



---

Publicly Accessible Penn Dissertations

---

2017

# Integration Of Fermentation And Organic Synthesis: Studies Of Roquefortine C And Biosynthetic Derivatives

Claire Marie Gober

University of Pennsylvania, [cgober@sas.upenn.edu](mailto:cgober@sas.upenn.edu)

Follow this and additional works at: <https://repository.upenn.edu/edissertations>

 Part of the [Organic Chemistry Commons](#)

---

## Recommended Citation

Gober, Claire Marie, "Integration Of Fermentation And Organic Synthesis: Studies Of Roquefortine C And Biosynthetic Derivatives" (2017). *Publicly Accessible Penn Dissertations*. 2312.  
<https://repository.upenn.edu/edissertations/2312>

This paper is posted at ScholarlyCommons. <https://repository.upenn.edu/edissertations/2312>  
For more information, please contact [repository@pobox.upenn.edu](mailto:repository@pobox.upenn.edu).

---

# Integration Of Fermentation And Organic Synthesis: Studies Of Roquefortine C And Biosynthetic Derivatives

## **Abstract**

Roquefortine C is one of the most ubiquitous indoline alkaloids of fungal origin. It has been isolated from over 30 different species of *Penicillium* fungi and has garnered attention in recent years for its role as a biosynthetic precursor to the triazaspirocyclic natural products glandicoline B, meleagrins, and oxaline. The triazaspirocyclic motif, which encompasses three nitrogen atoms attached to one quaternary carbon forming a spirocyclic scaffold, is a unique chemical moiety that has been shown to impart a wide array of biological activity, from anti-bacterial activity and antiproliferative activity against cancer cell lines to anti-biofouling against marine organisms. Despite the promise of these compounds in the pharmaceutical and materials industries, few syntheses of triazaspirocycles exist in the literature. The biosynthesis of roquefortine C-derived triazaspirocycles, however, provides inspiration for the synthesis of these compounds, namely through a nitron-promoted transannular rearrangement. This type of internal rearrangement has never been carried out synthetically and would provide an efficient stereoselective synthesis of triazaspirocycles. This work encompasses efforts towards elucidating the biosynthetic pathway of roquefortine C-derived triazaspirocycles as well as synthetic efforts towards the construction of triazaspirocycles. Chapter 1 will discuss a large-scale fermentation procedure for the production of roquefortine C from *Penicillium crustosum*. Chapters 2 and 3 explore (through enzymatic and synthetic means, respectively) the formation of the key indoline nitron moiety required for the proposed transannular rearrangement. Finally, chapter 4 will discuss synthetic efforts towards the synthesis of triazaspirocycles. This work has considerably enhanced our understanding of the roquefortine C biosynthetic pathway and the unique chemistry of this natural product, and our efforts towards the synthesis of triazaspirocycles will facilitate the use of these compounds in numerous applications.

## **Degree Type**

Dissertation

## **Degree Name**

Doctor of Philosophy (PhD)

## **Graduate Group**

Chemistry

## **First Advisor**

Madeleine M. Joullie

## **Keywords**

Fermentation, Indole alkaloid, Roquefortine

## **Subject Categories**

Organic Chemistry

INTEGRATION OF FERMENTATION AND ORGANIC SYNTHESIS: STUDIES OF  
ROQUEFORTINE C AND BIOSYNTHETIC DERIVATIVES

Claire Marie Gober

A DISSERTATION

in

Chemistry

Presented to the Faculties of the University of Pennsylvania

in

Partial Fulfillment of the Requirements for the

Degree of Doctor of Philosophy

2017

Supervisor of Dissertation

---

Madeleine M. Joullié, Professor of Chemistry

Graduate Group Chairperson

---

Gary A. Molander, Hirschmann-Makineni Professor of Chemistry

Dissertation Committee

William P. Dailey, Associate Professor of Chemistry

Donna Huryn, Adjunct Professor of Chemistry

Ian Blair, A.N. Richards Professor of Pharmacology

INTEGRATION OF FERMENTATION AND ORGANIC SYNTHESIS: STUDIES  
OF ROQUEFORTINE C AND BIOSYNTHETIC DERIVATIVES

COPYRIGHT

2017

Claire Marie Gober

## **ACKNOWLEDGMENT**

Through the ups and downs of the last five years, I have grown both personally and professionally in more ways than I can imagine. This program has instilled in me independence and a tremendous work ethic that will continue to serve me throughout my professional career. I am tremendously proud to present this dissertation and would not be where I am today without the help, guidance, and support of countless mentors, colleagues, friends, and family.

First and foremost, I would like to acknowledge my research advisor, Dr. Madeleine Joullié. She accepted me into her research group as an eager first year graduate student and believed in my talents and abilities at a time when I often found it difficult to believe in myself. She remains one of the most dedicated and hard-working people I have known, and her commitment to her work and her students has always been inspirational. Over the years, she has supported me not only in my scientific endeavors, but also in my personal and professional development. She allowed me the freedom to explore different areas of chemistry and science I found interesting, which helped me broaden my scientific horizons and kept me constantly engaged in my research. Dr. Joullié recognized early on my passion and talent for writing and communicating science, and has given me many opportunities to improve in these areas.

I would like to extend special thanks to my dissertation committee members, Dr. Donna Huryn, Dr. Ian Blair, and particularly my chair Dr. Bill Dailey. Their

support, career guidance, and helpful suggestions over the years have molded me into the scientist I am today and have helped me create a body of work I am proud and honored to present.

I owe a great debt of gratitude to a number of mentors and former teachers. Thank you to my high school chemistry teachers Mr. D'Aquanno and Mr. Keagy who helped instill my passion for chemistry. I would also like to thank my high school physics teacher Mrs. Wakefield, who was not only an amazing teacher but also an excellent role model as a female scientist. My first research experience was as an REU student in the Kozlowski group during the summer of 2011. Thank you to Dr. Marisa Kozlowski for taking a chance on an undergraduate with no research experience and special thanks to my graduate student mentors in that lab, Dr. Ryan Walvoord, Dr. John Curto, and particularly Dr. Alison Metz for helping to shape me as a scientist. I would like to thank my undergraduate research advisor at Cornell, Dr. Bruce Ganem, for allowing me to take the lead on my first project in his lab and for all of his encouragement and guidance. Thank you also to Dr. David Chenoweth, whose wealth of knowledge, infectious passion for science, and helpful suggestions during group meetings have been particularly motivating.

None of this work would be possible without the help from the incredible facilities and staff here in the Chemistry Department. Thank you to Drs. George Furst and Jun Gu for their extraordinary help, particularly in developing the  $^{15}\text{N}$  NMR protocols. Thanks to Drs. Rakesh Kohli and Chuck Ross for their support in

our mass spectrometry facility and to Dr. Pat Carroll for his assistance in X-ray crystallography. Thank you to Judith Currano for all her assistance in preparing our manuscripts and for always being available to give advice. Thank you to all the administrative staff in our department: Robert Wertz, Kristen Muscat, Chris Jeffrey, Dr. James Tarver, Dr. Kersten Forsthoefel, Yvonne Kline and Bruno Fiorenza.

I would like to acknowledge all my colleagues and peers for providing helpful insight and whose advice and training has proved invaluable to my research. Thank you to former labmates Dr. Jisun Lee, Dr. Brandon Kelly, and Michael Persun; to Chenoweth group members, particularly Dr. Stephanie Barros, whose biological expertise was instrumental in developing the fermentation protocol; to Matt Bunner for his countless hours assisting me with LC-MS studies; to my collaborators at the University of Michigan, including Dr. Sean Newmister, Dr. Roberto Berlinck, and Dr. David Sherman; and to Dr. Robert Rarig, Dr. Mai Tran, Dr. Yitao Zhang, Roy Malamakal, Sung-Eun Suh, and Melissa Grenier for their essential experimental input.

My time at Penn has not only molded me into an excellent scientist, but has also allowed me to develop professionally through a number of student organizations. Thank you to my friends and colleagues on the Women in Chemistry board, including Dr. Lyndsay Leal, Dr. Kelsey VanGelder, Melissa Grenier, Dr. Rachel Abaskharon, Dr. Katie Pulsipher, Teresa Rapp, Althea Gaffney, Adriana Jemison, and others. Thank you to the Chemistry-Biology Interface Training

Program, which not only supported my stipend for two and a half years, but also allowed me to develop professional connections and learn about a wide range of scientific fields.

Special thanks go out to all my friends who have been there for me through it all, helping me celebrate the accomplishments and supporting me through the hardships and stress. Thank you to all my friends in my incoming graduate class including Chris Walters, Dr. Geraint Davies, Dr. John Tellis, Roy Malamakkal, David Primer, and Jake Nagy; to my wonderful friends outside the department Chris Bailey, Dan Lane, Elise Chen, Lauren Allegrezza, and Charlotte Sacksteder; and to my PhilHarmonia family.

Finally, I would like to thank Ethan and my mom, dad, and sister for their amazing support over the years, and particularly in this last year.



## ABSTRACT

### INTEGRATION OF FERMENTATION AND ORGANIC SYNTHESIS: STUDIES OF ROQUEFORTINE C AND BIOSYNTHETIC DERIVATIVES

Claire Marie Gober

Madeleine M. Joullié

Roquefortine C is one of the most ubiquitous indoline alkaloids of fungal origin. It has been isolated from over 30 different species of *Penicillium* fungi and has garnered attention in recent years for its role as a biosynthetic precursor to the triazaspirocyclic natural products glandicoline B, meleagrins, and oxaline. The triazaspirocyclic motif, which encompasses three nitrogen atoms attached to one quaternary carbon forming a spirocyclic scaffold, is a unique chemical moiety that has been shown to impart a wide array of biological activity, from anti-bacterial activity and antiproliferative activity against cancer cell lines to anti-biofouling against marine organisms. Despite the promise of these compounds in the pharmaceutical and materials industries, few syntheses of triazaspirocycles exist in the literature. The biosynthesis of roquefortine C-derived triazaspirocycles, however, provides inspiration for the synthesis of these compounds, namely through a nitrene-promoted transannular rearrangement. This type of internal rearrangement has never been carried out synthetically and would provide an efficient stereoselective synthesis of triazaspirocycles. This work encompasses efforts towards elucidating the biosynthetic pathway of roquefortine C-derived

triazaspirocycles as well as synthetic efforts towards the construction of triazaspirocycles. Chapter 1 will discuss a large-scale fermentation procedure for the production of roquefortine C from *Penicillium crustosum*. Chapters 2 and 3 explore (through enzymatic and synthetic means, respectively) the formation of the key indoline nitron moiety required for the proposed transannular rearrangement. Finally, chapter 4 will discuss synthetic efforts towards the synthesis of triazaspirocycles. This work has considerably enhanced our understanding of the roquefortine C biosynthetic pathway and the unique chemistry of this natural product, and our efforts towards the synthesis of triazaspirocycles will facilitate the use of these compounds in numerous applications.

## TABLE OF CONTENTS

ACKNOWLEDGMENT .....	iii
ABSTRACT .....	vii
LIST OF FIGURES AND SCHEMES.....	xv
CHAPTER ONE.....	1
I. Introduction.....	2
II. Background .....	3
A. Isolation and Structure Determination .....	3
B. Biological Properties of Roquefortine C .....	5
C. Biosynthesis of Roquefortine C and Related Metabolites .....	6
D. Total Synthesis of Roquefortine C.....	11
E. Prior Art: Small Scale Fermentation of Roquefortine C .....	12
III. Results and Discussion .....	14
A. Large Scale Fermentation of Roquefortine C.....	14
B. Comparison to Other Methods of Roquefortine C Production .....	17
IV. Conclusions.....	18
V. Experimental Details.....	18
General Information .....	18
Isolation of roquefortine C ( <b>1</b> ) from <i>P. crustosum</i> .....	19
VI. References .....	20
Appendix 1A: Species of <i>Penicillium</i> that Produce Roquefortine C .....	27
Appendix 1B: Spectra Relevant to Chapter 1 .....	29
CHAPTER TWO.....	36
I. Introduction.....	37
II. Background .....	37

A. Nitrones.....	37
B. Nitrene Biosynthesis .....	40
III. Results and Discussion .....	42
A. Oxaline Biosynthetic Gene Cluster.....	42
B. OxaD, a Flavin-Dependent Nitrene Synthase .....	43
C. Investigating the Mechanism of Oxidation.....	46
D. Roquefortine L Undergoes 1,3-Dipolar Cycloaddition .....	48
E. Oxidation of Roquefortine C Derivatives by OxaD .....	50
F. OxaD Catalyzes Indole 2,3-Oxidation of Notoamide S.....	54
G. Speculation on Glandicoline A Formation in <i>P. glandicola</i> .....	57
IV. Conclusions.....	59
V. Experimental .....	60
<i>P. oxalicum</i> genomic DNA sequencing.....	60
Molecular cloning of oxaD gene.....	62
Overexpression and purification of OxaD .....	62
Isolation of <sup>15</sup> N-enriched roquefortine C ( <b>1</b> ) from <i>P. crustosum</i> .....	64
Semi-synthesis of roquefortine C analogues: General Information .....	65
11-Bromoroquefortine C ( <b>39</b> ) .....	66
11-Iodoroquefortine C ( <b>40</b> ).....	67
20-Phenylsulfonylroquefortine C ( <b>41</b> ).....	68
Isoroquefortine C ( <b>9</b> ).....	69
Enzymatic generation of roquefortine L and derivatives: General Information.....	70
Roquefortine L ( <b>17</b> ) .....	71
Roquefortine L ( <b>17</b> ), <sup>15</sup> N enriched .....	72
11-Bromoroquefortine L ( <b>44</b> ).....	72
Isoroquefortine L ( <b>43</b> ).....	73
20-Phenylsulfonylroquefortine L ( <b>46</b> ) .....	73
Enzymatic conversion of notoamide S ( <b>50</b> ).....	76

Single turnover studies with OxaD .....	77
Steady state kinetics of OxaD with roquefortine C .....	78
1,3-Dipolar cycloaddition of roquefortine L ( <b>17</b> ) with methyl acrylate .....	81
Total turnover number calculation.....	82
VI. References .....	82
Appendix 2A: Spectra Relevant to Chapter 2.....	88
CHAPTER THREE .....	137
I. Introduction.....	138
II. Background .....	138
A. Nitrones.....	138
B. Chemical Kinetics and Reaction Progress Kinetic Analysis .....	140
III. Results and Discussion .....	144
A. Roquefortine C N-Oxidation Products .....	144
B. Derivation of N-Oxidation Rate Laws .....	146
C. Attempts to Monitor Reaction Kinetics .....	148
D. N-Oxidation Product Analysis.....	150
IV. Conclusions.....	153
V. Experimental Section.....	154
General Information .....	154
Roquefortine C hydroxylamine ( <b>16</b> ) .....	155
Roquefortine L ( <b>17</b> ) .....	156
11-Hydroxyroquefortine L ( <b>61</b> ) .....	157
Oxidation with DMDO .....	158
Oxidation with mCPBA.....	159
Oxidation with sodium tungstate/hydrogen peroxide.....	159
Oxidation with trichloroacetonitrile/hydrogen peroxide.....	159
Oxidation with Davis oxaziridine .....	159

Oxidation with OXONE ®.....	160
LC-MS calibration .....	160
VI. References .....	161
Appendix 3A: Spectra Relevant to Chapter 3.....	164
CHAPTER FOUR .....	169
I. Introduction.....	170
II. Background .....	170
A. Triazaspirocycle Natural Products.....	170
B. Triazaspirocycles: Properties and Applications .....	172
C. Synthesis of Triazaspirocycles .....	176
III. Results and Discussion .....	180
A. Geometry Optimization Studies of Roquefortine C Transannular Rearrangement.....	180
B. Efforts toward Transannular Rearrangement Methodology using Roquefortine C.....	183
C. First Generation Model System.....	186
D. Second Generation Model System: Design and Computational Studies.....	189
E. Second Generation Model System: Synthetic Efforts.....	192
IV. Conclusions and Future Directions.....	199
V. Experimental Details.....	200
General information .....	200
2-(((Benzyloxy)carbonyl)amino)-2-hydroxyacetic acid ( <b>113</b> ).....	201
Methyl 2-(((benzyloxy)carbonyl)amino)-2-methoxyacetate ( <b>114</b> ).....	202
Methyl 2-(((benzyloxy)carbonyl)amino)-2-(dimethoxyphosphoryl)- acetate ( <b>115</b> ).....	203

<i>tert</i> -Butyl (2 <i>S</i> )-2-((1-(dimethoxyphosphoryl)-2-methoxy-2-oxoethyl)- carbamoyl)pyrrolidine-1-carboxylate ( <b>118</b> ).....	204
1-Tosyl-1 <i>H</i> -imidazole-4-carbaldehyde ( <b>119</b> ).....	205
<i>tert</i> -Butyl ( <i>S,Z</i> )-2-((3-methoxy-3-oxo-1-(1-tosyl-1 <i>H</i> -imidazol-4-yl)prop- 1-en-2-yl)carbamoyl)pyrrolidine-1-carboxylate ( <b>120</b> ) .....	206
( <i>S,Z</i> )-3-((1-Tosyl-1 <i>H</i> -imidazol-4-yl)methylene)hexahydropyrrolo[1,2- <i>a</i> ]- pyrazine-1,4-dione ( <b>121</b> ).....	207
Benzyl 2-(2,2,2-trifluoroacetamido)acrylate ( <b>126b</b> ).....	208
1-Allyl-3-methyl-1 <i>H</i> -indole ( <b>133</b> ) .....	209
( <i>R</i> )-2,2'-Bis(methoxymethoxy)-1,1'-binaphthalene ( <b>144</b> ).....	210
( <i>R</i> )-3,3'-Dichloro-2,2'-bis(methoxymethoxy)-1,1'-binaphthalene ( <b>145</b> ).....	211
( <i>R</i> )-3,3'-Dichloro-BINOL ( <b>142</b> ) .....	212
Benzyl (2 <i>S</i> ,3 <i>aS</i> ,8 <i>aS</i> )-8-allyl-3 <i>a</i> -methyl-1-(2,2,2-trifluoroacetyl)- 1,2,3,3 <i>a</i> ,8,8 <i>a</i> -hexahydropyrrolo[2,3- <i>b</i> ]indole-2-carboxylate ( <b>140b</b> ) .....	213
Methyl (2 <i>S</i> ,3 <i>aS</i> ,8 <i>aS</i> )-8-allyl-3 <i>a</i> -methyl-1-(2,2,2-trifluoroacetyl)- 1,2,3,3 <i>a</i> ,8,8 <i>a</i> -hexahydropyrrolo[2,3- <i>b</i> ]indole-2-carboxylate ( <b>140a</b> ).....	214
Methyl (2 <i>S</i> ,3 <i>aS</i> ,8 <i>aS</i> )-3 <i>a</i> -methyl-1-(2,2,2-trifluoroacetyl)-1,2,3,3 <i>a</i> ,8,8 <i>a</i> - hexahydropyrrolo[2,3- <i>b</i> ]indole-2-carboxylate ( <b>146</b> ).....	215
Methyl (2 <i>S</i> ,3 <i>aS</i> ,8 <i>aR</i> )-3 <i>a</i> -methyl-1,2,3,3 <i>a</i> ,8,8 <i>a</i> -hexahydropyrrolo[2,3- <i>b</i> ]indole-2-carboxylate ( <b>148</b> ) .....	216
2-(( <i>tert</i> -Butoxycarbonyl)amino)-2-methylpropanoic acid ( <b>127a</b> ).....	217
Methyl (2 <i>S</i> ,3 <i>aS</i> ,8 <i>aS</i> )-1-(2-(( <i>tert</i> -butoxycarbonyl)amino)-2- methylpropanoyl)-3 <i>a</i> -methyl-1,2,3,3 <i>a</i> ,8,8 <i>a</i> -hexahydropyrrolo[2,3- <i>b</i> ]indole-2-carboxylate ( <b>149</b> ) .....	218
Methyl (2 <i>S</i> ,3 <i>aS</i> ,8 <i>aR</i> )-1-(2-(( <i>tert</i> -butoxycarbonyl)amino)-2-methyl- propanoyl)-3 <i>a</i> -methyl-8-(phenylsulfonyl)-1,2,3,3 <i>a</i> ,8,8 <i>a</i> -hexahydro- pyrrolo[2,3- <i>b</i> ]indole-2-carboxylate ( <b>150</b> ) .....	219

(5a <i>R</i> ,10b <i>S</i> ,11a <i>S</i> )-3,3,10b-Trimethyl-6-(phenylsulfonyl)-2,3,6,10b,11,11a-hexahydro-4 <i>H</i> -pyrazino[1',2':1,5]pyrrolo[2,3- <i>b</i> ]indole-1,4(5a <i>H</i> )-dione ( <b>151</b> ).....	220
(5a <i>R</i> ,10b <i>S</i> ,11a <i>S</i> )-2-(4-Methoxybenzyl)-3,3,10b-trimethyl-6-(phenylsulfonyl)-2,3,6,10b,11,11a-hexahydro-4 <i>H</i> -pyrazino[1',2':1,5]pyrrolo[2,3- <i>b</i> ]indole-1,4 (5a <i>H</i> )-dione ( <b>154</b> ).....	221
(5a <i>R</i> ,10b <i>S</i> )-11a-Hydroxy-2-(4-methoxybenzyl)-3,3,10b-trimethyl-6-(phenylsulfonyl)-2,3,6,10b,11,11a-hexahydro-4 <i>H</i> -pyrazino[1',2':1,5]pyrrolo[2,3- <i>b</i> ]indole-1,4(5a <i>H</i> )-dione ( <b>155</b> ).....	222
VI. References .....	223
Appendix 4A: Description of Human Cell Lines.....	230
Appendix 4B: Spectra Relevant to Chapter 4.....	231
Appendix 4C: X-Ray Crystal Structures Relevant to Chapter 4.....	261
List of Acronyms and Abbreviations .....	274
Bibliography.....	283



## LIST OF FIGURES AND SCHEMES

Figure 1.1: Roquefortine C and related metabolites .....	3
Scheme 1.1: Structural determination of roquefortine C ( <b>1</b> ) by chemical reduction and hydrolysis .....	4
Scheme 1.2: Photoisomerization of roquefortine C and configuration of the dehydrohistidine moiety .....	5
Figure 1.2: Inhibition of hepatic cytochrome P450s as a result of intramolecular hydrogen bonding .....	6
Scheme 1.3: Biosynthesis of roquefortine C ( <b>1</b> ) .....	8
Scheme 1.4: Roquefortine biosynthetic pathway proposed by Vleggaar et al., with potential intermediates in brackets .....	9
Scheme 1.5: Biosynthesis of roquefortine C-derived metabolites.....	11
Scheme 1.6: Total synthesis of roquefortine C ( <b>1</b> ).....	12
Scheme 1.7: Roquefortine C fermentation process .....	14
Table 1.1: Roquefortine C fermentation growth media composition .....	15
Figure 1.3: Effects of light on <i>P. crustosum</i> mycelial growth .....	16
Figure 2.1: Known indoline nitronone natural products.....	39
Scheme 2.1: Cytochrome P450 oxidation mechanism .....	41
Scheme 2.2: Flavin monooxygenase mechanism .....	41
Scheme 2.3: Oxaline biosynthetic gene cluster .....	43
Figure 2.2: Reactions with OxaD and <b>1</b> led to the detection of a hydroxylamine intermediate <b>16</b> and the hydrolysis product <b>36</b> .....	45
Scheme 2.4: Possible mechanisms of roquefortine L ( <b>17</b> ) biosynthesis by OxaD .....	47
Table 2.1: Single turnover studies of OxaD .....	48
Table 2.2: Potential dipolarophile candidates for 1,3-dipolar cycloaddition with roquefortine L ( <b>17</b> ).....	49

Scheme 2.5: Roquefortine L ( <b>17</b> ) undergoes 1,3-dipolar cycloaddition with methyl acrylate to generate <b>38</b> .....	50
Figure 2.3: (A) Roquefortine C and derivatives. (B) Nitrones derived from OxaD N-oxidation .....	51
Scheme 2.6: Semisynthesis of roquefortine C derivatives <b>9</b> , <b>39</b> , and <b>40</b> .....	51
Figure 2.4: Electrophilic fluorinating reagents.....	52
Scheme 2.7: Unexpected NFSI phenylsulfonyl transfer .....	53
Figure 2.5: Total turnover number of roquefortine C and derivatives by OxaD .....	54
Scheme 2.8: OxaD reactivity with notoamides .....	56
Scheme 2.9: NotB-catalyzed formation of notoamides C ( <b>56</b> ) and D ( <b>57</b> ) from notoamide E ( <b>51</b> ).....	57
Scheme 2.10: Proposed biogenesis of glandicoline A ( <b>15</b> ) and B ( <b>2</b> ).....	59
Scheme 3.1: Nitrones as chemical building blocks.....	139
Scheme 3.2: Mechanism of amine oxidation to nitrones .....	139
Scheme 3.3: Roquefortine C N-oxidation products.....	144
Scheme 3.4: Roquefortine C oxidation pathway.....	147
Scheme 3.5: Determination of <i>K</i> for the formation of peroxyimidic acid <b>62</b> .....	149
Figure 3.1: <sup>1</sup> H NMR spectra of roquefortine C ( <b>1</b> ) and N-oxidation products....	150
Table 3.1: Roquefortine C N-oxidation distribution of products .....	152
Table 3.2: Electrophilicity of electrophilic oxidizing reagents .....	153
Figure 4.1: Triazaspirocycle scaffolds .....	170
Figure 4.2: Triazaspirocyclic natural products .....	171
Scheme 4.1: Biogenesis of roquefortine C derived triazaspirocycles in <i>P. chrysogenum</i> and <i>P. oxalicum</i> .....	172
Scheme 4.2: Photochromic triazaspirocycles .....	175
Scheme 4.3: Surface functionalization with triazaspirocycles.....	176
Scheme 4.4: Synthesis of triazaspirocycles via 1,3-dipolar cycloaddition .....	177

Scheme 4.5: Pummerer reaction to access dibromoagelaspongin triazaspirocyclic core .....	178
Scheme 4.6: Synthesis of dibromoagelaspongin core via intramolecular epoxide ring opening .....	178
Scheme 4.7: Synthesis of fused $\beta$ -lactams via acetic anhydride promoted transannular rearrangements .....	179
Scheme 4.8: Triazaspirocyclic formation in the total syntheses of oxaline and meleagrins .....	180
Figure 4.3: Reaction coordinate diagram of roquefortine C transannular rearrangement to glandicoline B .....	182
Figure 4.4: Geometry optimized structure of compound <b>59b</b> .....	182
Scheme 4.9: Retrosynthetic analysis of glandicoline B formation .....	184
Figure 4.5: Representative epidithiodiketopiperazine alkaloids synthesized by Movassaghi and Sodeoka .....	184
Scheme 4.10: Formation of diketoamine <b>106</b> from hemiaminal <b>108</b> .....	185
Scheme 4.11: Representative protection of a pyrroloindoline diketopiperazine .....	186
Scheme 4.12: Synthetic route towards first generation model system <b>121</b> .....	188
Scheme 4.13: Oxaphosphetane internal hydrogen bonding leads to exclusive formation of the <i>Z</i> isomer .....	189
Scheme 4.14: Retrosynthesis of second generation model system <b>124</b> and triazaspirocyclic <b>123</b> .....	190
Table 4.1: Calculated folding energy ( $\Delta E_{\text{folding}}$ ) of <b>128</b> .....	191
Figure 4.6: Reaction coordinate diagram of transannular rearrangement to <b>123a</b> .....	192
Scheme 4.15: Proposed mechanism of pyrroloindoline synthesis by formal [3+2] cycloaddition .....	193
Scheme 4.16: Synthesis of pyrroloindolines <b>140a</b> and <b>140b</b> .....	194
Scheme 4.17: Synthesis of ( <i>R</i> )-3,3'-Cl <sub>2</sub> -BINOL <b>142</b> .....	195

Scheme 4.18: Synthesis of phenylsulfonyl protected model system <b>151</b> .....	196
Scheme 4.19: Calculation of diketopiperazine $\alpha$ C-H BDE as heat of reaction $\Delta H$ .....	197
Table 4.2: Captodative character of select diketopiperazines .....	198
Scheme 4.20: $\alpha$ -Hydroxylation of model system <b>155</b> .....	199
Scheme 4.21: Future work towards the synthesis of triazaspirocycle <b>123a</b> .....	200

## CHAPTER ONE

### LARGE SCALE FERMENTATION OF ROQUEFORTINE C

Material in this chapter reproduced in part with permission from:

Newmister, S. A.; Gober, C. M.; Romminger, S.; Yu, F.; Tripathi, A.; Parra, L. L. L.;

Williams, R. M.; Berlinck, R. G. S.; Joullié, M. M.; Sherman, D. H. *J. Am. Chem. Soc.*

**2016**, *138*(35), 11176-11184. Copyright 2016 American Chemical Society.

Gober, C.; Joullié, M. M. *Athens Journal of Science* **2015**, *3*(4), 257-264

Gober, C.; Carroll, P. J.; Joullié, M. M. *Mini Rev. Org. Chem.* **2016**, *13*, 126-142.

Copyright 2016 Bentham Science.

## I. Introduction

Prenylated indoline alkaloids make up one of the largest classes of biologically active compounds of microbial origin. Fungal alkaloids in particular comprise a large portion of this class of compounds. The biological activity displayed by prenylated indoline alkaloids of fungal origin is wide ranging, from anti-bacterial activity<sup>1,2</sup> and antiproliferative activity against human T-cell leukemia<sup>3</sup> to anti-fouling against marine organisms.<sup>4</sup>

One of the most ubiquitous prenylated indoline alkaloids is roquefortine C (**1**, Figure 1.1). Roquefortine C is found in low levels in industrially produced blue cheese,<sup>5</sup> grain,<sup>6-9</sup> and animal feedstocks,<sup>10</sup> and has been isolated from 30 different *Penicillium* species<sup>11-26</sup> (see Appendix 1A). It has been a subject for research for several years due to its unique structure, its biological activity, and its role as a biosynthetic precursor to related metabolites glandicoline B (**2**), meleagrins (**3**), and oxalines (**4**). The first total synthesis of roquefortine C was carried out in the Joullié laboratory in 2008; however, this synthesis was lengthy, expensive, and low yielding, thus limiting further studies of roquefortine C and its downstream metabolites. Therefore, it was of interest to develop a fermentation-based approach towards roquefortine C production.

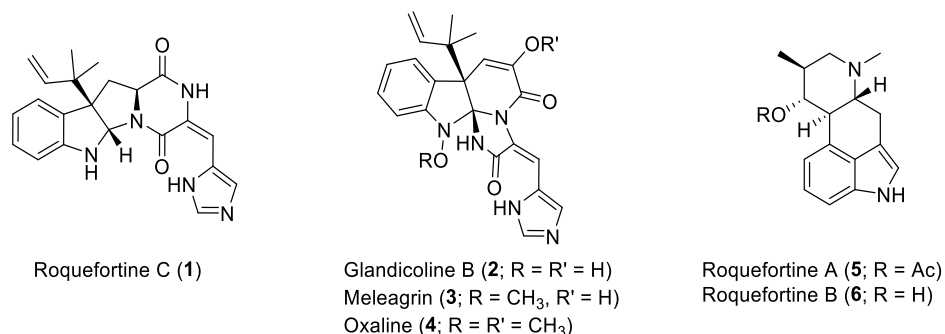


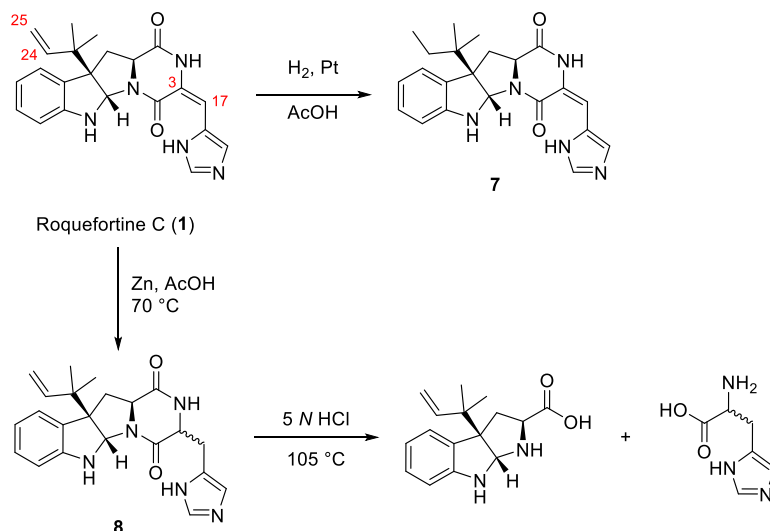
**Figure 1.1:** Roquefortine C and related metabolites

## II. Background

### A. Isolation and Structure Determination

Roquefortine C was first isolated from cultures of *Penicillium roqueforti* Thom along with the related compounds roquefortines A (5) and B (6) by Matazo Abe and coworkers in 1975.<sup>14</sup> Though characterization data was reported for roquefortine C, Abe et al. were unable to propose a structure for this novel compound. The following year, Scott and coworkers isolated roquefortine C from a sample of *P. roqueforti* (strain CS1) and determined its structure via a series of chemical and spectroscopic studies. Similar to many indoline alkaloids, roquefortine C was found to be composed of a tryptophan-proline diketopiperazine skeleton. Platinum-catalyzed hydrogenation of roquefortine C yielded 24,25-dihydroroquefortine C (7), and nuclear magnetic resonance (NMR) analysis of this compound as compared to roquefortine C suggested that the prenyl group was positioned in the reverse orientation to the indoline moiety (Scheme 1.1). Reduction with zinc in acetic acid at 70 °C afforded two 3,17-dihydroroquefortine C isomers (8) and corresponded with the disappearance of a singlet at 6.40 ppm in

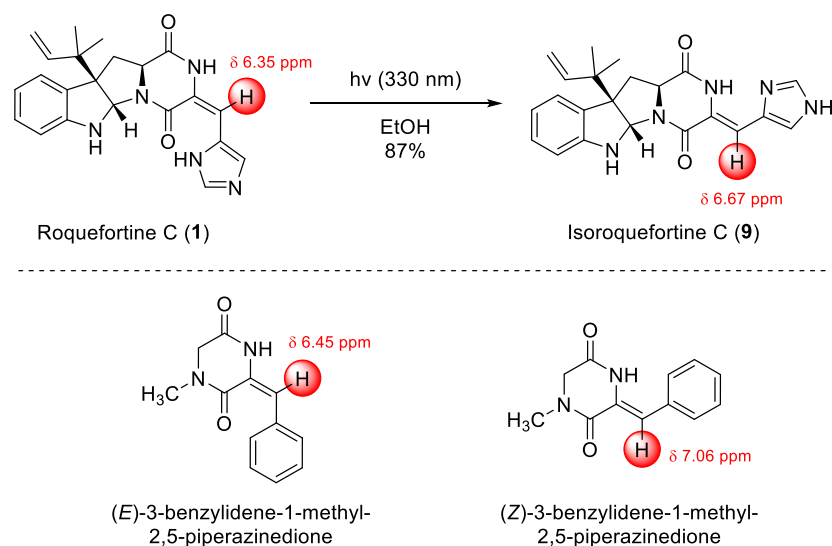
the  $^1\text{H}$  NMR spectra. Acidic hydrolysis of these two isomers yielded histidine, leading Scott and coworkers to conclude that roquefortine C possessed a unique dehydrohistidine side chain extending from the diketopiperazine.<sup>12</sup>



**Scheme 1.1:** Structural determination of roquefortine C (1) by chemical reduction and hydrolysis

The stereochemistry of the dehydrohistidine moiety was confirmed in 1979 by Scott and coworkers.<sup>27</sup> Photoisomerization of roquefortine C corresponded to a shift of H17 in the  $^1\text{H}$  NMR spectrum from 6.35 ppm in roquefortine C to 6.67 ppm in the photoisomer isoroquefortine C (9, Scheme 1.2). In previous comparisons between (*E*) and (*Z*)-3-benzylidene-1-methyl-2,5-piperazinedione, deshielding of this nature had been observed in the *E* species due to the adjacent carbonyl.<sup>28</sup> The dehydrohistidine moiety in roquefortine C was thus determined to be in the *E* configuration.





**Scheme 1.2:** Photoisomerization of roquefortine C and configuration of the dehydrohistidine moiety

## B. Biological Properties of Roquefortine C

The cytotoxicity of roquefortine C has been a subject of debate for many years. The toxicity of this compound appears to be highly organism-specific; roquefortine C has been reported to induce neurotoxic and inflammatory responses in mice<sup>12,29,30</sup> and paralytic activity in cockerels,<sup>31</sup> but it has shown little to no cytotoxicity in a number of human cell lines.<sup>9,32,33</sup> Roquefortine C may also be significant in indoor air contamination, as it has been isolated from numerous mold-contaminated indoor environments and as inflammatory responses have been reported for mouse lungs intratracheally instilled with roquefortine C.<sup>29,34-36</sup>

Roquefortine C is known to inactivate hepatic cytochrome P450s<sup>37</sup> and inhibit growth of gram-positive bacteria containing heme proteins.<sup>38,39</sup> The *E*-dehydrohistidine moiety of roquefortine C has been shown to be a key factor in

this inhibition. Computational studies of roquefortine C suggest internal hydrogen bonding between H19 and the C4 carbonyl oxygen (Figure 1.2).<sup>40</sup> As a consequence of this intramolecular hydrogen bonding, the imidazole moiety does not experience tautomerization. The nitrogen on the periphery of roquefortine C, N21, forms a strong Fe-N interaction through its lone pair, inhibiting hepatic cytochrome P450s and peroxidases.

Interestingly, isoroquefortine C demonstrates no such inhibition of heme proteins. Isoroquefortine C also possesses intramolecular hydrogen bonding; however, in this case, N19 becomes the hydrogen bond acceptor. As isoroquefortine C also does not experience tautomerization, the N21 lacks the  $sp^2$  lone pair needed to form a strong bond to iron and fails to inhibit hepatic cytochrome P450s.<sup>37</sup>

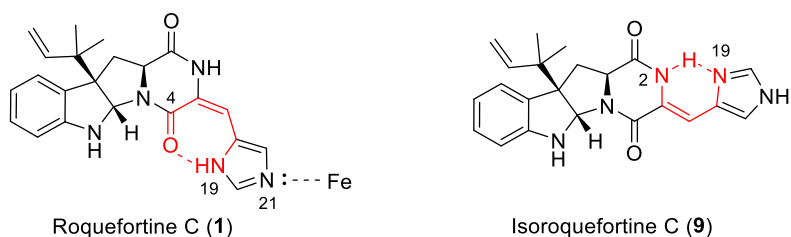
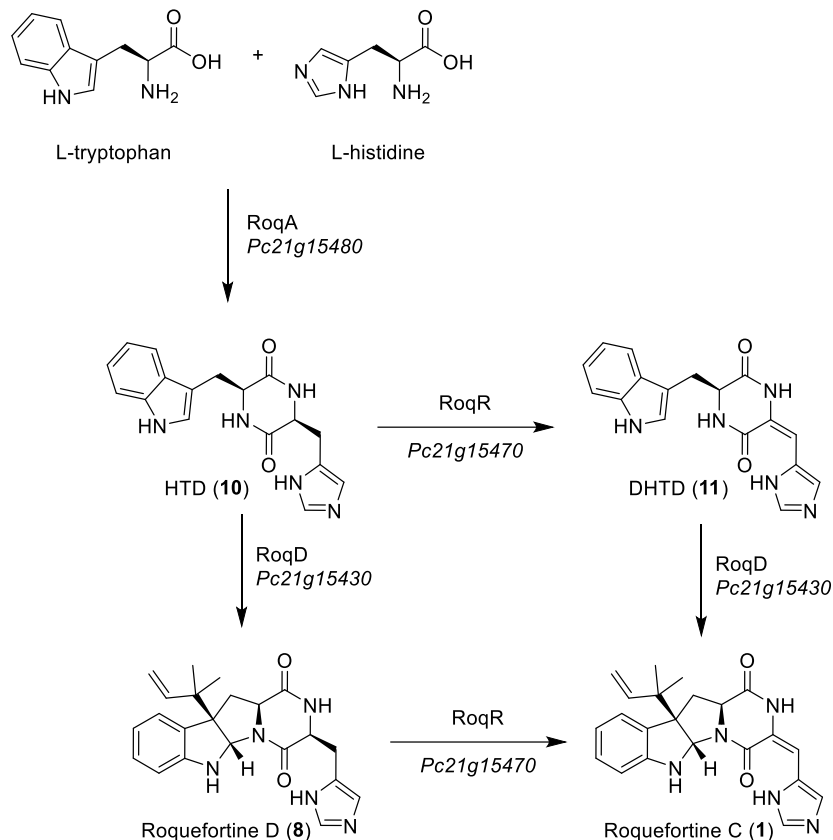


**Figure 1.2:** Inhibition of hepatic cytochrome P450s as a result of intramolecular hydrogen bonding

### C. Biosynthesis of Roquefortine C and Related Metabolites

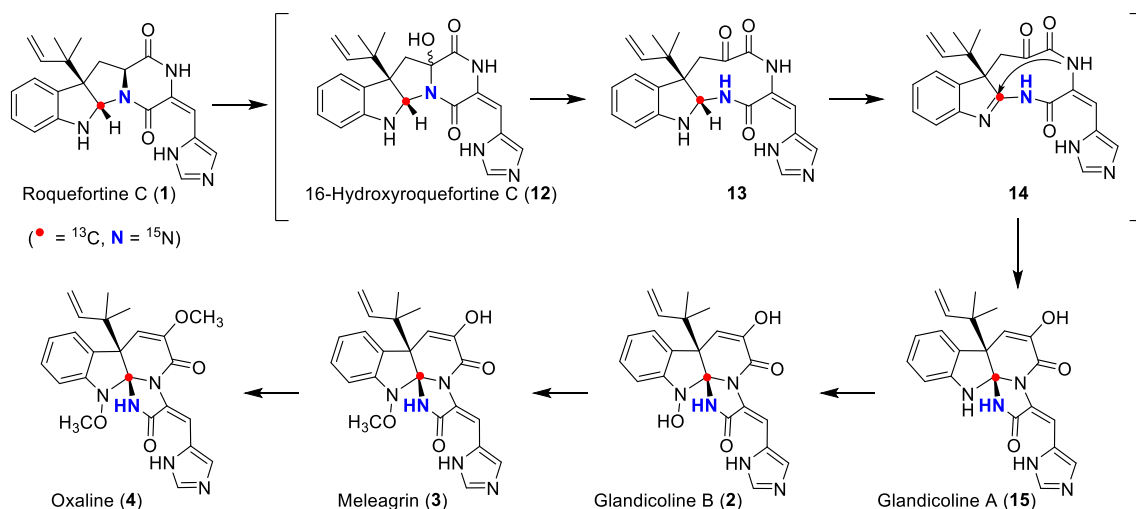
The genome of *Penicillium chrysogenum* was sequenced in 2008, setting the stage for the exploration of roquefortine C biosynthesis.<sup>41</sup> In 2011, a single cluster of coregulated genes encoding the biosynthesis of roquefortine C and

meleagrins were discovered by Martín and coworkers (Scheme 1.3). Open reading frames (ORFs) within the roquefortine-meleagrins gene cluster in the *P. chrysogenum* genome have been subjected to a series of RNA silencing experiments, which enabled a putative biochemical assignment for each step of the biosynthetic pathway.<sup>42</sup> *Pc21g15480* was found to encode a nonribosomal peptide synthetase (NRPS) RoqA, which is proposed to promote the biosynthesis of histidyltryptophanyldiketopiperazine (HTD, **10**) from histidine and tryptophan. RoqA was shown to contain two modules each containing activation, thiolation, and condensation domains. Subsequent gene deletion studies by Vreeken and coworkers uncovered a branched pathway leading to the biosynthesis of roquefortine C.<sup>43</sup> A gene encoding prenyltransferase RoqD (*Pc21g15430*) was found to promote the biosynthesis of roquefortine D (**8**) from HTD and roquefortine C from dehydrohistidyltryptophanyldiketopiperazine (DHTD, **11**). *Pc21g15470* encodes cytochrome P450 oxidoreductase RoqR, which was found to promote the dehydrogenation of HTD to DHTD and of roquefortine D to roquefortine C.



**Scheme 1.3:** Biosynthesis of roquefortine C (1)

The biosynthetic pathway connecting roquefortine C to its downstream metabolites has been a subject of investigation for several years. A radiolabeling study by Vlegaar (Scheme 1.4) was the first evidence to suggest a biosynthetic pathway containing *Penicillium* indole alkaloids roquefortine C, glandicolines A (15) and B (2), meleagrins (3), and oxaline (4).<sup>44</sup> He proposed that the pathway began with the hydroxylation of roquefortine C, followed by a rearrangement to give glandicoline A, N-oxidation to give glandicoline B, and methylation to give meleagrins and oxaline.



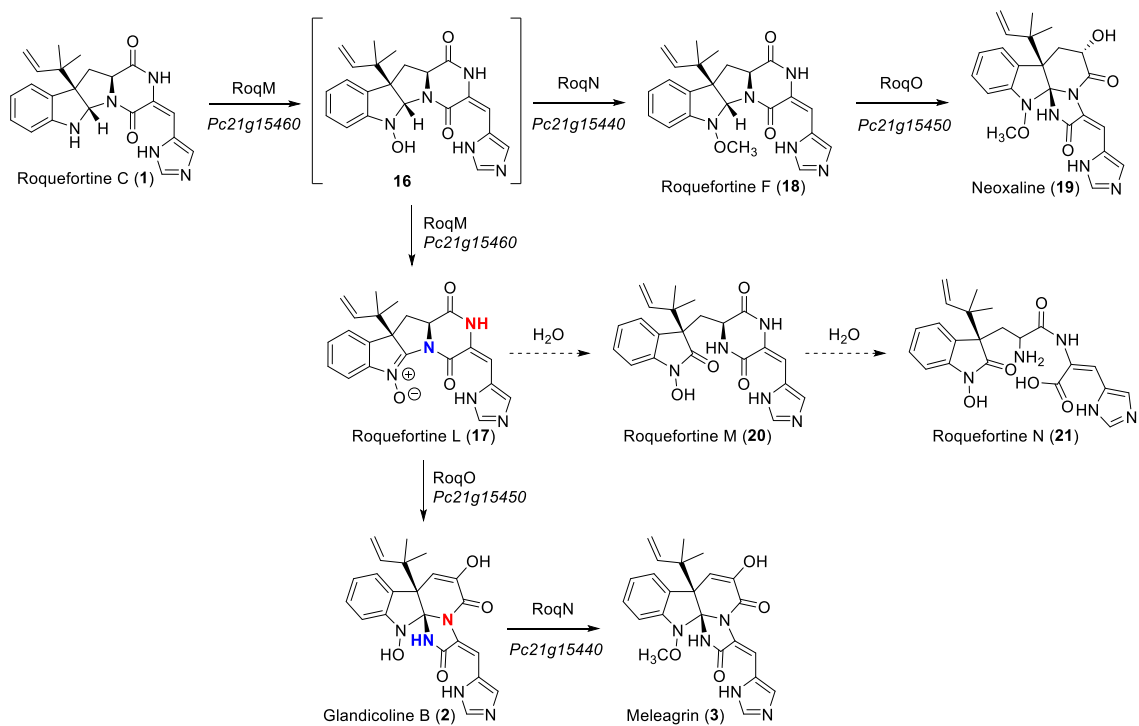
**Scheme 1.4:** Roquefortine biosynthetic pathway proposed by Vleggaar et al., with potential intermediates in brackets

It was unclear from this study, however, whether oxaline was made biosynthetically via a direct oxidation and rearrangement of roquefortine C, as is suggested in Scheme 1.4, or if it were instead made via a separate pathway. A later study by Reshetilova provided evidence of direct oxidation and rearrangement as incorporation of exogenous  $^{14}\text{C}$  labeled roquefortine C into the proposed downstream metabolites was shown to occur in cell suspensions and growing cultures of *Penicillium glandicola*.<sup>45,46</sup>

Whole genome sequencing, analysis, and substrate modeling with *P. chrysogenum* Wis54-1255 have enabled the determination of the gene cluster that encodes the biosynthesis of roquefortine C derived metabolites.<sup>41</sup> In the first reports of this gene cluster, Martín and coworkers found the transformation of roquefortine C (1) into glandicoline A (15) to be promoted by a MAK1-like monooxygenase RoqM (encoded by *Pc21g15460*), as evidenced by loss of

production of **2**, **15**, and **4** upon gene silencing. Subsequent gene deletion analysis of the *P. chrysogenum* strain DS54555 roquefortine C gene cluster<sup>43</sup> confirmed the results obtained by gene silencing,<sup>42</sup> leading to a mechanism identical to the one previously proposed by Steyn and Vlegaar.<sup>44</sup>

More recently, rigorous structural elucidation of the metabolites of this pathway prompted a revision of the biosynthetic mechanism for this particular rearrangement.<sup>47</sup> The key revision to this newly proposed metabolic pathway is the generation of the nitrene-bearing intermediate roquefortine L (**17**) by RoqM from **1** (Scheme 1.5). Since roquefortine L (**17**) has a molecular weight identical to that of glandicoline A (**15**), it was proposed that **17** had been mistakenly characterized as **15** in the initial gene silencing and gene deletion studies. Cytochrome P450 monooxygenase RoqO (encoded by *Pc21g15450*) was proposed to catalyze the rearrangement of **15** to give the triazaspirocyclic core of glandicoline B (**2**) as deletion of this gene resulted in loss of production of **3** and **2**. Novel metabolites roquefortine F (**18**) and neoxaline (**19**), presumably formed from hydroxylamine **16**, were also reported in this work as well as roquefortines M (**20**) and N (**21**), which were formed following non-enzymatic hydrolysis of roquefortine L.



**Scheme 1.5:** Biosynthesis of roquefortine C-derived metabolites

#### D. Total Synthesis of Roquefortine C

The first and only total synthesis of roquefortine C was published by our laboratory in 2008 (Scheme 1.6).<sup>40</sup> This total synthesis included a novel elimination strategy to construct the thermodynamically disfavored *E*-dehydrohistidine moiety. However, this synthesis did little to improve the availability or cost of the compound: only 17 milligrams were produced as a result of the total synthesis, and the cost of raw materials to produce 1 gram of **1** by total synthesis is estimated to be over \$1800.





production by four strains of *P. roqueforti* using five unique growth conditions.<sup>48</sup> Roquefortine C production was found to parallel mycelial growth, with the majority of roquefortine C being isolated from the mycelia as opposed to the liquid growth media. Extractions of roquefortine C from the mycelia were carried out with acetone, which was determined to be the ideal extraction solvent. Growth media containing yeast extract and higher concentrations of sucrose gave superior yields of roquefortine C, with maximum yields from mycelia estimated at 295 mg per liter of growth media at 40 days from *P. roqueforti* strain HPB 111275.

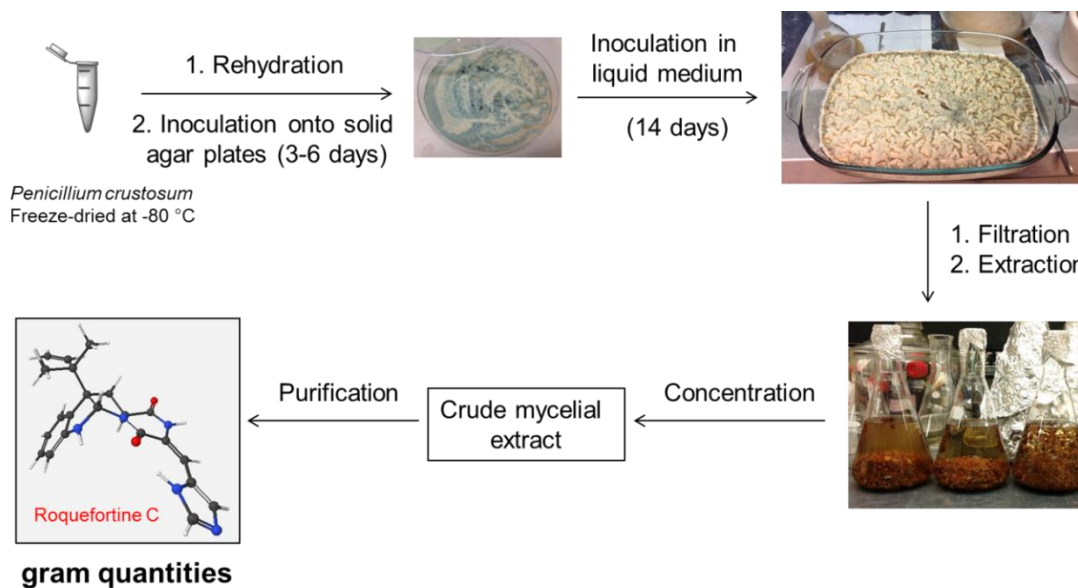
Roquefortine C has also been isolated in high yields from other species of *Penicillia*. In 1980, Diener et al. isolated roquefortine C in 101 mg per liter from mycelia of *Pencillium commune* grown in a yeast extract-sucrose growth medium and determined that stationary cultures were imperative for roquefortine C production.<sup>31</sup> Alkaline environments tended to correlate with higher roquefortine production, as the pH of growth media yielding the largest quantities of roquefortine C rose to 8 or 9 following 10 days of mycelial growth. Initial mycelial growth rate was shown to be more rapid with smaller volumes of growth media in conical flasks. Roquefortine C was also isolated from *Penicillium crustosum* by Mantle and coworkers in 1983.<sup>49</sup> Grown for 12 days in Czapek-Dox liquid growth media supplemented with 0.5% yeast extract, roquefortine C production was found to approach 13 mg per 50 mL growth media, which equates to 260 mg per liter. Mantle also observed the necessity of mycelial growth for roquefortine C

production and found that poor mycelial growth negatively impacted roquefortine C production.

### III. Results and Discussion

#### A. Large Scale Fermentation of Roquefortine C

While *P. roqueforti*, in particular the HPB 111275 strain, would have been the ideal strain for our fermentation based on the previously discussed work by P. M. Scott, its limited availability in the United States led us to select *P. crustosum* ATCC 90174 (strain NHL 6491 [I-31]) for development of the fermentation process (Scheme 1.7). Czapek-Dox broth supplemented with 5% yeast extract (Table 1.1) was selected as the growth media for the fermentation of roquefortine C as roquefortine C production was previously shown to be accelerated with high concentrations of sucrose and yeast extract.



**Scheme 1.7:** Roquefortine C fermentation process

Geometry optimization of roquefortine C was carried out at the HF/6-311+G(2d,p) level of theory

**Table 1.1:** Roquefortine C fermentation growth media composition

<b>Reagent</b>	<b>Quantity<sup>†</sup></b>
Sucrose	30.000 g
Sodium nitrate	3.000 g
Dipotassium phosphate	1.000 g
Magnesium sulfate	0.500 g
Potassium chloride	0.500 g
Ferrous sulfate	0.010 g
Yeast extract	5.000 g

<sup>†</sup>Per liter ultrapure (Type 1) water

Preliminary fermentation trials were carried out in Erlenmeyer flasks (1, 2, 4, and 6 L) containing relatively small volumes (200-1000 mL) of growth media. Pyrex borosilicate trays (3.5 L) eventually proved to be a superior vessel for the fermentation process. These trays eliminated the extraneous headspace present in the Erlenmeyer flask system, which provided greater ease of storage and harvest of the mycelial cultures as well as cleaning of the growth vessels.

Exposure to light (both sunlight and standard laboratory lighting) was found to negatively impact mycelial growth, and subsequently roquefortine C production. In particular, exposure to light in the initial stages of mycelial growth was found to impede mycelial growth, even if cultures were subsequently shielded from light (Figure 1.3). As a result, liquid cultures of *P. crustosum* were grown in darkness for the entirety of the fermentation process.

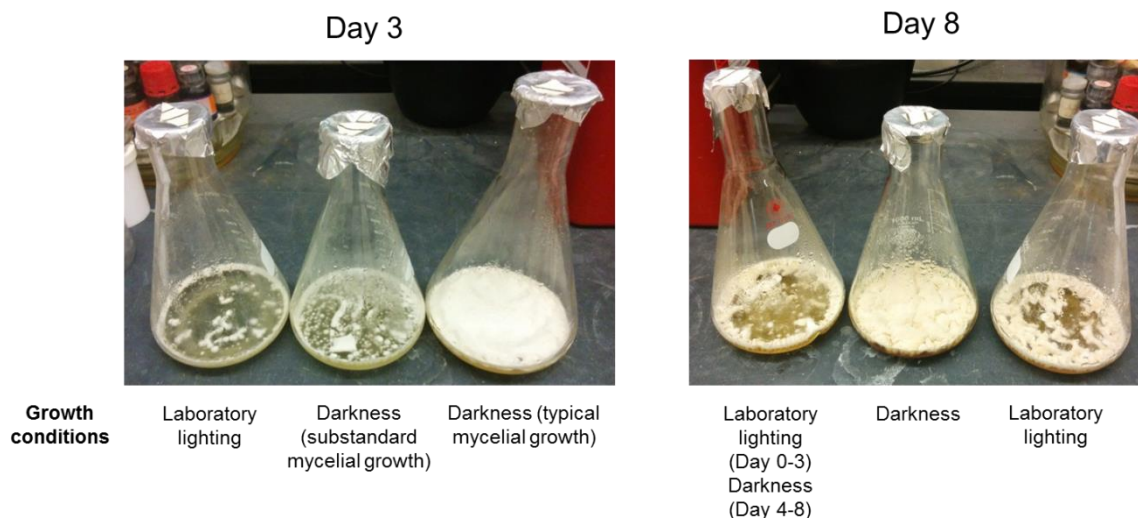


**Figure 1.3:** Effects of light on *P. crustosum* mycelial growth

Roquefortine C in this fermentation procedure was isolated exclusively from the mycelia, as the liquid growth media has been shown to yield minimal amounts of roquefortine C. Lyophilization of the mycelia to remove water proved to be extremely important to obtaining good yields of roquefortine C. The polarity of roquefortine C allows for straightforward extraction and purification. Roquefortine C exhibits high solubility in polar aprotic solvents such as chloroform, acetone, and dichloromethane, which permits its extraction from the mycelial material. Two extractions were performed in this fermentation procedure: one 3 hour extraction in a 1:1 mixture of chloroform and acetone and one 18 hour extraction in acetone. The polarity of roquefortine C with respect to the other metabolites extracted from the *P. crustosum* mycelia allowed for its purification by column chromatography using an 85:10:5 mixture of  $\text{CH}_2\text{Cl}_2/\text{CH}_3\text{OH}/\text{acetone}$ , providing roquefortine C in excellent purity in quantities of 150 mg per liter of growth media.

## B. Comparison to Other Methods of Roquefortine C Production

The production of roquefortine C by fermentation has proven to be much more efficient than production by traditional organic synthesis. The total synthesis of roquefortine C only yielded 17 mg after 12 steps, which included 7 extractions and 10 chromatography purifications. Two major challenges in this synthesis include the installation of the reverse prenyl moiety, which required the use of stoichiometric organostannane, and the installation of the *E*-dehydrohistidine moiety, which could only be synthesized in a 1:1 mixture with the *Z* isomer. Fermentation of roquefortine C requires only one extraction and one chromatography purification and allows for a significant reduction in cost of raw materials. To produce a gram of roquefortine C by total synthesis is estimated to cost over 100 times the amount to produce one gram of roquefortine C by fermentation. Additionally, the amount of active experimental time of the researcher is significantly reduced.

While our production of roquefortine C ultimately gave less of the title compound per liter than the two highest yielding procedures by Abe and Scott, this fermentation procedure is scalable and can afford good yields, comparable to the majority of small scale fermentations of roquefortine C. Following the development of this fermentation procedure, a patent was filed by researchers at the First Institute of Oceanography in China describing a fermentation procedure for the production of roquefortine C.<sup>50</sup> This patent detailed the fermentation of *Penicillium* sp. Y32 in a variety of growth media. The fungal liquid cultures were allowed to

grow for 25-35 days, after which the mycelia was extracted with acetone and ethyl acetate and purified by column chromatography. This procedure gave roquefortine C yields between 6.8 and 33  $\mu\text{g}$  per mL liquid growth media, paling in comparison to the procedure described in this chapter.

#### **IV. Conclusions**

The fermentation procedure described herein allows for the production of gram quantities of roquefortine C in excellent purity. With yields of 150 mg per liter, this method provides significant benefits over the traditional organic synthesis of roquefortine C and will allow for further exploration of roquefortine C and its downstream metabolites.

#### **V. Experimental Details**

##### **General Information**

Roquefortine C was purified by flash column chromatography (FCC) on 230-400 mesh silica gel.  $^1\text{H}$  and  $^{13}\text{C}$  NMR spectra were recorded on a spectrometer operating at 500 MHz for  $^1\text{H}$  and 125 MHz for  $^{13}\text{C}$  unless otherwise stated. Chemical shifts are reported in ppm relative to tetramethylsilane (TMS) as the internal standard for  $^1\text{H}$  and chloroform as the internal standard for  $^{13}\text{C}$ . NMR data is reported as follows: chemical shift, multiplicity (s = singlet, d = doublet, dd = doublet of doublets, t = triplet, q = quartet, br = broad, m = multiplet), coupling constants (Hz), and integration.  $^1\text{H}$ - $^1\text{H}$  Homonuclear correlation spectroscopy

(COSY),  $^1\text{H}$ - $^{13}\text{C}$  heteronuclear single quantum correlation experiment (HSQC), and  $^1\text{H}$ - $^{13}\text{C}$  heteronuclear multiple bond correlation (HMBC) NMR spectra were recorded on a spectrometer operating at 500 MHz. High-resolution mass spectra (HRMS) were recorded on an electrospray ionization time-of-flight (ESI-TOF) spectrometer (Agilent). Waters software calibrates and reports by use of neutral atomic mass. The mass of the electron is not included.

### **Isolation of roquefortine C (1) from *P. crustosum***

Freeze-dried samples of *P. crustosum* were rehydrated for 1 hour in double distilled (dd) water and inoculated onto malt extract agar plates (Blakeslee's formula). Fungal samples were allowed to grow on plates for 3-5 days in darkness at room temperature until colonies of blue-green fungus were observed. Twelve borosilicate glass trays (9 by 13 inch) were each filled with 825 mL autoclave-sterilized Czapek-Dox yeast extract (CDY) liquid media, prepared using 35 g/L Czapek-Dox broth and 5 g/L yeast extract. The CDY broth was inoculated with fungal culture using a sterile loop. *P. crustosum* samples were grown in liquid culture for 12-14 days until a sufficient mycelial mat covered the surface of the liquid media. Mycelial material was harvested by filtering off liquid media, macerating the mycelial mat using a mortar and pestle, and lyophilizing. Lyophilized samples were extracted in 1:1  $\text{CHCl}_3$ /acetone for 3 hours and then again in acetone for 18 hours. Organic extracts were then concentrated by rotary evaporation to give a crude mycelial extract. Roquefortine C was purified by flash chromatography (retention factor ( $R_f$ ) 0.26, 85:10:5  $\text{CH}_2\text{Cl}_2$ / $\text{CH}_3\text{OH}$ /acetone), to

yield 1 g of purified material.  $^1\text{H}$  NMR (500 MHz,  $\text{CDCl}_3$ )  $\delta$  12.92 (s, br, 1H), 10.27 (s, 1H), 7.68 (s, 1H), 7.23 (s, 1H), 7.17 (d,  $J = 6.0$  Hz, 1H), 7.09 (t,  $J = 6.0$  Hz, 1H), 6.76 (t,  $J = 6.0$  Hz, 1H), 6.59 (d,  $J = 6.5$  Hz, 1H), 6.35 (s, 1H), 5.97 (dd,  $J = 9, 14.5$  Hz, 1H), 5.63 (s, 1H), 5.14 (s, 1H), 5.11 (d,  $J = 7.0$  Hz, 1H), 5.08 (s, 1H), 4.03 (dd,  $J = 5.0, 9.5$  Hz, 1H), 2.58 (dd,  $J = 4.5, 15.0$  Hz, 1H), 2.45 (t,  $J = 10.0$  Hz, 1H), 1.13 (s, 1H), 1.02 (s, 1H).  $^{13}\text{C}$  NMR (125 MHz,  $\text{CDCl}_3$ )  $\delta$  167.3, 159.6, 150.2, 143.6, 137.1, 135.7, 129.3, 128.8, 125.7, 125.4, 121.9, 119.4, 115.0, 111.6, 109.4, 78.6, 61.8, 59.0, 41.2, 37.0, 23.1, 22.7.  $^{15}\text{N}$  NMR (600 MHz,  $\text{CDCl}_3$ )  $\delta$ : 257.9, 167.8, 147.4, 138.1, 83.4. IR (KBr): 3199, 1681, 1607, 1435, 1412, 1215, 1102, 752  $\text{cm}^{-1}$  (lit. (Ohmomo et al., 1975)<sup>14</sup> IR (KBr) 3180, 1690, 1660, 1604  $\text{cm}^{-1}$ ).  $[\alpha]_D^{22}$  -700.5 (c 0.77,  $\text{CHCl}_3$ ) (lit. (Ohmomo et al., 1975)<sup>14</sup>  $[\alpha]_D^{15}$  -764 (c 0.50, pyr.)). HRMS (ESI-TOF)  $m/z$   $[\text{M} + \text{H}]^+$  calcd for  $\text{C}_{22}\text{H}_{24}\text{N}_5\text{O}_2$  390.1930, found 390.1930 (lit. (Joullié et al., 2008)<sup>40</sup> calcd for  $\text{C}_{22}\text{H}_{24}\text{N}_5\text{O}_2$  390.1930, found 390.1920).

## VI. References

- (1) Koolen, H. H. F.; Soares, E. R.; da Silva, F. M. A.; de Almeida, R. A.; de Souza, A. D. L. *Quim. Nova* **2012**, 35(4), 771-774.
- (2) Zheng, C. J.; Sohn, M.-J.; Lee, S.; Kim, W.-G. *PLoS ONE* **2013**, 8(11), e78922.
- (3) Koizumi, Y.; Arai, M.; Tomoda, H.; Ōmura, S. *Biochim. Biophys. Acta.* **2004**, 1693(1), 47-55.



- (4) Han, Z.; Sun, J.; Zhang, Y.; He, F.; Xu, Y.; Matsumura, K.; He, L. S.; Qiu, J. W.; Qi, S. H.; Qian, P. Y. *J. Proteome Res.* **2013**, *12*(5), 2090-2100.
- (5) Hymery, N.; Vasseur, V.; Coton, M.; Mounier, J.; Jany, J. L.; Barbier, G.; Coton, E. *Compr Rev Food Sci F* **2014**, *13*(4), 437-456.
- (6) Driehuis, F.; Spanjer, M. C.; Scholten, J. M.; te Giffel, M. C. *J. Dairy Sci.* **2008**, *91*(11), 4261-4271.
- (7) Mansfield, M. A.; Jones, A. D.; Kuldau, G. A. *Phytopathology* **2008**, *98*(3), 330-336.
- (8) Spanjer, M. C.; Rensen, P. M.; Scholten, J. M. *Food Addit. Contam. Part A Chem. Anal. Control Expo. Risk Assess.* **2008**, *25*(4), 472-489.
- (9) Rasmussen, R. R.; Rasmussen, P. H.; Larsen, T. O.; Bladt, T. T.; Binderup, M. L. *Food Chem. Toxicol.* **2011**, *49*(1), 31-44.
- (10) Monbaliu, S.; Van Poucke, C.; Detavernier, C.; Dumoulin, F.; Van De Velde, M.; Schoeters, E.; Van Dyck, S.; Averkieva, O.; Van Peteghem, C.; De Saeger, S. *J. Agric. Food Chem.* **2010**, *58*(1), 66-71.
- (11) Yamaguchi, T.; Nozawa, K.; Nakajima, S.; Kawai, K.; Udagawa, S. *Maikotokishin* **1991**, *34*, 485-487.
- (12) Scott, P. M.; Merrien, M. A.; Polonsky, J. *Experientia* **1976**, *32*(2), 140-142.

- (13) Banke, S.; Frisvad, J. C.; Rosendahl, S. *Mycol. Res.* **1997**, *101*(5), 617-624.
- (14) Ohmomo, S.; Sato, T.; Utagawa, T.; Abe, M. *Agr. Biol. Chem. Tokyo* **1975**, *39*(6), 1333-1334.
- (15) Ohmomo, S.; Ohashi, T.; Abe, M. *Agr. Biol. Chem. Tokyo* **1980**, *44*(8), 1929-1930.
- (16) Kyriakidis, N.; Waight, E. S.; Day, J. B.; Mantle, P. G. *Appl. Environ. Microb.* **1981**, *42*(1), 61-62.
- (17) Kozlovsky, A. G.; Solovieva, T. F.; Reshetilova, T. A.; Skryabin, G. K. *Experientia* **1981**, *37*, 472-473.
- (18) El-Banna, A. A.; Pitt, J. I.; Leistner, L. *Syst. Appl. Microbiol.* **1987**, *10*, 42-46.
- (19) Frisvad, J. C.; Filtenborg, O. *Appl. Environ. Microb.* **1983**, *46*(6), 1301-1310.
- (20) Frisvad, J. C.; Filtenborg, O. *Mycologia* **1989**, *81*(6), 837-861.
- (21) Frisvad, J. C.; Filtenborg, O. In *Modern concepts in Penicillium and Aspergillus classification*; Samson, R. A., Pitt, J. I., Eds.; Plenum Press: New York, 1990, p 159-170.
- (22) Frisvad, J. C.; Filtenborg, O. In *Modern concepts in Penicillium and Aspergillus classification*; Samson, R. A., Pitt, J. I., Eds.; Plenum Press: New York, 1990, p 373-384.

- (23) Frisvad, J. C.; Smedsgaard, J.; Larsen, T. O.; Samson, R. A. *Stud. Mycol.* **2004**, *49*, 201-241.
- (24) Ohmomo, S.; Utagawa, T.; Abe, M. *Agr. Biol. Chem. Tokyo* **1977**, *41*(10), 2097-2098.
- (25) Overy, D. P.; Frisvad, J. C. *Syst. Appl. Microbiol.* **2003**, *26*(4), 631-639.
- (26) Boysen, M.; Skouboe, P.; Frisvad, J.; Rossen, L. *Microbiology* **1996**, *142*, 541-549.
- (27) Scott, P. M.; Polonsky, J.; Merrien, M. A. *J. Agric. Food Chem.* **1979**, *27*(1), 201-202.
- (28) Blake, K. W.; Sammes, P. G. *J. Chem. Soc. C.* **1970**, *7*, 980-984.
- (29) Rand, T. G.; Giles, S.; Flemming, J.; Miller, J. D.; Puniani, E. *Toxicol. Sci.* **2005**, *87*(1), 213-222.
- (30) Arnold, D. L.; Scott, P. M.; McGuire, P. F.; Harwig, J.; Nera, E. A. *Food Cosmet. Toxicol.* **1978**, *16*, 369-371.
- (31) Wagener, R. E.; Davis, N. D.; Diener, U. L. *Appl. Environ. Microb.* **1980**, *39*(4), 882-887.
- (32) Larsen, T. O.; Gareis, M.; Frisvad, J. C. *J. Agric. Food Chem.* **2002**, *50*, 6148-6152.

- (33) Bunger, J.; Westphal, G.; Monnich, A.; Hinnendahl, B.; Hallier, E.; Muller, M. *Toxicology* **2004**, *202*(3), 199-211.
- (34) Vishwanath, V.; Sulyok, M.; Labuda, R.; Bicker, W.; Krska, R. *Anal. Bioanal. Chem.* **2009**, *395*(5), 1355-1372.
- (35) Taubel, M.; Sulyok, M.; Vishwanath, V.; Bloom, E.; Turunen, M.; Jarvi, K.; Kauhanen, E.; Krska, R.; Hyvarinen, A.; Larsson, L.; Nevalainen, A. *Indoor Air* **2011**, *21*(5), 368-375.
- (36) Vishwanath, V.; Sulyok, M.; Weingart, G.; Kluger, B.; Taubel, M.; Mayer, S.; Schuhmacher, R.; Krska, R. *Talanta* **2011**, *85*(4), 2027-2038.
- (37) Aninat, C.; Andre, F.; Delaforge, M. *Food Addit. Contam.* **2005**, *22*(4), 361-368.
- (38) Kopp-Holtwiesche, B. B. *J. Environ. Pathol. Toxicol. Oncol.* **1990**, *10*(1-2), 41-44.
- (39) Kopp, B.; Rehm, H. J. *Eur. J. Appl. Microbiol. Biotechnol.* **1979**, *6*, 397-401.
- (40) Shangguan, N.; Hehre, W. J.; Ohlinger, W. S.; Beavers, M. P.; Joullié, M. M. *J. Am. Chem. Soc.* **2008**, *130*(19), 6281-6287.
- (41) van den Berg, M. A.; Albang, R.; Albermann, K.; Badger, J. H.; Daran, J. M.; Driessen, A. J.; García-Estrada, C.; Fedorova, N. D.; Harris, D. M.; Heijne, W. H.; Joardar, V.; Kiel, J. A.; Kovalchuk, A.; Martin, J. F.; Nierman, W. C.; Nijland, J. G.;

Pronk, J. T.; Roubos, J. A.; van der Klei, I. J.; van Peij, N. N.; Veenhuis, M.; von Döhren, H.; Wagner, C.; Wortman, J.; Bovenberg, R. A. *Nat. Biotechnol.* **2008**, 26(10), 1161-1168.

(42) García-Estrada, C.; Ullán, R. V.; Albillos, S. M.; Fernández-Bodega, M. A.; Durek, P.; von Döhren, H.; Martín, J. F. *Chem. Biol.* **2011**, 18(11), 1499-1512.

(43) Ali, H.; Ries, M. I.; G., N. J.; Lankhorst, P. P.; Hankemeier, T.; Bovenberg, R. A. L.; Driessen, A. J. M.; Vreeken, R. J. *PLoS ONE* **2013**, 8(6), e65328.

(44) Steyn, P. S.; Vleggaar, R. *J. Chem. Soc. Chem. Commun.* **1983**, 10, 560.

(45) Reshetilova, T. A.; Vinokurova, N. G.; Khmelenina, V. N.; Kozlovskii, A. G. *Microbiology* **1995**, 64(1), 27-29.

(46) Reshetilova, T. A.; Kozlovsky, A. G. *J. Basic Microbiol.* **1990**, 30(2), 109-114.

(47) Ries, M. I.; Ali, H.; Lankhorst, P. P.; Hankemeier, T.; Bovenberg, R. A.; Driessen, A. J.; Vreeken, R. J. *J. Biol. Chem.* **2013**, 288(52), 37289-37295.

(48) Scott, P. M.; Kennedy, B. P.; Harwig, J.; Blanchfield, B. J. *Appl. Environ. Microb.* **1977**, 33(2), 249-253.

(49) Mantle, P. G.; Perera, K. P. W. C.; Maishman, N. J.; Mundy, G. R. *Appl. Environ. Microb.* **1983**, 45(5), 1486-1490.

(50) Chen, H.; Fan, Y.; Du, N.; Li, P., Roquefortine C preparing method.  
CN104894182, 2015.

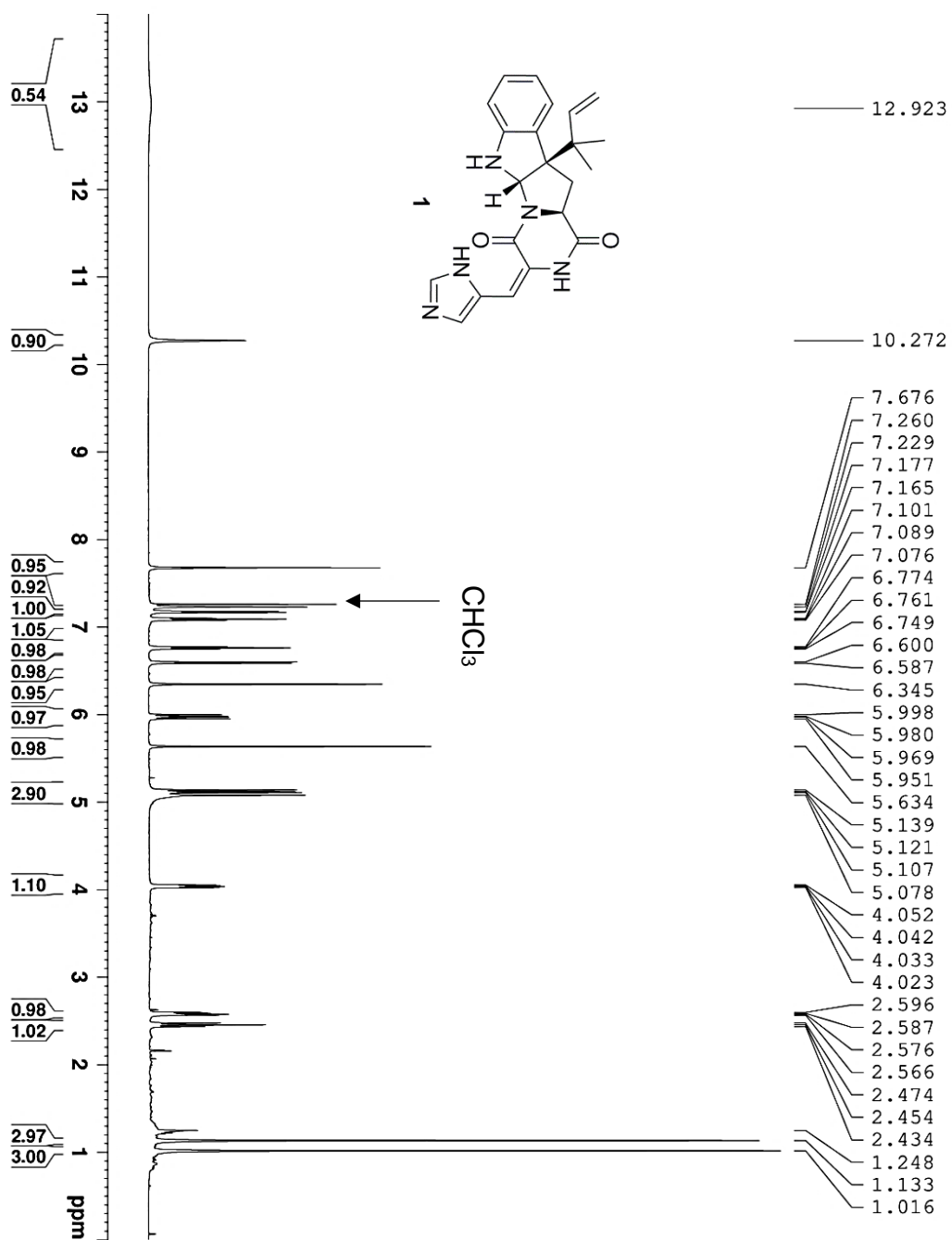
### Appendix 1A: Species of *Penicillium* that Produce Roquefortine C

Penicillium species	Investigator	Reference number
<i>P. albocoremium</i>	Frisvad, 1989 Overy, 2003	20, 25
<i>P. allii</i>	Frisvad, 1989	20
<i>P. atramentosum</i>	Frisvad, 1989	20
<i>P. carneum</i>	Boysen, 1996	26
<i>P. chrysogenum</i>	El-Banna, 1987 Frisvad, 1989	18, 20
<i>P. concentricum</i> ,	Frisvad, 1989	20
<i>P. confertum</i> ,	Frisvad, 1989	20
<i>P. coprobium</i>	Frisvad, 1989	20
<i>P. coprophilum</i>	Frisvad, 1989	20
<i>P. crustosum</i>	Kyriakidis, 1981 Kozlovsky, 1981 (as <i>P. farinosum</i> )	16, 17
<i>P. expansum</i>	Ohmomo, 1980 Frisvad, 1983	15, 19
<i>P. flavigenum</i>	Banke, 1997	13
<i>P. glandicola</i>	Frisvad, 1983 (as <i>P. granulatum</i> ) Frisvad, 1989	19, 20
<i>P. griseofulvum</i>	Ohmomo, 1980 (as <i>P. urticae</i> ) Frisvad, 1983	15, 19

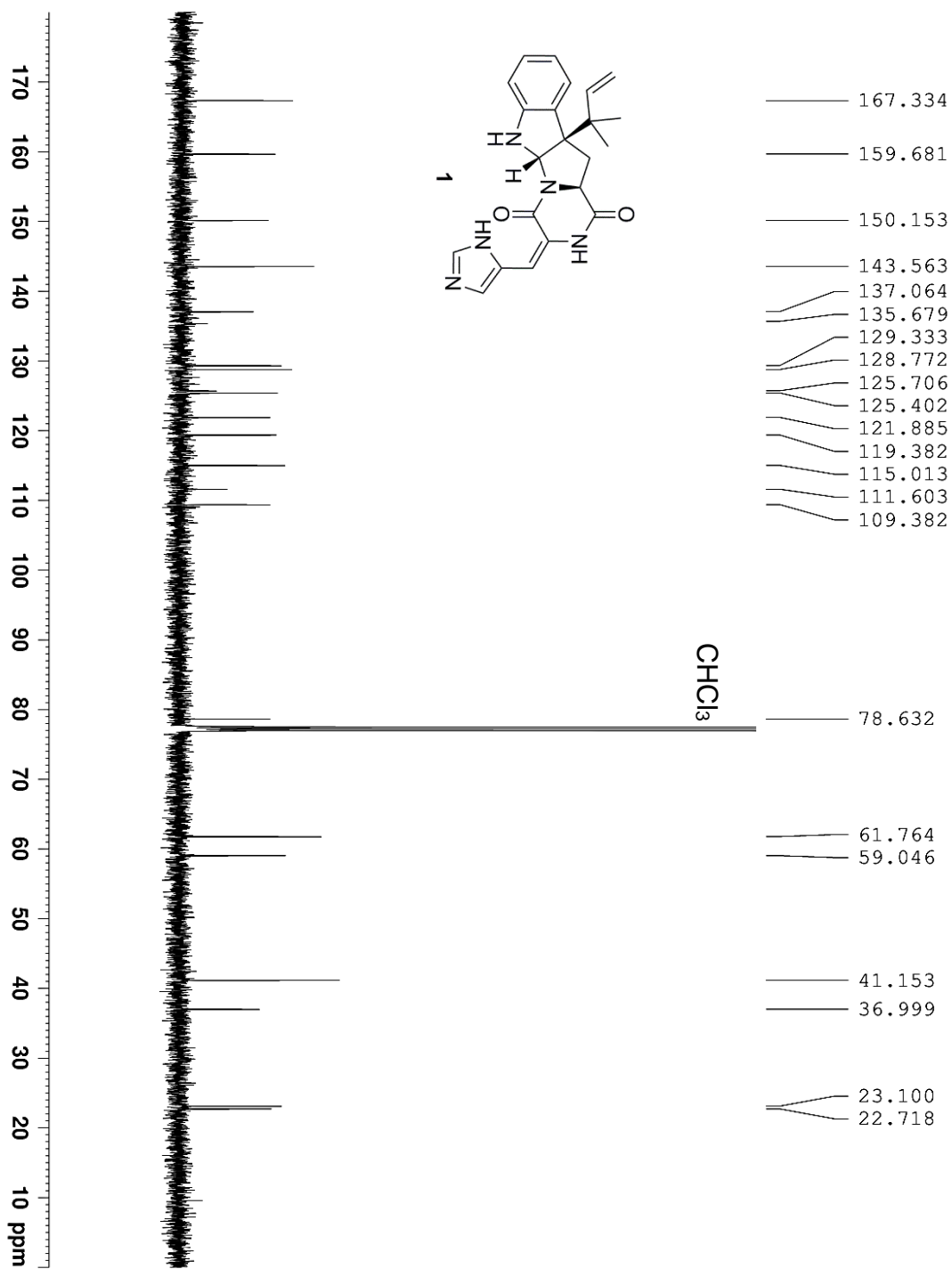
<i>P. hirsutum</i>	Ohmomo, 1980 (as <i>P. corymbiferum</i> ) Frisvad, 1989 (as <i>P. corymbiferum</i> )	15, 20
<i>P. hordei</i>	Frisvad, 1989	20
<i>P. marinum</i>	Frisvad, 2004	23
<i>P. melanoconidium</i>	Frisvad, 1989	20
<i>P. paneum</i>	Boysen, 1996	26
<i>P. persicinum</i>	Frisvad, 2004	23
<i>P. radiccicola</i>	Overy, 2003	25
<i>P. roqueforti</i>	Ohmomo, 1975 Scott, 1976 Yamaguchi, 1991	11, 12, 14
<i>P. sclerotigenum</i>	Frisvad, 1990	21, 22
<i>P. tulipae</i>	Overy, 2003	25
<i>P. venetum</i>	Frisvad, 1989	20
<i>P. vulpinum</i>	Frisvad, 1983 (as <i>P. claviforme</i> )	19



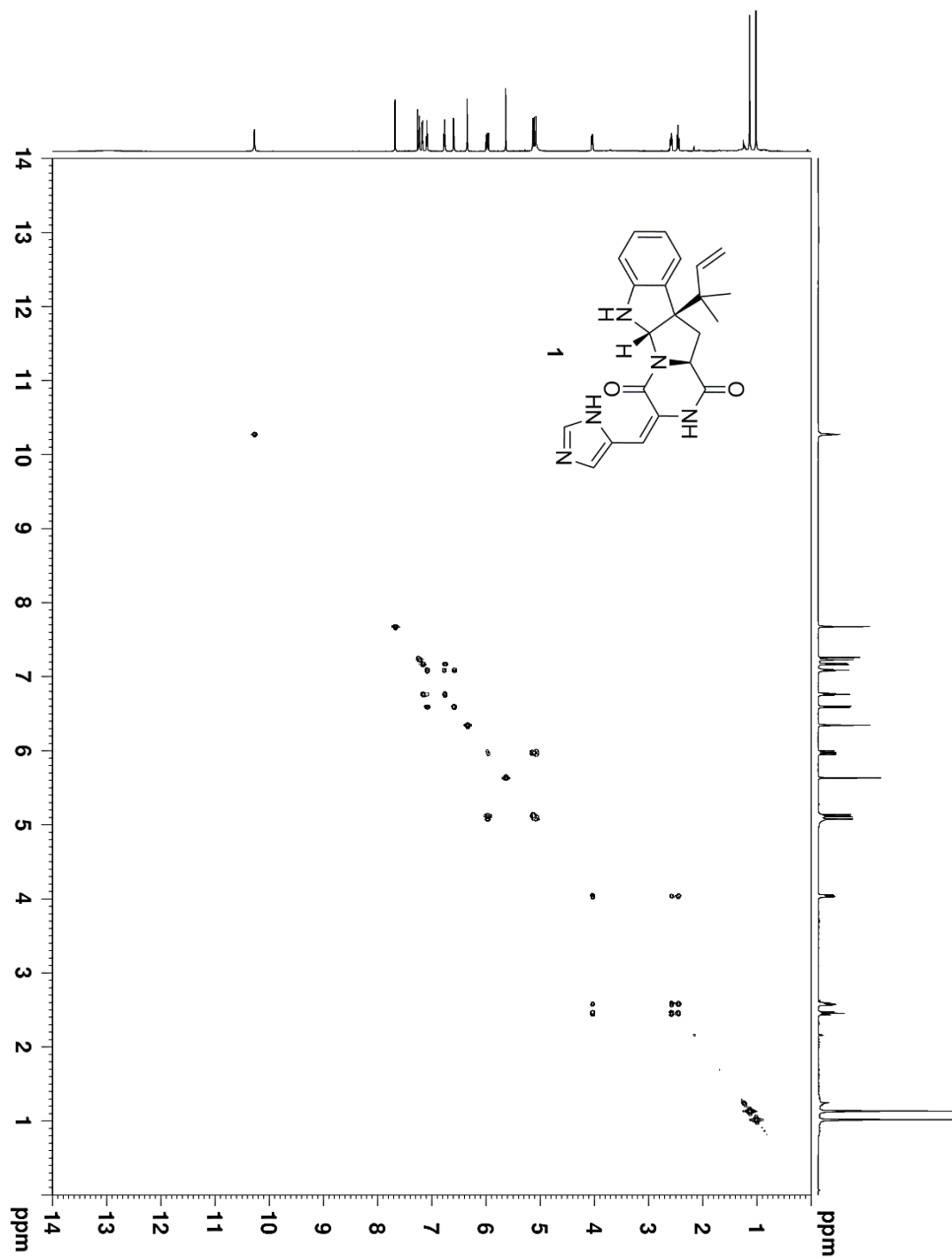
## **Appendix 1B: Spectra Relevant to Chapter 1**



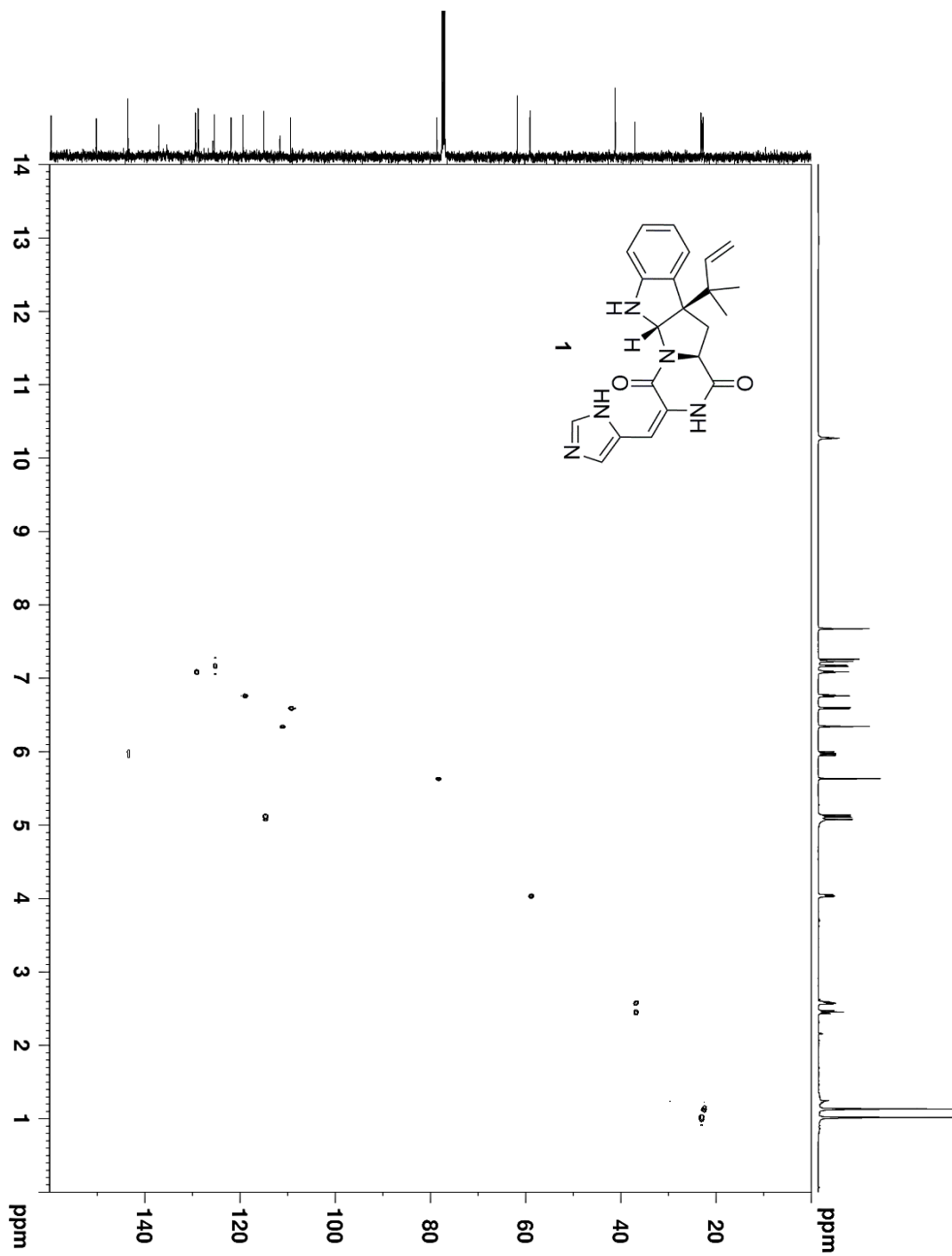
Supplementary Figure 1.1: <sup>1</sup>H NMR (500 MHz, CDCl<sub>3</sub>) Spectrum of 1



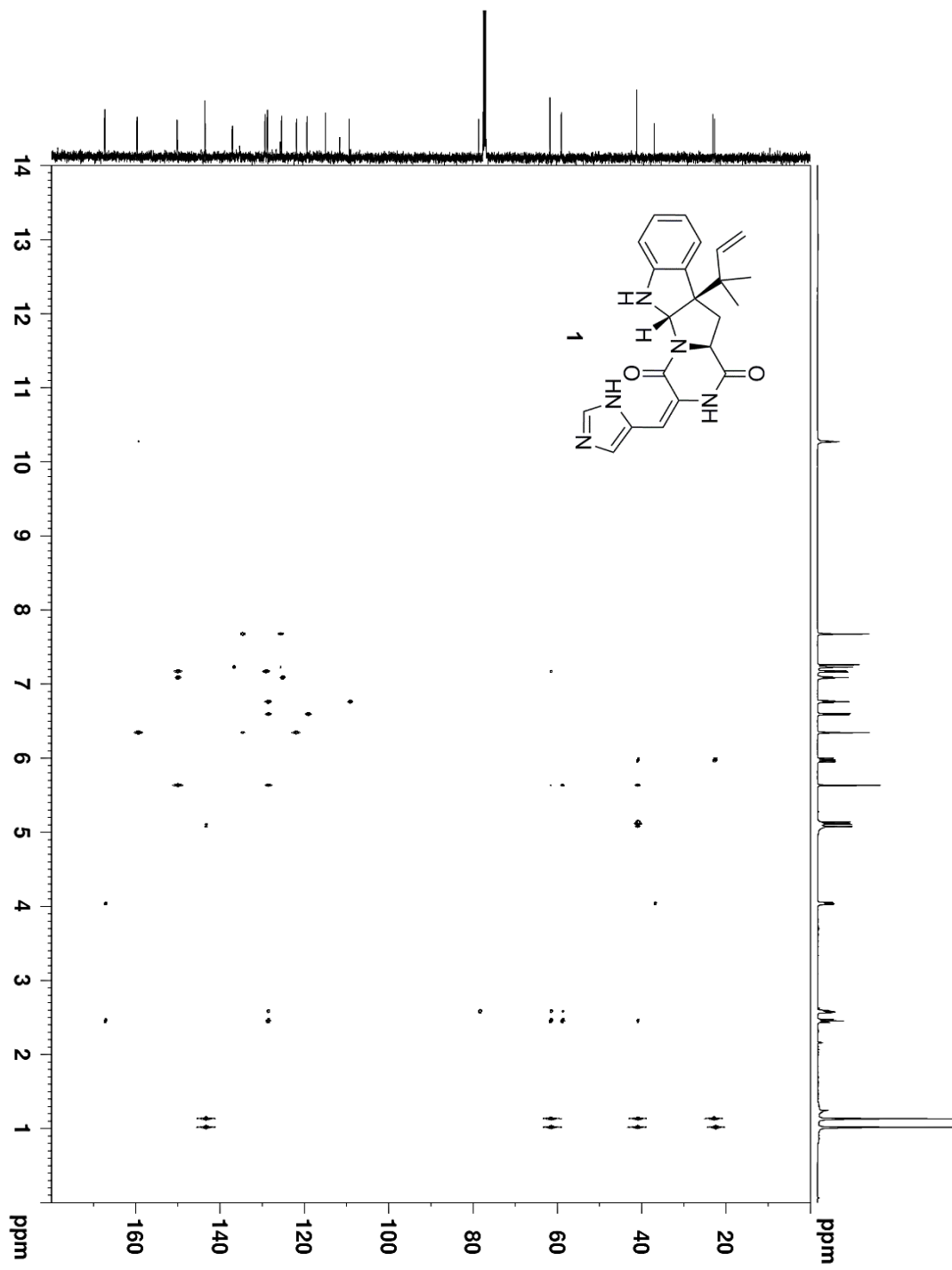
Supplementary Figure 1.2:  $^{13}\text{C}$  NMR (125 MHz,  $\text{CDCl}_3$ ) Spectrum of **1**



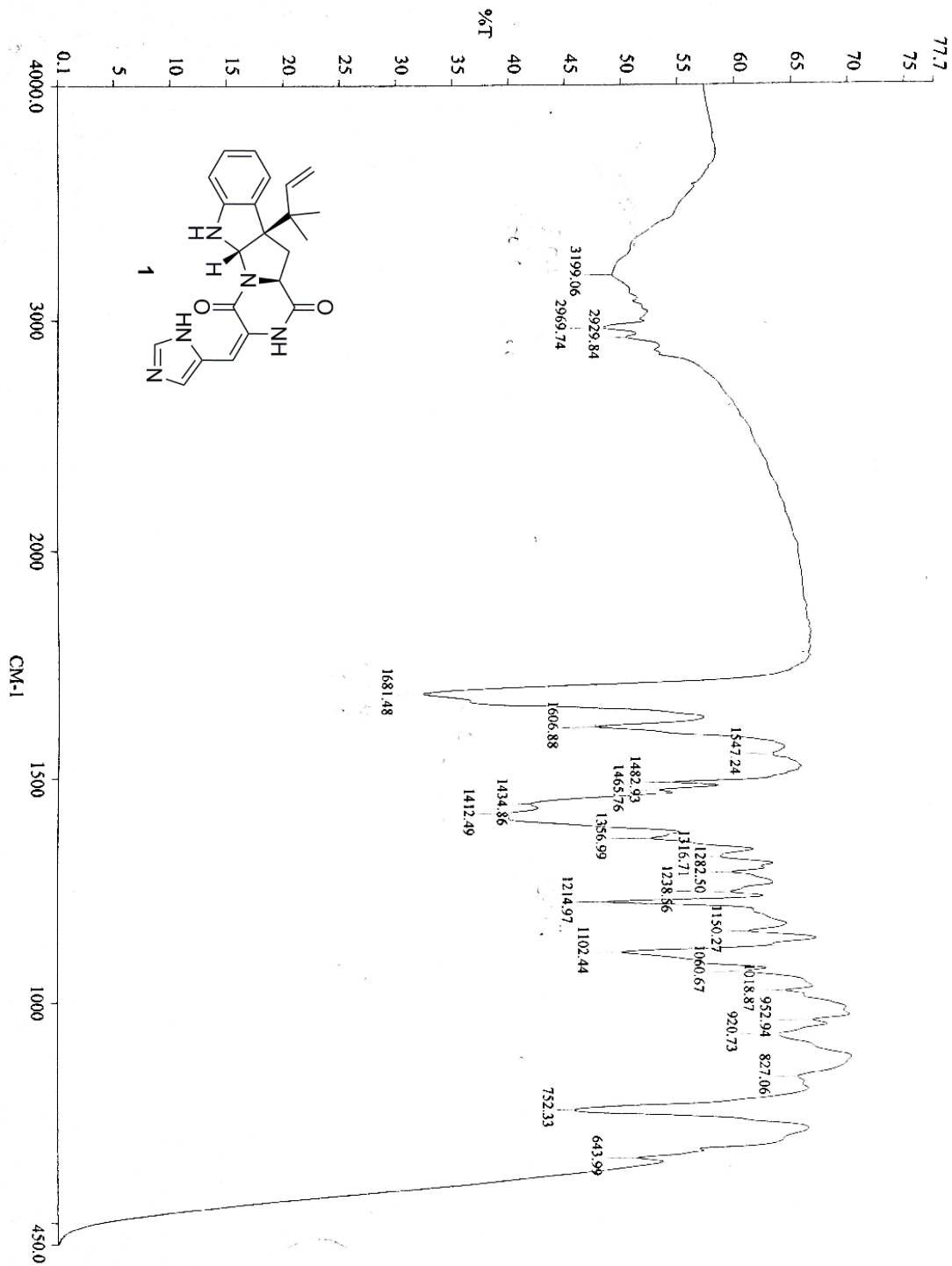
**Supplementary Figure 1.3:**  $^1\text{H}$ - $^1\text{H}$  COSY NMR (500 MHz,  $\text{CDCl}_3$ ) Spectrum of **1**



Supplementary Figure 1.4:  $^1\text{H}$ - $^{13}\text{C}$  HSQC NMR (500 MHz,  $\text{CDCl}_3$ ) Spectrum of **1**



**Supplementary Figure 1.5:**  $^1\text{H}$ - $^{13}\text{C}$  HMBC NMR (500 MHz,  $\text{CDCl}_3$ ) Spectrum of **1**



Supplementary Figure 1.6: IR (KBr pellet) Spectrum of 1

**CHAPTER TWO**  
**N-OXIDATION OF ROQUEFORTINE C BY OXAD**

Material in this chapter reproduced in part with permission from:

Newmister, S. A.; Gober, C. M.; Romminger, S.; Yu, F.; Tripathi, A.; Parra, L. L. L.; Williams, R. M.; Berlinck, R. G. S.; Joullié, M. M.; Sherman, D. H. *J. Am. Chem. Soc.* **2016**, *138*(35), 11176-11184. Copyright 2016 American Chemical Society



## I. Introduction

In recent years, downstream metabolites of roquefortine C have acquired renewed interest due to their unique triazaspirocyclic core and their biological activity. Until recently, the triazaspirocyclic core of glandicoline B, meleagrins, and oxaline was thought to be biosynthesized via an indole imine intermediate glandicoline A. Recent work by the Vreeken lab, however, indicates that these metabolites are formed via a nitron intermediate, roquefortine L. The uniqueness of this nitron natural product as well as the general lack of robust synthetic methods towards synthesizing indoline nitrones led us, in collaboration with the Sherman laboratory at the University of Michigan, to develop flavin monooxygenase OxaD as a biocatalyst for indoline nitron synthesis. We herein report the isolation, characterization, and enzymatic activity of OxaD, which can be produced in significant yields by heterologous expression. OxaD is a flavoprotein that has been harnessed for the biocatalytic conversion of roquefortine C and roquefortine C semisynthetic derivatives to afford the resulting indoline nitrones in very good yield and in a single step. To the best of our knowledge, this work represents the first biocatalytic synthesis of indoline nitrones.

## II. Background

### A. Nitrones

The nitron functional group, which is an *N*-oxide of an imine, is a unique and versatile chemical moiety. The extreme electrophilicity of the nitron carbon allows for its participation in nucleophilic addition reactions as well as 1,3-dipolar

cycloaddition reactions. Synthesis of nitrones generally occurs through either condensation of a ketone with a hydroxylamine or oxidation of an *N,N*-disubstituted hydroxylamine.

Chemical conversion of indolines into their respective nitrones has been reported in only a few instances. This transformation requires either mild oxidative conditions to give very moderate yields,<sup>1,2</sup> or a multi-step procedure affording good yield.<sup>3</sup> Oxidation of *N*-aryl secondary amines generally gives poor yields, as electron transfer from the amine to the oxidant typically results in C-N bond cleavage and subsequent oxidation of the fragments. The powerful electrophilicity of the nitron  $\alpha$ -carbon makes it susceptible to intra- and intermolecular nucleophilic attack, often resulting in numerous side products.

Fungal production of roquefortine L (**17**) is particularly relevant, since very few indoline nitrones are known as natural products.<sup>4-8</sup> With the exception of the recently isolated versicamide E (**30**), alstoyunine D (**31**), and perakine *N*<sup>1</sup>,*N*<sup>4</sup>-dioxide (**32**), the remaining fungal indole nitrones share a common avrainvillamide (**33**) core (Figure 2.1). Nitron incorporation into these compounds can promote several biologically relevant events. For example, the nitron functional group on avrainvillamide is required for dimerization to stephacidin B (**35**).<sup>9</sup> The nitron function of avrainvillamide also plays a vital role in its anti-proliferative activity. Avrainvillamide has been shown to bind to oncogenic protein nucleophosmin, which is frequently overexpressed in solid tumors, with expression levels often

correlating to tumor metastasis. The proposed mechanism of anti-proliferation involves nucleophilic attack of the nitron functionality by cysteine residues in cellular proteins.<sup>8,10-12</sup> Such properties generate great interest in the chemical synthesis of these molecules, as evidenced by the syntheses of avrainvillamide (**33**) and stephacidin B (**35**) published in recent years.<sup>1,13,14</sup>

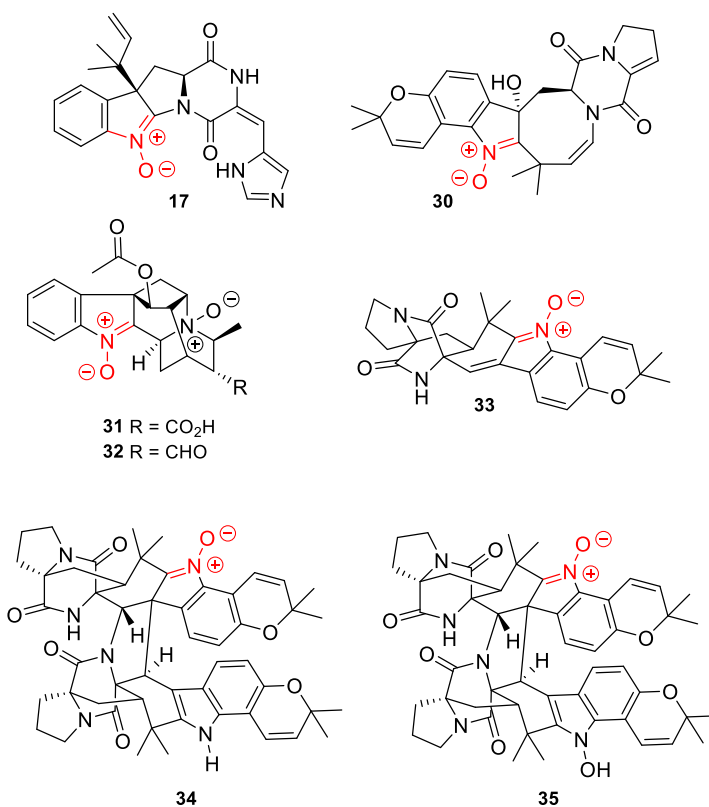


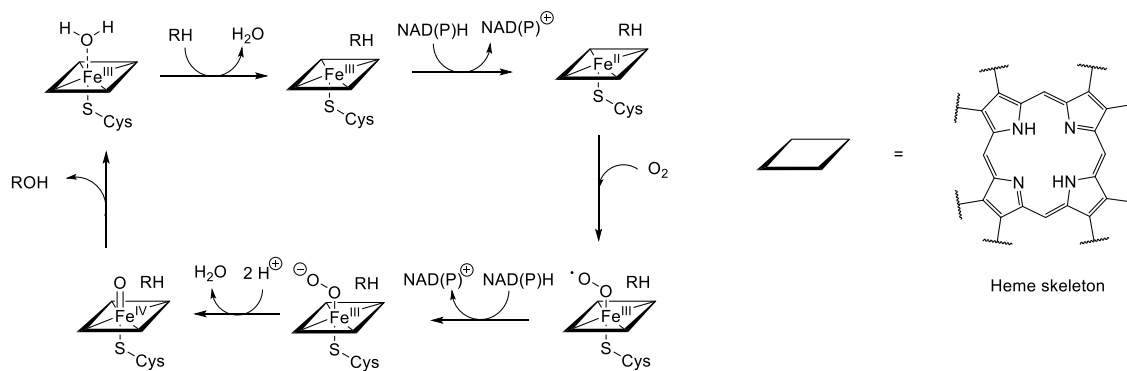
**Figure 2.1:** Known indoline nitron natural products

Discovery of a biocatalyst that could efficiently perform such a reaction in a single high-yielding step would be of major interest for the synthesis of nitron functionalized indolines, particularly of complex and biologically active indoline alkaloids.

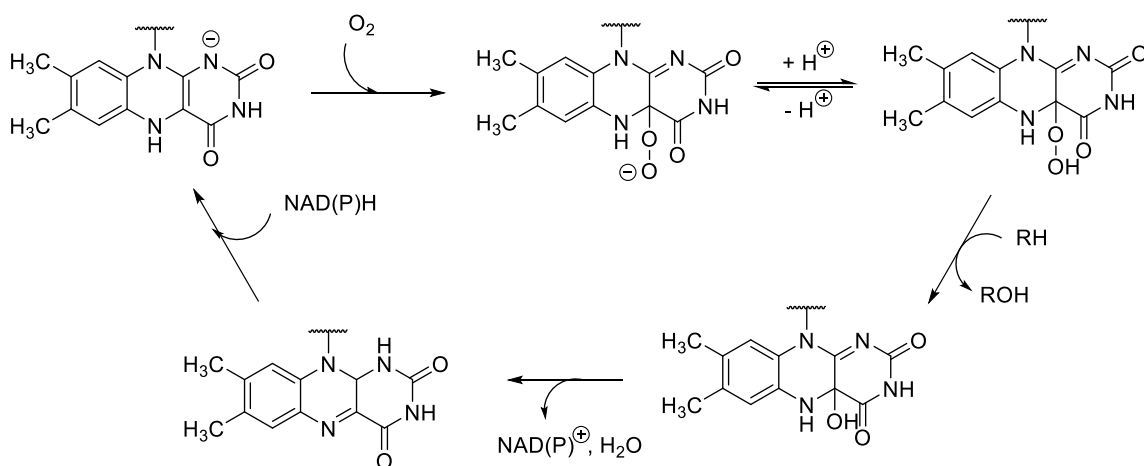
## B. Nitron Biosynthesis

The biosynthetic oxidation of amines to hydroxylamines is well documented; however, the biosynthesis of nitrones has been observed in relatively few instances. The biosynthetic oxidation of amines is typically carried out by either flavin-dependent monooxygenases or cytochrome P450s. These enzymes both implement cofactors for the activation of molecular oxygen. Cytochrome P450s carry out oxidations through use of iron bound to an organic cofactor such as a heme (Scheme 2.1). The iron is attached to the P450 via a cysteine residue. The substrate first binds proximal to the heme, displacing water. Electron transfer from reduced nicotinamide adenine dinucleotide (NADH) or nicotinamide adenine dinucleotide phosphate (NADPH) converts the iron(III) to the iron(II) species. Molecular oxygen binds to iron(II) giving a peroxy radical, which is converted to the corresponding peroxy anion via a second electron transfer. Rapid protonation of the peroxy anion generates the highly reactive iron(IV) oxo species, which allows for oxidation of the substrate and regeneration of the initial iron-water complex.

Flavin-dependent monooxygenases incorporate molecular oxygen using an organic flavin cofactor (Scheme 2.2). Molecular oxygen is incorporated into the reduced flavin species, giving a peroxy anion. Protonation generates a reactive hydroperoxyflavin, which delivers oxygen in an electrophilic fashion on its substrate. The reduced flavin is regenerated via dehydration and subsequent electron transfer.



**Scheme 2.1:** Cytochrome P450 oxidation mechanism



**Scheme 2.2:** Flavin monooxygenase mechanism

Previous accounts of enzymatic nitrene formation have focused on metabolism of xenobiotic secondary amines and hydroxylamines by hepatic microsomal enzymes;<sup>15-20</sup> however, in the majority of these instances, nitrene formation was accompanied by a number of additional oxidative side reactions. Additionally, thorough characterization of the nitrene products in these instances is generally lacking, with nitrene formation often assumed following observation of nitrene addition or degradation products.

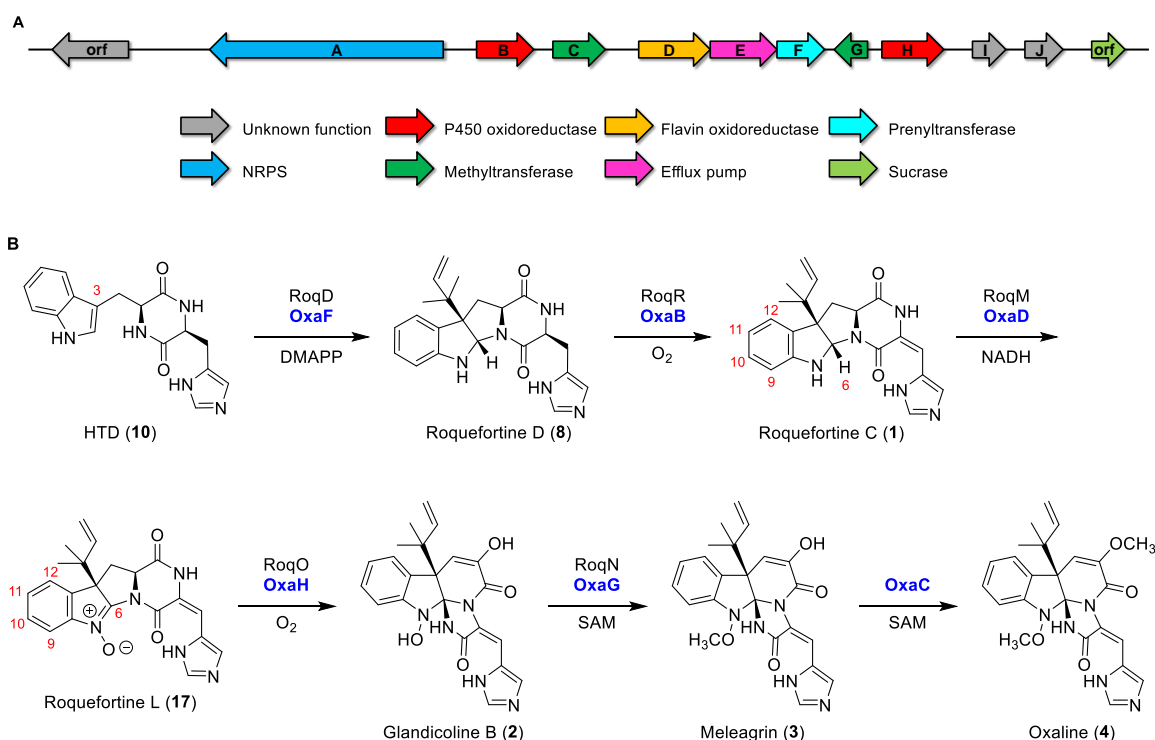
### III. Results and Discussion

#### A. Oxaline Biosynthetic Gene Cluster

While the biosynthesis of the roquefortine C-derived alkaloids **1-4** has been the subject of investigations employing genetic approaches,<sup>21-23</sup> enzymatic characterization relating to assembly and processing steps is completely lacking for these indoline alkaloid pathways.

In order to investigate the biogenesis of oxaline in mechanistic detail, the genome of *P. oxalicum* F30 was sequenced by the Sherman group and gene cluster analysis was performed using antiSMASH (antibiotics & Secondary Metabolite Analysis Shell), followed by a deep annotation of the oxaline biosynthetic pathway (Scheme 2.3A). The composition of the oxaline (*oxa*) gene cluster is highly similar to that of roquefortine/meleagrins (*roq*) cluster from *P. chrysogenum*,<sup>21</sup> with an average 78.4% similarity between homologous ORFs in the respective systems. One exception is a second methyltransferase (OxaC), which is absent in *P. chrysogenum* and suggests that this enzyme is responsible for the enol O-methylation that distinguishes **3** from **4**. By homology, we reason that the initial biosynthetic steps toward **4** match those previously reported for **3** (Scheme 2.3B). Briefly, the first biosynthetic intermediate HTD (**10**), is generated by an NRPS-mediated condensation of the corresponding L-amino acids. HTD undergoes reverse prenylation at C3 catalyzed by OxaF and dehydrogenation catalyzed by OxaB to give **1**. The flavin oxidase, OxaD, and the P450 monooxygenase, OxaH, are homologous to *P. chrysogenum* RoqM and RoqO,

respectively. RoqM and RoqO have been proposed to generate the core intermediate **2** from **1** by proceeding through intermediate **17**, as identified by Vreeken et al.<sup>22</sup> The conversion of **17** to **2** is proposed to arise from a P450-dependent hydroxylation catalyzed by OxaH, although this transformation has not been observed *in vitro*. Two O-methylations by OxaG and OxaC generate the final product **4**.



### Scheme 2.3: Oxaline biosynthetic gene cluster

(A) Schematic representation of the ORFs in the oxaline (*oxa*) gene cluster. (B) Proposed biosynthetic pathway in *P. oxalicum* F30. The homologous enzymes from the roquefortine C/meleagrins (*roq*) gene cluster in *P. chrysogenum* are also shown. A second methyltransferase, OxaC, lacks a homolog in *P. chrysogenum*.

## B. OxaD, a Flavin-Dependent Nitron Synthase

OxaD was cloned by the Sherman group from a *P. oxalicum* F30 cDNA library and heterologously expressed in *Escherichia coli*. The purified enzyme

exhibited an intense yellow color. High-performance liquid chromatography-mass spectrometry (HPLC-MS) analysis of the supernatant of boiled OxaD shows near quantitative incorporation of flavin adenine dinucleotide (FAD). In order to obtain sufficient quantities of roquefortine C, a fermentation-based isolation using *P. crustosum* was implemented, as described in Chapter 1.<sup>24</sup> Gram quantities of pure **1** were obtained for enzymatic testing and chemical derivatization. Both NADH and NADPH were shown by the Sherman group to be effective in the oxidation of **1** by OxaD. Incubation of OxaD with **1** and reduced nicotinamide cofactor resulted in the formation of several products. After 4 hours incubation of **1** with OxaD, HPLC-MS analysis (50:50 CH<sub>3</sub>OH:H<sub>2</sub>O) showed peaks with molecular weights corresponding to the nitrone **17**, the hydrated product **36**, and a presumed CH<sub>3</sub>OH adduct (Figure 2.2). Low levels of the hydroxylamine **16** were also detected. Preparative scale enzymatic reactions were conducted in the Joullié laboratory using **1** (20 mg) in order to characterize the major reaction product. As reverse-phase C18 chromatography led exclusively to the hydrolysis product **36**, subsequent reactions were designed to minimize the exposure of **17** to aqueous conditions, acidic or basic pH, and light. Biocatalytic reactions were performed for 1 hour prior to extraction with EtOAc and normal phase chromatography purification on deactivated silica gel in the absence of unhindered alcohols. These conditions led to **17** in a single step in good yield.



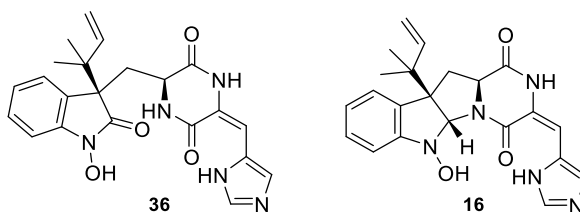


**Figure 2.2:** Reactions with OxaD and **1** led to the detection of a hydroxylamine intermediate **16** and the hydrolysis product **36**

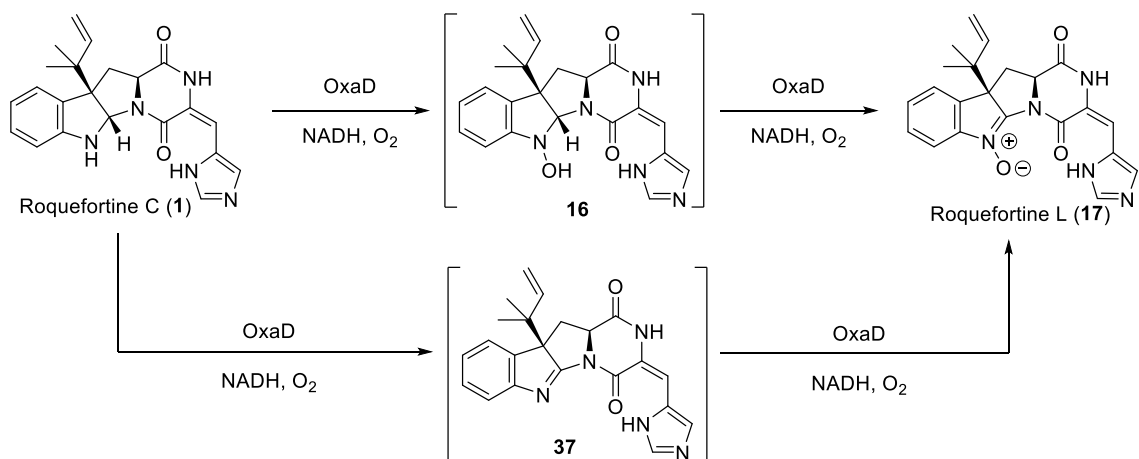
Identification of nitrones has long been a challenge with regard to their differentiation from other products of N-oxidation, such as imines, amine oxides, or oxaziridines. The presence of the nitron functionality in **17** was confirmed by analysis of  $^1\text{H}$  NMR,  $^{13}\text{C}$  NMR, and infrared (IR) spectra. Analysis of the  $^1\text{H}$  NMR spectrum of **17** confirms the double oxidation event at the indoline nitrogen, demonstrated conclusively by the disappearance of the H6 signal at  $\delta$  6.35 ppm. Moreover, chemical shifts of H9, H10, H11 and H12 were observed further downfield. Analysis of the  $^{13}\text{C}$  NMR spectrum of **17** was further indicative of the nitron formation, as the chemical shift of the C-6 peak shifted from  $\delta$  78 ppm to  $\delta$  150 ppm. Additionally, previous infrared analysis of *N*-phenyl nitrones shows a very strong band between  $1000\text{-}1100\text{ cm}^{-1}$  corresponding to the N-O stretch.<sup>25</sup> This band disappears upon isomerization of *N*-phenyl nitrones to the corresponding oxaziridines. Following the oxidation of roquefortine C by OxaD, an intense band was observed at  $1014\text{ cm}^{-1}$  in the IR spectrum of **17**, providing additional support for the presence of a nitron functionality rather than an oxaziridine.

As the natural abundance of  $^{15}\text{N}$  is quite low (0.36%), 20 mg of roquefortine L proved to be an insufficient amount to carry out  $^{15}\text{N}$  NMR experiments. Thus,

*P. crustosum* was cultured in  $^{15}\text{N}$ -enriched medium to give  $^{15}\text{N}$ -labeled **1** (86%  $^{15}\text{N}$  incorporation). This material was subjected to the same reaction conditions as **1** to provide  $^{15}\text{N}$ -labeled **17**, which was characterized by analysis of the  $^1\text{H}$ - $^{15}\text{N}$  HMBC spectrum. Nitrogen atoms in *N*-aryl nitrones display a characteristic peak between  $\delta$  270-300 ppm, while the corresponding amine nitrogens are observed between  $\delta$  0-100 ppm. In the  $^1\text{H}$ - $^{15}\text{N}$  HMBC spectrum of  $^{15}\text{N}$ -enriched **17** the signal at  $\delta$  83 ppm disappeared, and a new peak was observed at  $\delta$  281 ppm, which correlated to H9 and H10.

### C. Investigating the Mechanism of Oxidation

The observation of hydroxylamine **16** led us to investigate the mechanism of roquefortine C (**1**) oxidation by OxaD. The full catalytic cycle encompasses a four-electron reduction, in which two equivalents of NADH are consumed *en route* to the nitrone product. We considered two possible mechanisms for this reaction, the first proceeding via a hydroxylamine intermediate and the second proceeding via the indole imine (**37**, Scheme 2.4).



**Scheme 2.4:** Possible mechanisms of roquefortine L (**17**) biosynthesis by OxaD

Single turnover experiments were performed in which only one equivalent of NADH was provided to equimolar concentrations of OxaD and roquefortine C. Analysis of the reaction products showed an approximate 1:2 ratio of singly-oxidized hydroxylamine **16** species relatively to the doubly-oxidized nitrone product (Table 2.1), conclusively demonstrating that the reaction proceeds through a hydroxylamine intermediate. The abundance of **16** with respect to **17** under single turnover conditions also suggested that oxidation by OxaD is catalyzed in an iterative rather than a processive manner. To further support this proposal, single-turnover reactions were run with a 10-fold stoichiometric excess of roquefortine C with respect to NADH and OxaD in an effort to preclude re-binding of dissociated hydroxylamine. Under these conditions, **16** was the dominant reaction product, further supporting an iterative mechanism for OxaD. This iterative N-oxidation mechanism has been previously reported with human flavin containing monooxygenase 3 (FMO3) using various substrates.<sup>20,26</sup> The steady state kinetic

constants of OxaD with roquefortine C were determined by the Sherman group using an high-performance liquid chromatography (HPLC) based assay. These data show a turnover number ( $k_{\text{cat}}$ ) of  $0.017 \text{ s}^{-1}$  with a Michaelis constant ( $K_M$ ) of 71 nM resulting in a catalytic efficiency ( $k_{\text{cat}}/K_M$ ) of  $2.3 \times 10^5 \text{ M}^{-1}\text{s}^{-1}$ .

**Table 2.1:** Single turnover studies of OxaD

Entry	Roquefortine C ( <b>1</b> ) equiv.	Conversion (%)	Product ratio	
			Hydroxylamine ( <b>16</b> )	Roquefortine L ( <b>17</b> )
1	1	75	1	2
2	10	10	1	0

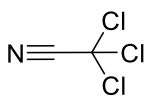
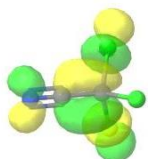
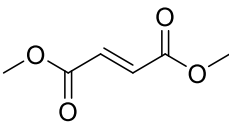
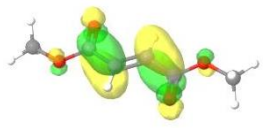
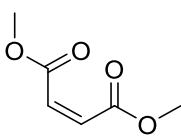
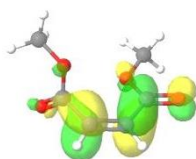
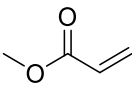
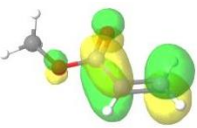
#### D. Roquefortine L Undergoes 1,3-Dipolar Cycloaddition

Since nitrones undergo 1,3 dipolar cycloadditions with dipolarophiles such as alkenes, alkynes, and nitriles, **17** was screened with known dipolarophiles for 1,3-dipolar cycloaddition reactions. Appropriate dipolarophile candidates for 1,3-dipolar cycloaddition with **17** were predicted by computational HOMO-LUMO analysis performed by the Joullié group (Table 2.2).

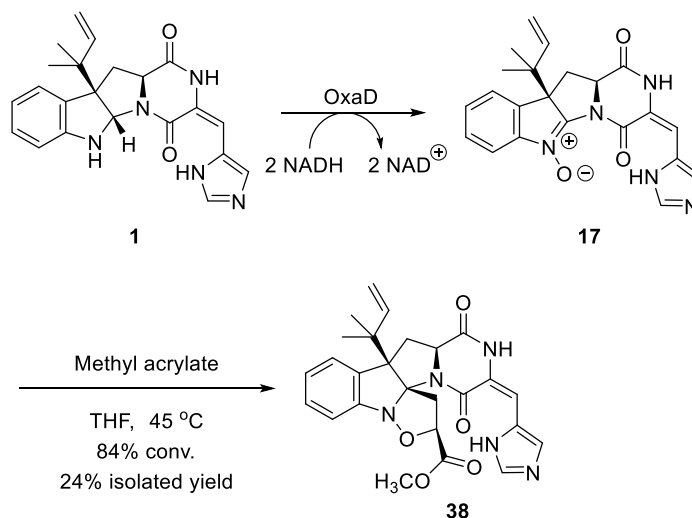
Methyl acrylate showed the best reactivity toward **17**. Optimized reaction conditions developed by the Sherman group generated cycloadduct **38** in a single step with 84% conversion, 24% yield (Scheme 2.5). The observed regiochemistry of this reaction is consistent with predictions based on frontier molecular orbital interactions described by Sustmann and Trill.<sup>27</sup> The stereochemistry of this species was determined by NOESY (Nuclear Overhauser effect spectroscopy). While this

cycloaddition is highly indicative of the presence of a nitron functionality in **17**, oxaziridines are also known to thermally rearrange to nitrones before undergoing 1,3-dipolar cycloadditions.<sup>28,29</sup>

**Table 2.2:** Potential dipolarophile candidates for 1,3-dipolar cycloaddition with roquefortine L (**17**)

Dipolarophile	LUMO structure	HOMO-LUMO gap <sup>†</sup> (eV)
 Trichloroacetonitrile		11.54
 Dimethyl fumarate		10.56
 Dimethyl maleate		11.33
 Methyl acrylate		11.78

<sup>†</sup>HOMO-LUMO energy gaps calculated using HOMO of roquefortine L (**17**) and LUMO of dipolarophile. Calculations was carried out at the HF/6-311+G(2d,p) level of theory.



**Scheme 2.5:** Roquefortine L (**17**) undergoes 1,3-dipolar cycloaddition with methyl acrylate to generate **38**

### E. Oxidation of Roquefortine C Derivatives by OxaD

In order to explore the substrate scope of OxaD, the roquefortine C derivatives **9**, **39–42** were assayed under the same conditions as described above for the native substrate **1** (Figure 2.3A). Compounds **9**, **39–41** were generated by semisynthesis from **1** (Scheme 2.6) while roquefortine E (**42**) was purchased from Enzo (Ann Arbor, MI). Iso Roquefortine C (**9**) was obtained by photochemical reaction of **1** using broad spectrum UV light.<sup>30</sup> Isomerization of roquefortine C was also observed upon exposure to direct sunlight over the course of several days. Electrophilic aromatic substitution of **1** using *N*-bromosuccinimide (NBS) and *N*-iodosuccinimide (NIS) yielded 11-bromo Roquefortine C (**39**)<sup>31</sup> and 11-iodo Roquefortine C (**40**), respectively.

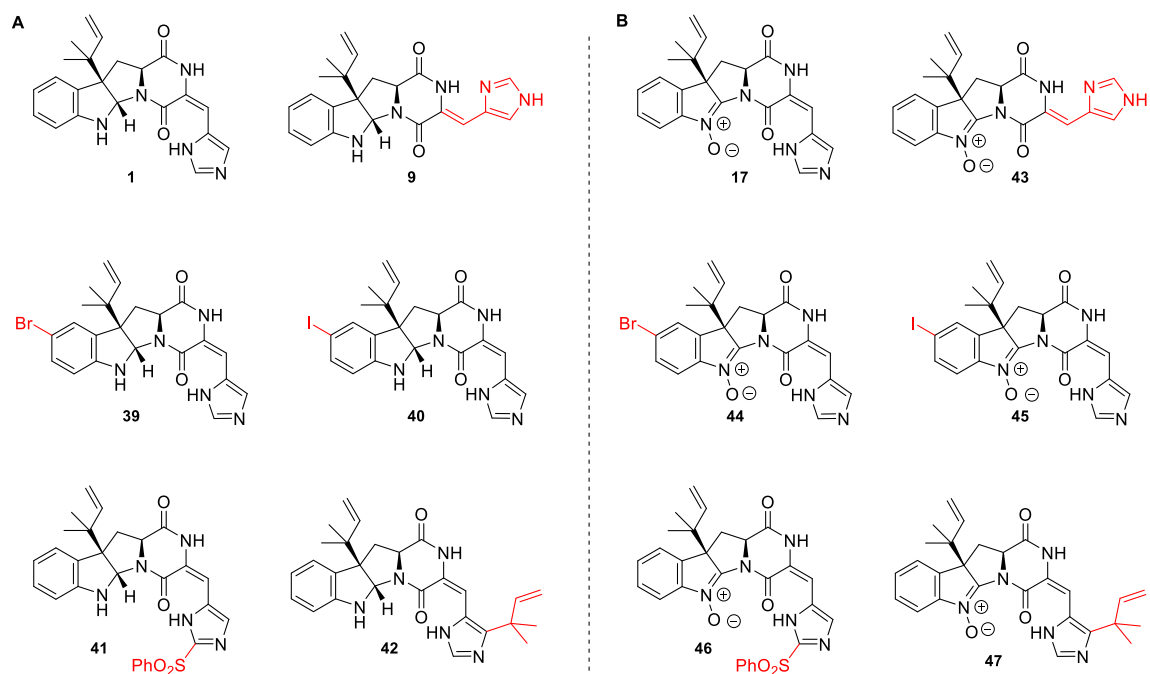
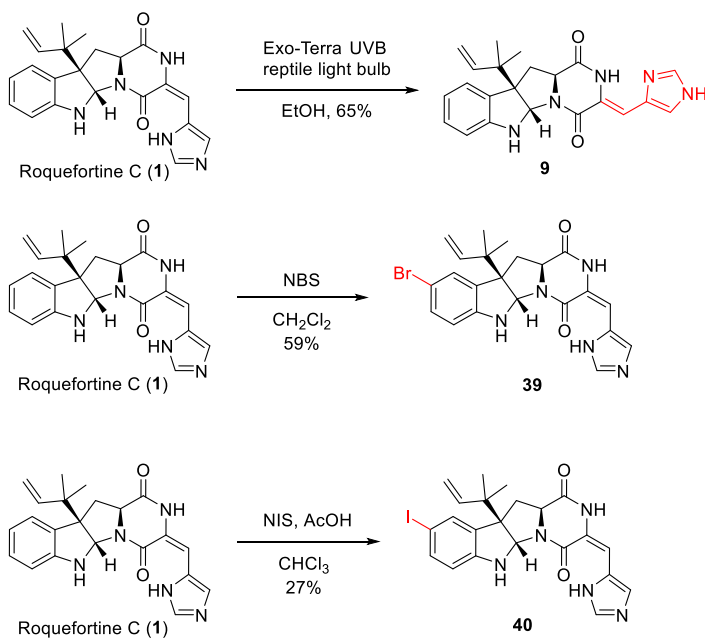


**Figure 2.3:** (A) Roquefortine C and derivatives. (B) Nitrones derived from OxalD N-oxidation  
Modifications to the roquefortine C scaffold highlighted in red.



**Scheme 2.6:** Semisynthesis of roquefortine C derivatives 9, 39, and 40

A number of fluorination and trifluoromethylation methods were attempted, including trifluoromethylation using the Baran sodium and zinc trifluoromethanesulfonates and electrophilic fluorination using SelectFluor, 1-(chloromethyl)-4-fluoro-1,4-diazoniabicyclo[2.2.2]octane dihexafluorophosphate (F-TEDA-PF<sub>6</sub>), and 1-fluoro-2,4,6-trimethylpyridin-1-ium tetrafluoroborate (Figure 2.4). Unfortunately, reactions using these conditions gave only starting material. Synthesis of the arylstannane derivative from 11-iodo roquefortine C (**40**), in preparation for silver-catalyzed electrophilic fluorination as described by Ritter,<sup>32</sup> also proceeded poorly.

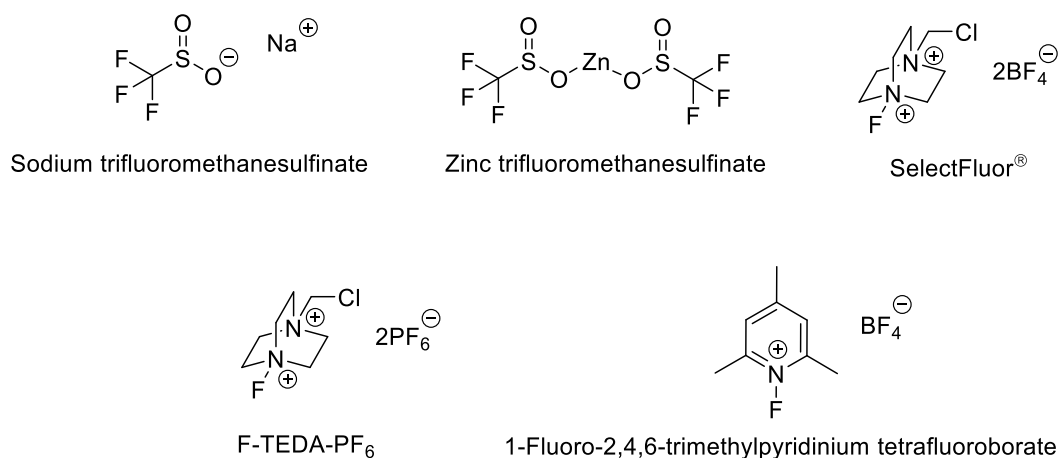
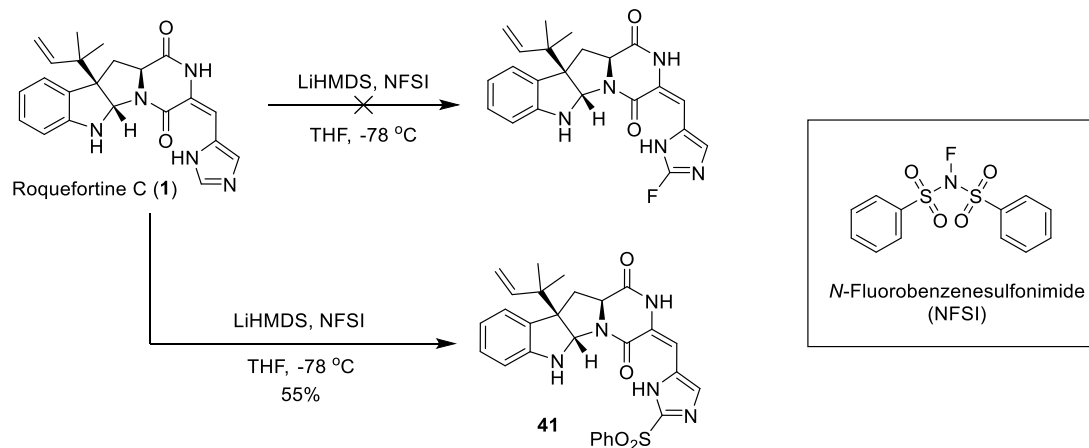


**Figure 2.4:** Electrophilic fluorinating reagents

Attempted electrophilic fluorination with *N*-fluorobis(phenyl)sulfonamide (NFSI) did not afford a fluoro derivative but instead introduced a sulfonyl group on the C20 position of the imidazole ring (Scheme 2.7). Although the reaction was unexpected, there is precedent for a similar reaction on a purine derivative proposed to occur via a single electron transfer (SET) mechanism.<sup>33</sup>





**Scheme 2.7:** Unexpected NFSI phenylsulfonyl transfer

A number of synthesized roquefortine C derivatives were tested for antimicrobial activity in collaboration with the Moulder Center for Drug Discovery Research at Temple University and the University of Rochester. Compounds **40** along with the imidazole N21 carboxybenzyl (Cbz) protected derivative of **1** showed modest activity (64  $\mu\text{g}/\text{mL}$ ) against *Staphylococcus aureus* UAMS 1 (a penicillin sensitive strain) despite their low aqueous solubility.

Processing **9**, **39–42** to their corresponding nitron products (**43–47**, Figure 2.3B) demonstrated that OxaD can accommodate variation at several positions in the roquefortine C skeleton. Total turnover numbers (TTN) were measured by the Sherman group to quantify the effect of these variations on the OxaD biocatalyst (Figure 2.5). Modifications to the histidine moiety, including both alkene isomerization (**43**) and reverse prenylation (**47**), were well tolerated. Only the

phenylsulfonyl derivative (**46**) showed a substantial decrease in TTN. To test whether the diminished turnover of **46** was observed due to the poor solubility of this substrate, TTNs were measured using both 10% and 20% dimethyl sulfoxide (DMSO) cosolvent. While elevated cosolvent increased the solubilization of **46**, only a modest increase in TTN was observed, likely indicating that the benefit was offset by attenuated enzymatic activity. Modifications to the indole ring via halogenation (compounds **44** and **45**) were also processed efficiently by OxaD.

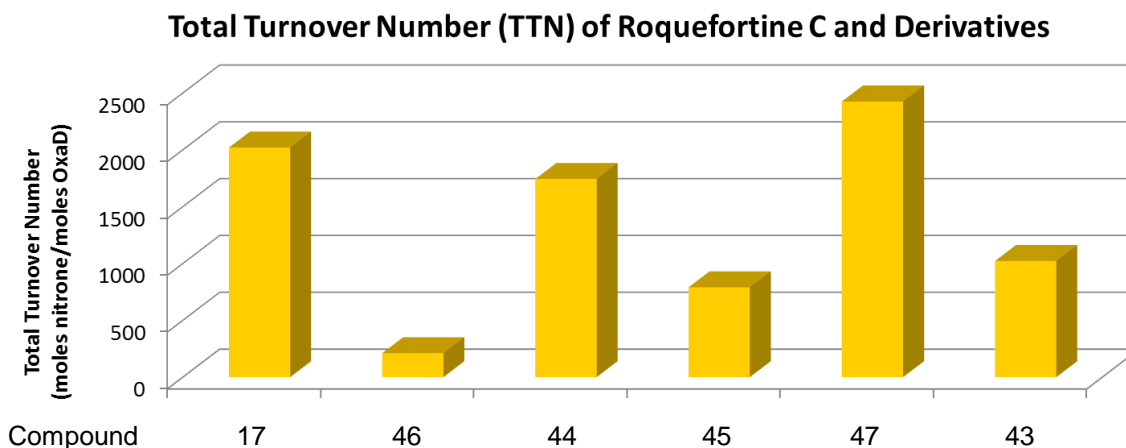
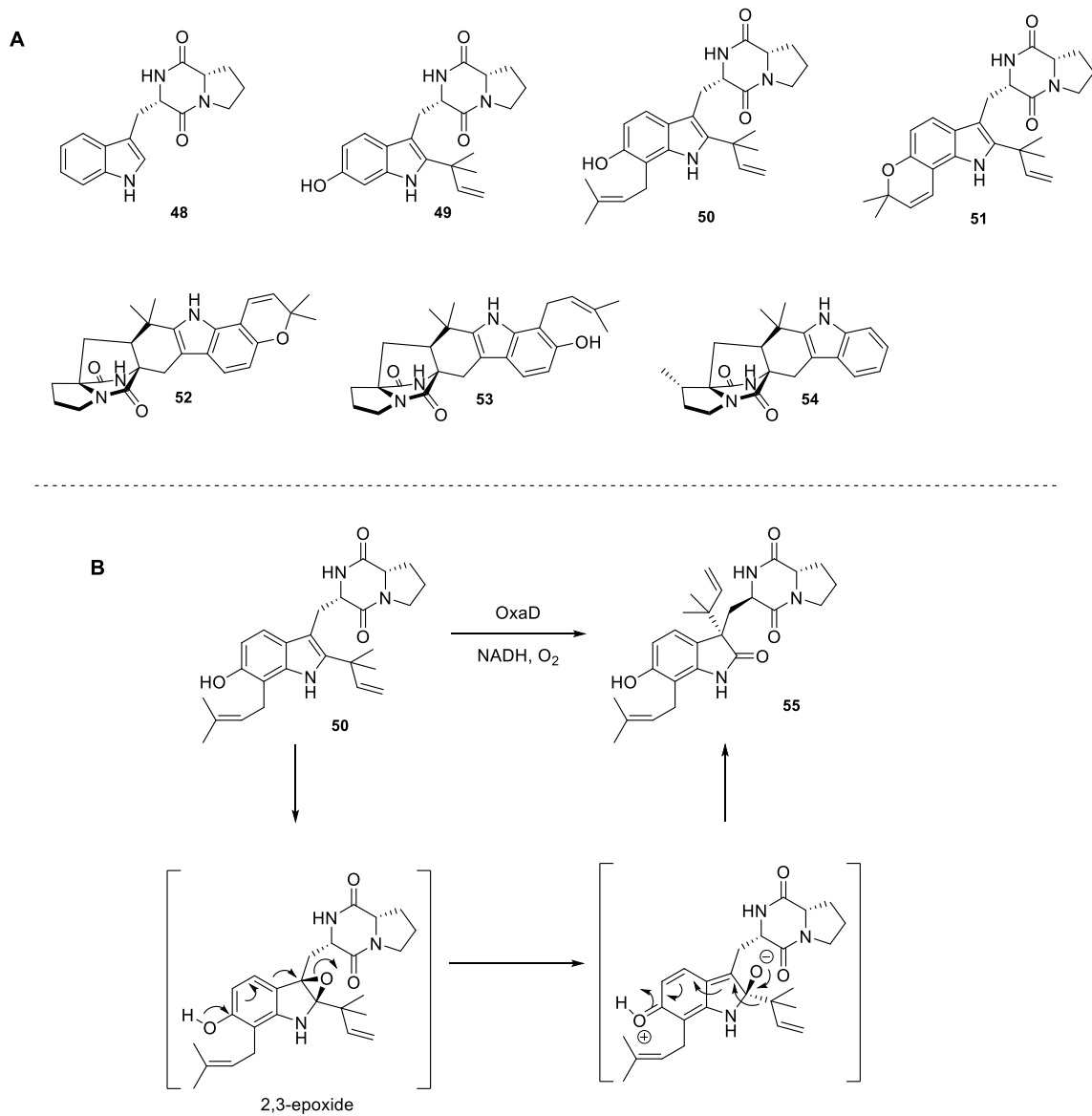


**Figure 2.5:** Total turnover number of roquefortine C and derivatives by OxaD. TTN was calculated as moles product/moles enzyme.

#### F. OxaD Catalyzes Indole 2,3-Oxidation of Notoamide S

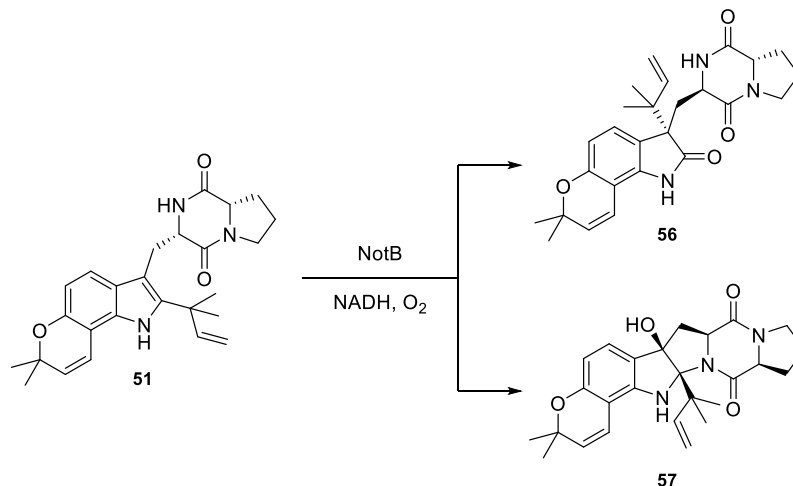
Based on the broad reactivity that OxaD displayed with roquefortine C derivatives, the Sherman group subjected additional indole alkaloids to the enzyme

to examine whether this substrate flexibility extended beyond the roquefortine C scaffold. These include brevianamide F (**48**), 6-OH-deoxybrevianamide E (**49**), notoamide S (**50**), notoamide E (**51**), (+)-stephacidin A (**52**), notoamide T (**53**) and pre-paraherquamide (**54**) (Scheme 2.8A). Of particular interest was to assay **52**, a presumed biosynthetic precursor to the nitron-bearing avrainvillamide (**32**),<sup>34</sup> however no reaction was observed for substrates **48**, **49**, and **51-53**. Enzyme-dependent generation of a new product with  $m/z = +16$  Da was uniquely observed by liquid chromatography-mass spectrometry (LC-MS) with **50**. The total conversion (20%) was lower than that of the roquefortine C alkaloids. Biocatalytic reaction of **50** with OxaD gave rise to a 2-indolinone **55** rather than the expected indole *N*-hydroxylamine (Scheme 2.8B). The product **55** is presumed to arise via 2,3-epoxidation followed by a pinacol-like rearrangement in an analogous fashion to the NotB catalyzed formation of notoamides C (**56**) and D (**57**) (Scheme 2.9).<sup>35</sup> Compound **55** was observed as a single reaction product between **50** and OxaD, as opposed to the reaction between notoamide E (**51**) and NotB which generated notoamides C (**56**) and D (**57**). OxaD appears to play a role in directing reaction selectivity, although low enzyme activity with notoamide S (**50**) could limit the detection of minor reaction products. This outcome shows that OxaD presents remarkable functional plasticity in addition to its broad substrate scope. Further structural investigation would be required to determine the mechanistic basis of this branch in reaction specificity.



**Scheme 2.8:** OxaD reactivity with notoamides

(A) Synthetic notoamides tested with OxaD. Only **50** was converted by the enzyme.  
 (B) Pinacol-like rearrangement of the OxaD catalyzed 2,3-indole epoxidation on **50** gives rise to the novel product **55**.



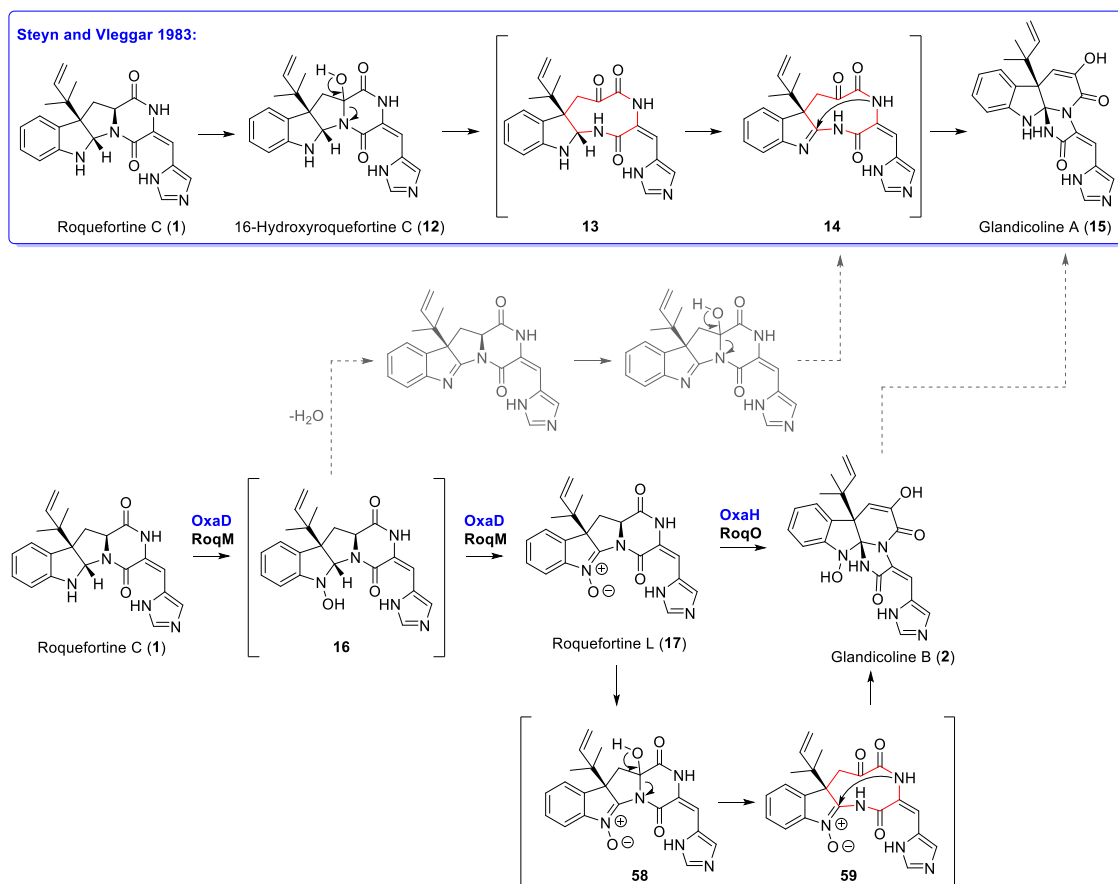
**Scheme 2.9:** NotB-catalyzed formation of notoamides C (**56**) and D (**57**) from notoamide E (**51**)

### G. Speculation on Glandicoline A Formation in *P. glandicola*

Our extensive work with OxaD coupled with the striking similarities of the roquefortine C gene clusters in *P. oxalicum* and *P. chrysogenum* give further support to the role of roquefortine L as the exclusive biosynthetic precursor to glandicoline B. Hydroxylation at C16 of **1** leading to **12** appears insufficient to induce rearrangement, since this metabolite has been previously isolated and identified;<sup>36,37</sup> therefore, both hydroxylation at C16 and nitron generation to give **58** are likely required for the core rearrangement to occur. Roquefortine L (**17**) involvement is supported by the fact that glandicoline A (**15**) has not been observed in *P. chrysogenum*, and that disruption of *roqM* (81% homology with *oxaD*) abolished the production of glandicoline B (**2**).<sup>22</sup> The first report of **15** in *P. glandicola* is sufficiently supported by spectroscopic data;<sup>38</sup> however, subsequent reports of **15** were based on mass spectrometry analysis,

chromatographic retention time ( $R_f$ ) and/or UV signature, but not by NMR analysis.<sup>21,23,39</sup> As substantial structural characterization of metabolites is imperative in differentiating glandicoline A from **17**, we have unequivocally assigned the nitron group in **17** by NMR, IR, and chemical transformation.

At present, the mechanism of formation of **15** in *P. glandicola* is unclear. It could require a yet unknown route to the 1,2-imine in **14** proposed by Steyn and Vleggaar<sup>33</sup> or arise by modification of **2** (Scheme 2.10). Investigation of the biosynthetic gene clusters in strains that produce **15** will be necessary to identify candidate enzymes that could give rise to **15**, either through a different oxidation cascade involving **1** or enzymatic processing of **2**. Understanding the role of the oxidative enzymes involved in the rearrangement of **1** to **2** will be critical for in vitro reconstitution and for future mutasynthetic efforts based on derivatives of **1**. There is ample precedence for plasticity in these pathways, as mutasynthesis with *roqA* gene disruption mutant strains has been used to generate novel roquefortine D derivatives.<sup>40</sup> Characterization of OxaD reported in this study also reveals the ability of the roquefortine C nitron synthase to accept an array of modified substrates that enables the generation of novel indoline nitrones that would be synthetically appealing for the preparation of further elaborated alkaloid scaffolds.



**Scheme 2.10:** Proposed biogenesis of glandicoline A (**15**) and B (**2**)

#### IV. Conclusions

The enzymatic characterization of OxaD, along with the results of gene disruptions,<sup>23</sup> indicates that formation of roquefortine L (**17**) is a key biosynthetic intermediate toward formation of the glandicoline core. The results herein illustrate that the combination of biological and chemical approaches for the generation of new and diverse natural products can lead to a number of applications in chemistry and chemical biology. Understanding the genetic and metabolic information of biological systems can provide access to complex chiral molecular scaffolds, which can be further synthetically elaborated into novel molecules. These natural

product-based modified frameworks are of considerable interest in chemistry, biochemistry, and chemical biology as bioactive chemical entities or as unique biochemical tools. Heterologous production and enzymatic characterization of OxaD constitutes a proof of concept that unique biocatalysts can generate versatile and powerful chemical and biochemical tools for structural diversification.

## V. Experimental

### *P. oxalicum* genomic DNA sequencing

*P. oxalicum* was cultivated in liquid medium (20% artificial seawater with 12.0 g/L glucose, 6.0 g/L starch, 12.0 g/L soytone, 3.0 g/L peptone, 0.18 g/L meat extract, 3.0 g/L yeast extract) in still mode at 28 °C for 14 days. The mycelia were harvested by filtration and genomic DNA was extracted using the Wizard Genomic DNA isolation kit (Promega). Genomic DNA was analyzed by using a HiSeq 2000 sequence analyzer using 100 cycle paired end reads (Illumina). *De novo* assembly of genomes was performed using Velvet version 0.7.63. The summary of dataset and parameters of genome sequencing and assembly is shown in **Tables S1-2**. Probes from the published sequence for meleagrins biosynthetic gene cluster were used to identify the contig containing the oxaline biosynthetic gene cluster.

**Supplementary Table 2.1:** *P. oxalicum* F30 genome sequencing and assembly

Genome	Number of reads	k-mer	Coverage cutoff	N50	Number of contigs
<i>P. oxalicum</i>	62,981,204	71	28	24,473	9,807



**Supplementary Table 2.2: Annotation of OXA gene cluster**

Proteins	Size (AA)*	Function	Relative (identity/similarity) (%)	Accession number
ORF01	800	hypothetical protein, phosphoenolpyruvate synthase	Hypothetical protein ATEG 02219 [ <i>Aspergillus terreus</i> NIH2624] (72/83)	XP_001211397.1
OxaA	2390	NRPS	Pc21g15480 [ <i>Penicillium chrysogenum</i> Wisconsin 54-1255] (53/69)	XP_002568558.1
OxaB	477	cytochrome P450 oxidoreductase	Pc21g15470 [ <i>Penicillium chrysogenum</i> Wisconsin 54-1255] (73/84)	XP_002568557.1
OxaC	405	O-methyltransferase	O-methyltransferase [ <i>Aspergillus flavus</i> NRRL3357](49/65)	XP_002384741.1
OxaD	456	MAK1	Pc21g15460 [ <i>Penicillium chrysogenum</i> Wisconsin 54-1255] (66/79)	XP_002568556.1
OxaE	482	MFS toxin efflux pump	Pc21g15420 [ <i>Penicillium chrysogenum</i> Wisconsin 54-1255] (69/81)	XP_002568552.1
OxaF	419	dimethylallyl tryptophan synthase, putative	Pc21g15430 [ <i>Penicillium chrysogenum</i> Wisconsin 54-1255] (70/80)	XP_002568553.1
OxaG	288	UbiE/COQ5 family methyltransferase, putative	Pc21g15440 [ <i>Penicillium chrysogenum</i> Wisconsin 54-1255] (73/84)	XP_002568554.1
OxaH	499	cytochrome P450 monooxygenase	Pc21g15450 [ <i>Penicillium chrysogenum</i> Wisconsin 54-1255](64/77)	XP_002568555.1
OxaI	322	hp**	Pc12g13620 [ <i>Penicillium chrysogenum</i> Wisconsin 54-1255](62/75)	XP_002558169.1
OxaJ	419	hp**	hypothetical protein AKAW_10943 [ <i>Aspergillus kawachii</i> IFO 4308](57/72)	GAA92830.1
OxaK	322	sucrase/ferredoxin-like family protein Fmi1	Pc12g04290 [ <i>Penicillium chrysogenum</i> Wisconsin 54-1255](73/83)	XP_002557299.1

\*AA: amino acid; \*\*hypothetical protein

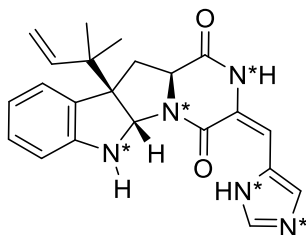
### **Molecular cloning of *oxaD* gene**

*P. oxalicum* F30 was cultivated in liquid medium as above. RNA was isolated from filter paper-dried mycelia using the TRIzol® Reagent (Ambion RNA, Life Technologies) and protocol. The reverse transcription PCR (RT-PCR) was performed using the High Capacity cDNA Reverse Transcription Kit (Applied Biosystems) using Oligo dT primer (Life Technologies). The cDNA generated from one microgram of total RNA was used as the template for PCR amplification of the *oxaD* gene. The forward primer based on the *oxaD* gene is 5'-aattcgGCTAGCATGACTGTTCCGAACAGCGCC-3' (the NheI restriction site is underlined) and reverse, 5'-cgaattCTCGAGCTATGTTGAGACAGTCTTTTTGTAGTCATG-3' (the XhoI site is underlined). The amplified *oxaD* gene was doubly digested by NheI and XhoI, and then ligated into an NheI/XhoI digested pET28b vector, which was modified to include eight His residues followed by a tobacco etch virus (TEV) protease recognition sequence, to generate the pET28b-*oxaD* construct for protein expression.

### **Overexpression and purification of OxaD**

The *Escherichia coli* BL21 (DE3) pRARE transformant carrying pET28b-*oxaD* was grown at 37 °C overnight in lysogeny broth (LB) containing 50 µg/mL of kanamycin. Baffled Fernbach flasks (6 x 1.5 L of LB in 2.8 L) containing 50 µg/mL of kanamycin were inoculated with 20 mL overnight culture. Cells were grown at 37 °C until A<sub>600</sub> reached ~ 0.6. Isopropyl β-D-thiogalactoside (IPTG, 1 mM) was added to induce

protein overexpression. Cells were cultured at 18 °C overnight, harvested by centrifugation, and frozen directly into liquid nitrogen prior to storage at -80 °C. All subsequent purification steps were performed on ice or at 4 °C. Frozen cells (15 g) were resuspended in 100 mL of lysis buffer (10 mM 4-(2-hydroxyethyl)-1-piperazineethanesulfonic acid (HEPES) pH 7.6, 50 mM NaCl, 10% glycerol, 0.2 mM tris(2-carboxyethyl)phosphine (TCEP)). Lysis was achieved by the addition of lysozyme (0.5 mg/mL), benzonase (Merck kGaA, 1 kU), and MgSO<sub>4</sub> (5 mM) followed by sonication on ice. The lysate was clarified by centrifugation at 60,000 g for 30 minutes at 4 °C. NaCl and imidazole were added to the supernatant to final concentrations of 300 mM and 20 mM, respectively, prior to loading a column containing 7 mL of Ni-NTA resin (Qiagen) equilibrated with NiNTA wash buffer (20 mM HEPES pH 7.6, 300 mM NaCl, 20 mM imidazole, 10% glycerol, 0.2 mM TCEP). The column was washed with 150 mL of wash buffer. The bound N-terminal His<sub>8</sub>-tagged OxaD was eluted by elution buffer (300 mM imidazole pH 8.0, 10% glycerol, 0.2 mM TCEP). The eluant was concentrated on a Millipore Amicon Ultra centrifugal concentrator (30 kDa MWCO). The concentrated protein was exchanged into storage buffer (10 mM HEPES pH 7.6, 50 mM NaCl, 10% glycerol, 0.2 mM TCEP) using a PD-10 desalting column (GE Healthcare). The purified OxaD protein was flash frozen in liquid nitrogen, and stored at -80 °C.



### Isolation of $^{15}\text{N}$ -enriched roquefortine C (1) from *P. crustosum*

Freeze-dried samples of *P. crustosum* were inoculated onto malt extract agar plates as described in Chapter 1.  $^{15}\text{N}$ -Enriched Czapek-Dox liquid media was prepared as follows: 10 g sucrose; 1 g  $^{15}\text{N}$ -enriched (98%+)  $\text{NaNO}_3$ ; 0.33 g  $\text{K}_2\text{HPO}_4$ ; 0.167 g  $\text{MgSO}_4$ ; 0.167 g  $\text{KCl}$ ; 0.003 g  $\text{FeSO}_4$ ; and 333 mL dd  $\text{H}_2\text{O}$ . Media was inoculated with fungal culture as described above and was grown in liquid culture for 21 days. Mycelial material was harvested and extracted as described above and  $^{15}\text{N}$ -enriched roquefortine C was purified from the other metabolites by flash chromatography ( $R_f$  0.33, 85:10:5  $\text{CH}_2\text{Cl}_2/\text{CH}_3\text{OH}/\text{acetone}$ ). HRMS (ESI-TOF)  $m/z$   $[\text{M} + \text{H}]^+$  calcd for  $\text{C}_{22}\text{H}_{24}^{15}\text{N}_5\text{O}_2$  395.1782, found 395.1787.

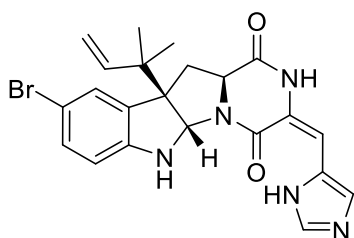
**Supplementary Table 2.3:**  $^{15}\text{N}$  Incorporation into roquefortine C (1) determined by mass spectrometry

Experimental			IDCalc prediction (86% $^{15}\text{N}$ incorporation)	
$m/z$	Intensity	Relative Abundance	$m/z$	Relative Abundance
391.2823	6080	5.20	391.1948	0.29
392.1895	16600	14.19	392.1972	3.64
393.1912	40400	34.53	393.1995	22.79
394.1828	90500	77.35	394.2019	72.82
395.1801	117000	100.00	395.2042	100.00
396.1850	29200	24.96	396.2066	22.57

## **Semi-synthesis of roquefortine C analogues: General Information**

Starting materials, reagents and solvents were purchased from commercial suppliers and used without further purification unless otherwise noted. Anhydrous tetrahydrofuran (THF) and CH<sub>2</sub>Cl<sub>2</sub> were obtained from a solvent dispensing system stored under positive pressure of argon. The sample of roquefortine E (**42**) was purchased from Enzo (Ann Arbor, MI). All reactions were conducted in oven-dried glassware. The progress of reactions was monitored by silica gel thin layer chromatography (TLC) plates (250 μm with fluorescent indicator), visualized under UV, and stained using a phosphomolybdic acid (PMA) stain. Products were purified by flash column chromatography (FCC) on 230-400 mesh silica gel. <sup>1</sup>H and <sup>13</sup>C NMR spectra were recorded on a spectrometer operating at 500 MHz for <sup>1</sup>H and 125 MHz for <sup>13</sup>C unless otherwise stated. Chemical shifts are reported in ppm relative to tetramethylsilane (TMS) as the internal standard for <sup>1</sup>H and chloroform as the internal standard for <sup>13</sup>C. <sup>15</sup>N NMR spectra were recorded on a spectrometer operating at 600 MHz. Chemical shifts are reported in ppm relative to nitromethane as the external standard. <sup>1</sup>H-<sup>1</sup>H Homonuclear correlation spectroscopy (COSY), <sup>1</sup>H-<sup>1</sup>H NOESY, <sup>1</sup>H-<sup>13</sup>C heteronuclear single quantum correlation experiment (HSQC), <sup>1</sup>H-<sup>13</sup>C heteronuclear multiple quantum coherence (HMQC), and <sup>1</sup>H-<sup>13</sup>C heteronuclear multiple bond correlation (HMBC) NMR spectra were recorded on a spectrometer operating at 500 MHz. <sup>1</sup>H-<sup>1</sup>H Gradient correlation spectroscopy (gCOSY), <sup>1</sup>H-<sup>13</sup>C gradient heteronuclear single quantum coherence adiabatic (gHSQCAD), and <sup>1</sup>H-<sup>13</sup>C gradient heteronuclear multiple

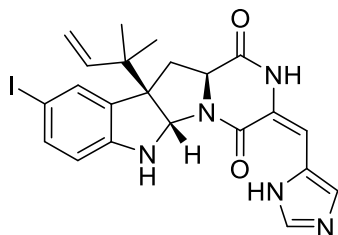
bond correlation adiabatic (gHMBCAD) NMR spectra were recorded on a spectrometer operating at 700 MHz. NMR data is reported as follows: chemical shift, multiplicity (s = singlet, d = doublet, dd = doublet of doublets, t = triplet, q = quartet, br = broad, m = multiplet), coupling constants (Hz), and integration. High-resolution mass spectra (HRMS) were recorded on an electrospray ionization time-of-flight (ESI-TOF) spectrometer (Agilent). Waters software calibrates and reports by use of neutral atomic mass. The mass of the electron is not included.



### 11-Bromoroquefortine C (39)

In a round-bottomed flask under argon, roquefortine C (100 mg, 0.26 mmol) was dissolved in dry  $\text{CH}_2\text{Cl}_2$  (6 mL). A solution of NBS (46 mg, 0.26 mmol) in dry  $\text{CH}_2\text{Cl}_2$  (6 mL) was prepared and added dropwise via syringe to the round-bottomed flask containing roquefortine C. The reaction mixture was allowed to stir overnight (15 hours), after which it was washed three times with saturated aqueous  $\text{NaHCO}_3$ . The organic solution was then dried over  $\text{Na}_2\text{SO}_4$  and concentrated in vacuo. The crude product was purified by flash chromatography (98:2 to 90:10  $\text{CH}_2\text{Cl}_2$ - $\text{CH}_3\text{OH}$ ) to give 11-bromoroquefortine C (72 mg, 59%) as a yellow powder.  $^1\text{H}$  NMR (500 MHz,  $\text{CDCl}_3$ )  $\delta$  9.83 (s, 1H), 7.70 (s, 1H), 7.28 (d,  $J = 1.5$  Hz, 1H), 7.26 (s, 1H), 7.20 (dd,  $J = 8.5, 1.5$  Hz, 1H), 6.49 (d,  $J = 8.0$  Hz, 1H), 6.35 (s, 1H),

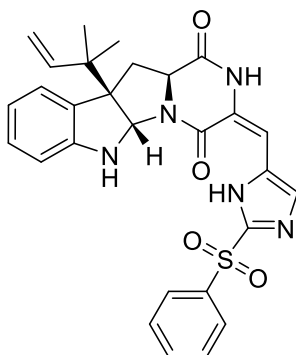
5.99 (s, 1H), 5.96 (d,  $J = 6.5$  Hz, 1H), 5.93 (s, 1H), 4.09 (dd,  $J = 6.0, 11.5$  Hz, 1H), 2.56 (dd,  $J = 5.0, 12.5$  Hz, 1H), 2.47 (t,  $J = 12.0$  Hz, 1H), 1.15 (s, 1H), 1.05 (s, 1H).  $^{13}\text{C}$  NMR (125 MHz,  $\text{CDCl}_3$ )  $\delta$  166.9, 159.6, 149.2, 143.0, 137.0, 135.1, 132.0, 131.3, 128.3, 125.7, 121.9, 115.4, 111.6, 110.8, 110.6, 78.7, 61.9, 58.9, 41.1, 37.0, 23.0, 22.6. HRMS (ESI-TOF)  $m/z$   $[\text{M} + \text{H}]^+$  calcd for  $\text{C}_{22}\text{H}_{23}^{79}\text{BrN}_5\text{O}_2$  468.1035, found 468.1035 (lit. (da Silva et al., 2014)<sup>31</sup> HRMS (ESI)  $m/z$   $[\text{M} + \text{H}]^+$  calcd for  $\text{C}_{22}\text{H}_{23}^{81}\text{BrN}_5\text{O}_2$  470.1186, found 470.1182).



### 11-Iodoroquefortine C (40)

In a round-bottomed flask under argon, roquefortine C (40 mg, 0.1 mmol) was dissolved in  $\text{CHCl}_3$  (1 mL). NIS (27 mg, 0.12 mmol) and AcOH (0.3 mL) were added to the round-bottomed flask, and the reaction mixture was allowed to stir overnight (15 hours), after which it was washed three times with saturated aqueous  $\text{NaHCO}_3$ . The organic solution was then dried over  $\text{Na}_2\text{SO}_4$  and concentrated in vacuo. The crude product was purified by flash chromatography (100:0 to 90:10  $\text{CH}_2\text{Cl}_2$ - $\text{CH}_3\text{OH}$ ) to give 11-iodoroquefortine C (14 mg, 27%) as a yellow powder.  $^1\text{H}$  NMR (500 MHz,  $\text{CDCl}_3$ )  $\delta$  11.61 (s, 1H), 9.71 (s, 1H), 7.65 (s, 1H), 7.38 (d,  $J = 1.5$  Hz, 1H), 7.32 (dd,  $J = 8.0$  Hz, 1.5 Hz, 1H), 7.14 (s, 1H), 6.67 (s, 1H), 6.35 (d,  $J = 7.0$  Hz), 5.91 (dd,  $J = 17.0$  Hz, 6.0 Hz, 1H), 5.60 (s, 1H), 5.08 (m, 2H), 4.99 (s, 1H),

4.09 (dd,  $J=6.0, 11.5$  Hz, 1H), 2.50 (dd,  $J=5.5, 12.0$  Hz, 1H), 2.43 (t,  $J=12.0$  Hz, 1H), 1.09 (s, 3H), 1.00 (s, 3H).  $^{13}\text{C}$  NMR (125 MHz,  $\text{CDCl}_3$ )  $\delta$  165.4, 158.6, 150.2, 143.2, 137.8, 137.5, 135.4, 134.0, 132.0, 126.6, 117.5, 115.1, 111.1, 105.4, 79.5, 78.1, 61.8, 59.2, 41.1, 37.4, 23.0, 22.6 ppm. HRMS (ESI-TOF)  $m/z$   $[\text{M} + \text{H}]^+$  calcd for  $\text{C}_{22}\text{H}_{23}\text{N}_5\text{O}_2$  516.0897, found 516.0912.

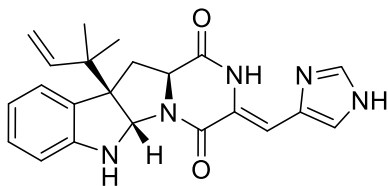


### 20-Phenylsulfonylroquefortine C (41)

In a round-bottomed flask under argon, roquefortine C (40 mg, 0.10 mmol) was dissolved in dry THF (1 mL) and chilled in a dry ice/acetone bath. A 1.0 M solution of lithium bis(trimethylsilyl)amide (LiHMDS) in THF (0.11 mL, 0.11 mmol) was added dropwise via syringe and the reaction mixture was allowed to stir for 10 minutes. NFSI (32 mg, 0.10 mmol) was then added and the reaction mixture was gradually warmed to room temperature. After stirring for 3 hours, the reaction mixture was concentrated in vacuo. The residue was diluted with  $\text{H}_2\text{O}$ , extracted three times with  $\text{CH}_2\text{Cl}_2$ , dried over  $\text{Na}_2\text{SO}_4$ , and concentrated in vacuo. The crude residue was purified by flash chromatography (98:2 to 90:10  $\text{CH}_2\text{Cl}_2$ - $\text{CH}_3\text{OH}$ ) to give 20-phenylsulfonylroquefortine C (29 mg, 55%) as a yellow solid.  $^1\text{H}$  NMR



(500 MHz, CDCl<sub>3</sub>) δ 9.31 (s, 1H), 8.57 (s, 1H), 7.96 (d, *J* = 10.0 Hz, 3H), 7.65 (t, *J* = 7.5 Hz, 1H), 7.53 (t, *J* = 8.0 Hz, 2H), 7.12 (d, *J* = 7.5 Hz, 1H) 7.06 (t, *J* = 7.5 Hz, 1H), 6.72 (t, *J* = 7.5 Hz, 1H), 6.57 (d, *J* = 8.0 Hz, 1H), 6.34 (s, 1H), 5.93 (dd, *J* = 17.0, 11.0 Hz, 1H), 5.60 (s, 1H), 5.07 (m, 3H), 4.00 (dd, *J* = 6.0, 11.5 Hz, 1H), 2.52 (dd, *J* = 12.5 Hz, 6.0 Hz, 1H), 2.38 (t, *J* = 12.0 Hz, 1H), 1.09 (s, 1H), 0.98 ppm (s, 1H). <sup>13</sup>C NMR (125 MHz, CDCl<sub>3</sub>) δ 167.6, 158.0, 150.4, 143.6, 137.9, 137.5, 136.1, 135.1, 130.0, 129.1, 128.8, 127.7, 126.8, 125.4, 120.3, 119.0, 114.9, 114.7, 109.2, 78.1, 61.6, 59.1, 41.1, 37.0, 23.0, 22.6 ppm. HRMS (ESI-TOF) *m/z* [M + H]<sup>+</sup> calcd for C<sub>28</sub>H<sub>28</sub>N<sub>5</sub>O<sub>4</sub>S 530.1862, found 530.1866.



### Isoroquefortine C (9)

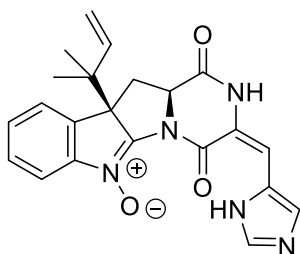
In a round-bottomed flask, roquefortine C (90 mg, 0.23 mmol) was dissolved in EtOH (90%, 100 mL) and degassed with argon for 15 minutes. The solution was then irradiated with a broad-spectrum UV light bulb (Exo-Terra UVB 200 Intense Compact Fluorescent Lamp, 26 W) under argon for 2 days. The reaction mixture was concentrated in vacuo, and the residue was purified by flash chromatography (95:5 CH<sub>2</sub>Cl<sub>2</sub>:CH<sub>3</sub>OH) to furnish isoroquefortine C (59 mg, 66%) as a pale yellow solid. <sup>1</sup>H NMR (500 MHz, CDCl<sub>3</sub>) δ 11.67 (s, 1H), 7.63 (s, 1H), 7.24 (s, 1H), 7.11 (m, 2H), 7.05 (t, *J* = 7.5 Hz, 1H), 6.71 (t, *J* = 7.5 Hz, 1H), 6.63 (s, 1H), 6.56 (d, *J* = 7.5 Hz, 1H), 5.94 (dd, *J* = 11.0, 17.5 Hz, 1H), 5.62 (s, 1H), 5.07 (m, 2H), 5.03 (s,

1H), 4.03 (dd,  $J = 6.0, 11.5$  Hz, 1H), 2.53 (dd,  $J = 6.0, 12.5$  Hz, 1H), 2.42 (t,  $J = 12.0$  Hz, 1H), 1.10 (s, 1H), 0.99 (s, 1H).  $^{13}\text{C}$  NMR (125 MHz,  $\text{CDCl}_3$ )  $\delta$  165.9, 158.5, 150.5, 143.6, 136.9, 135.8, 129.1, 128.9, 126.2, 125.3, 119.0, 118.2, 114.7, 109.2, 105.8, 78.1, 61.7, 59.2, 41.1, 37.4, 23.1, 22.6. IR (KBr): 3149, 2969, 1685, 1609, 1438, 1216, 1082, 748.31  $\text{cm}^{-1}$  (lit. (Joullié et al., 2002)<sup>41</sup> IR (KBr) 1680, 1630  $\text{cm}^{-1}$ ).  $\alpha_D^{22}$  -281.5146 (c 0.96,  $\text{CHCl}_3$ ) (lit. (Joullié et al., 2002)<sup>41</sup>  $\alpha_D^{20}$  -390 (c 0.05,  $\text{CHCl}_3$ )). HRMS (ESI-TOF):  $m/z$   $[\text{M} + \text{H}]^+$  calcd for  $\text{C}_{22}\text{H}_{23}\text{N}_5\text{O}_2$  390.1930, found 390.1932 (lit. (Joullié et al., 2002)<sup>41</sup> HRMS (ESI-TOF)  $m/z$   $[\text{M} + \text{H}]^+$  calcd for  $\text{C}_{22}\text{H}_{24}\text{N}_5\text{O}_2$  390.1930, found 390.1956).

#### **Enzymatic generation of roquefortine L and derivatives: General Information**

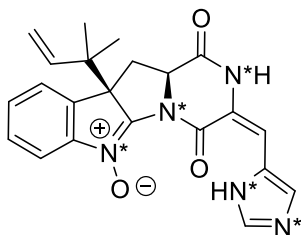
The biocatalytic reaction was set up as follows: 10  $\mu\text{M}$  OxaD (0.05 mg), 0.5 mM roquefortine C (20 mg), 5 mM NADH (382 mg), 10% DMSO, 50 mM Na/K/PO<sub>4</sub> pH 7.3, 10% glycerol, 1 mM EDTA. A 100 mL reaction was run in 10 mL aliquots in 9 dram glass vials for 2 hours at room temperature with mild agitation (100 rpm, orbital shaker). Solid NaCl was added to saturation and the reaction was extracted 3 times with an equal volume of EtOAc. Centrifugation at 1000 x  $g$  for 2 minutes in a swinging bucket centrifuge was necessary to break the emulsion which formed upon addition of solvent. The combined organic fractions were washed twice with an equal volume of saturated aqueous NaCl, dried over  $\text{Na}_2\text{SO}_4$ , concentrated by rotary evaporation, and placed under high vacuum to remove DMSO. The product was applied to a silica column equilibrated with 2%  $\text{Et}_3\text{N}$  in  $\text{CH}_2\text{Cl}_2$ , washed with  $\text{CH}_2\text{Cl}_2$ , followed by step-gradient elution with increasing  $i$ -PrOH (0-20%) in  $\text{CH}_2\text{Cl}_2$

to give the nitrone product as a pale yellow solid. The solid was dissolved in a minimal volume of HPLC grade EtOAc and triturated with HPLC grade hexanes in an ice bath. The resulting fine solid was precipitated via centrifuge, and pellets were washed three times with HPLC grade hexanes, vortexing vigorously before centrifuging. Residual EtOAc was removed by dissolving the pellets in a small volume of CCl<sub>4</sub>, concentrating via rotary evaporator to give a fluffy solid, and drying under reduced pressure overnight.



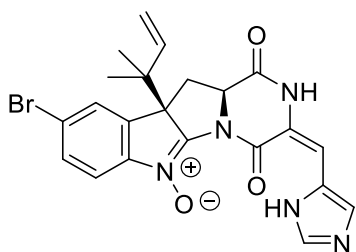
### Roquefortine L (17)

(86% conversion, 8 mg (40%) isolated yield). <sup>1</sup>H NMR (600 MHz, DMSO-d<sub>6</sub>/CDCl<sub>3</sub>) δ 10.69 (s, 1H), 7.75 (s, 1H), 7.60 (s, 1H), 7.58 (d, *J* = 8.0 Hz, 1H), 7.48 (m, 2H), 7.40 (t, *J* = 7.4 Hz; 1H), 6.53 (s, 1H), 5.76 (dd, *J* = 11.0, 17.3 Hz, 1H), 5.08 (dd, *J* = 3.7, 11.4 Hz, 1H), 5.03 (d, *J* = 11.4 Hz, 1H), 4.99 (s, 1H), 2.86 (dd, *J* = 3.8, 14.1 Hz, 1H), 2.21 (dd, *J* = 11.5, 13.6 Hz, 1H), 1.03 (s, 3H), 0.83 (s, 3H). <sup>13</sup>C NMR (150 MHz, CDCl<sub>3</sub>) δ 164.7, 156.4, 148.6, 146.8, 141.7, 138.0, 128.7, 128.3, 124.1, 121.6, 115.5, 114.5, 63.4, 27.9, 22.3, 22.2. IR (KBr): 2961.82, 1682.40, 1384.58, 1258.38, 1091.79, 1014.45, 794.80 cm<sup>-1</sup>. HRMS (ESI-TOF) *m/z* [M + H]<sup>+</sup> calcd for C<sub>22</sub>H<sub>22</sub>N<sub>5</sub>O<sub>3</sub> 404.1723, found 404.1727 (lit. (Vreeken et al., 2013)<sup>22</sup> HRMS (FTICR-MS) *m/z* [M + H]<sup>+</sup> calcd for C<sub>22</sub>H<sub>22</sub>N<sub>5</sub>O<sub>3</sub> 404.1723, found 404.1706).



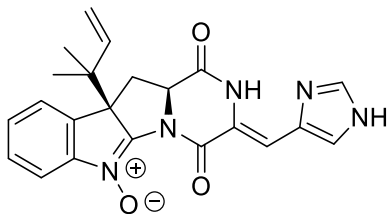
**Roquefortine L (17), <sup>15</sup>N enriched**

(93% conversion, 5 mg (21%) isolated yield). <sup>15</sup>N NMR (600 MHz, DMSO-d<sub>6</sub>/CDCl<sub>3</sub>) δ 282.3, 134.7, 126.9. HRMS (ESI-TOF) *m/z* [M + H]<sup>+</sup> calcd for C<sub>22</sub>H<sub>22</sub><sup>15</sup>N<sub>5</sub>O<sub>3</sub> 409.1574, found 409.1574.



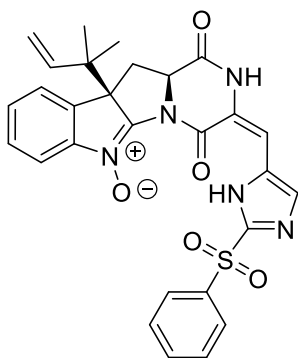
**11-Bromo-roquefortine L (44)**

(70% conversion, 5 mg (60%) isolated yield). <sup>1</sup>H NMR (500 MHz, CDCl<sub>3</sub>) δ 12.40 (s, 1H), 8.64 (br. s, 1H), 7.70, (s, 1H), 7.66 (d, *J* = 8.0 Hz, 1H), 7.06 (m, 2H), 7.34 (s, 1H), 6.44 (s, 1H), 5.81 (dd, *J* = 10.5, 17.5 Hz, 1H), 5.16 (d, *J* = 11.0 Hz, 1H), 5.12 (s, 1H), 5.03 (m, 1H), 3.05 (dd, *J* = 3.5, 14.0 Hz, 1H), 2.29 (t, *J* = 12.5 Hz, 1H), 1.15 (s, 1H), 0.99 (s, 1H). <sup>13</sup>C NMR (125 MHz, CDCl<sub>3</sub>) δ 165.1, 157.6, 148.1, 143.6, 141.6, 140.2, 138.1, 135.7, 132.9, 129.5, 127.9, 125.4, 123.3, 119.4, 117.5, 115.0, 63.9, 59.0, 43.9, 23.1, 23.0. HRMS (ESI-TOF) *m/z* [M + H]<sup>+</sup> calcd for C<sub>22</sub>H<sub>21</sub><sup>79</sup>BrN<sub>5</sub>O<sub>3</sub> 482.0828, found 482.0833.



### Isoroquefortine L (43)

(81% conversion, 10 mg (52%) isolated yield).  $^1\text{H}$  NMR (500 MHz,  $\text{CDCl}_3$ )  $\delta$  11.92 (br. s, 1H), 11.71 (br. s, 1H), 7.77 (m, 2H), 7.51 (m, 2H), 7.42 (m, 2H), 6.92 (s, 1H), 5.82 (dd,  $J = 11.0, 16.5$  Hz, 1H), 5.12 (m, 2H), 5.03 (m, 1H), 3.06 (dd,  $J = 3.5, 14.0$  Hz, 1H), 2.25 (t,  $J = 11.5$  Hz, 1H), 1.12 (s, 1H), 0.88 (s, 1H).  $^{13}\text{C}$  NMR (125 MHz,  $\text{CDCl}_3$ )  $\delta$  163.8, 156.9, 150.1, 149.2, 141.8, 138.1, 136.7, 136.5, 129.5, 129.0, 128.8, 124.6, 124.5, 120.7, 117.1, 115.8, 109.4, 64.3, 29.3, 44.0, 25.2, 22.9. HRMS (ESI-TOF)  $m/z$   $[\text{M} + \text{H}]^+$  calcd for  $\text{C}_{22}\text{H}_{22}\text{N}_5\text{O}_3$  404.1723, found 404.1720.

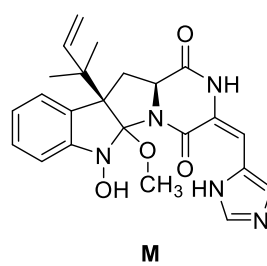
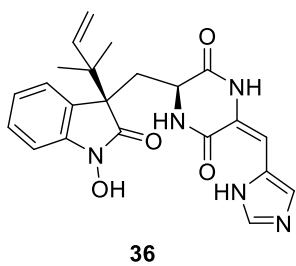
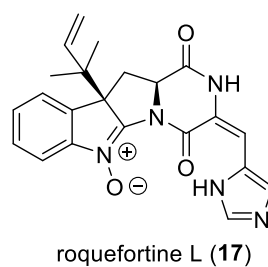
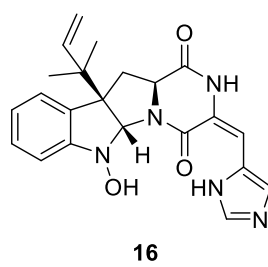
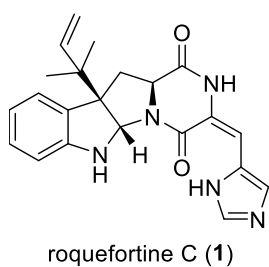
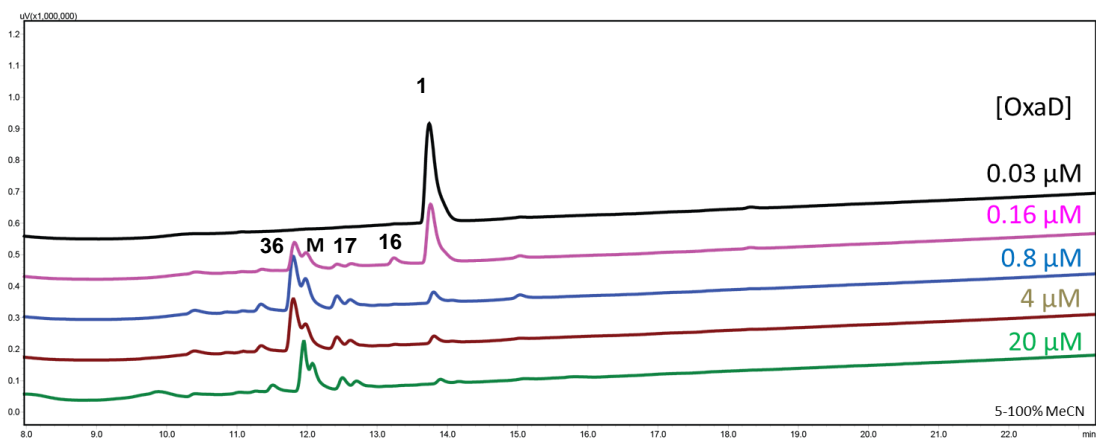


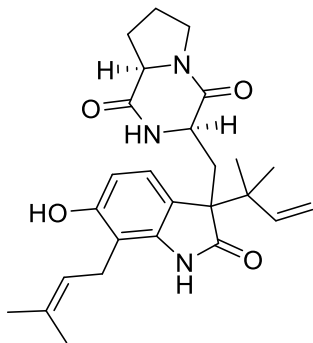
### 20-Phenylsulfonylroquefortine L (46)

(90% conversion, 11 mg (42%) isolated yield).  $^1\text{H}$  NMR (500 MHz,  $\text{CDCl}_3$ )  $\delta$  9.14 (s, 1H), 8.64 (s, 1H), 8.02 (m, 2H), 7.74 (d,  $J = 7.5$  Hz, 1H), 7.65 (t,  $J = 7.0$  Hz, 1H), 7.56 (m, 2H), 7.51 (t,  $J = 12.5$  Hz, 1H), 7.42 (m, 2H), 6.55 (s, 1H), 5.81 (dd,  $J = 10.5, 17.5$  Hz, 1H), 5.10 (d,  $J = 4.5$  Hz, 1H), 5.08 (s, 1H), 4.96 (d,  $J = 11.0$  Hz, 1H),

3.03 (dd,  $J = 3.5, 14.5$  Hz, 1H), 2.23 (t,  $J = 11.0$  Hz, 1H), 1.13 (s, 1H), 0.88 (s, 1H).  
 $^{13}\text{C}$  NMR (125 MHz,  $\text{CDCl}_3$ )  $\delta$  165.9, 155.5, 149.2, 148.2, 142.2, 138.6, 137.9,  
137.1, 136.4, 135.1, 130.1, 129.6, 128.9, 127.9, 125.2, 124.5, 120.9, 117.3, 117.0,  
116.1, 64.1, 58.9, 43.8, 25.6, 23.2, 22.8. HRMS (ESI-TOF)  $m/z$   $[\text{M} + \text{H}]^+$  calcd for  
 $\text{C}_{28}\text{H}_{26}\text{N}_5\text{O}_5\text{S}$  544.1655, found 544.1655.

## Supplementary Figure 2.1: OxaD reaction products





### Enzymatic conversion of notoamide S (50)

Notoamide S (**50**) was synthesized as previously described.<sup>42</sup> Notoamide S (**50**) (6 mg) was subjected to the same biocatalytic reaction conditions that were used for the roquefortine C derivatives and extracted in the same manner. The extracted material was purified by HPLC on a Waters XBridge Prep Phenyl 5  $\mu\text{m}$  (10 x 250 mm) column using isocratic separation (33% acetonitrile in water) at flow rate of 4 mL/min.  $^1\text{H}$  NMR (700 MHz,  $\text{DMSO-}d_6$ )  $\delta$  10.67 (s, 1H), 8.51 (s, 1H), 6.73 (d,  $J = 8.1$  Hz, 1H), 6.65 (s, 1H), 6.38 (d,  $J = 8.0$  Hz, 1H), 6.01 (dd,  $J = 17.5, 10.8$  Hz, 1H), 5.11 (t,  $J = 6.4$  Hz, 1H), 5.06 (d,  $J = 10.9$  Hz, 1H), 4.96 (d,  $J = 17.4$  Hz, 1H), 4.05 (t,  $J = 7.9$  Hz, 1H), 3.3 (m, 2H), 3.2 (m, 2H), 3.18 (m, 2H), 2.86 (d,  $J = 14.5$  Hz, 1H), 2.00 (m, 2H), 1.79 (m, 2H), 1.68 (s, 3H), 1.60 (s, 3H), 1.87 (s, 3H), 0.94 (s, 3H).  $^{13}\text{C}$  NMR (175 MHz,  $\text{DMSO-}d_6$ )  $\delta$  182.3, 165.6, 165.4, 155.6, 143.2, 142.3, 130.7, 123.1, 122.5, 119.2, 112.9, 110.5, 107.5, 57.8, 56.5, 51.6, 44.7, 30.2, 27.1, 25.2, 23.1, 21.7, 17.5 (obtained from HSQC/HMBC). HRMS (ESI-TOF)  $m/z$   $[\text{M} + \text{H}]^+$  calcd for  $\text{C}_{26}\text{H}_{34}\text{N}_3\text{O}_4$  452.2544, found 452.2545.

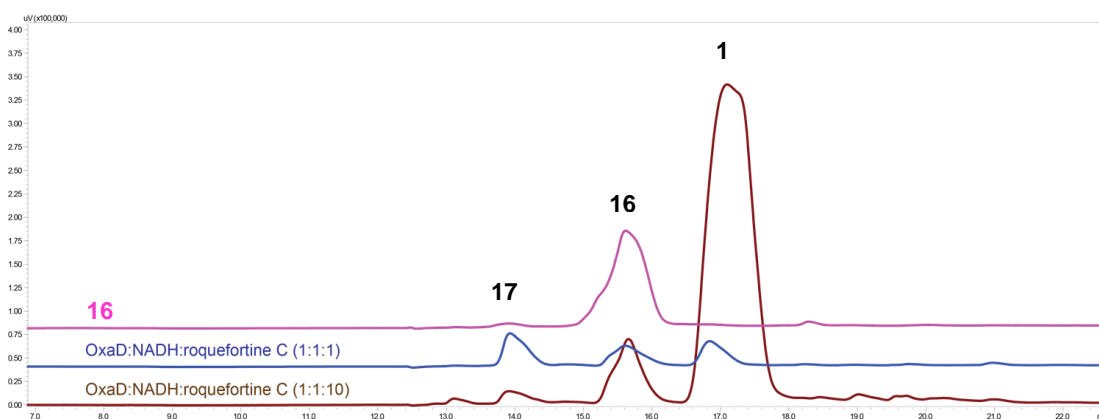
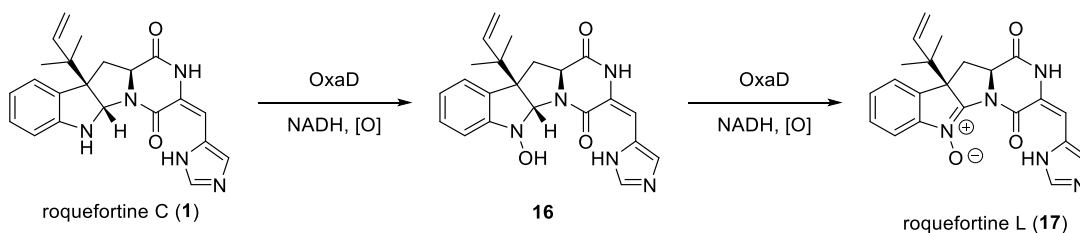


### Single turnover studies with OxaD

Single turnover reactions were set up with 120  $\mu\text{M}$  OxaD, 100  $\mu\text{M}$  NADH, 110  $\mu\text{M}$  or 1 mM roquefortine C, 10% DMSO, 50 mM Na/K/PO<sub>4</sub> pH 7.3, 10% glycerol, 1 mM EDTA and run for 4 minutes at room temperature. The reactions were quenched by extraction using EtOAc/saturated aqueous NaCl and analyzed by LC-MS, in which the intermediates were resolved using a linear gradient of 5-100% CH<sub>3</sub>CN in H<sub>2</sub>O over 20 minutes (0.3 mL/min flow rate) on an Agilent Extend C18 column (4.6x150 mm, 5  $\mu\text{m}$ ).

Standards for the roquefortine C hydroxylamine (**16**) were generated by reduction of roquefortine L (**17**) using 5 equivalents NaBH<sub>4</sub> in CH<sub>3</sub>OH. The reduction was run for 15 minutes at room temperature and quenched using an equal volume deionized water to give **16** as a single stereoisomer. <sup>1</sup>H NMR (500 MHz, CD<sub>3</sub>OD)  $\delta$  7.74 (s, 1H), 7.30 (s, 1H), 7.25 (d,  $J = 8$  Hz, 1H), 7.21 (t,  $J = 8$  Hz, 1H), 6.96 (t,  $J = 7.5$  Hz, 1H), 6.90 (d,  $J = 7.5$  Hz, 1H), 6.36 (s, 1H), 5.99 (dd,  $J = 6.5, 11$  Hz, 1H), 5.89 (s, 1H), 5.09 (m, 2H), 3.98 (t,  $J = 8.5$  Hz, 1H), 2.41 (m, 2H), 1.08 (s, 1H), 0.95 (s, 1H). <sup>13</sup>C NMR (125 MHz, CD<sub>3</sub>OD)  $\delta$  168.0, 159.8, 154.2, 145.0, 137.7, 131.8, 130.3, 126.0, 125.0, 124.4, 119.7, 115.9, 115.3, 111.1, 110.2, 87.9, 62.3, 59.7, 42.5, 40.1, 24.3, 23.5. HRMS (ESI-TOF)  $m/z$  [M + H]<sup>+</sup> calcd for C<sub>22</sub>H<sub>24</sub>N<sub>5</sub>O<sub>3</sub> 406.1879, found 406.1890.

## Supplementary Figure 2.2: OxaD single turnover reactions



## Steady state kinetics of OxaD with roquefortine C

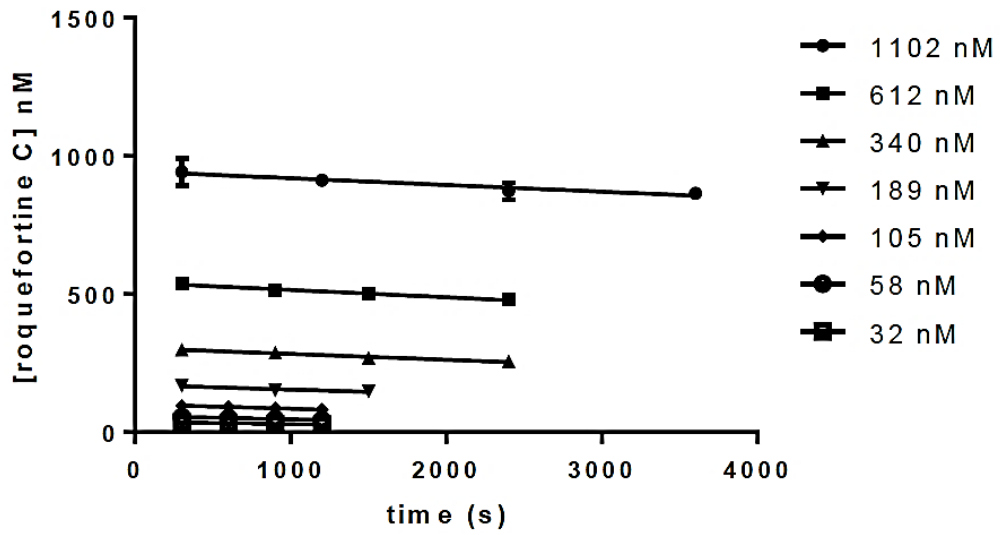
Initial experiments which sought to determine kinetic constants in a continuous spectrophotometric assay by following the oxidation of NADH at 340 nm were hampered by the low  $K_M$  for roquefortine C. Similarly, direct HPLC analysis could not achieve the sensitivity required to detect initial velocities at nanomolar concentrations of roquefortine C. The steady state kinetic constants of OxaD with roquefortine C were ultimately determined using an HPLC-based assay following a lyophilization step to concentrate the enzymatic reactions prior to analysis. Reactions were initiated by the addition of 100  $\mu\text{L}$  of varied concentrations of roquefortine C in 100% DMSO to 4.1 mL of 1.6 nM OxaD, 200  $\mu\text{M}$  NADH, 50 mM

Na/K/PO4 pH 7.4, 1 mM EDTA at room temperature (23 °C). 1.0 mL aliquots were quenched by plunging into liquid N<sub>2</sub> at various time points (5-60 min) to achieve less than 20% substrate consumption over the reaction time course. Four time points were taken in each time course. All reactions were performed in duplicate. The frozen aliquots were lyophilized to dryness over 24 hours and resuspended in 80 µL CH<sub>3</sub>OH. The resuspended samples were analyzed by HPLC in which the reaction mixture was resolved using a linear gradient of 15-65% CH<sub>3</sub>CN in dd H<sub>2</sub>O + 0.1% formic acid over 6 minutes (2.5 mL/min flow rate) on a ZORBAX SB-Phenyl column (4.6x150 mm, 5 µm) at 35 °C column oven temperature. Initial velocities were determined by the loss of roquefortine C signal and quantified using a standard curve for the substrate. The product signals were often below the UV detection limit at low substrate concentrations, and additionally the nitron product was prone to hydrolysis and CH<sub>3</sub>OH addition, giving rise to multiple product peaks. Initial velocities were plotted against substrate concentration (Supplementary Figure 2.3) and fit by non-linear regression to the Michaelis-Menten equation (Supplementary Figure 2.4) using GraphPad Prism Version 6.01 software to determine the kinetic constants  $k_{cat}$  and  $K_M$  (Supplementary Table 2.4).

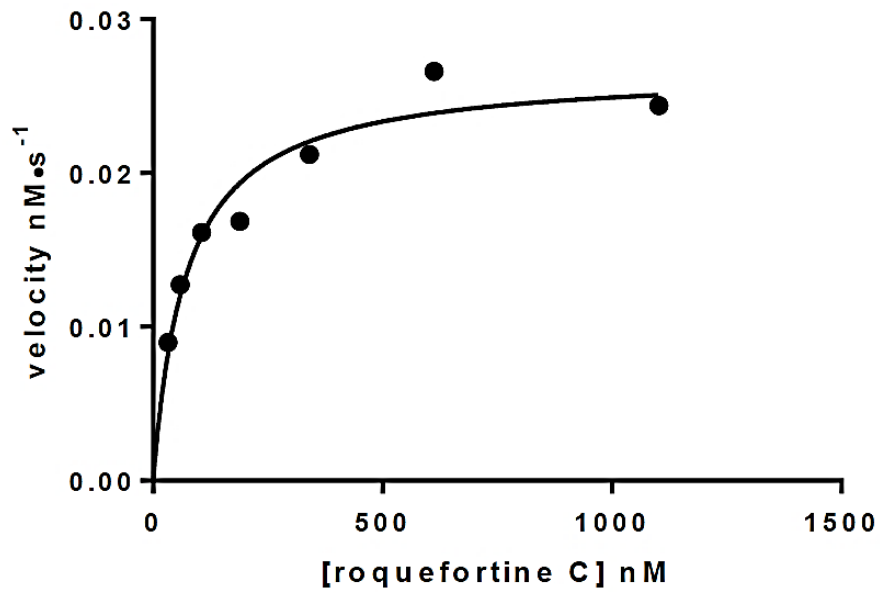
**Supplementary Table 2.4:** Steady state kinetics of OxaD with roquefortine C

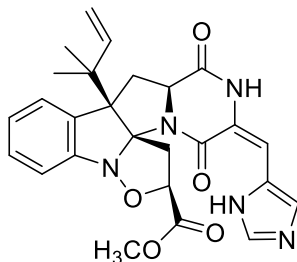
Enzyme	Substrate	$k_{cat}$ (s <sup>-1</sup> )	$K_M$ (nM)	$k_{cat}/K_M$ (M <sup>-1</sup> s <sup>-1</sup> )
OxaD	Roquefortine C	0.017 ± 0.001	71 ± 15	2.3 x 10 <sup>5</sup>

Supplementary Figure 2.3: OxaD Initial Velocity



Supplementary Figure 2.4: OxaD Michaelis-Menten Plot





### 1,3-Dipolar cycloaddition of roquefortine L (17) with methyl acrylate

Roquefortine L (**17**) was generated as above with the omission of the silica gel flash chromatography step as the <sup>1</sup>H NMR for the crude product of the biocatalytic reaction showed >90% purity with trace amounts of **1** and the nitron hydrolysis product. After enzymatic conversion and extraction, ~20 mg of **17** was dried overnight under high vacuum in a 25 mL round-bottomed flask. To the dried material 10 mL of dry THF and 1 mL methyl acrylate were added, the flask was quickly purged with vacuum/dry nitrogen using a Schlenk line and left under positive pressure of nitrogen. The reaction was run in the dark at 45 °C for 60 hours without stirring. The material was evaporated to dryness and purified on silica using CH<sub>2</sub>Cl<sub>2</sub>:CH<sub>3</sub>OH (0-12% CH<sub>3</sub>OH step-gradient) as the mobile phase. This material was subjected to further purification on C18 reverse phase HPLC chromatography to give the cycloadduct **38** (84% conversion, 24% yield) as a pale brown solid. <sup>1</sup>H NMR (600 MHz, CHCl<sub>3</sub>) δ 8.50 (s, 1H), 7.87 (s, 1H), 7.39 (d, *J* = 7.7 Hz, 2H), 7.30 (m, 3H), 7.18 (td, *J* = 1.3, 7.9 Hz, 1H), 6.41 (s, 1H), 6.16 (dd, *J* = 11.0, 17.3 Hz, 1H), 5.66 (t, *J* = 7.9, 1H), 5.15 (s, 1H), 5.11 (d, *J* = 8.6 Hz, 1H), 4.13 (t, *J* = 8.5 Hz, 1H), 3.73 (s, 3H), 3.36 (dd, *J* = 8.9, 13.8 Hz, 1H), 3.23 (dd, *J* = 7.0, 13.7 Hz, 1H), 2.90 (dd, *J* = 9.5, 13.6 Hz, 1H), 2.47 (dd, *J* = 8.1, 13.3 Hz, 1H), 1.31

(s, 3H), 1.26 (s, 3H).  $^{13}\text{C}$  NMR (150 MHz,  $\text{CHCl}_3$ )  $\delta$  170.3, 167.4, 160.4, 148.0, 144.5, 136.9, 135.3, 134.4, 129.2, 126.5, 125.3, 125.1, 121.8, 120.0, 113.8, 112.3, 101.3, 80.0, 62.8, 57.0, 52.4, 41.9, 36.3, 35.9, 21.0. HRMS (ESI-TOF)  $m/z$   $[\text{M} + \text{H}]^+$  calcd for  $\text{C}_{26}\text{H}_{28}\text{O}_5\text{N}_5$  490.2085, found 490.2097.

### **Total turnover number calculation**

Total turnover numbers (TTN = mol product/mol enzyme) were calculated in triplicate for all derivatives using 250  $\mu\text{M}$  substrate in 50 mM Na/K/ $\text{PO}_4$  pH 7.3, 10% glycerol, 1 mM EDTA. The OxaD concentration was 40 nM for substrates **1**, **9**, **39**; 80 nM for substrates **41**, **42**; and 320 nM for substrate **40**, and the reactions were performed in 10% and 20% DMSO cosolvent. The reactions were run overnight at room temperature and analyzed by HPLC, in which products were resolved using a linear gradient of 5-100%  $\text{CH}_3\text{CN}$  in  $\text{H}_2\text{O}$  over 11 minutes (1.5 mL/min flow rate) on an Agilent Extend C18 column (4.6x150 mm, 5  $\mu\text{m}$ ). Moles of product formed in the assay were inferred by substrate consumption, which was quantified from standard curves of the respective substrate generated using the same separation method.

## **VI. References**

- (1) Baran, P. S.; Guerrero, C. A.; Hafensteiner, B. D.; Ambhaikar, N. B. *Angew. Chem. Int. Ed.* **2005**, *44*(25), 3892-3895.
- (2) Ideguchi, T.; Yamada, T.; Shirahata, T.; Hirose, T.; Sugawara, A.; Kobayashi, Y.; Omura, S.; Sunazuka, T. *J. Am. Chem. Soc.* **2013**, *135*(34), 12568-12571.

- (3) Hafensteiner, B. D.; Escribano, M.; Petricci, E.; Baran, P. S. *Bioorg. Med. Chem. Lett.* **2009**, *19*(14), 3808-3810.
- (4) Fenical, W.; Jensen, P. R.; Cheng, X. C., Avrainvillamide, a cytotoxic marine natural product, and derivatives thereof. U.S. Patent 6,066,635, May 23, 2000.
- (5) Wang, X. R.; You, J. L.; King, J. B.; Powell, D. R.; Cichewicz, R. H. *J. Nat. Prod.* **2012**, *75*(4), 707-715.
- (6) Peng, J. X.; Gao, H. Q.; Li, J.; Ai, J.; Geng, M. Y.; Zhang, G. J.; Zhu, T. J.; Gu, Q. Q.; Li, D. H. *J. Org. Chem.* **2014**, *79*(17), 7895-7904.
- (7) Sugie, Y.; Hirai, H.; Inagaki, T.; Ishiguro, M.; Kim, Y. J.; Kojima, Y.; Sakakibara, T.; Sakemi, S.; Sugiura, A.; Suzuki, Y.; Brennan, L.; Duignan, J.; Huang, L. H.; Sutcliffe, J.; Kojima, N. *J. Antibiot. (Tokyo)* **2001**, *54*(11), 911-916.
- (8) Qian-Cutrone, J.; Huang, S.; Shu, Y. Z.; Vyas, D.; Fairchild, C.; Menendez, A.; Krampitz, K.; Dalterio, R.; Klohr, S. E.; Gao, Q. *J. Am. Chem. Soc.* **2002**, *124*(49), 14556-14557.
- (9) von Nussbaum, F. *Angew. Chem. Int. Ed.* **2003**, *42*(27), 3068-3071.
- (10) Wulff, J. E.; Siegrist, R.; Myers, A. G. *J. Am. Chem. Soc.* **2007**, *129*(46), 14444-14451.
- (11) Wulff, J. E.; Herzon, S. B.; Siegrist, R.; Myers, A. G. *J. Am. Chem. Soc.* **2007**, *129*(16), 4898-4899.

- (12) Mikkola, R.; Andersson, M. A.; Hautaniemi, M.; Salkinoja-Salonen, M. S. *Toxicol* **2015**, *99*, 58-67.
- (13) Herzon, S. B.; Myers, A. G. *J. Am. Chem. Soc.* **2005**, *127*(15), 5342-5344.
- (14) Artman, G. D.; Grubbs, A. W.; Williams, R. M. *J. Am. Chem. Soc.* **2007**, *129*(19), 6336-6342.
- (15) Kadlubar, F. F.; McKee, E. M.; Ziegler, D. M. *Arch. Biochem. Biophys.* **1973**, *156*, 46-57.
- (16) Bondon, A.; Macdonald, T. L.; Harris, T. M.; Guengerich, F. P. *J. Biol. Chem.* **1989**, *264*(4), 1988-1997.
- (17) Cashman, J. R.; Yang, Z.-c.; Hogberg, T. *Chem. Res. Toxicol.* **1990**, *3*, 428-432.
- (18) Clement, B.; Lustig, K. L.; Ziegler, D. M. *Drug Metab. Dispos.* **1993**, *21*(1), 24-29.
- (19) Rodriguez, R. J.; Proteau, P. J.; Marquez, B. L.; Hetherington, C. L.; Buckholz, C. J.; O'Connell, K. L. *Drug Metab. Dispos.* **1999**, *27*(8), 880-886.
- (20) Sun, H.; Ehlhardt, W. J.; Kulanthaivel, P.; Lanza, D. L.; Reilly, C. A.; Yost, G. *S. J. Pharmacol. Exp. Ther.* **2007**, *322*(2), 843-851.

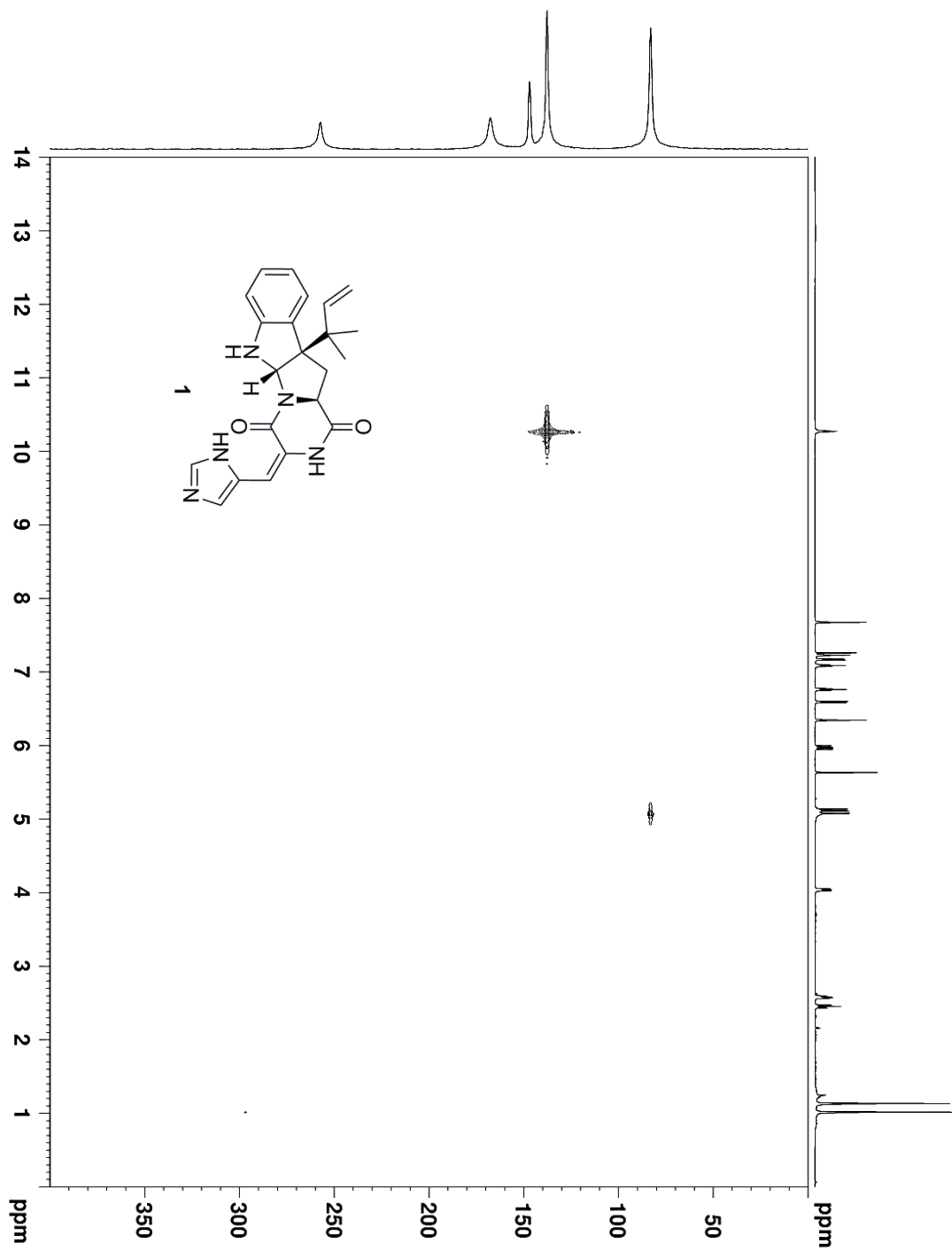


- (21) García-Estrada, C.; Ullán, R. V.; Albillos, S. M.; Fernández-Bodega, M. A.; Durek, P.; von Döhren, H.; Martín, J. F. *Chem. Biol.* **2011**, *18*(11), 1499-1512.
- (22) Ries, M. I.; Ali, H.; Lankhorst, P. P.; Hankemeier, T.; Bovenberg, R. A.; Driessen, A. J.; Vreeken, R. J. *J. Biol. Chem.* **2013**, *288*(52), 37289-37295.
- (23) Ali, H.; Ries, M. I.; Nijland, J. G.; Lankhorst, P. P.; Hankemeier, T.; Bovenberg, R. A.; Vreeken, R. J.; Driessen, A. J. *PLoS ONE* **2013**, *8*(6), e65328.
- (24) Gober, C.; Joullie, M. M. *Athens Journal of Science* **2015**, *3*(4), 257-264.
- (25) Shindo, H.; Umezawa, B. *Chem. Pharm. Bull. (Tokyo)* **1962**, *10*, 492-503.
- (26) Cashman, J. R.; Xiong, Y. N.; Xu, L.; Janowsky, A. *J. Pharmacol. Exp. Ther.* **1999**, *288*(3), 1251-1260.
- (27) Sustmann, R.; Trill, H. *Angew. Chem. Int. Ed.* **1972**, *11*(9), 838-&.
- (28) Williamson, K. S.; Michaelis, D. J.; Yoon, T. P. *Chem. Rev.* **2014**, *114*(16), 8016-8036.
- (29) Padwa, A.; Koehler, K. F. *Heterocycles* **1986**, *24*(2), 611–615.
- (30) Scott, P. M.; Polonsky, J.; Merrien, M. A. *J. Agric. Food Chem.* **1979**, *27*(1), 201-202.
- (31) da Silva, J. V.; Fill, T. P.; Lotufo, L. V.; do Ó. Pessoa, C.; Rodrigues-Filho, E. *Helv. Chim. Act.* **2014**, *97*, 1345-1353.

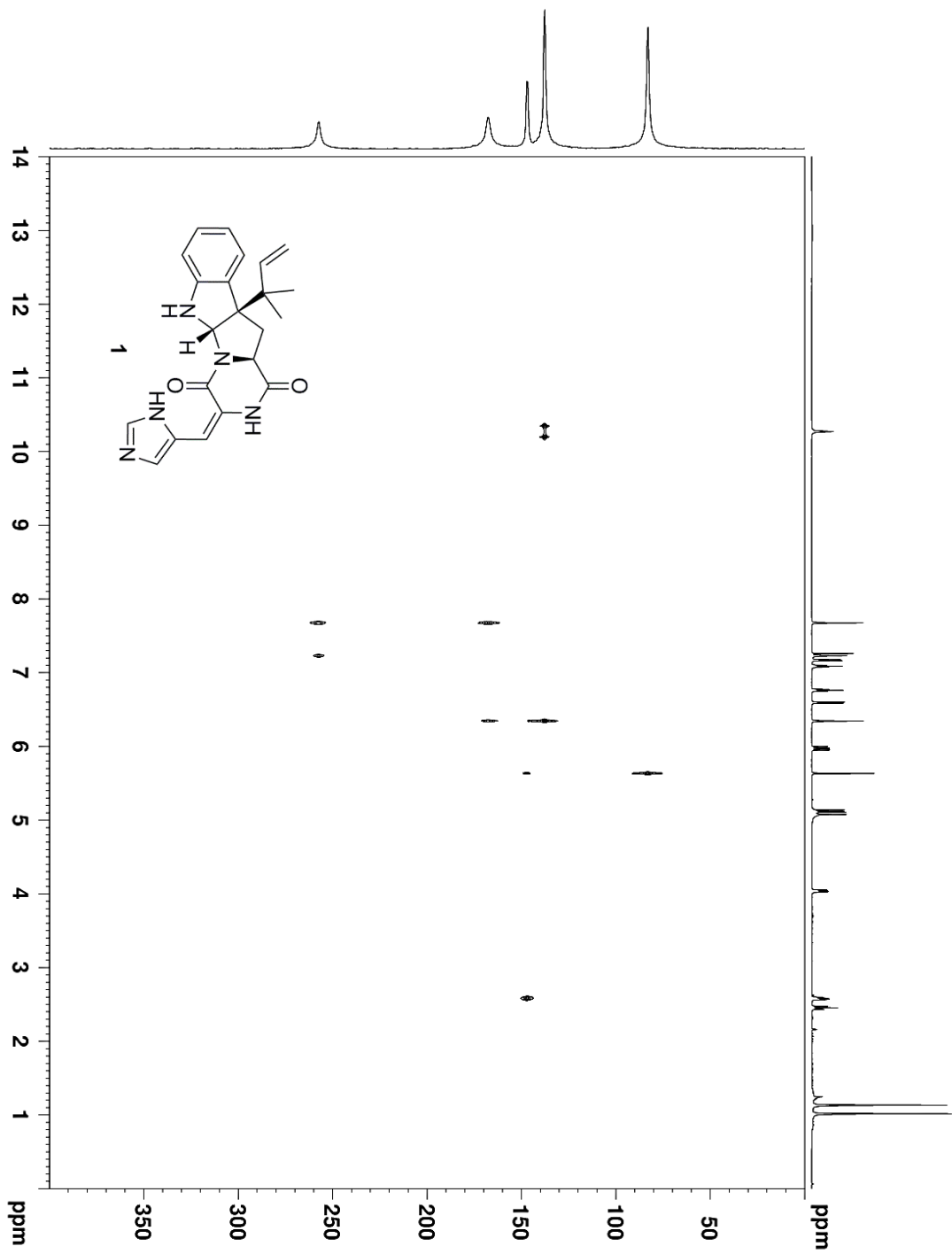
- (32) Tang, P.; Furuya, T.; Ritter, T. *J. Am. Chem. Soc.* **2010**, *132*, 12150-12154.
- (33) Roy, A.; Schneller, S. W. *Org. Lett.* **2005**, *7*(18), 3889-3891.
- (34) Nising, C. F. *Chem. Soc. Rev.* **2010**, *39*(2), 591-599.
- (35) Li, S.; Finefield, J. M.; Sunderhaus, J. D.; McAfoos, T. J.; Williams, R. M.; Sherman, D. H. *J. Am. Chem. Soc.* **2012**, *134*(2), 788-791.
- (36) Trimble, L. A.; Sumarah, M. W.; Blackwell, B. A.; Wrona, M. D.; Miller, J. D. *Tetrahedron Lett.* **2012**, *53*(8), 956-958.
- (37) Shan, W. G.; Ying, Y. M.; Yu, H. N.; Liu, W. H.; Zhan, Z. J. *Helv. Chim. Act.* **2010**, *93*(4), 772-776.
- (38) Kozlovsky, A. G.; Vinokurova, N. G.; Reshetilova, T. A.; Sakharovsky, V. G.; Baskunov, B. P.; Seleznyov, S. G. *Prikl. Biokhim. Mikrobiol.* **1994**, *30*(3), 410-414.
- (39) Overy, D. P.; Nielsen, K. F.; Smedsgaard, J. *J. Chem. Ecol.* **2005**, *31*(10), 2373-2390.
- (40) Ouchaou, K.; Maire, F.; Salo, O.; Ali, H.; Hankemeier, T.; van der Marel, G. A.; Filippov, D. V.; Bovenberg, R. A.; Vreeken, R. J.; Driessen, A. J.; Overkleeft, H. S. *ChemBioChem* **2015**, *16*(6), 915-923.
- (41) Schiavi, B. M.; Richard, D. J.; Joullié, M. M. *J. Org. Chem.* **2002**, *67*(3), 620-624.

(42) McAfoos, T. J.; Li, S.; Tsukamoto, S.; Sherman, D. H.; Williams, R. M.  
*Heterocycles* **2010**, *82*(1), 461-472.

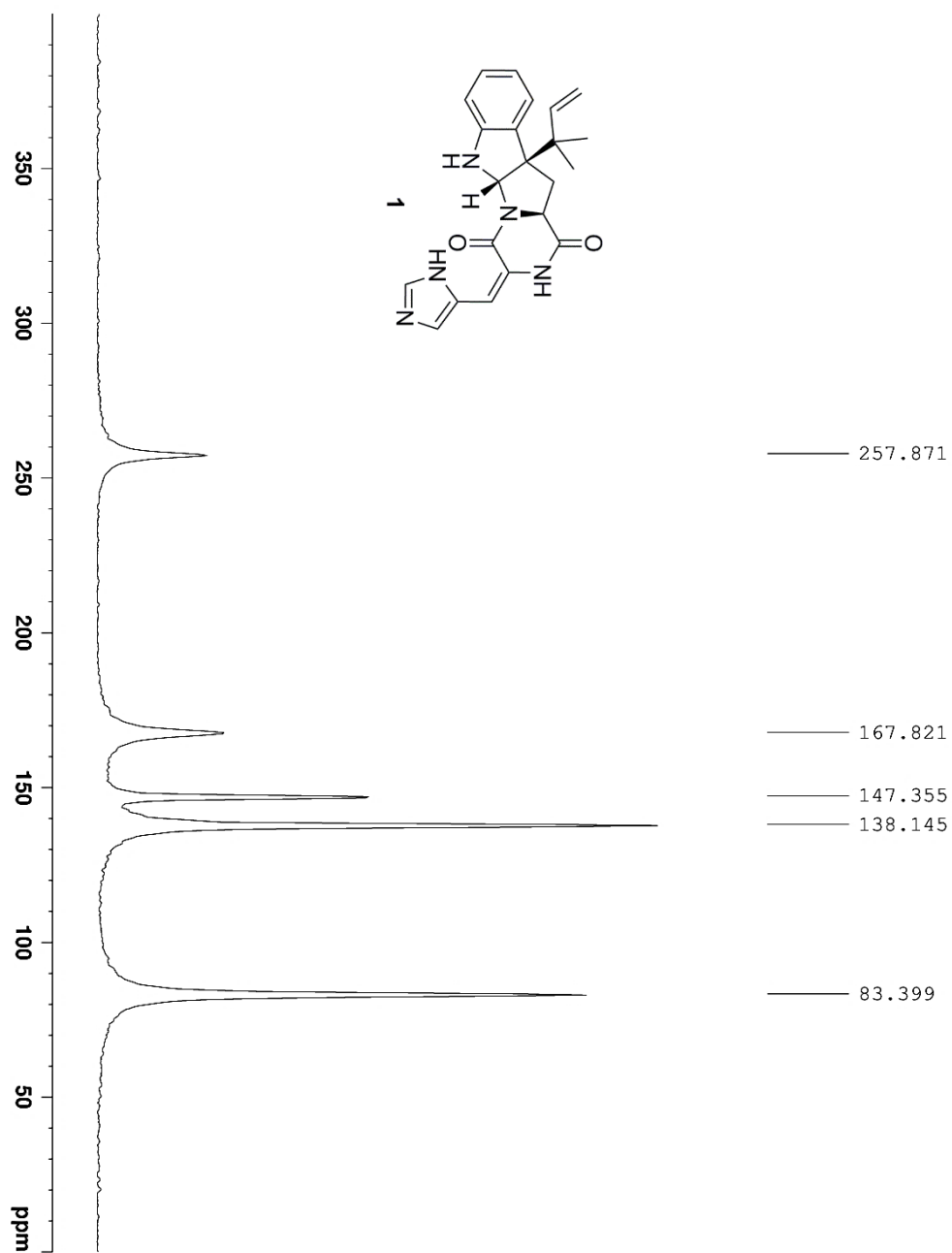
## **Appendix 2A: Spectra Relevant to Chapter 2**



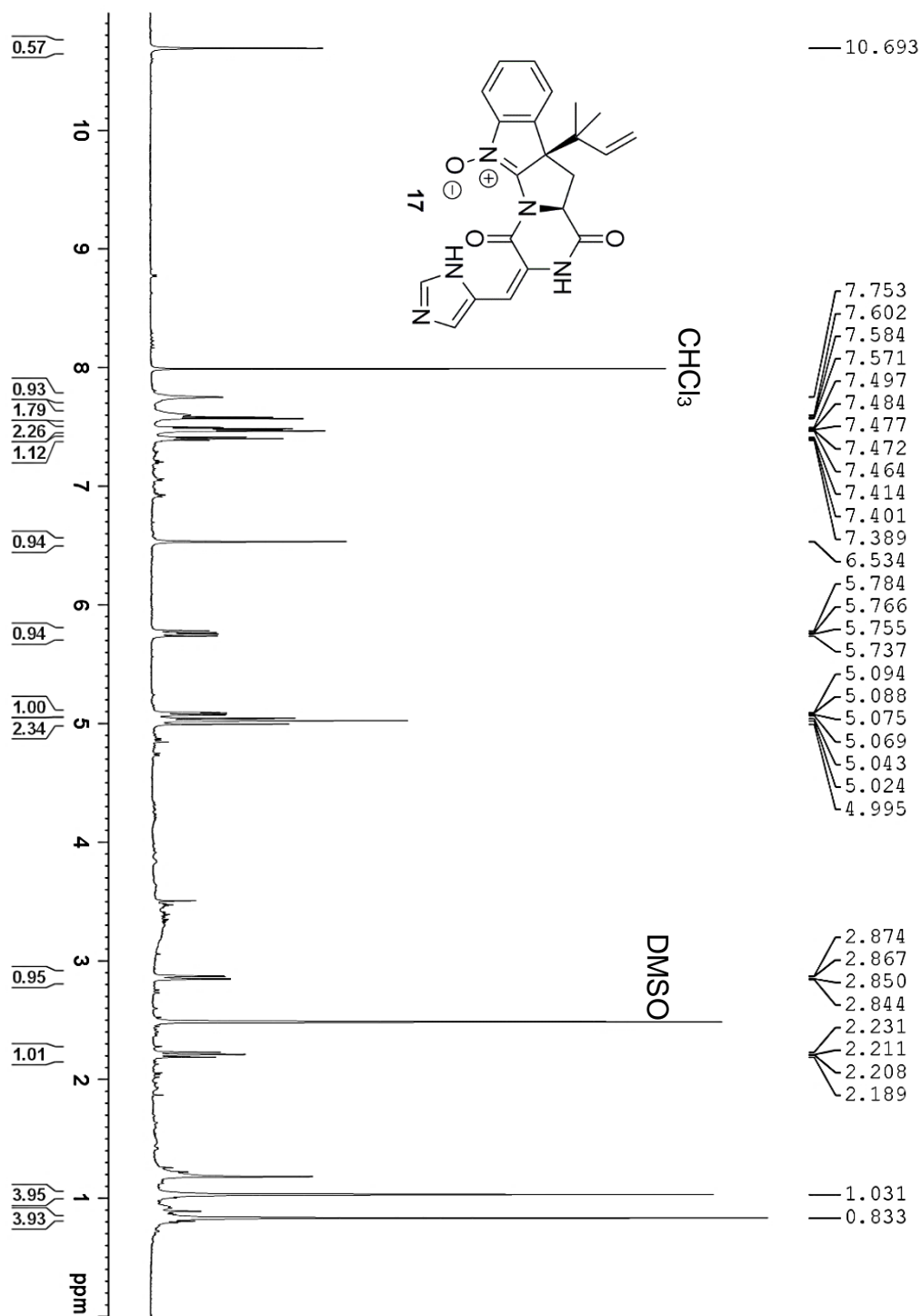
Supplementary Figure 2.5:  $^1\text{H}$ - $^{15}\text{N}$  HMQC NMR (600 MHz,  $\text{CDCl}_3$ ) Spectrum of **1**



**Supplementary Figure 2.6:**  $^1\text{H}$ - $^{15}\text{N}$  HMBC NMR (600 MHz,  $\text{CDCl}_3$ ) Spectrum of **1**

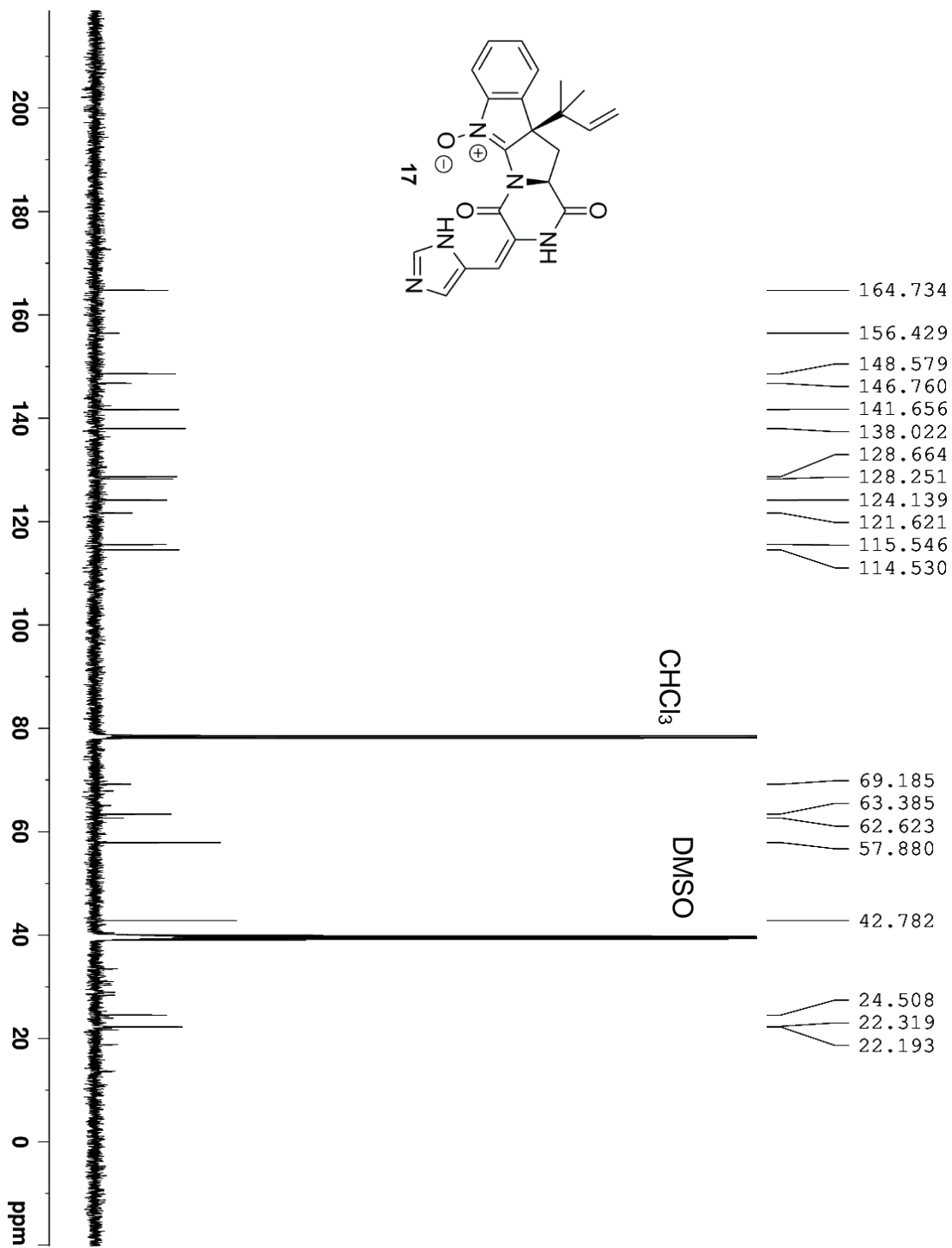


Supplementary Figure 2.7:  $^{15}\text{N}$  NMR (500 MHz,  $\text{CDCl}_3$ ) Spectrum of **1**



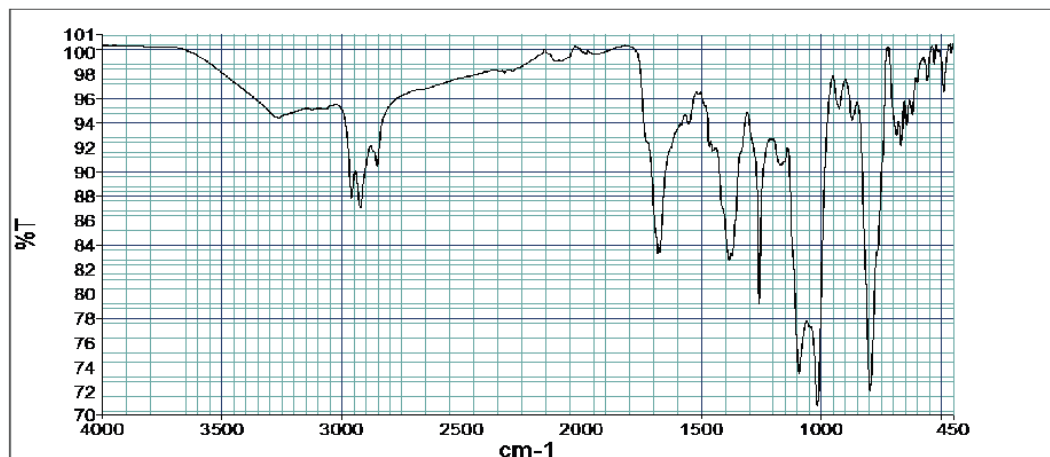
Supplementary Figure 2.8: <sup>1</sup>H NMR (600 MHz, DMSO-d<sub>6</sub>/CDCl<sub>3</sub>) Spectrum of 17





Supplementary Figure 2.9: <sup>13</sup>C NMR (150 MHz, DMSO-d<sub>6</sub>/CDCl<sub>3</sub>) Spectrum of 17

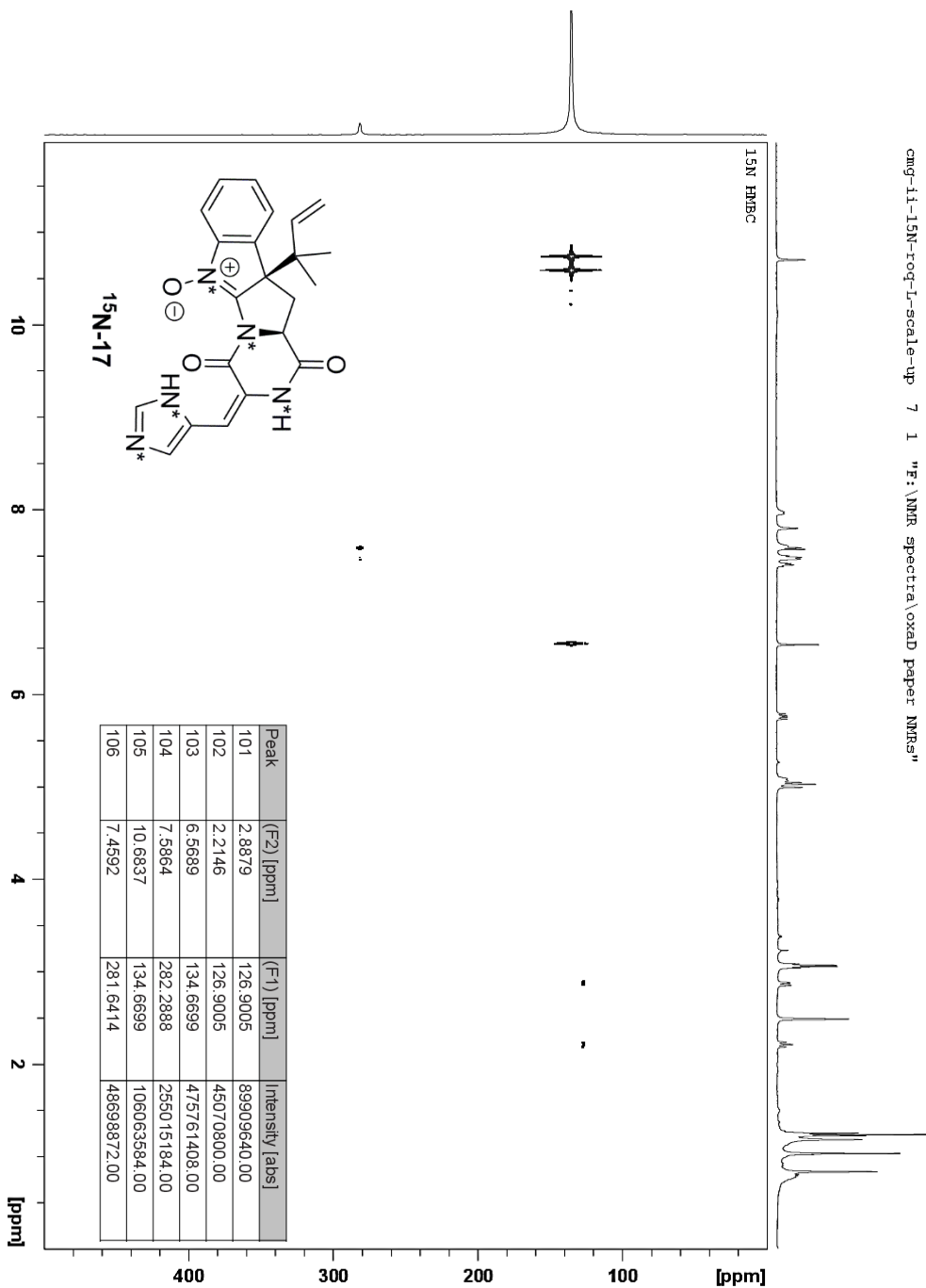
Supplementary Figure 2.10: IR Spectrum of 17



Spectrum Obtained on a Perkin Elmer Spectrum Two FT-IR

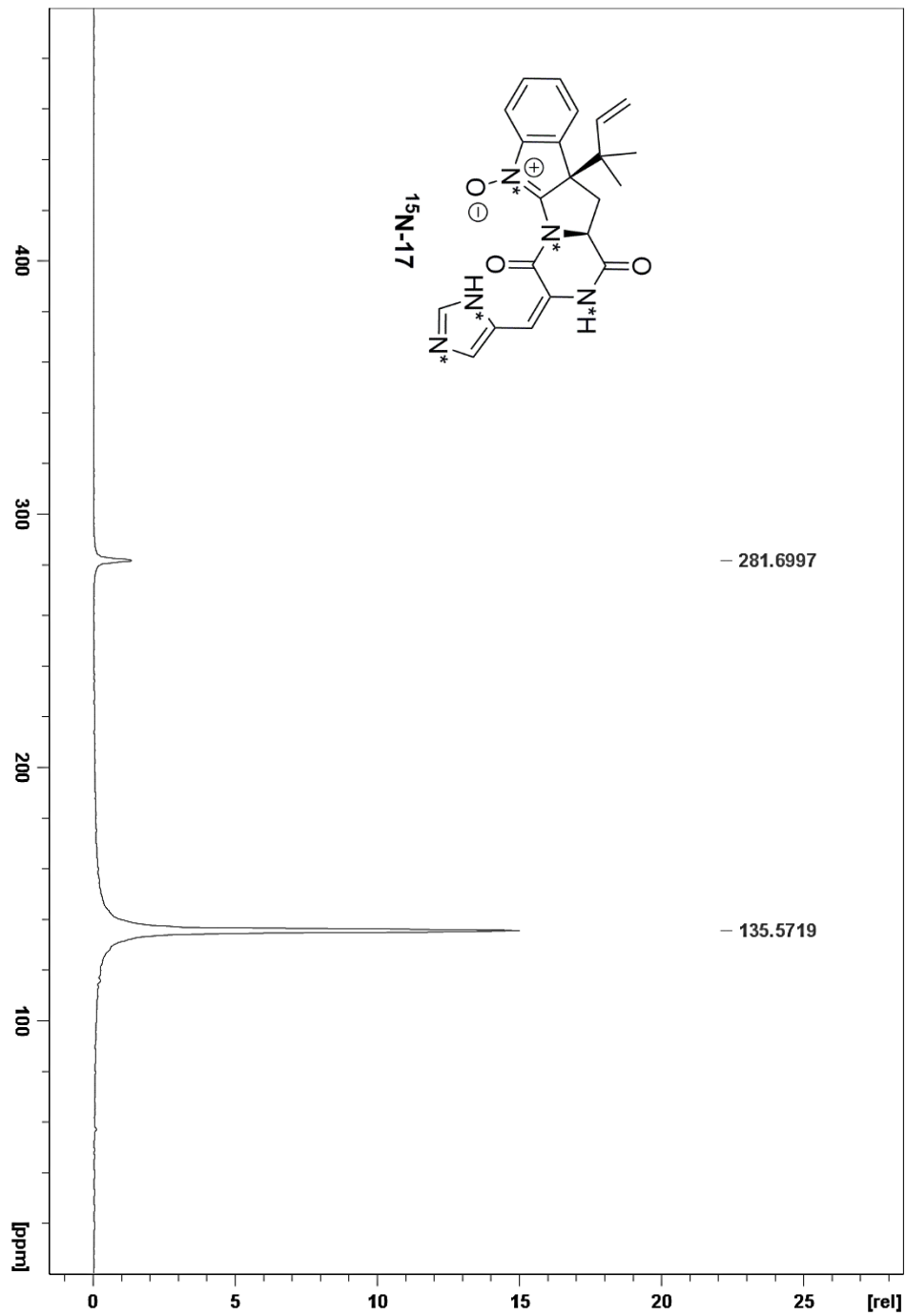
Peak List

Peak Number	X (cm-1)	Y (%T)
1	3268.41	94.4
2	2961.82	87.88
3	2925.05	87.03
4	2854.79	90.51
5	1682.4	83.34
6	1384.58	82.77
7	1258.38	79.11
8	1164.77	90.59
9	1091.79	73.48
10	1014.45	70.87
11	924.22	95.19
12	871.54	94.26
13	794.8	72.08
14	683.41	92.99
15	665.94	92.19
16	643.3	93.83

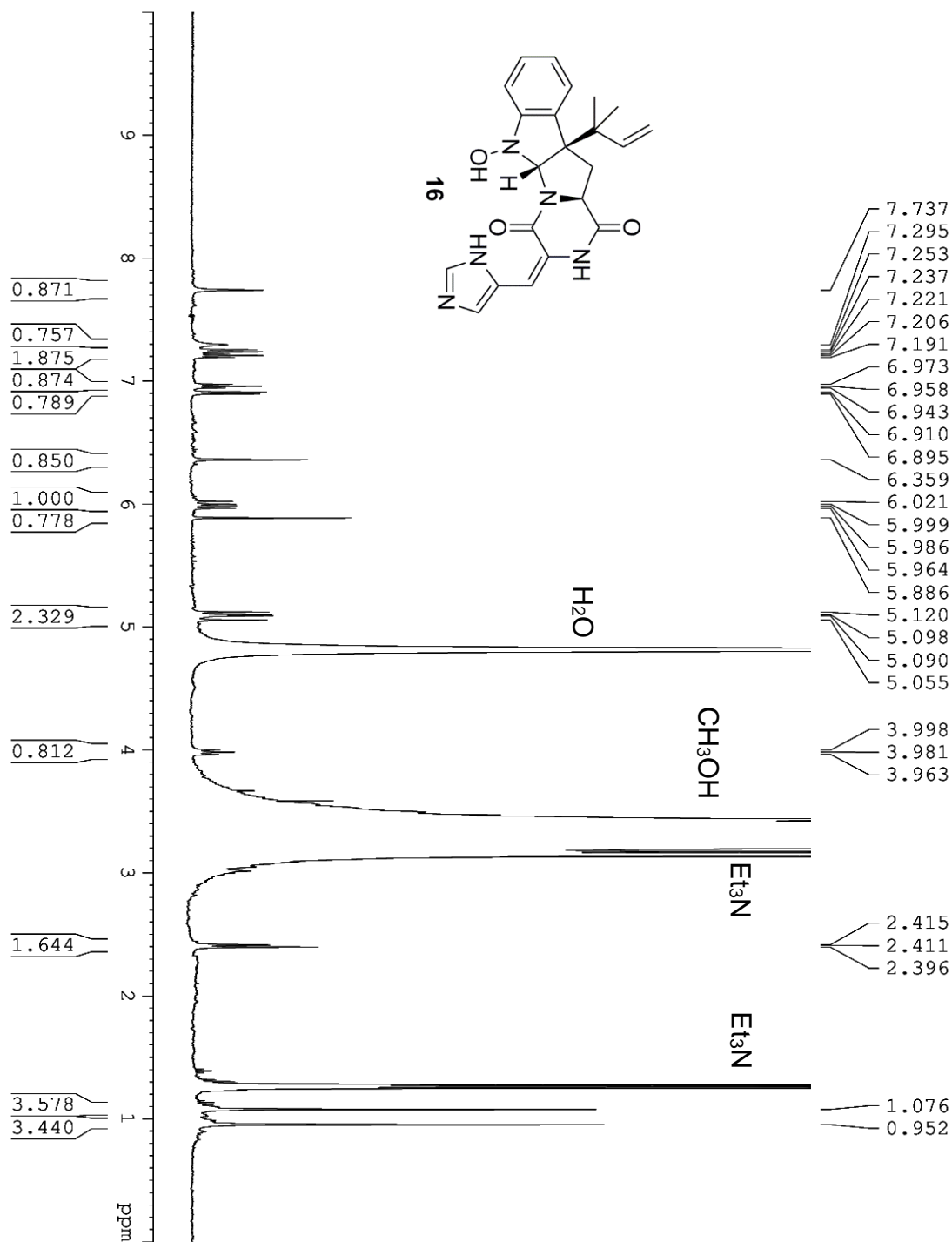


**Supplementary Figure 2.11:**  $^1\text{H}$ - $^{15}\text{N}$  HMBC NMR (600 MHz,  $\text{DMSO-}d_6/\text{CDCl}_3$ ) Spectrum of  $^{15}\text{N-17}$

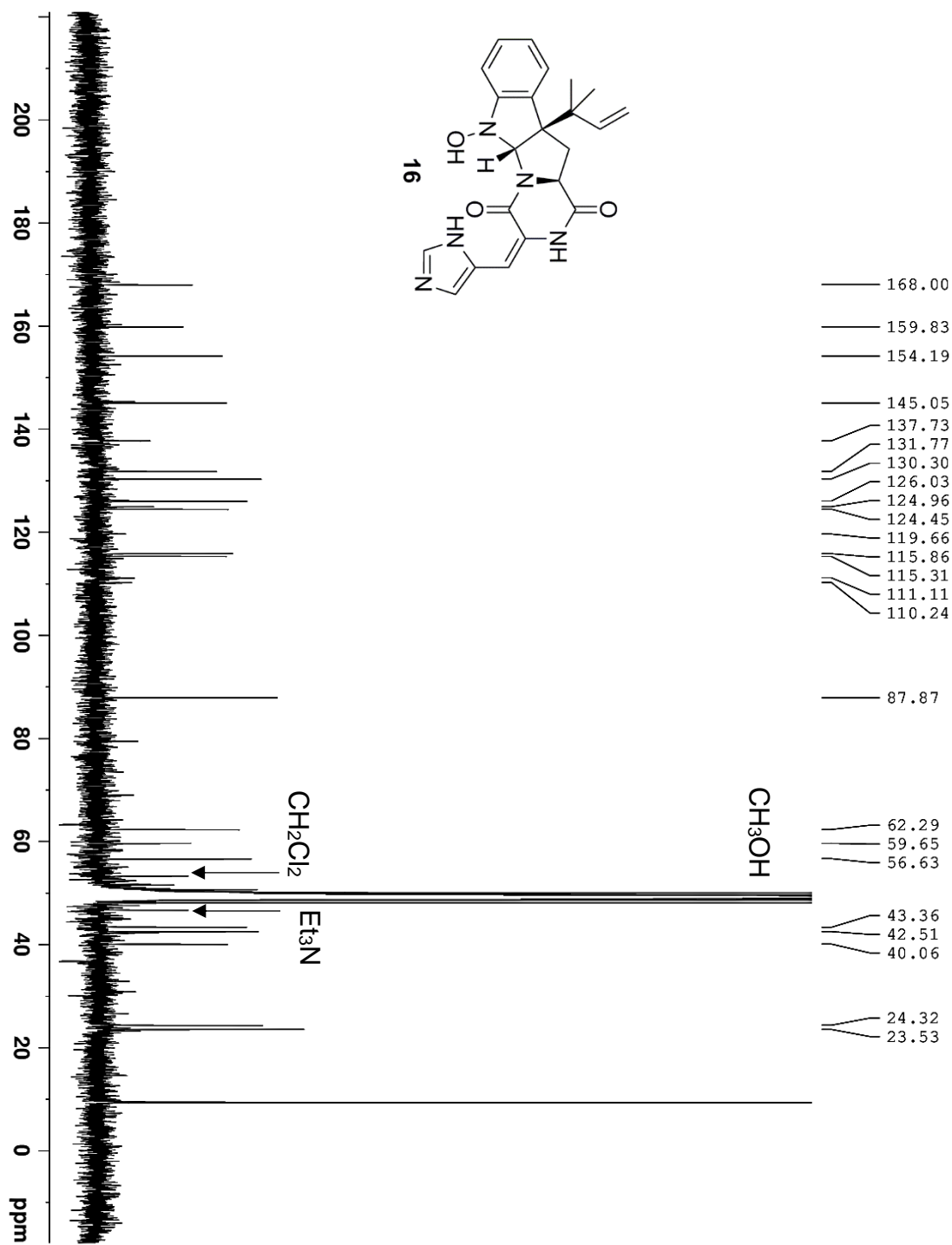
\*\*Signals corresponding to imidazole nitrogens not observed due to rapid tautomerization.



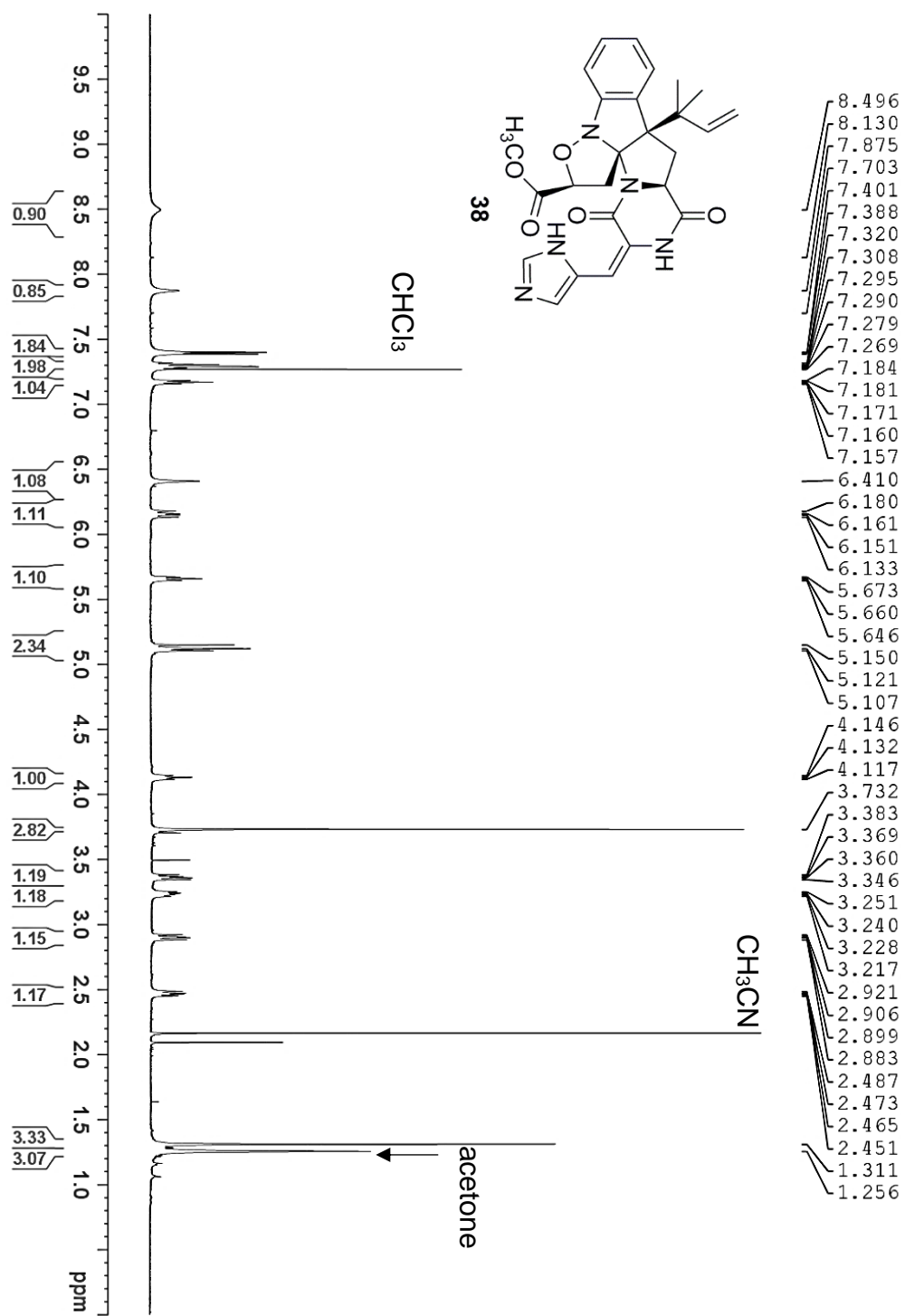
**Supplementary Figure 2.12:**  $^{15}\text{N}$  NMR (600 MHz,  $\text{DMSO-}d_6/\text{CDCl}_3$ ) Spectrum of  $^{15}\text{N-17}$   
\*\*Signals corresponding to imidazole nitrogens not observed due to rapid tautomerization.



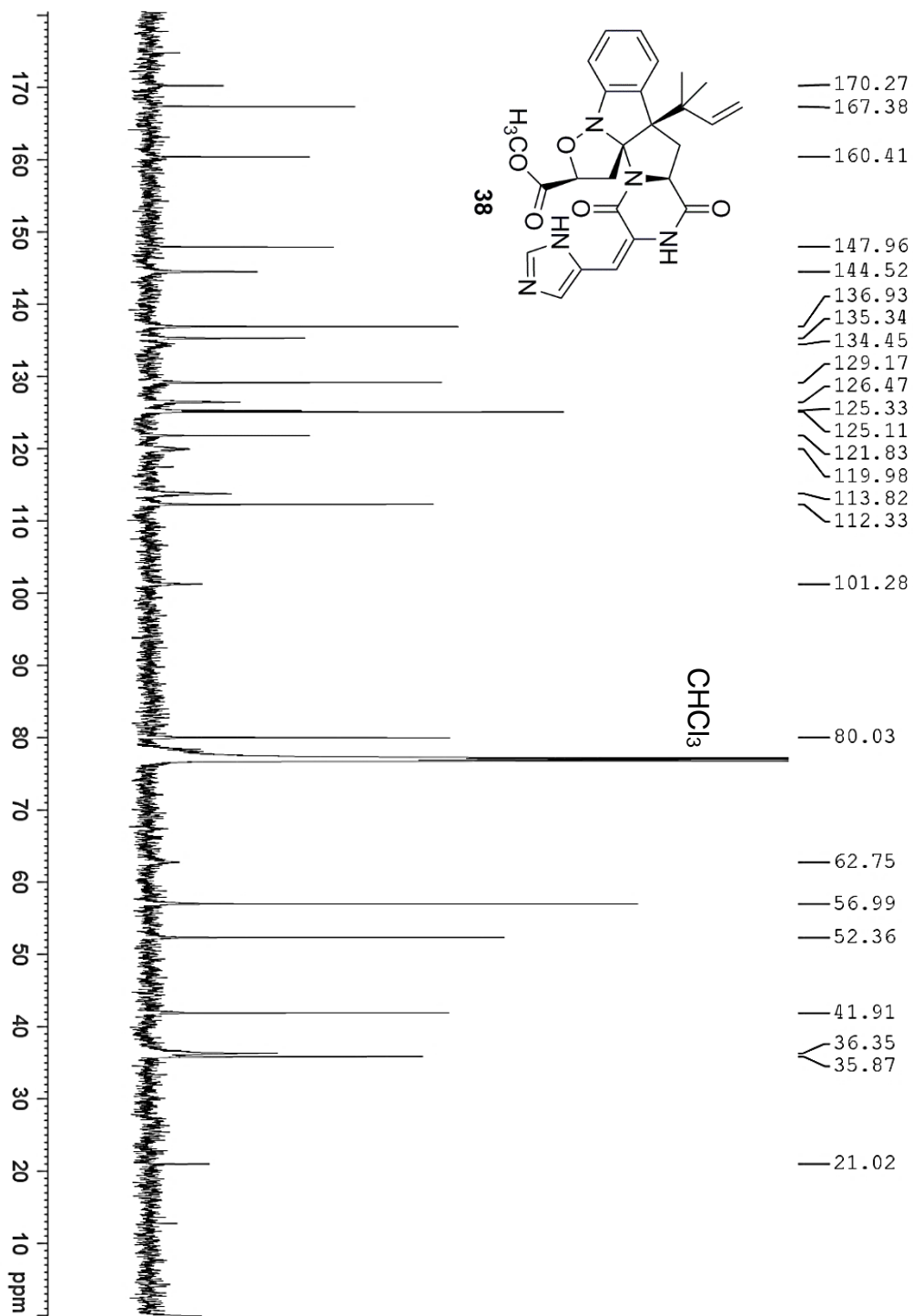
Supplementary Figure 2.13: <sup>1</sup>H NMR (500 MHz, CD<sub>3</sub>OD) Spectrum of **16**



Supplementary Figure 2.14: <sup>13</sup>C NMR (125 MHz, CD<sub>3</sub>OD) Spectrum of 16

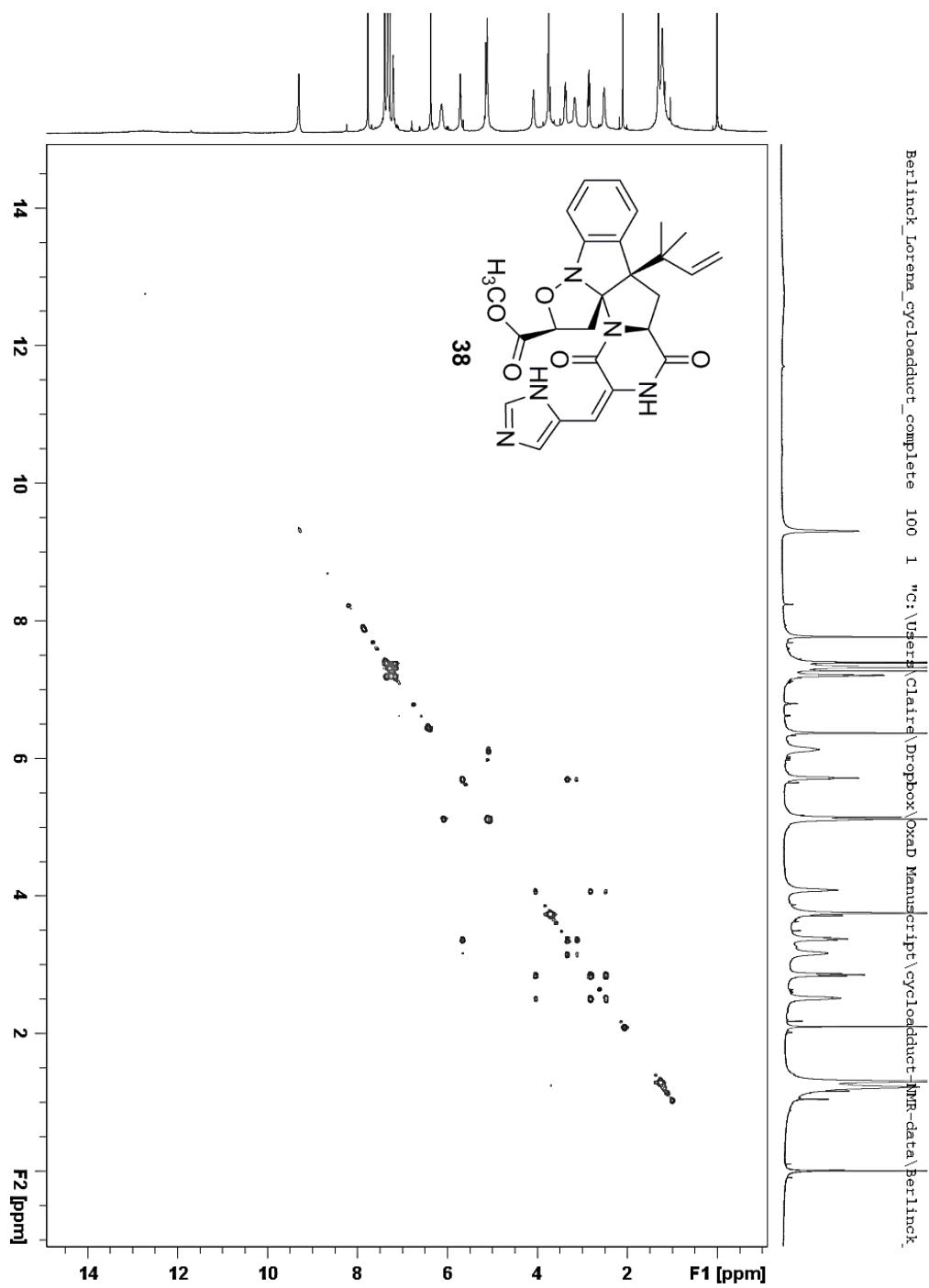


Supplementary Figure 2.15:  $^1\text{H}$  NMR (600 MHz,  $\text{CDCl}_3$ ) Spectrum of **38**

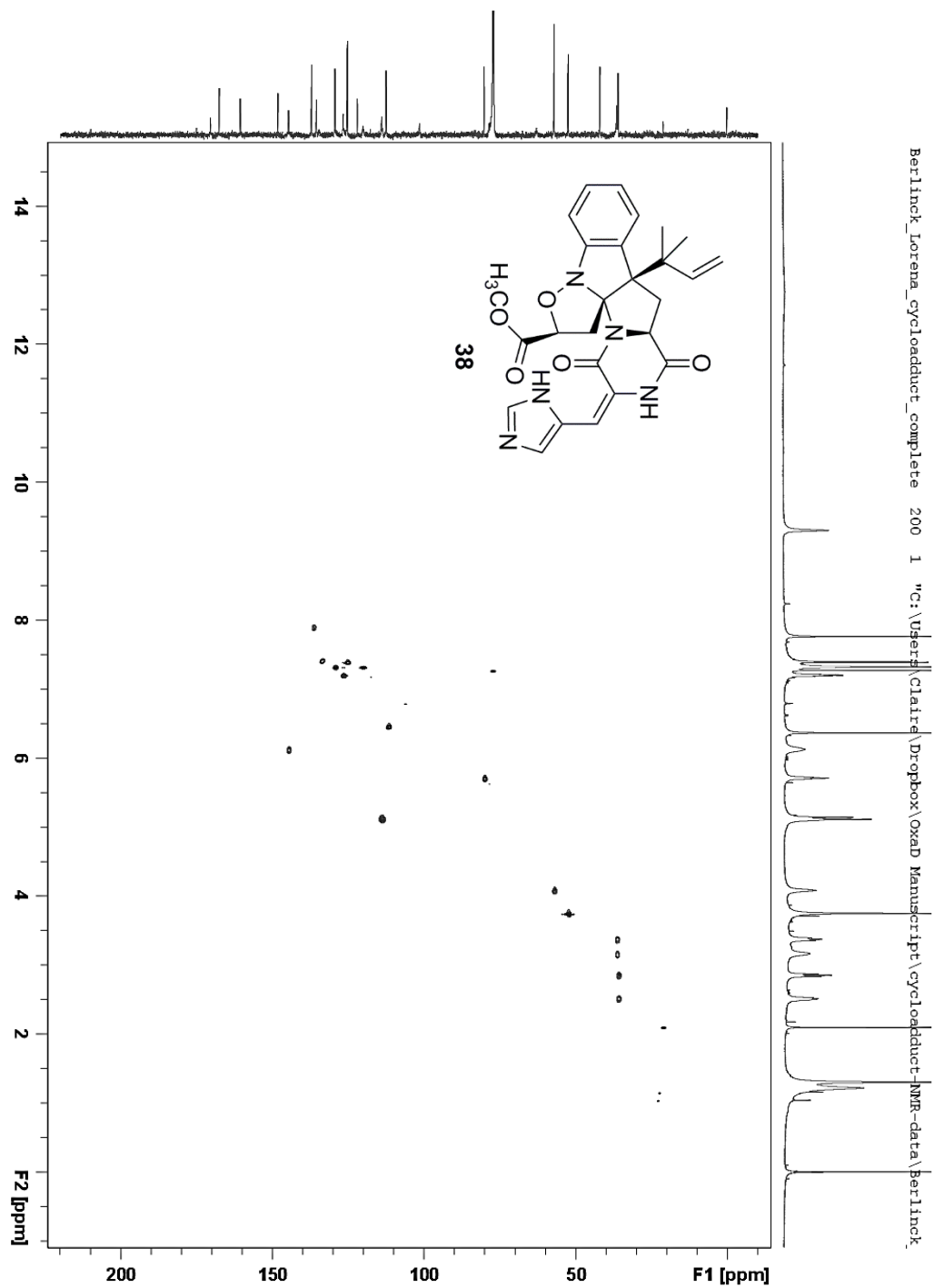


Supplementary Figure 2.16:  $^{13}\text{C}$  NMR (150 MHz,  $\text{CDCl}_3$ ) Spectrum of **38**

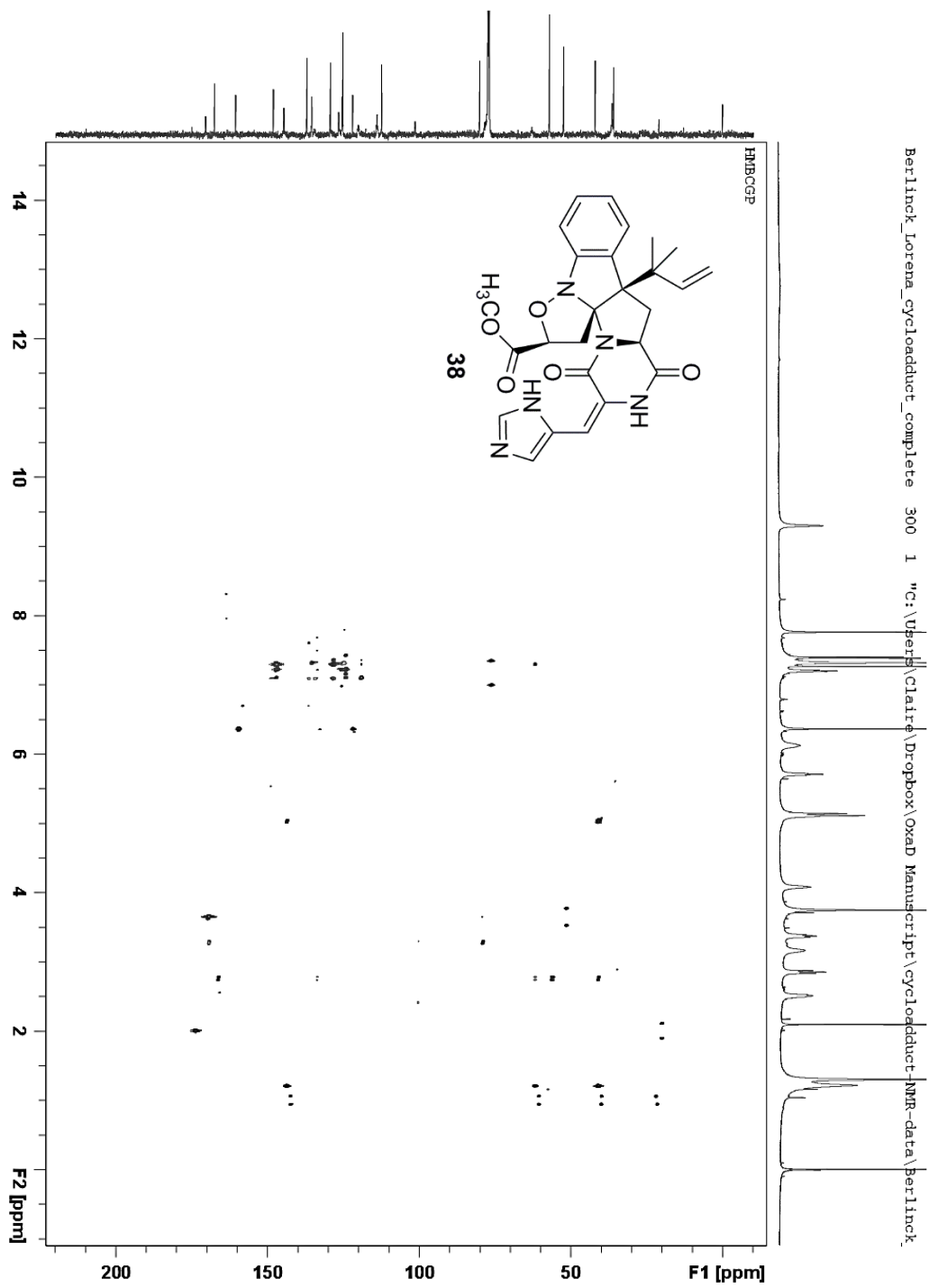




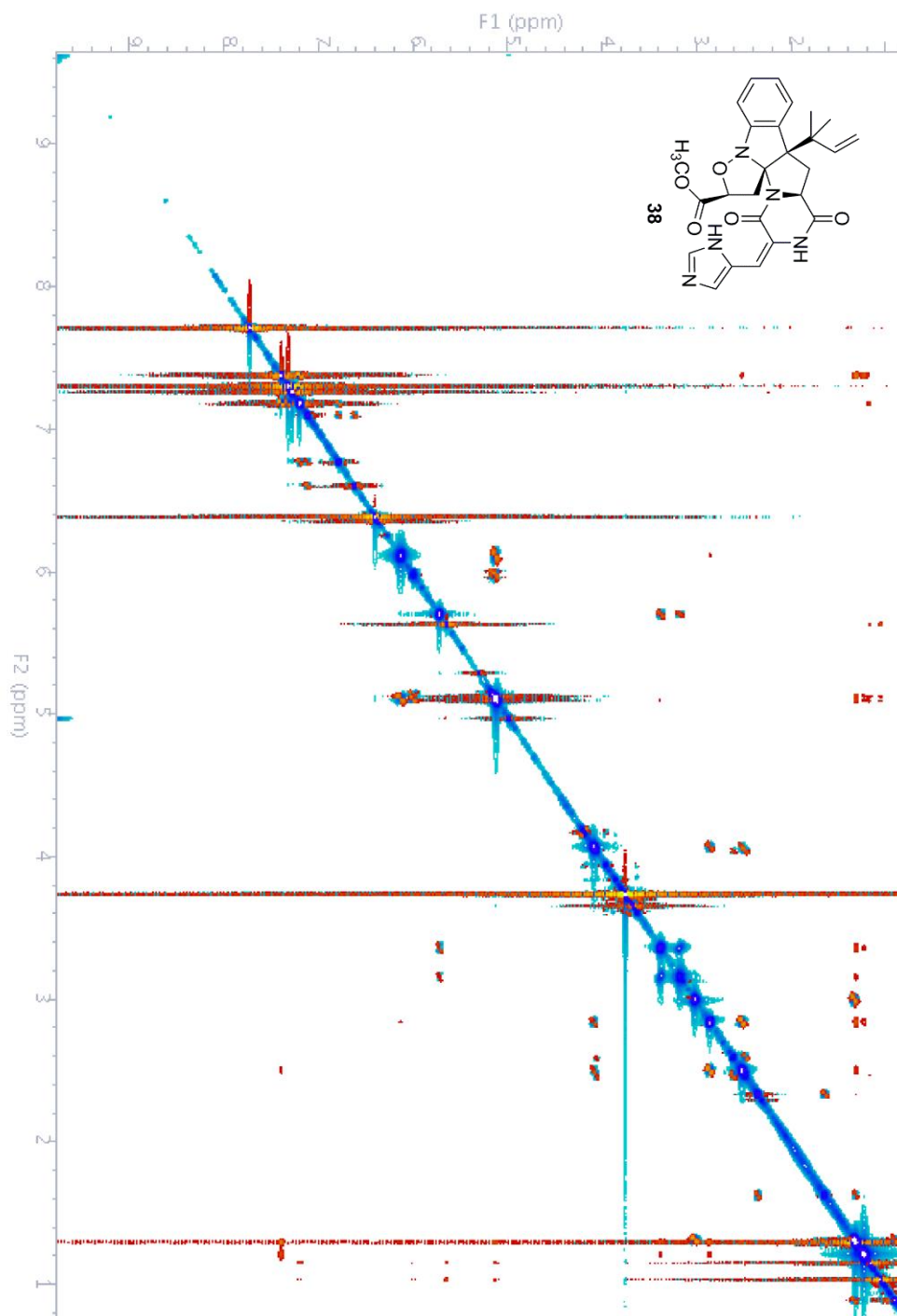
Supplementary Figure 2.17:  $^1\text{H}$ - $^1\text{H}$  COSY NMR (600 MHz,  $\text{CDCl}_3$ ) Spectrum of **38**



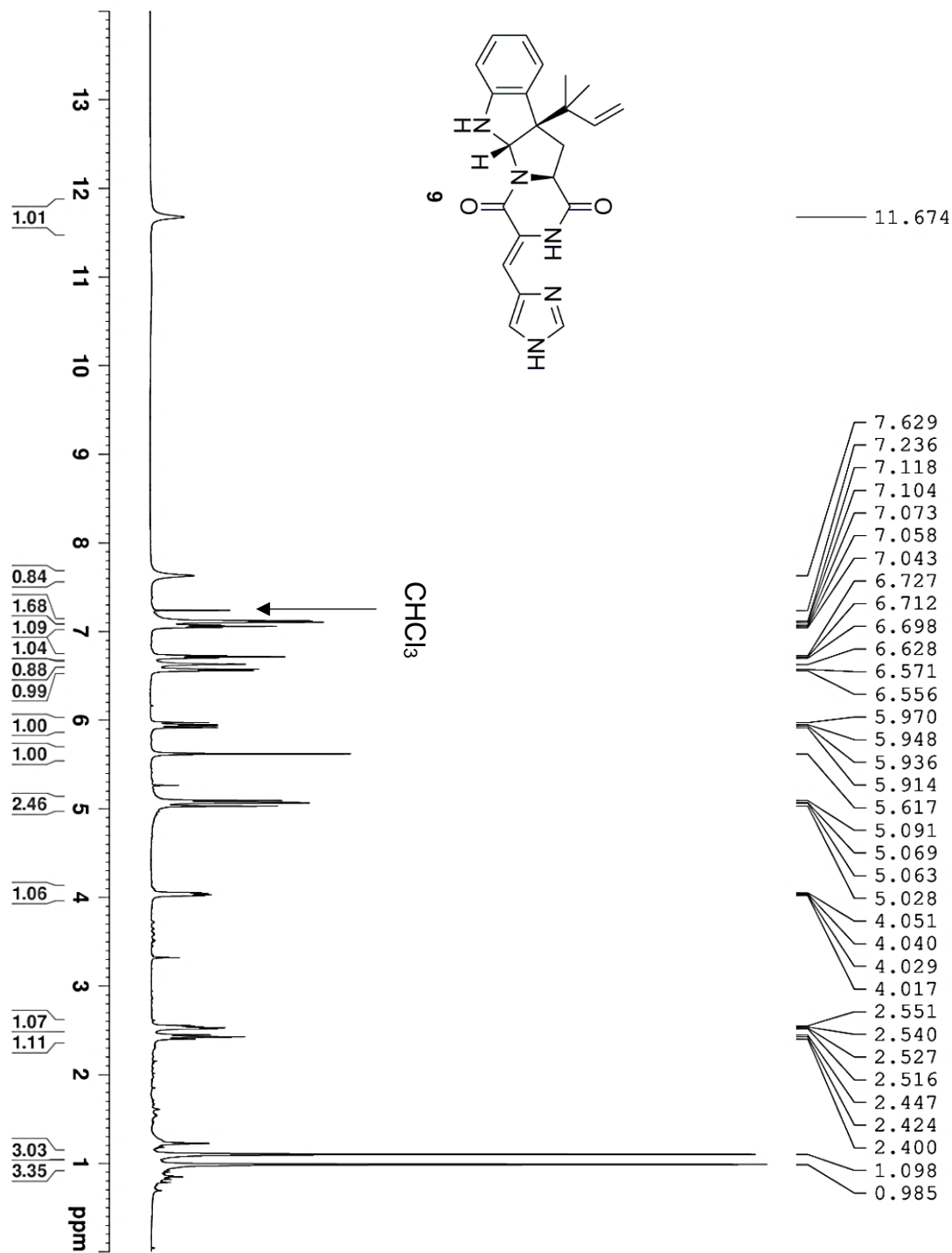
Supplementary Figure 2.18: <sup>1</sup>H-<sup>13</sup>C HSQC NMR (600 MHz, CDCl<sub>3</sub>) Spectrum of **38**



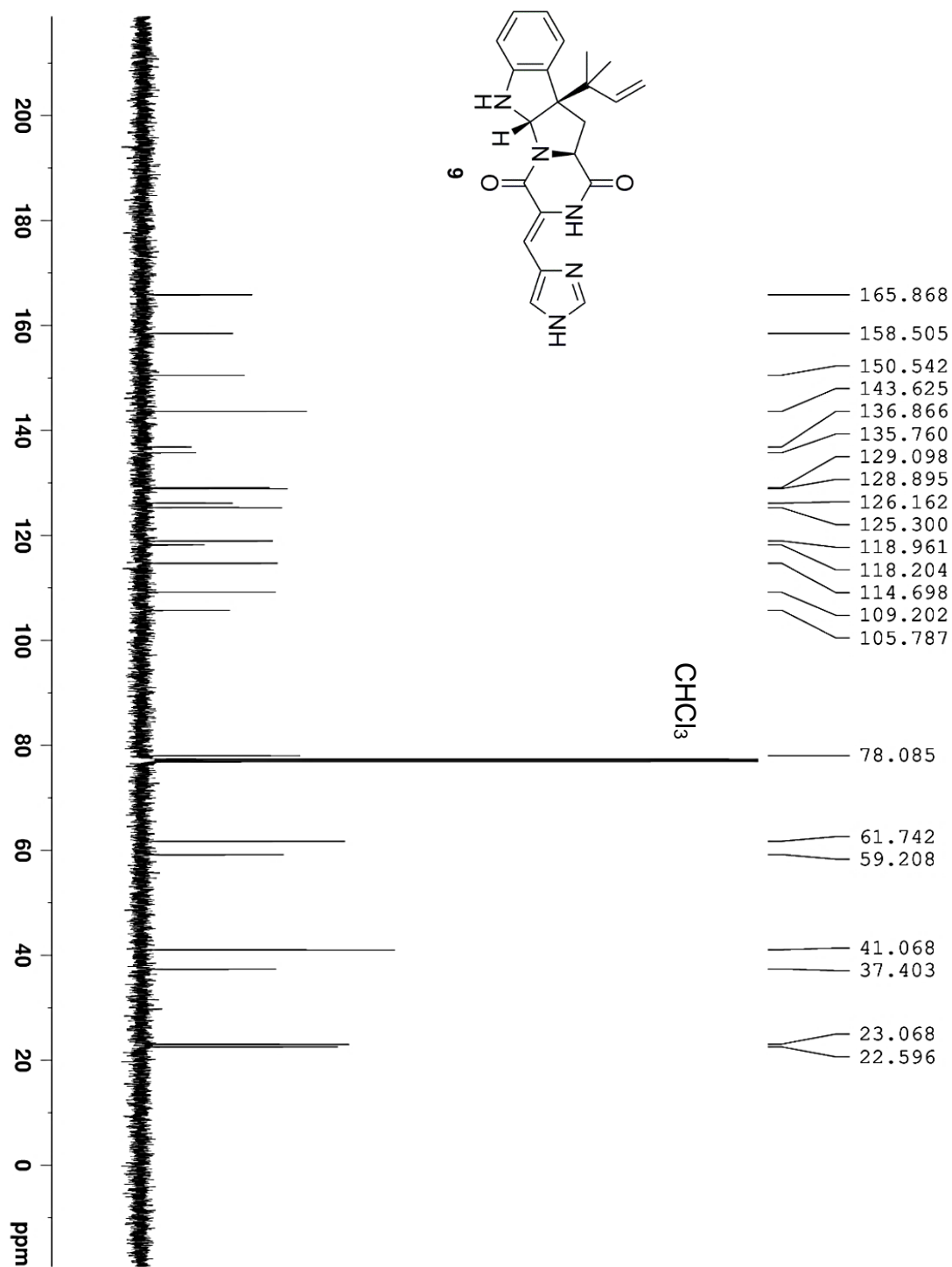
Supplementary Figure 2.19:  $^1\text{H}$ - $^{13}\text{C}$  HMBC NMR (600 MHz,  $\text{CDCl}_3$ ) Spectrum of **38**



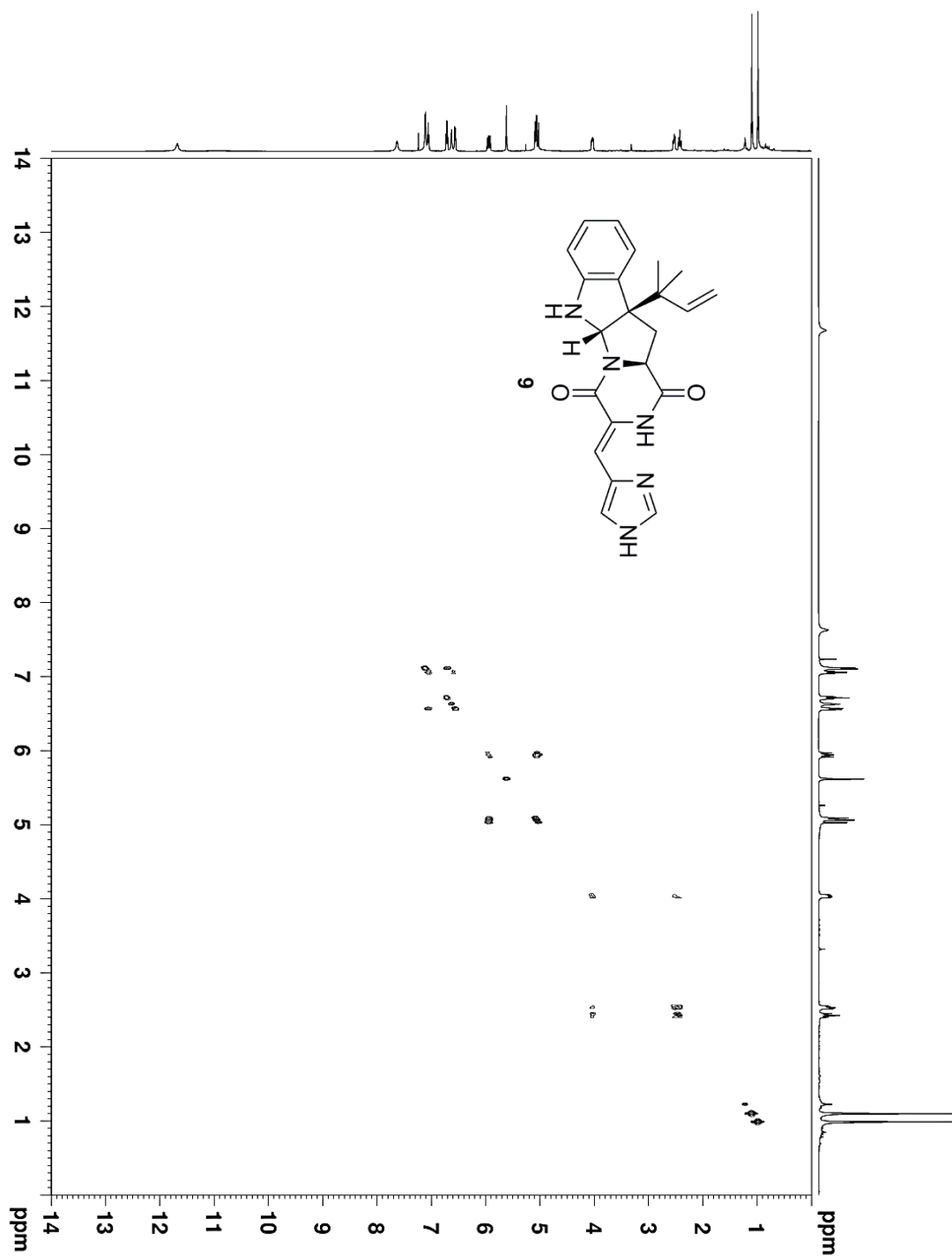
**Supplementary Figure 2.20:** <sup>1</sup>H-<sup>1</sup>H NOESY NMR (600 MHz, CDCl<sub>3</sub>) Spectrum of **38**



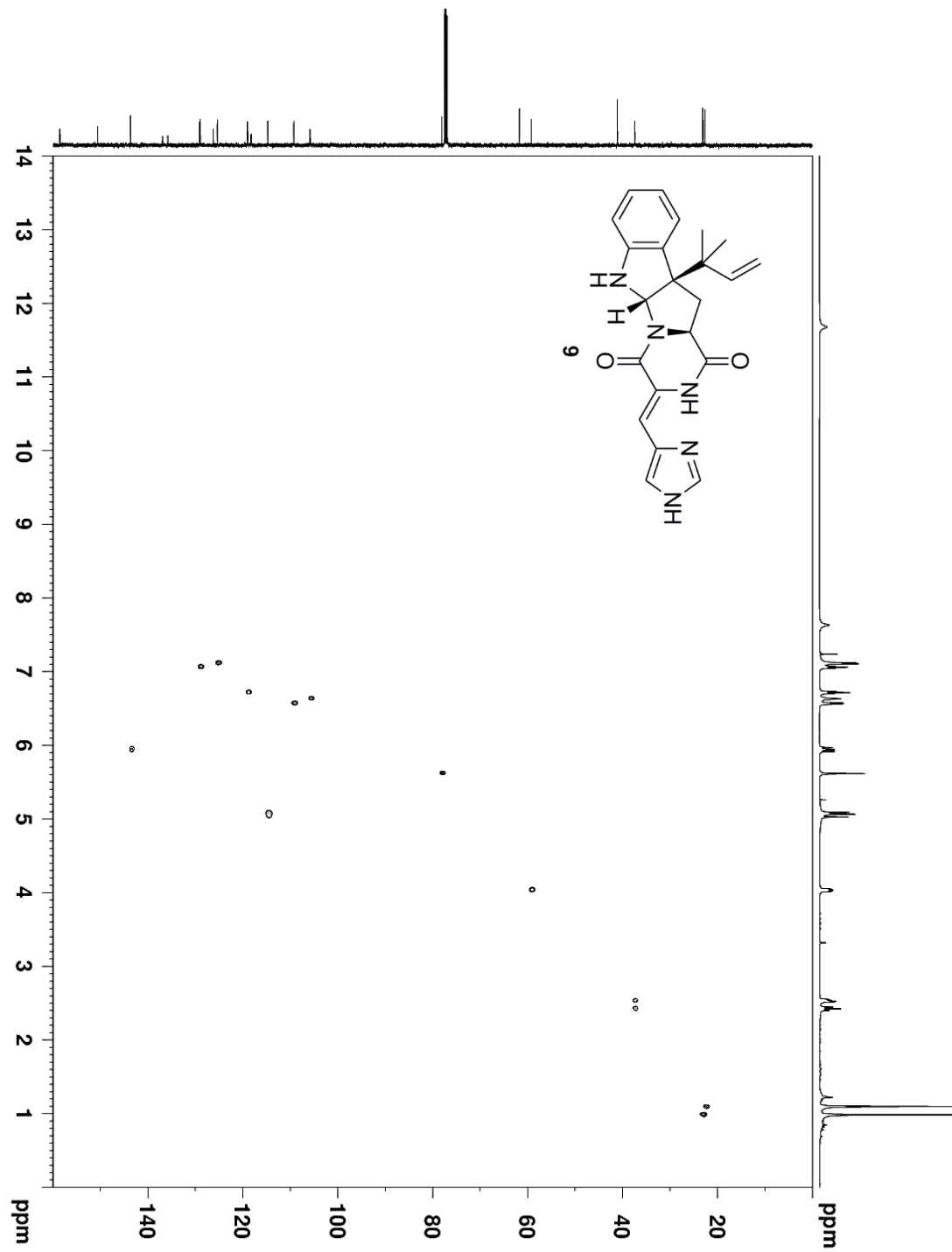
Supplementary Figure 2.21:  $^1\text{H NMR}$  (500 MHz,  $\text{CDCl}_3$ ) Spectrum of **9**



Supplementary Figure 2.22:  $^{13}\text{C}$  NMR (125 MHz,  $\text{CDCl}_3$ ) Spectrum of **9**

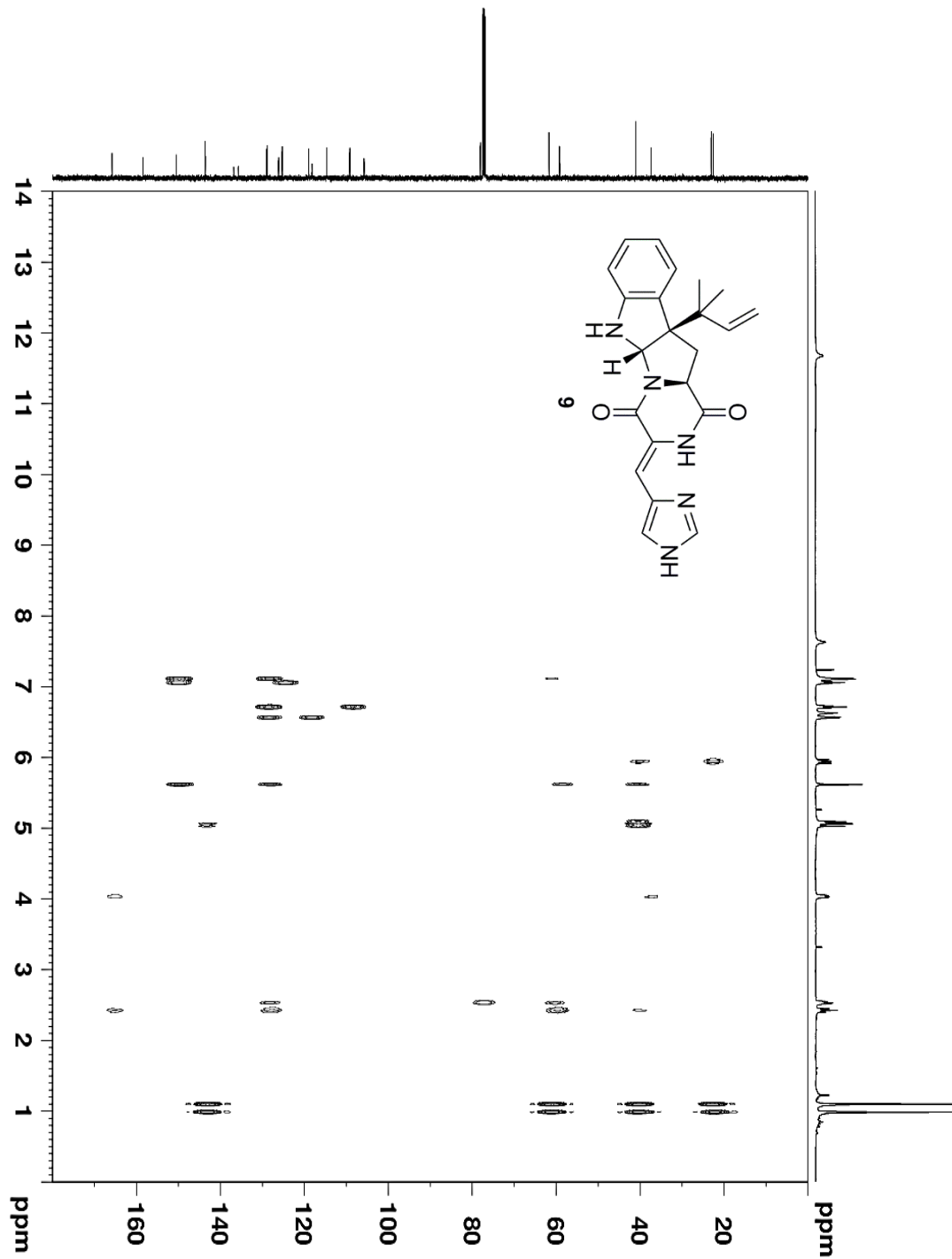


Supplementary Figure 2.23:  $^1\text{H}$ - $^1\text{H}$  COSY NMR (500 MHz,  $\text{CDCl}_3$ ) Spectrum of 9

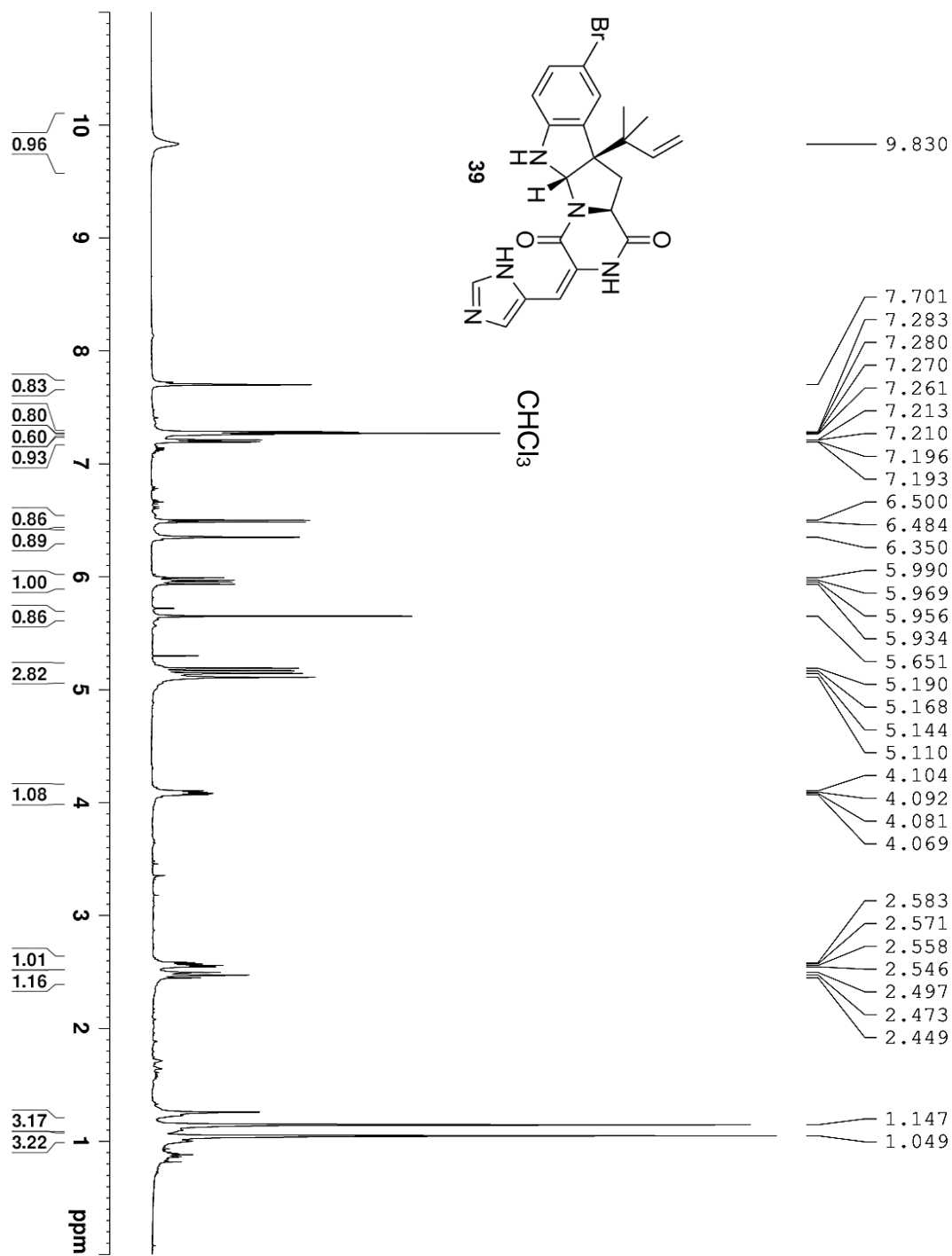


Supplementary Figure 2.24:  $^1\text{H}$ - $^{13}\text{C}$  HSQC NMR (500 MHz,  $\text{CDCl}_3$ ) Spectrum of 9

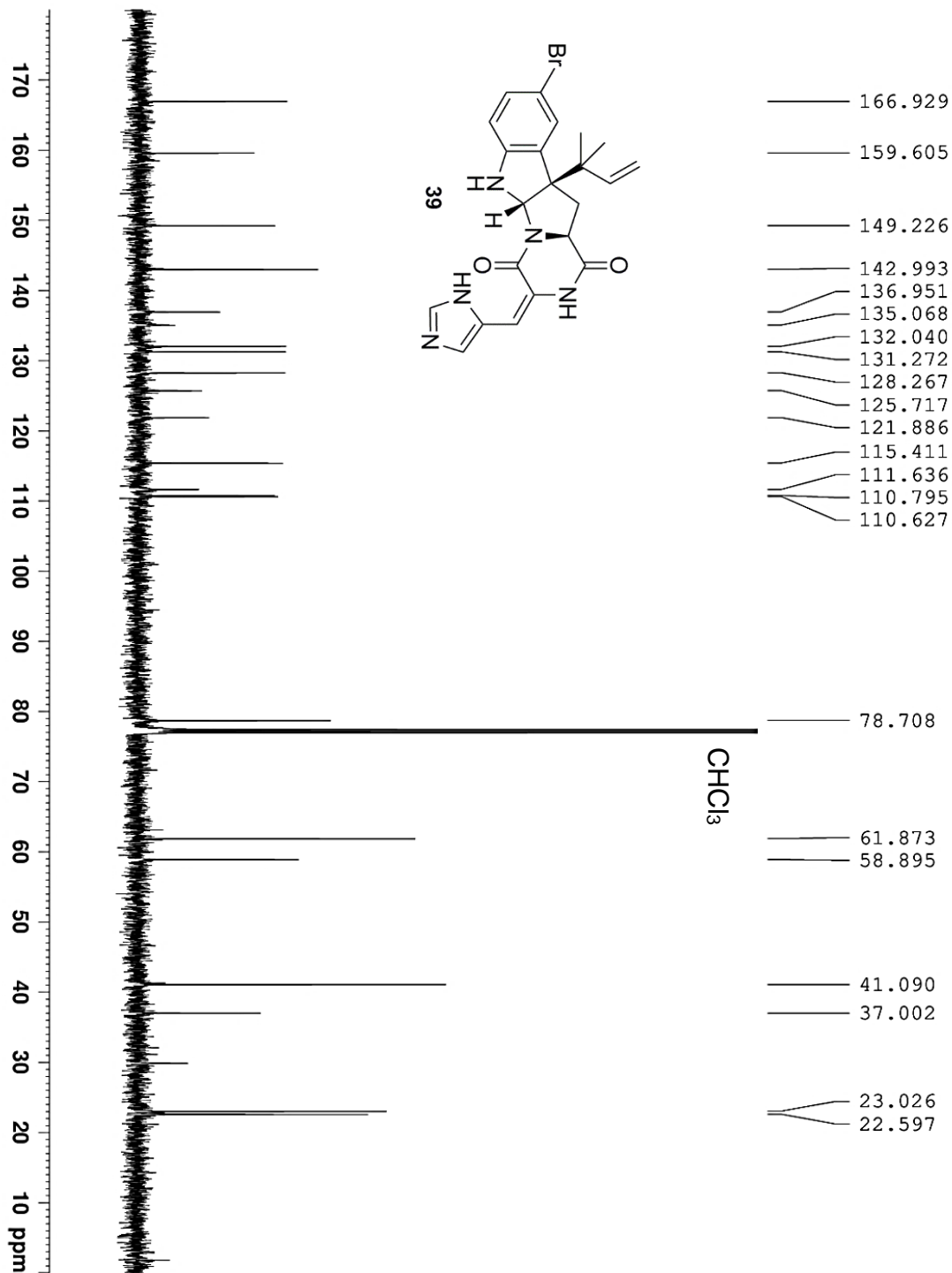




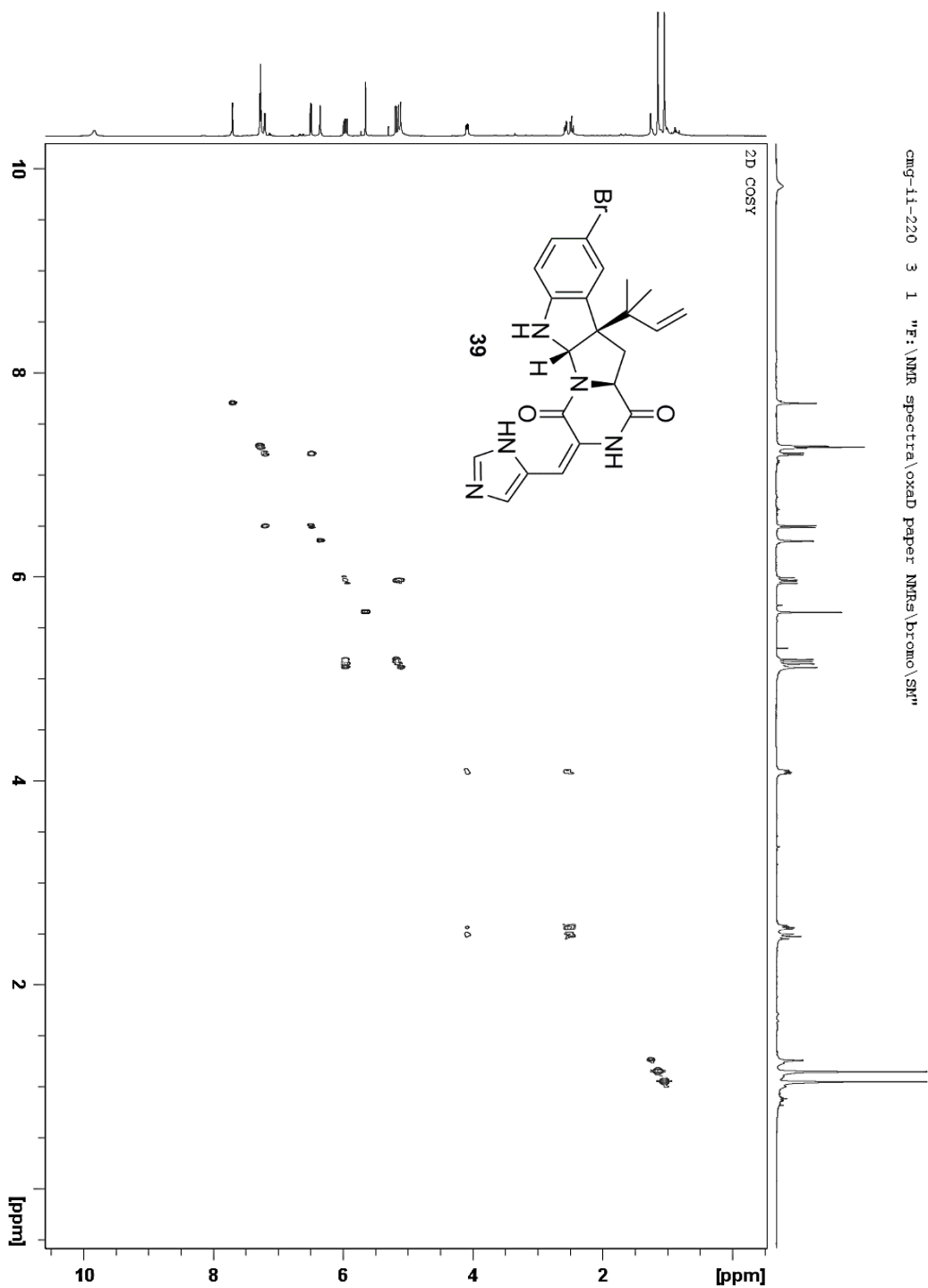
Supplementary Figure 2.25:  $^1\text{H}$ - $^{13}\text{C}$  HMBC NMR (500 MHz,  $\text{CDCl}_3$ ) Spectrum of **9**



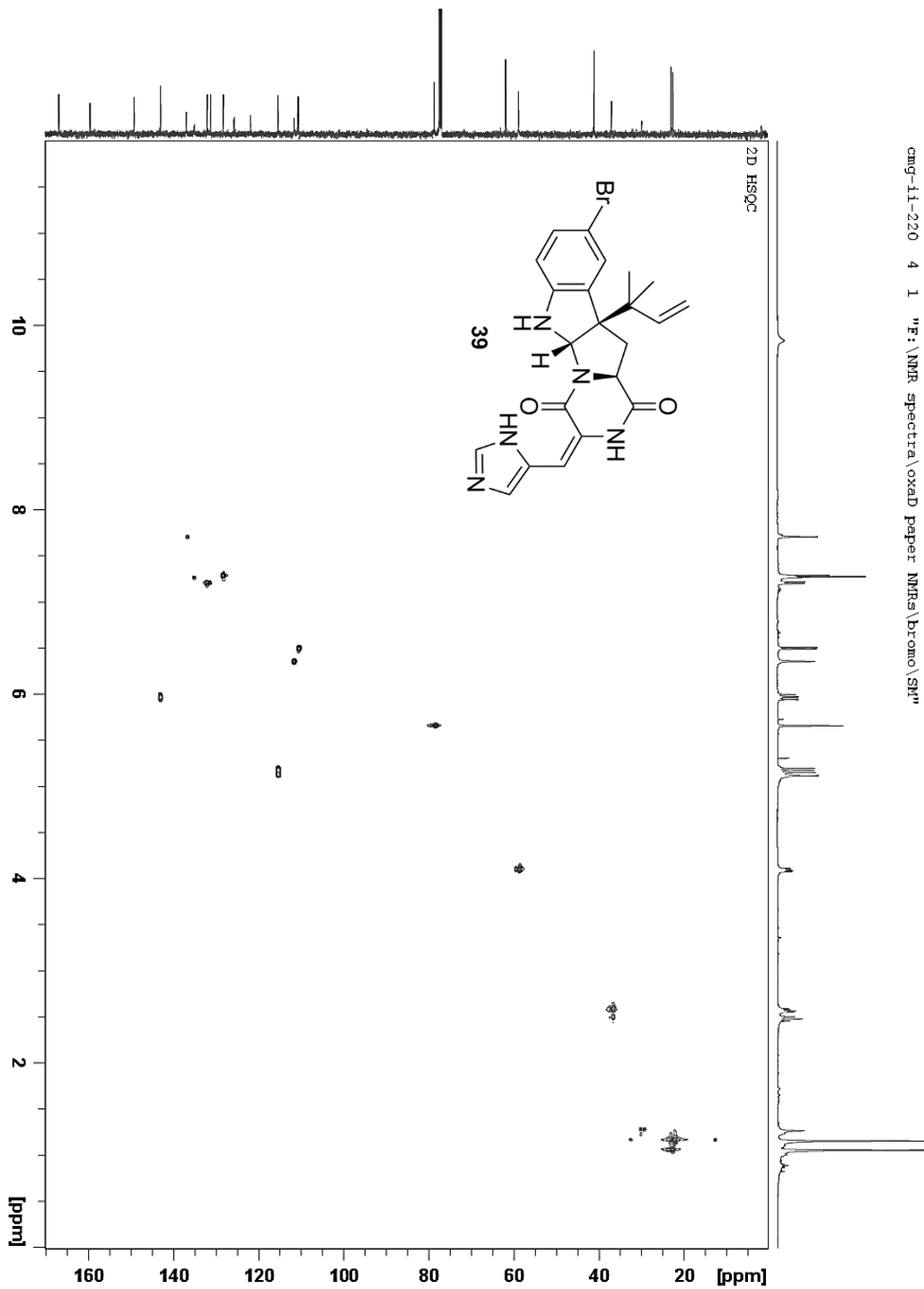
Supplementary Figure 2.26:  $^1\text{H NMR}$  (500 MHz,  $\text{CDCl}_3$ ) Spectrum of **39**



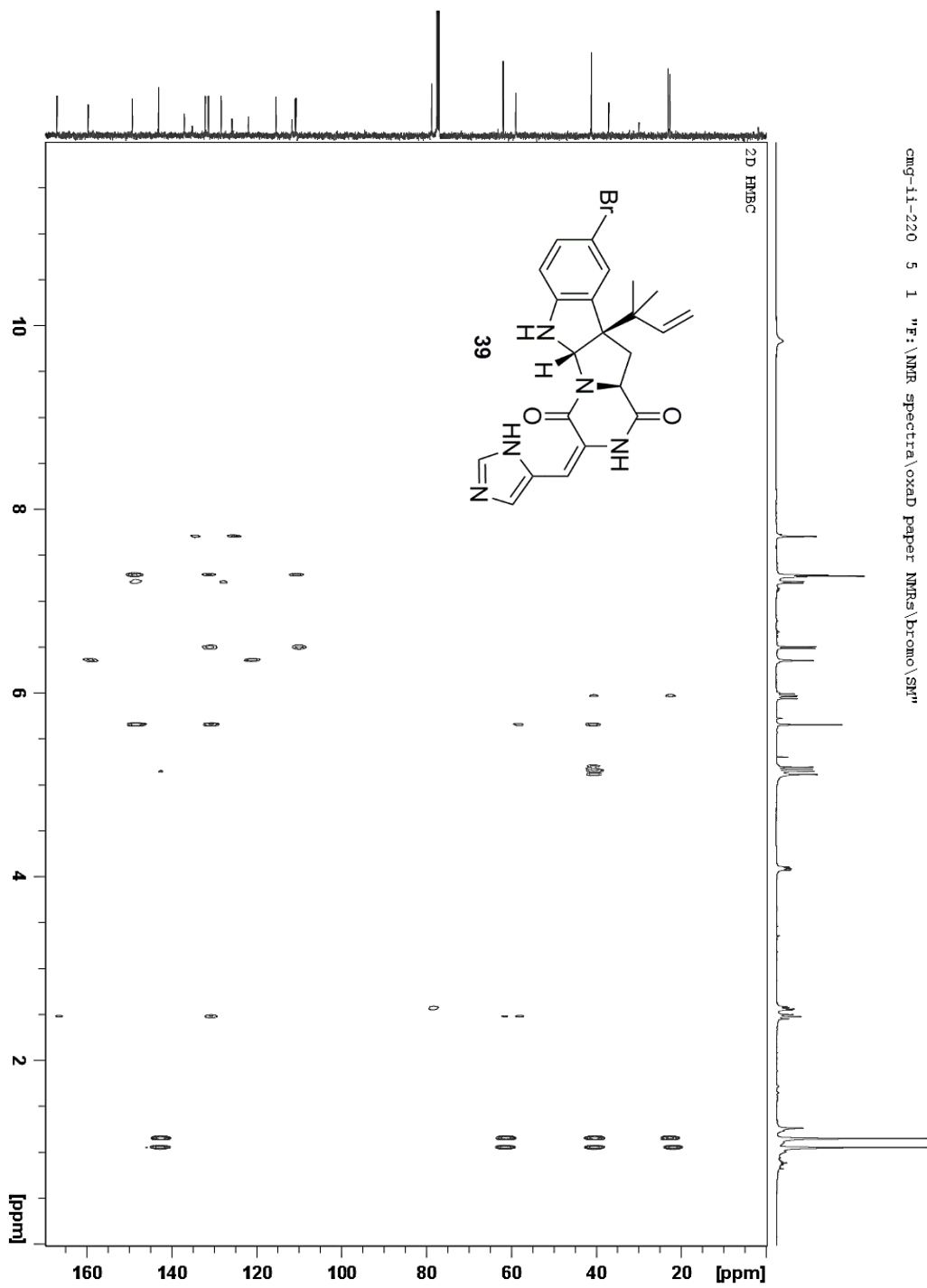
Supplementary Figure 2.27:  $^{13}\text{C}$  NMR (125 MHz,  $\text{CDCl}_3$ ) Spectrum of **39**



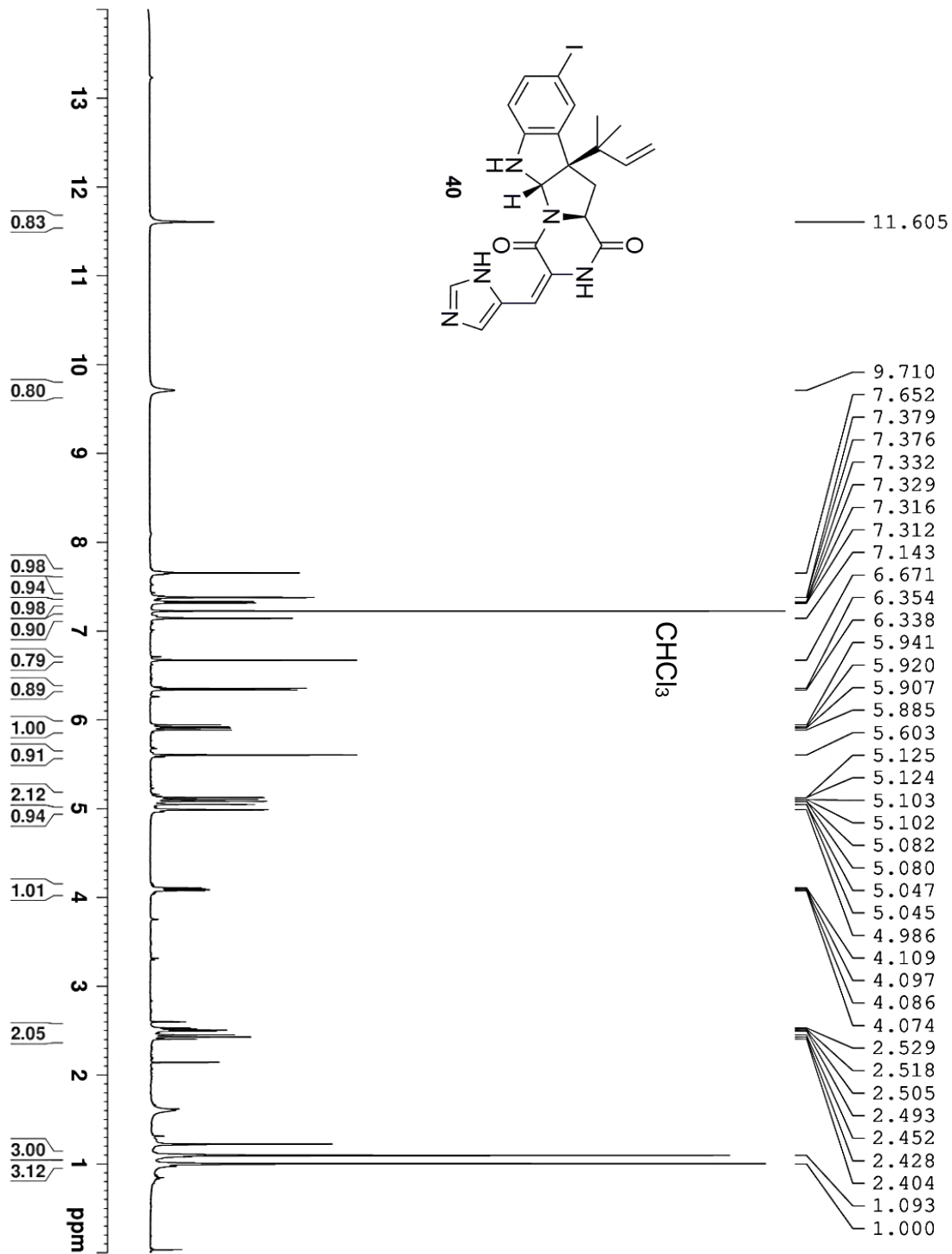
Supplementary Figure 2.28:  $^1\text{H}$ - $^1\text{H}$  COSY NMR (500 MHz,  $\text{CDCl}_3$ ) Spectrum of **39**



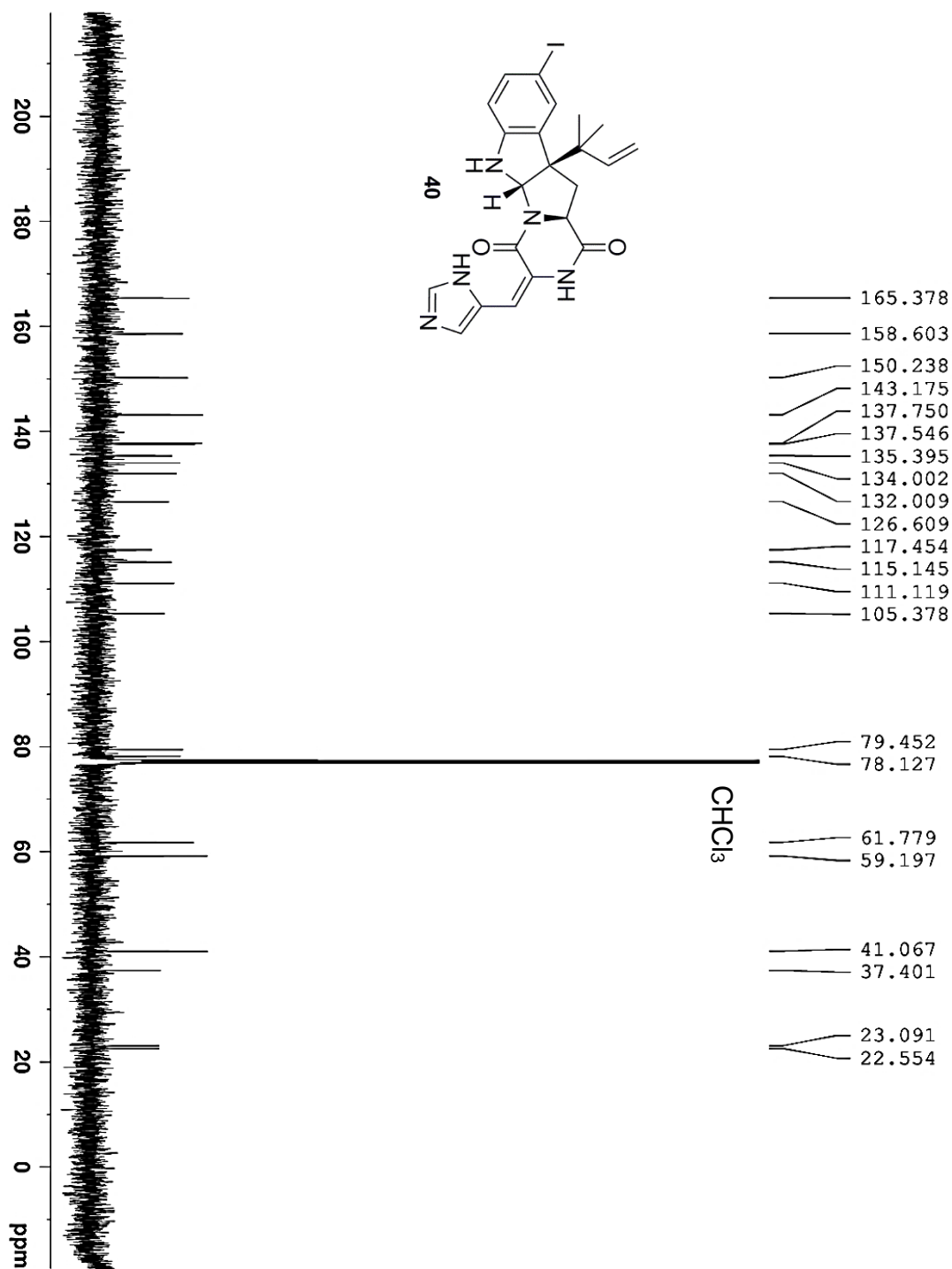
Supplementary Figure 2.29:  $^1\text{H}$ - $^{13}\text{C}$  HSQC NMR (500 MHz,  $\text{CDCl}_3$ ) Spectrum of **39**



Supplementary Figure 2.30:  $^1\text{H}$ - $^{13}\text{C}$  HMBC NMR (500 MHz,  $\text{CDCl}_3$ ) Spectrum of **39**

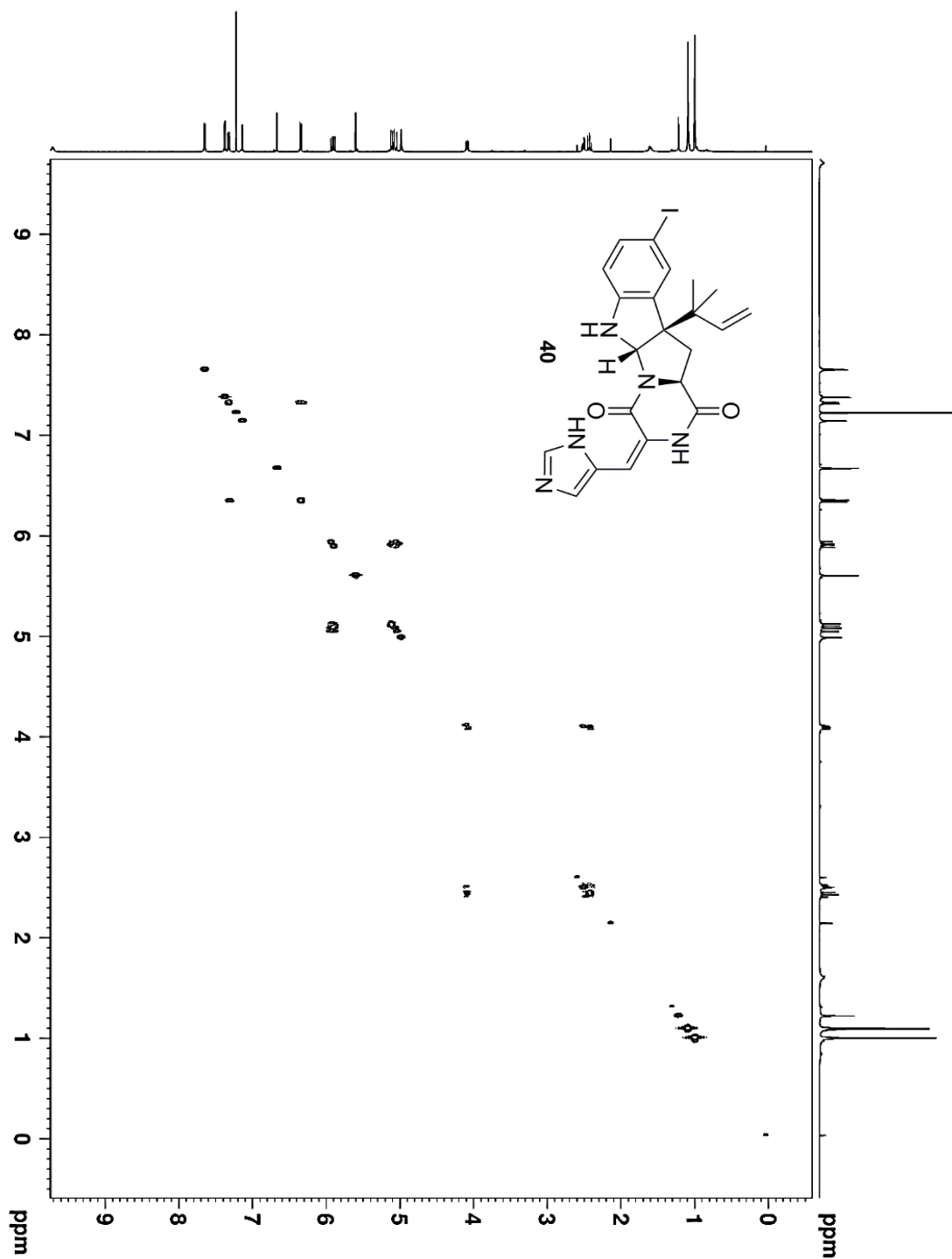


Supplementary Figure 2.31:  $^1\text{H NMR}$  (500 MHz,  $\text{CDCl}_3$ ) Spectrum of **40**

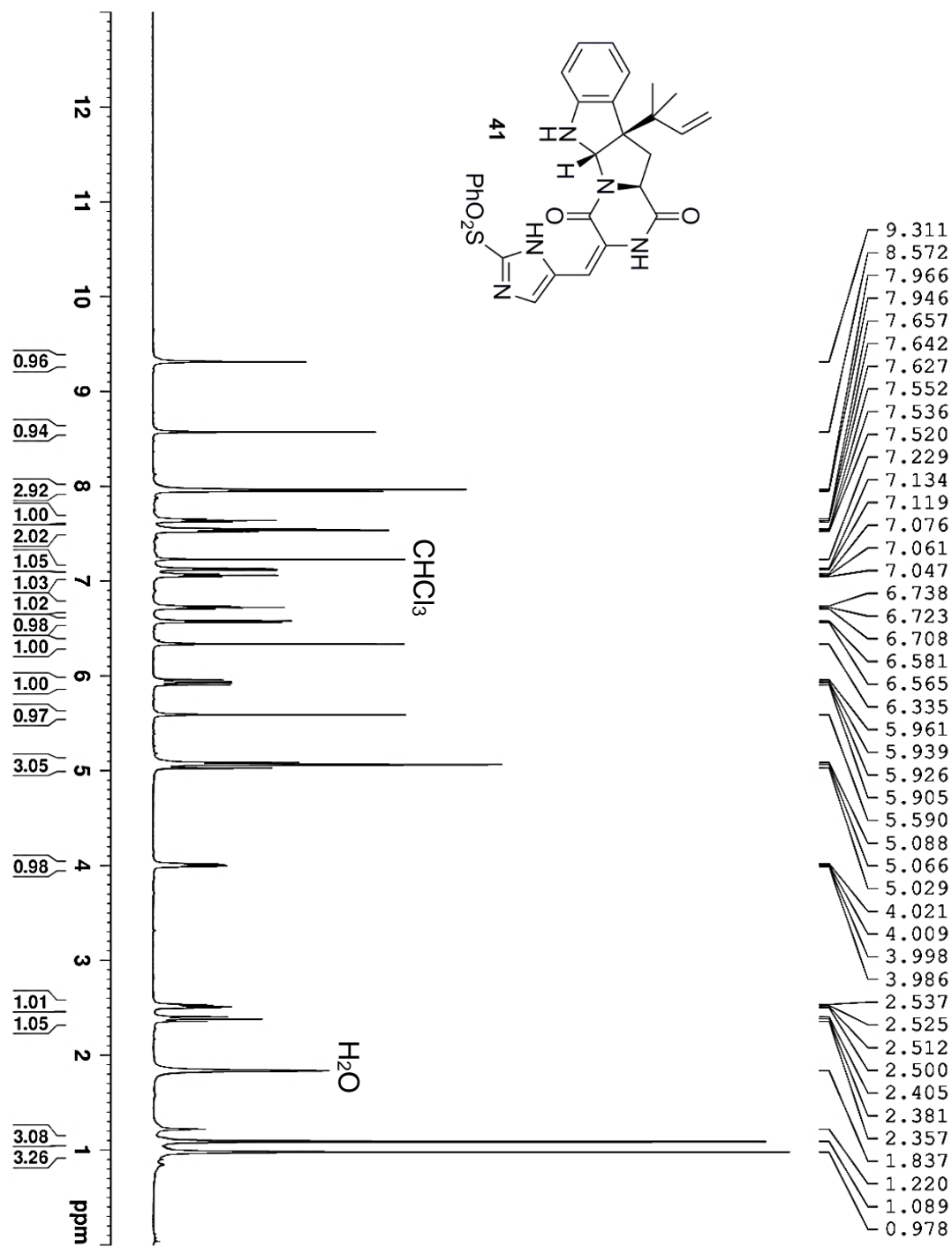


Supplementary Figure 2.32:  $^{13}\text{C}$  NMR (125 MHz,  $\text{CDCl}_3$ ) Spectrum of 40

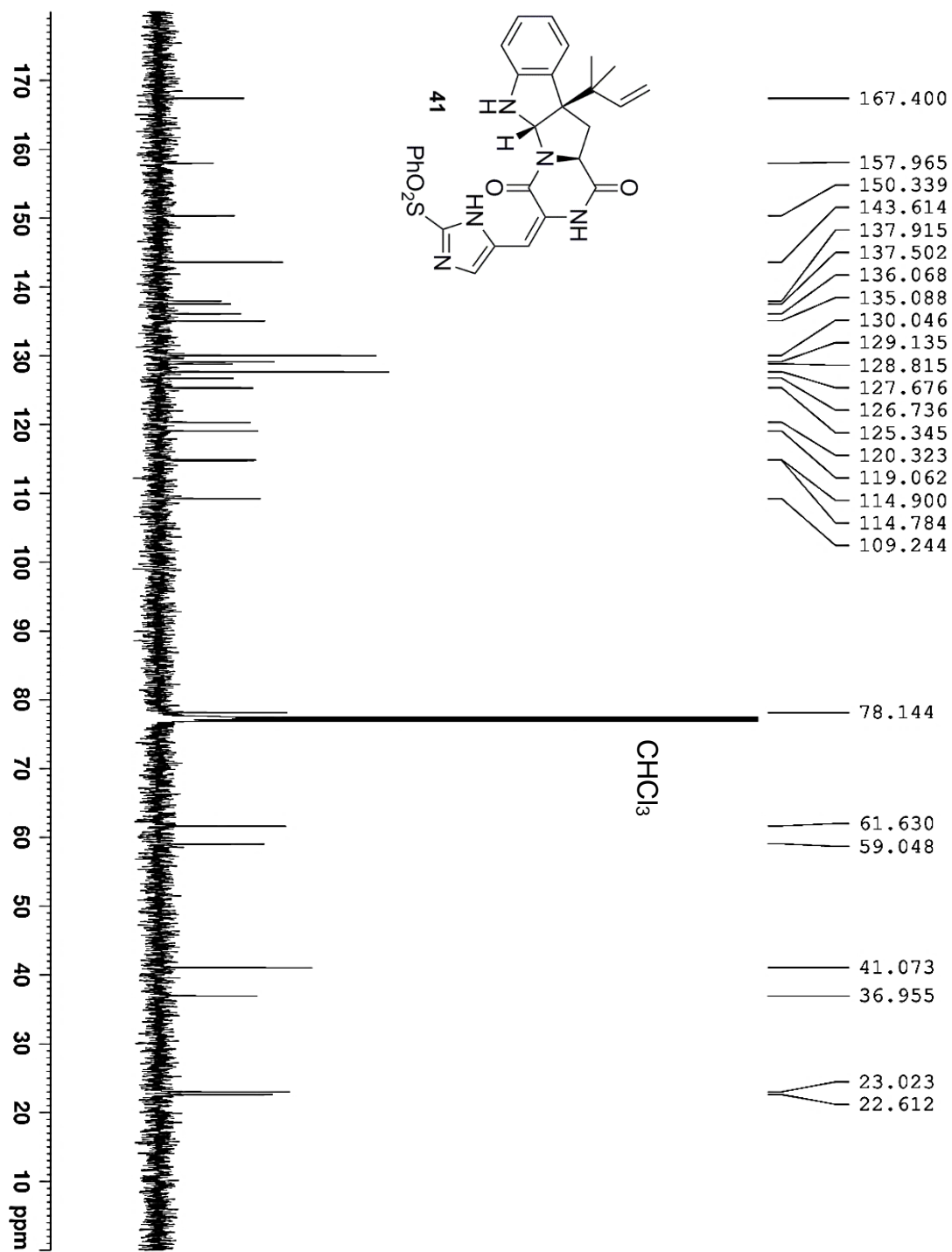




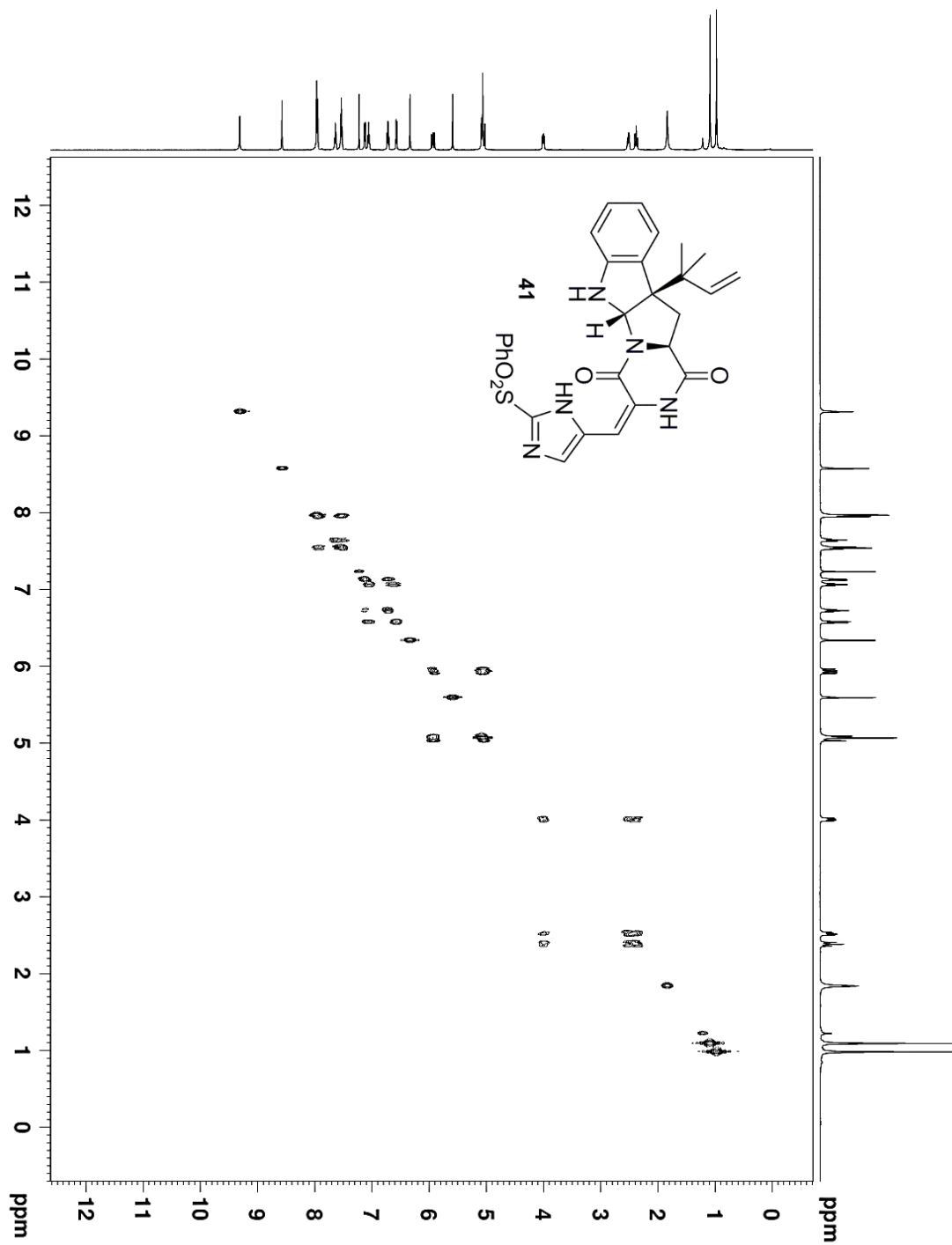
Supplementary Figure 2.33:  $^1\text{H}$ - $^1\text{H}$  COSY NMR (500 MHz,  $\text{CDCl}_3$ ) Spectrum of **40**



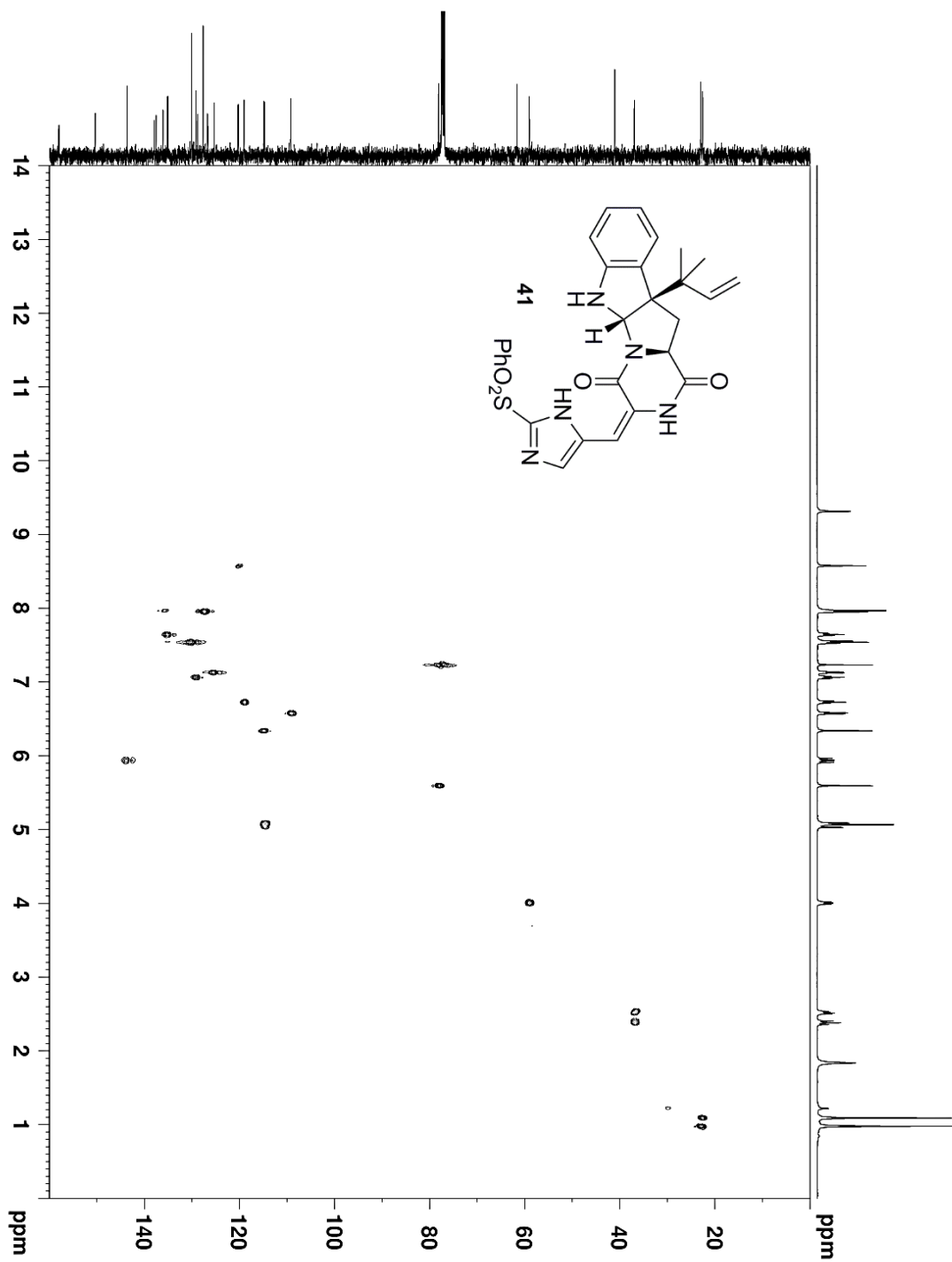
Supplementary Figure 2.34: <sup>1</sup>H NMR (500 MHz, CDCl<sub>3</sub>) Spectrum of 41



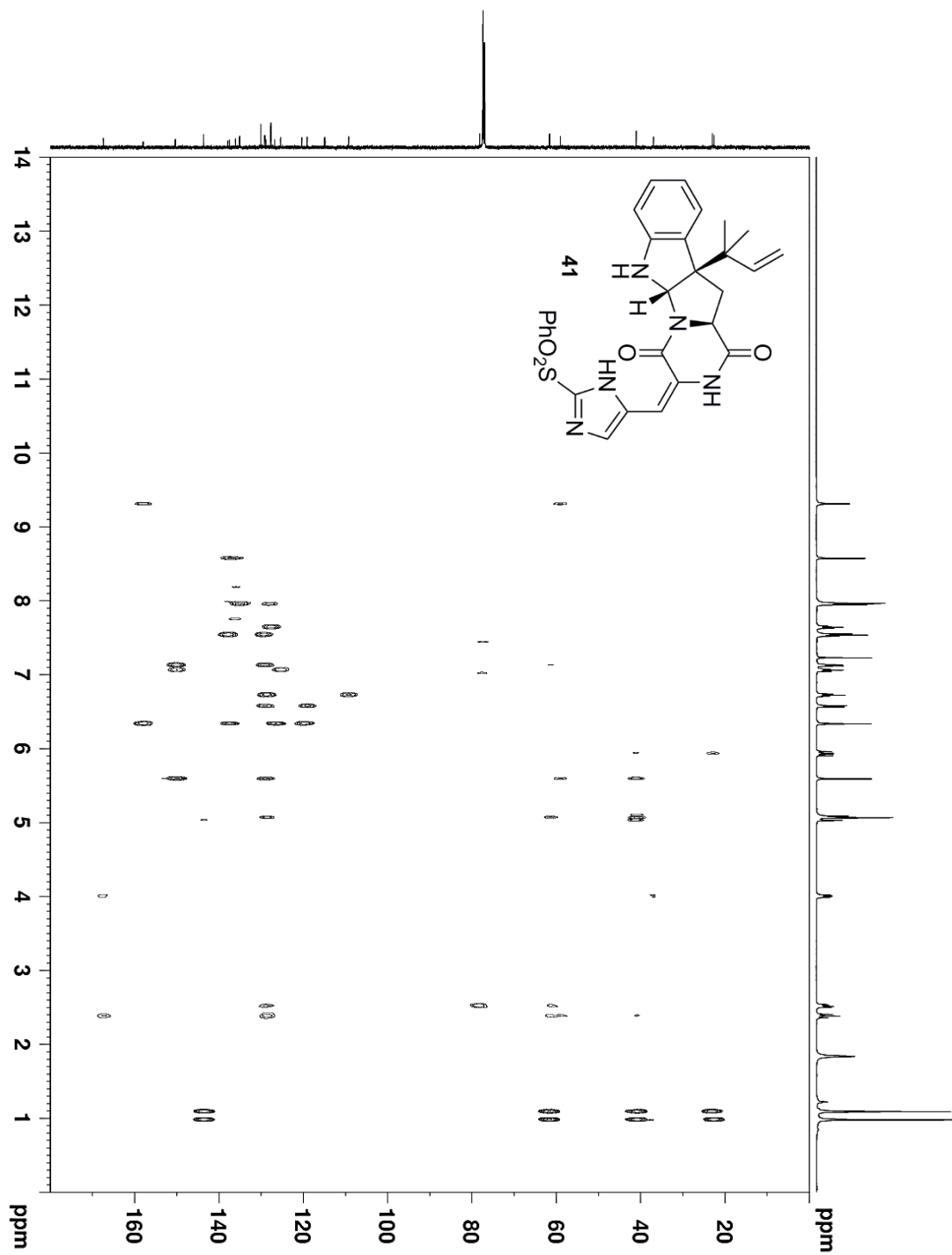
Supplementary Figure 2.35:  $^{13}\text{C}$  NMR (125 MHz,  $\text{CDCl}_3$ ) Spectrum of 41



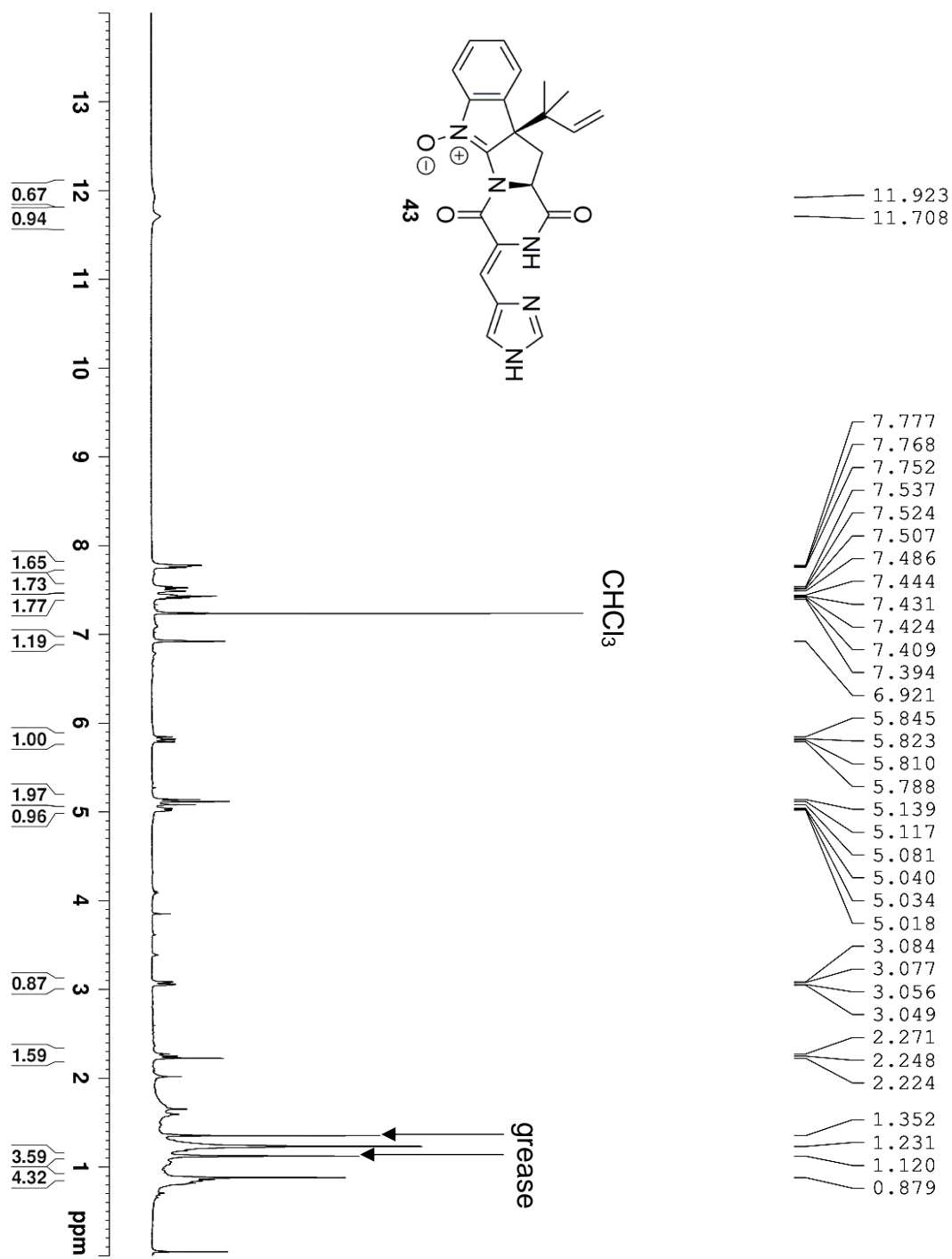
Supplementary Figure 2.36:  $^1\text{H}$ - $^1\text{H}$  COSY NMR (500 MHz,  $\text{CDCl}_3$ ) Spectrum of 41



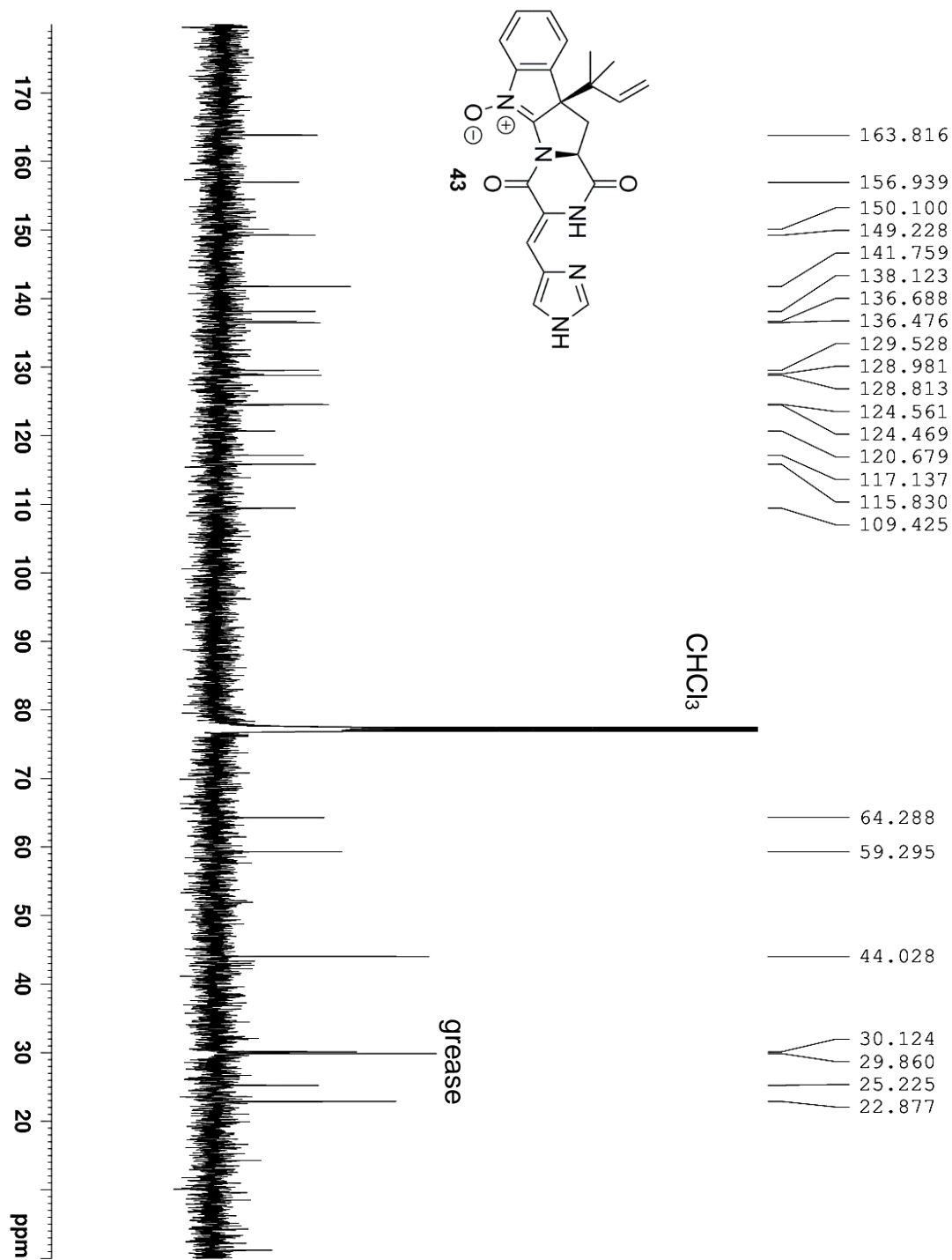
Supplementary Figure 2.37: <sup>1</sup>H-<sup>13</sup>C HSQC NMR (500 MHz, CDCl<sub>3</sub>) Spectrum of 41



Supplementary Figure 2.38:  $^1\text{H}$ - $^{13}\text{C}$  HMBC NMR (500 MHz,  $\text{CDCl}_3$ ) Spectrum of **41**

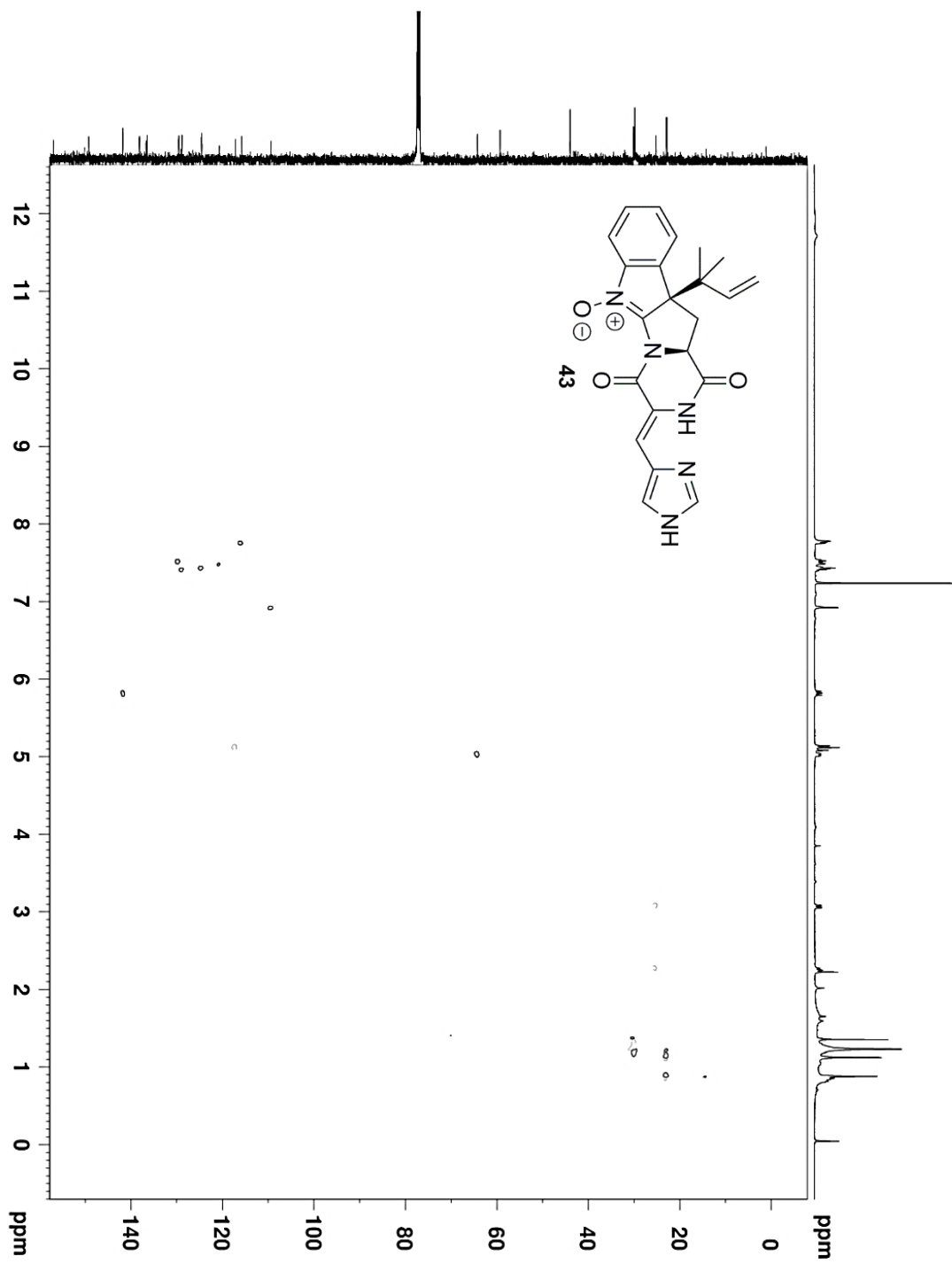


Supplementary Figure 2.39:  $^1\text{H}$  NMR (500 MHz,  $\text{CDCl}_3$ ) Spectrum of **43**

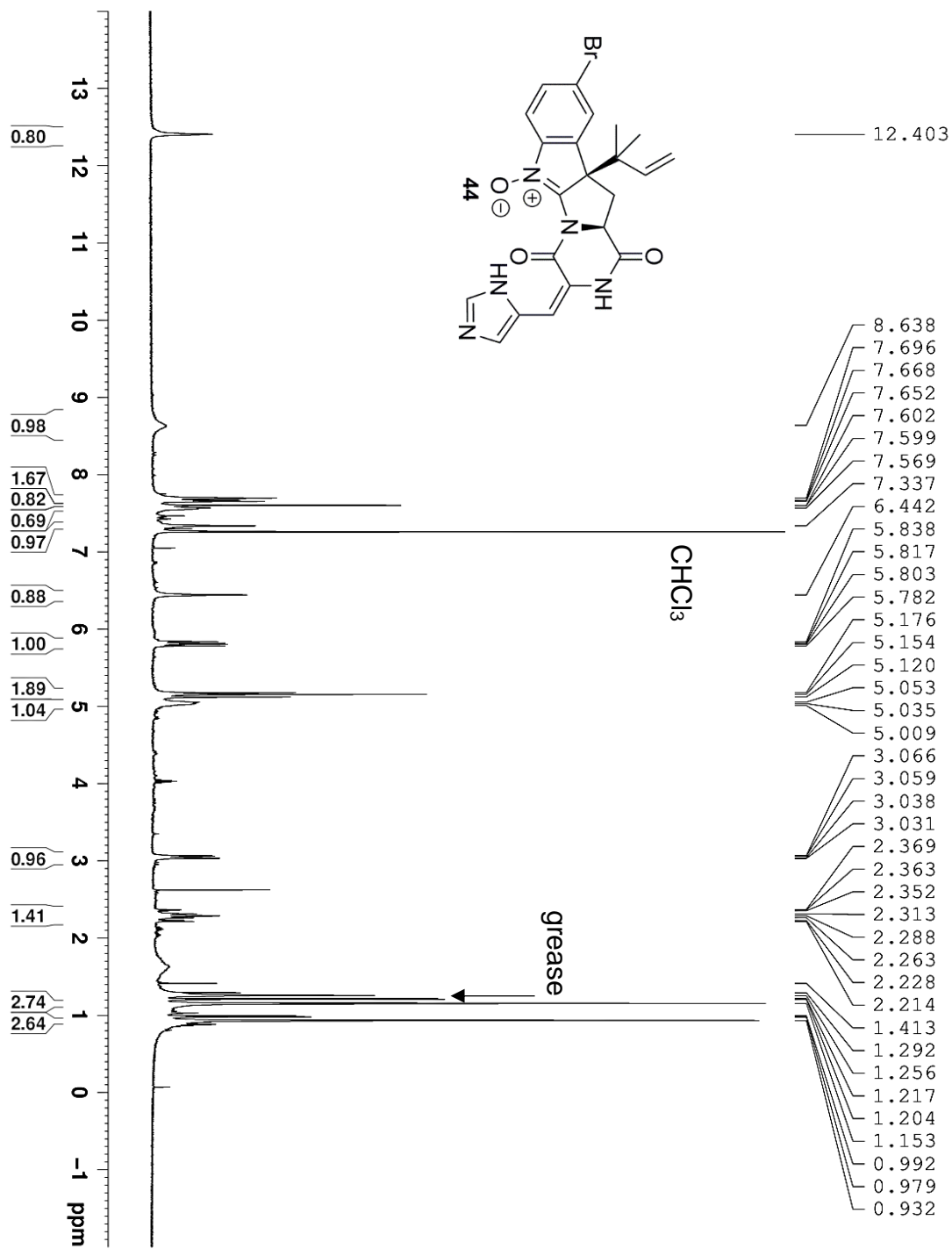


Supplementary Figure 2.40: <sup>13</sup>C NMR (125 MHz, CDCl<sub>3</sub>) Spectrum of **43**

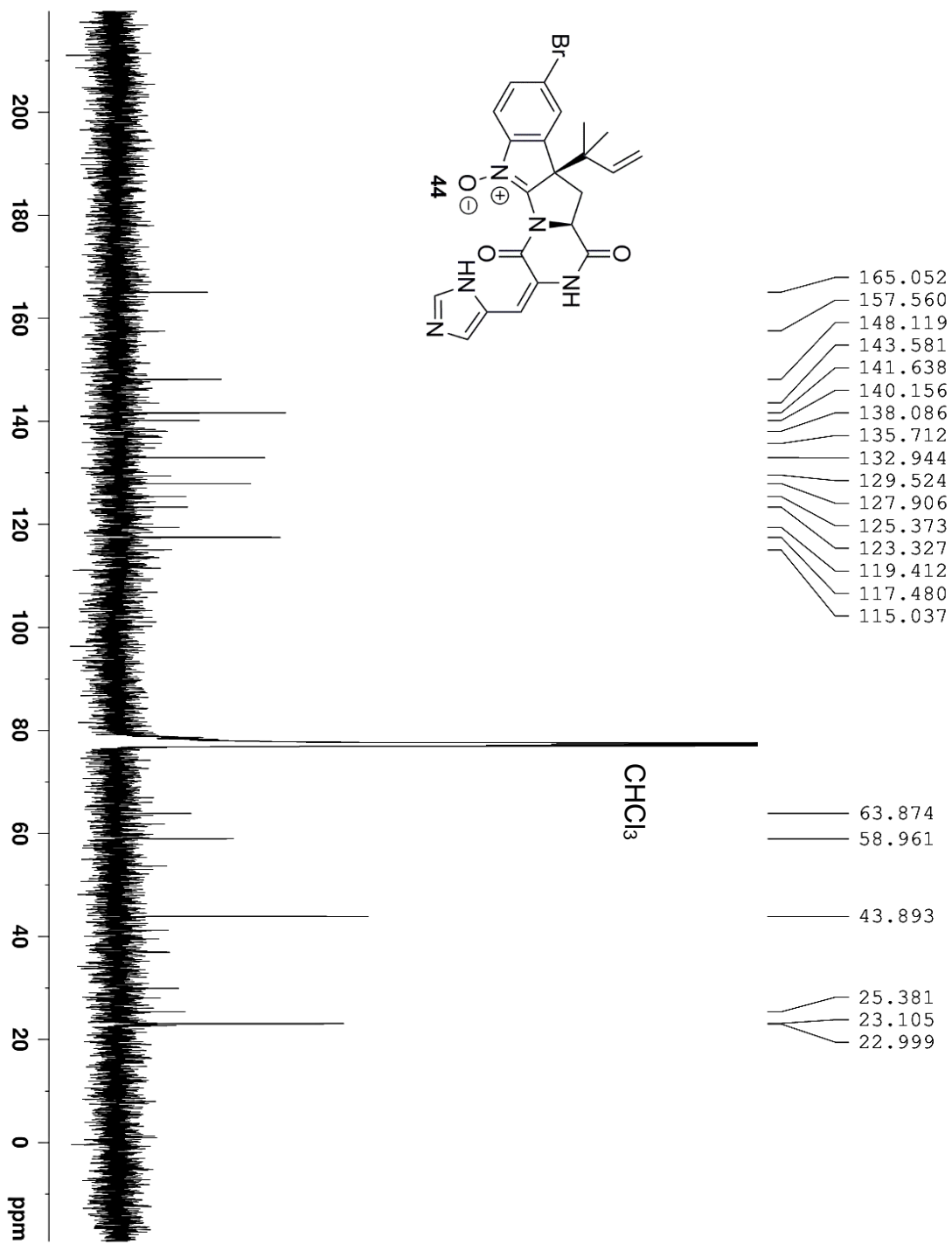




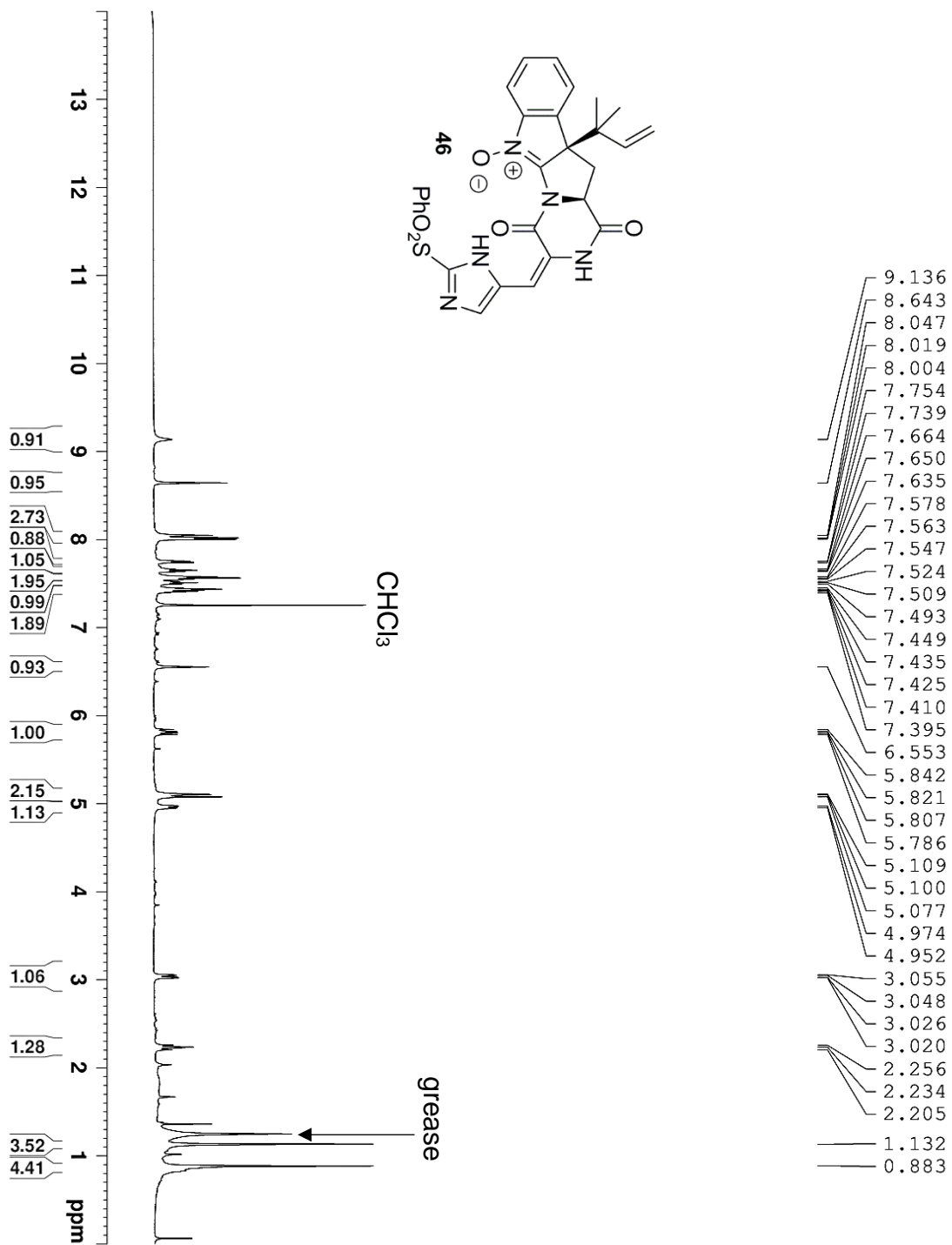
Supplementary Figure 2.41:  $^1\text{H}$ - $^{13}\text{C}$  HSQC NMR (500 MHz,  $\text{CDCl}_3$ ) Spectrum of 43



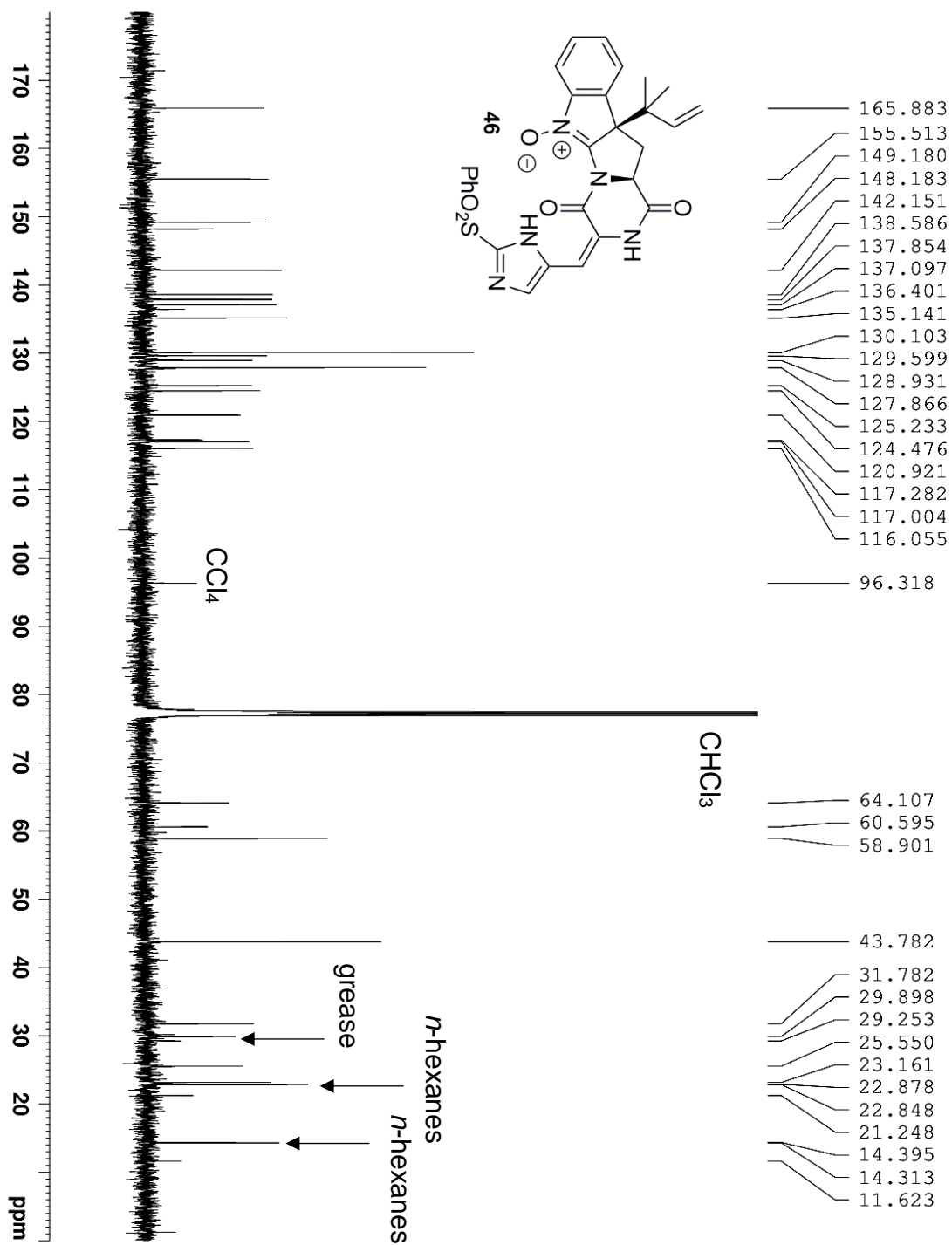
Supplementary Figure 2.42:  $^1\text{H NMR}$  (500 MHz,  $\text{CDCl}_3$ ) Spectrum of **44**



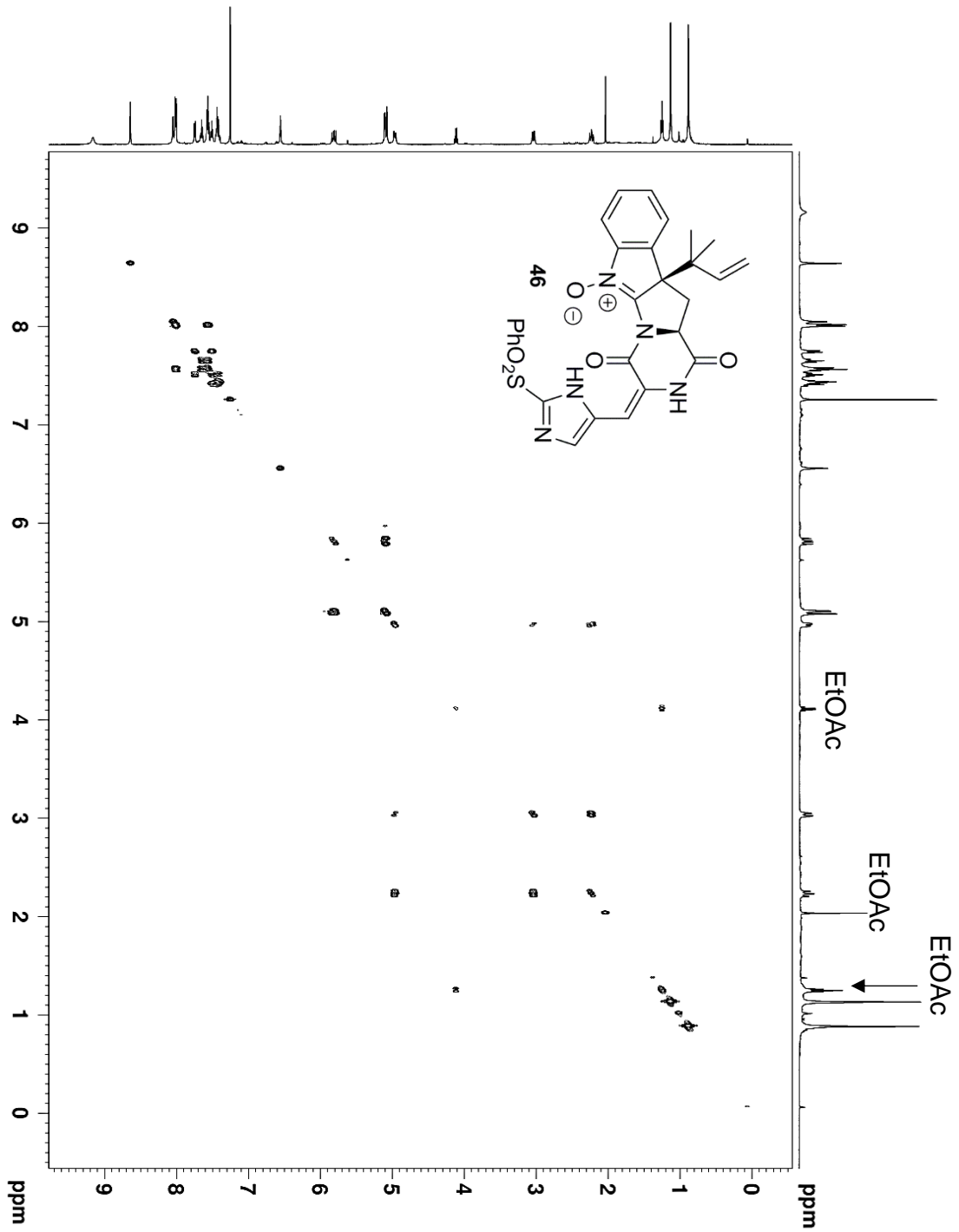
Supplementary Figure 2.43:  $^{13}\text{C}$  NMR (125 MHz,  $\text{CDCl}_3$ ) Spectrum of 44



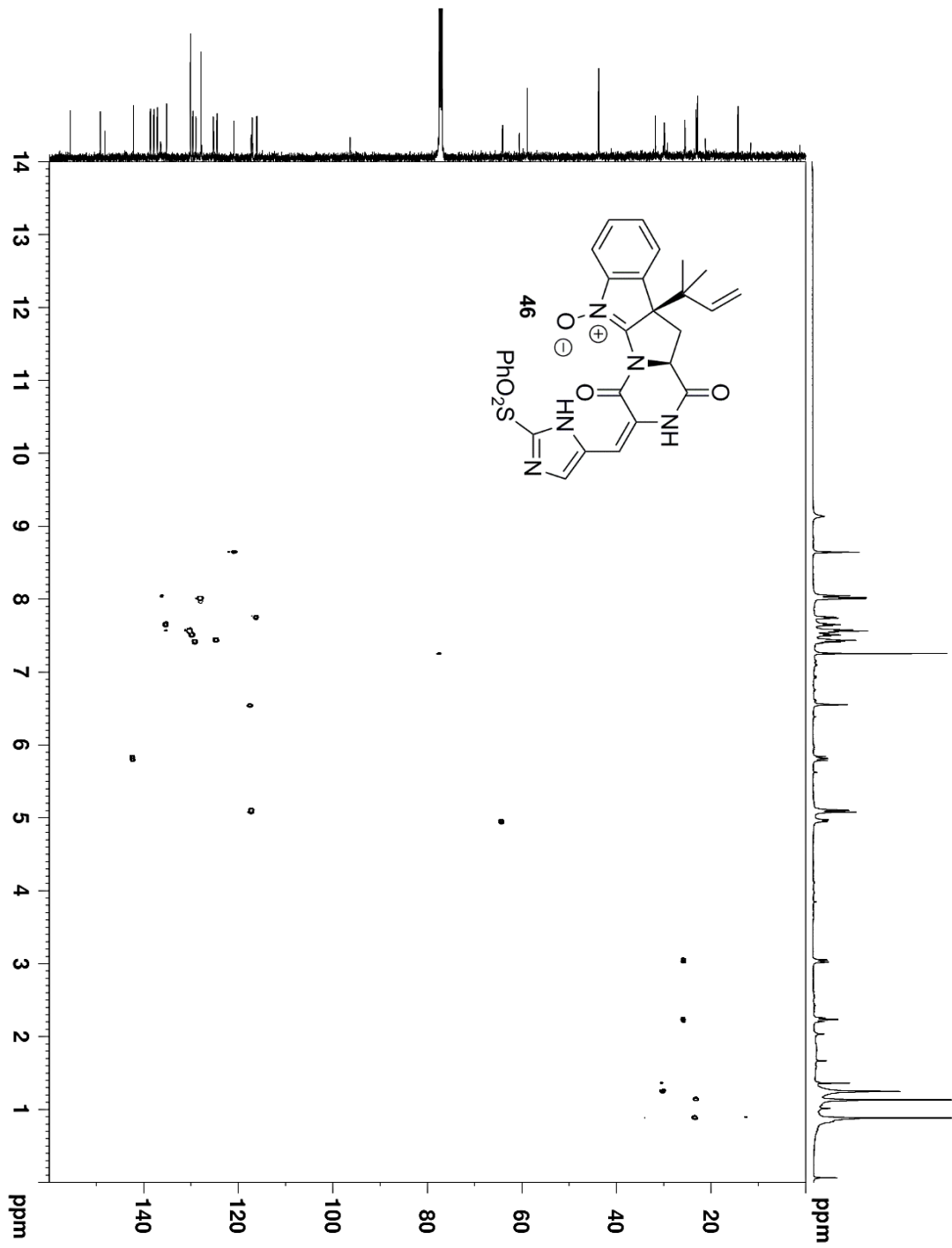
Supplementary Figure 2.44: <sup>1</sup>H NMR (500 MHz, CDCl<sub>3</sub>) Spectrum of **46**



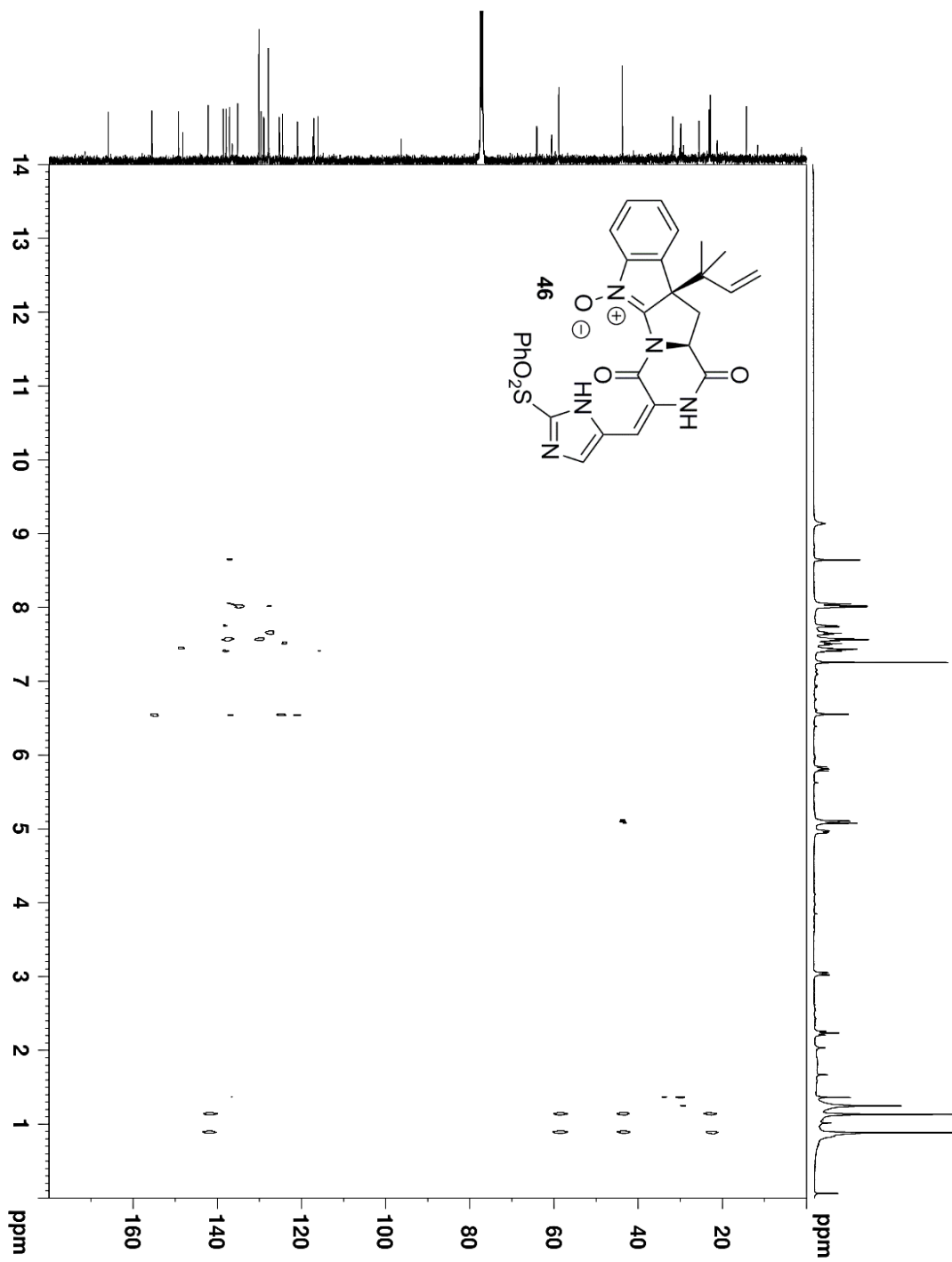
Supplementary Figure 2.45: <sup>13</sup>C NMR (125 MHz, CDCl<sub>3</sub>) Spectrum of **46**



Supplementary Figure 2.46: <sup>1</sup>H-<sup>1</sup>H COSY NMR (500 MHz, CDCl<sub>3</sub>) Spectrum of 46

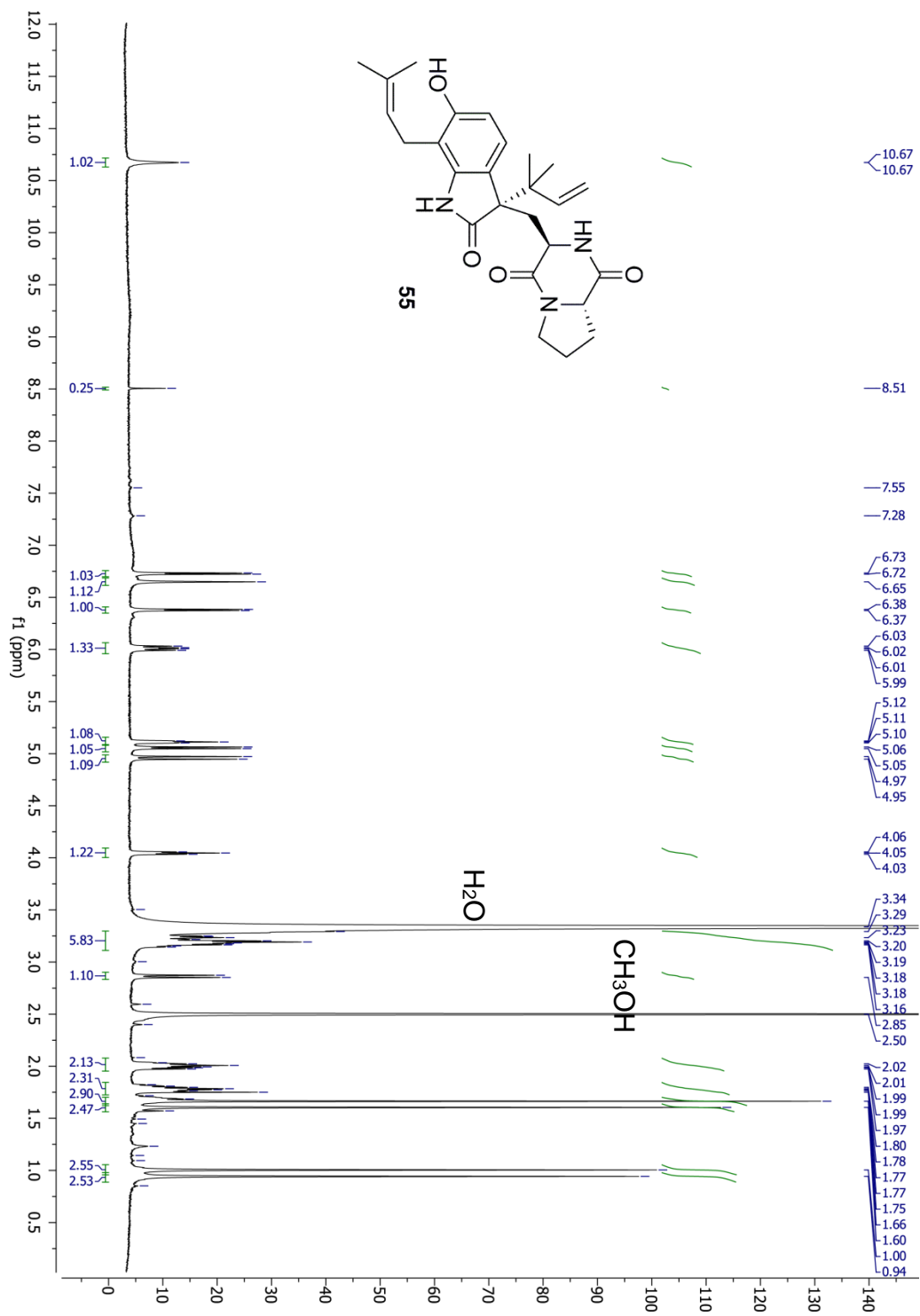


. Supplementary Figure 2.47: <sup>1</sup>H-<sup>13</sup>C HSQC NMR (500 MHz, CDCl<sub>3</sub>) Spectrum of 46

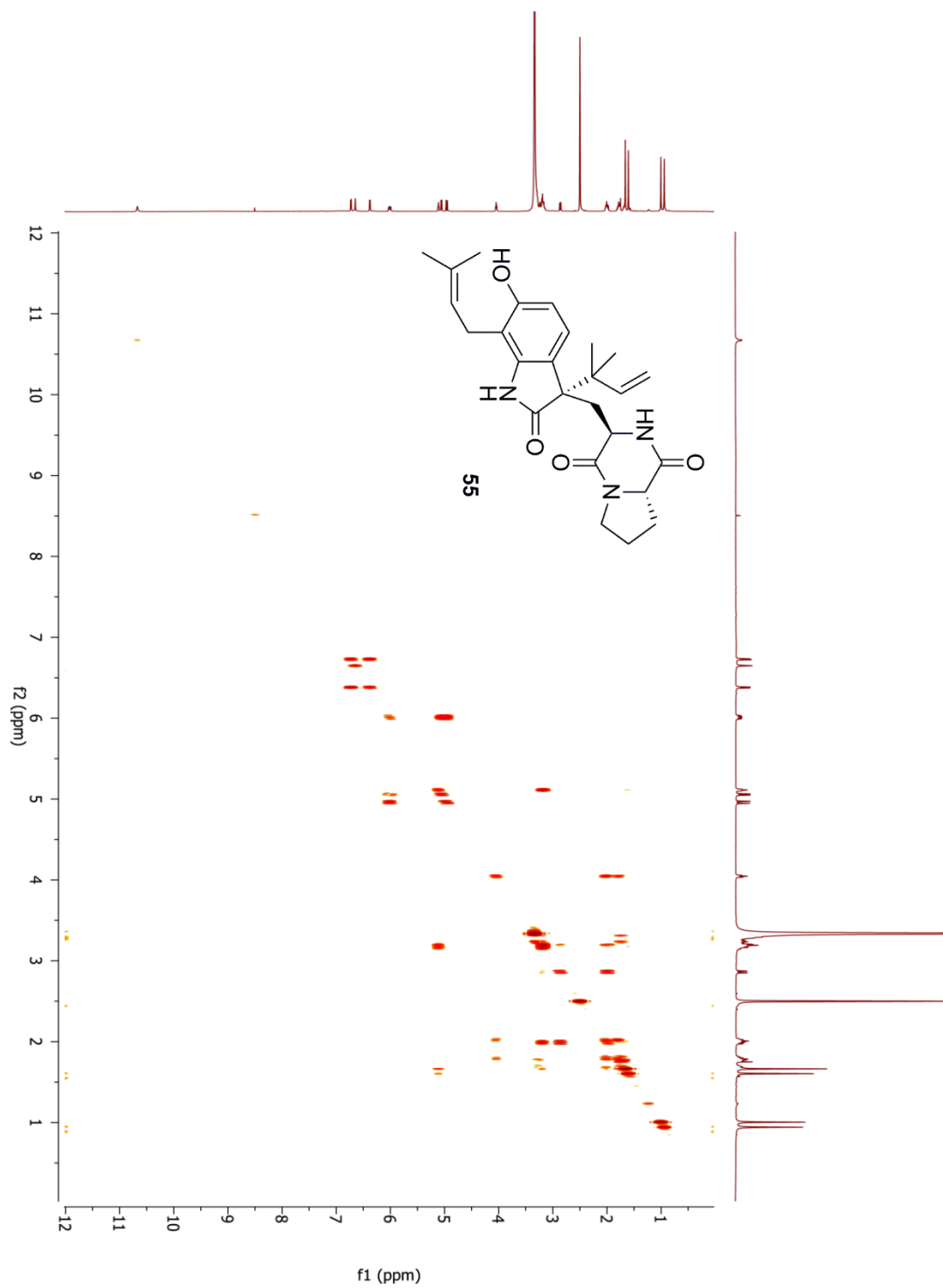


Supplementary Figure 2.48:  $^1\text{H}$ - $^{13}\text{C}$  HMBC NMR (500 MHz,  $\text{CDCl}_3$ ) Spectrum of 46

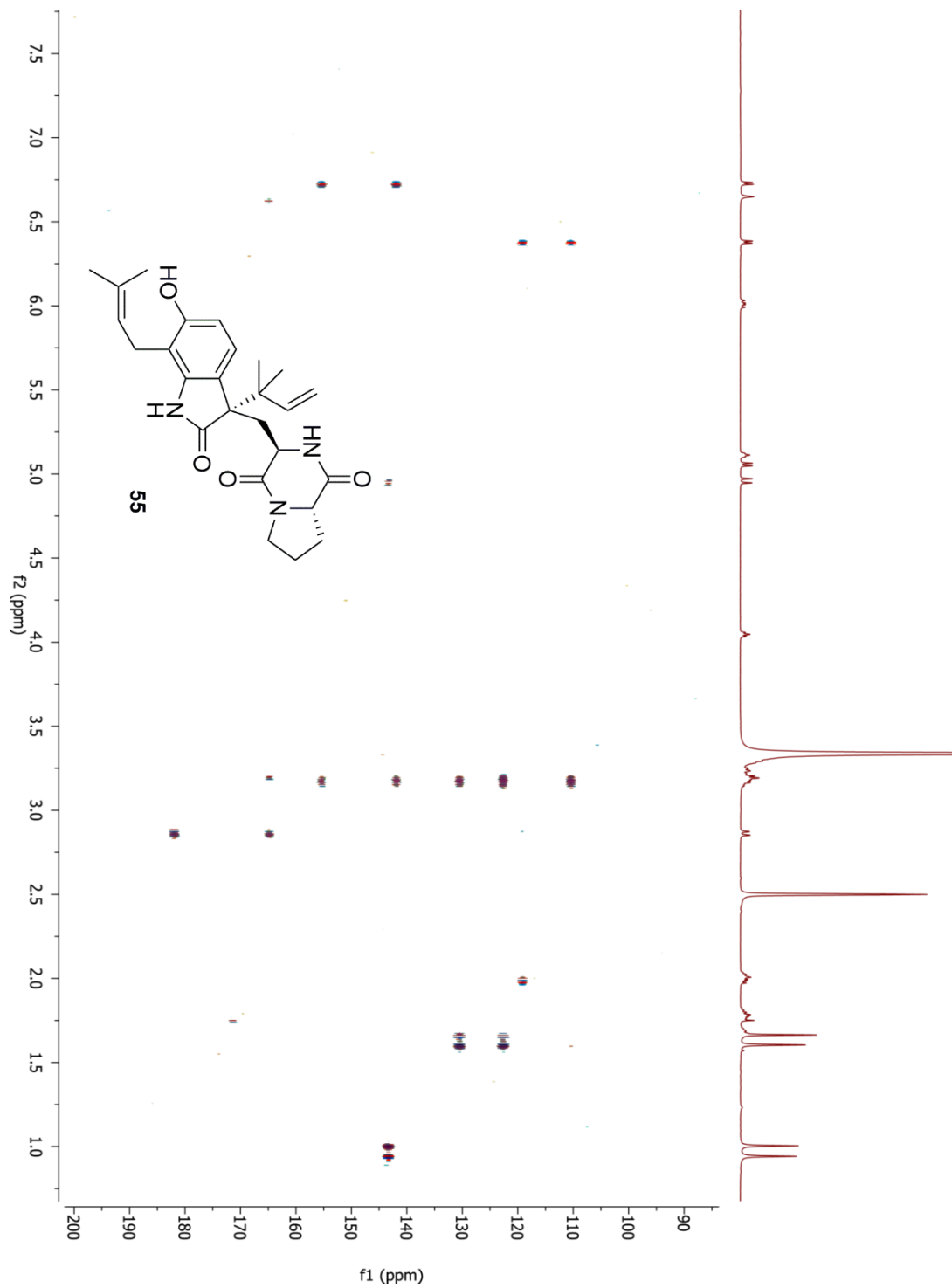




Supplementary Figure 2.49: <sup>1</sup>H NMR (700 MHz, DMSO-*d*<sub>6</sub>) Spectrum of **55**



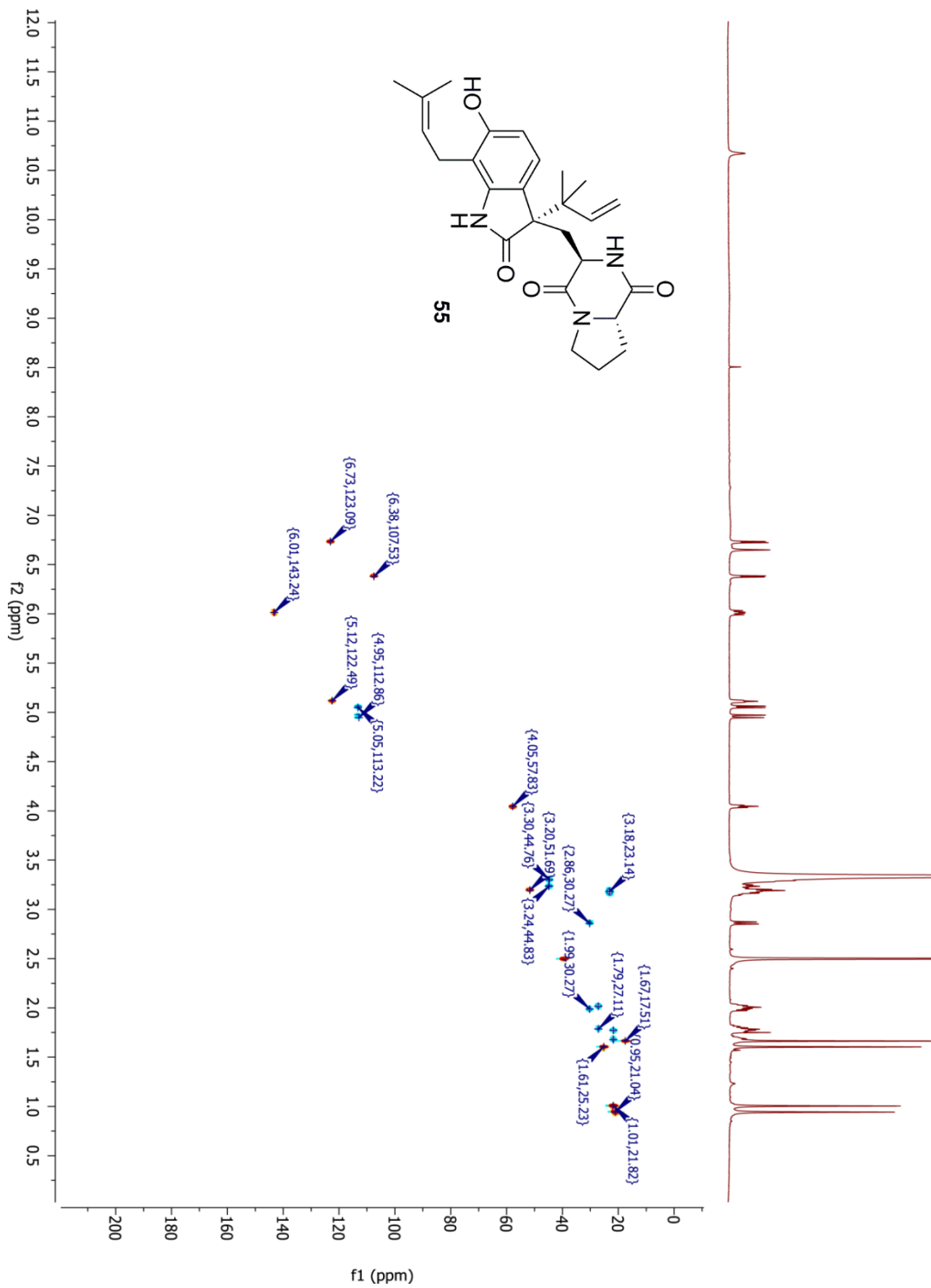
**Supplementary Figure 2.50:**  $^1\text{H}$ - $^1\text{H}$  gCOSY NMR (700 MHz,  $\text{DMSO}-d_6$ ) Spectrum of **55**



Supplementary Figure 2.51:  $^1\text{H}$ - $^{13}\text{C}$  gHMBCAD NMR (700 MHz,  $\text{DMSO}-d_6$ ) Spectrum

of 55

135



Supplementary Figure 2.52:  $^1\text{H}$ - $^{13}\text{C}$  gHSQC NMR (700 MHz,  $\text{DMSO}-d_6$ ) Spectrum of

55

136

## CHAPTER THREE

### ROQUEFORTINE C N-OXIDATION BY SYNTHETIC MEANS

Material in this chapter reproduced in part with permission from:

Gober, C.; Joullié, M. M. *Isr. J. Chem.* **2016**, 57(3-4), 303-308.

Copyright 2016 John Wiley and Sons.

## I. Introduction

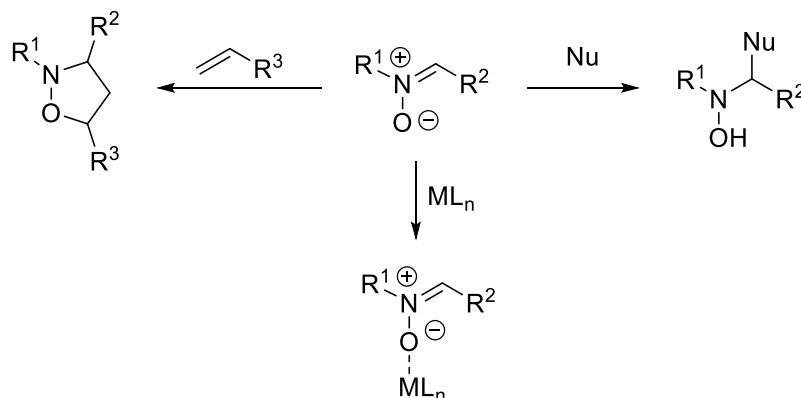
While the biomimetic synthesis of roquefortine L has been carried out using flavin monooxygenase OxaD,<sup>1</sup> the synthesis of roquefortine L by traditional synthetic methods has not yet been explored. Little has been done in the way of comparison studies to investigate the capacities of different oxidants towards N-oxidation,<sup>2</sup> particularly on systems as complex as roquefortine C. The fundamental differences between various oxidants are often not investigated, and investigation of the chemical kinetics of each of these oxidants may elicit new information regarding their reactivity towards complex systems. Therefore, it was of interest to examine the oxidation of the secondary amine functionality in roquefortine C to a nitron functionality by a variety of oxidizing reagents in an attempt to understand the etiology of the process.

## II. Background

### A. Nitrones

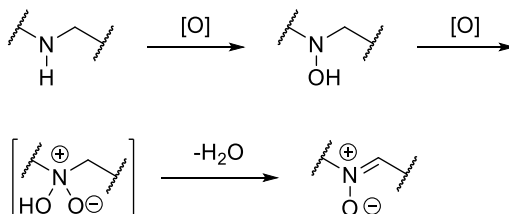
The nitron is simultaneously one of the most valuable yet underutilized functional groups in organic chemistry. These *N*-oxides are excellent building blocks for the synthesis of complex molecules, acting as electrophiles as well as 1,3-dipoles in cycloaddition reactions (Scheme 3.1).<sup>3</sup> Nitrones have also been implemented as ligands in transition metal complexes.<sup>4</sup> These compounds show promise in several applications; nitrones have been shown to inhibit oncogenic proteins as well as serving as spin traps for free radicals, which have been

implicated in neurodegenerative disease.<sup>5,6</sup> Aryl nitrones in particular have found use in photolithography techniques as photo-bleachable compounds used to enhance contrast.<sup>7</sup>



**Scheme 3.1:** Nitrones as chemical building blocks

The oxidation of amines, typically carried out with organic reagents such as dimethyldioxirane (DMDO), peroxyacids, and sulfonyloxaziridines as well as metal peroxo complexes, is one of the most common methods to synthesize nitrones. In this method of synthesis, a nitronium ion is formed following two sequential oxidations of the amine and subsequent elimination of water (Scheme 3.2).



**Scheme 3.2:** Mechanism of amine oxidation to nitrones

Despite the numerous approaches that have been developed for this transformation, the synthesis of nitrones is often fraught with complications. The

oxidation of unsymmetrical amines is plagued with regioselectivity issues,<sup>8</sup> and owing to its electrophilic  $\alpha$ -carbon, nitrones are subject to attack by nucleophiles, particularly in the presence of acidic media. *N*-Aryl amines such as roquefortine C are particularly difficult to oxidize as single electron transfer to form a relatively stable aminium radical cation results in C-N bond cleavage.<sup>9</sup> *N*-Aryl nitrones are also particularly unstable, as formation of the nitrone eliminates lone pair delocalization onto the aromatic ring.<sup>10</sup>

## B. Chemical Kinetics and Reaction Progress Kinetic Analysis

The study of chemical kinetics examines how one compound is converted to another. Chemical kinetics is particularly important in the field of organic chemistry as it can be implemented to elucidate mechanisms to new reactions or to compare rates of reaction between different reactants. Chemical reactions occur as a result of collisions between molecules, and as such, the rate of any reaction is proportional to the concentration of the reactant (Eq. 3.1). Reaction rate is also proportional to a rate constant  $k$ , which is a representation of a reaction's dependence on temperature and activation energy.

$$rate \propto k[R] \quad (\text{Eq. 3.1})$$

This relationship between rate, reactant concentration, and the rate constant is also time dependent. As more of reactant R (Eq. 3.2) is consumed over the course of a reaction, the rate of the reaction changes. This change can be reflected by writing the rate as a derivative as a function of time (Eq. 3.3).





$$\text{rate} = -k \frac{d[R]}{dt} = k \frac{d[P]}{dt} \quad (\text{Eq. 3.3})$$

Rate laws describe the rate of a chemical reaction as a function of rate constant and the concentration of reactants. The rate law for a given reaction  $A + B \rightarrow P$  (Eq. 3.4) is described in Eq. 3.5. The degree to which the rate of reaction is controlled by the concentration of the reactants is reflected in the partial reaction orders  $x$  and  $y$ . The sum of all partial reaction orders for a given reaction represents the overall reaction order.



$$\frac{d[P]}{dt} = k[A]^x[B]^y \quad (\text{Eq. 3.5})$$

Integration of differential rate equations provides integrated rate equations that describe the reactant concentration as a function of time. A simple first order reaction (Eq. 3.6) can be described by the rate law in Eq. 3.7. Integration of this equation gives the integrated rate law (Eq. 3.8), showing an exponential dependence of  $A$  with respect to the rate constant.



$$\frac{d[P]}{dt} = -\frac{d[A]}{dt} = k[A] \quad (\text{Eq. 3.7})$$

$$[A] = [A]_0 e^{-kt} \quad (\text{Eq. 3.8})$$

Integration of a second order bimolecular differential rate law (Eq. 3.10) leads to the integrated rate law as shown in Eq. 3.11.



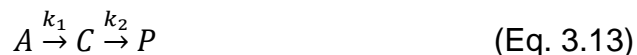
$$\frac{d[P]}{dt} = k[A][B] \quad (\text{Eq. 3.10})$$

$$\frac{1}{[B]_0 - [A]_0} \ln \left( \frac{[A]_0[B]}{[B]_0[A]} \right) = kt \quad (\text{Eq. 3.11})$$

Reactions that are second order in nature can often be simplified using experimental conditions to mimic first order behavior. This is accomplished by holding one of the reactants in great excess (usually more than 10 equivalents). In this way, the concentration of reactant B remains essentially constant over the course of the reaction, allowing for the reaction to be analyzed as if it were first order (Eq. 3.12). This process is known as pseudo-first order kinetics.

$$\frac{d[P]}{dt} = k[A][B]_0 = k'[A] \quad (\text{Eq. 3.12})$$

Many reactions have more than one step, which leads to rate laws involving the sum of two terms (Eq. 3.14).



$$\frac{d[C]}{dt} = k_1[A] - k_2[C] \quad (\text{Eq. 3.14})$$

The rate laws for multi-step reactions can become extraordinarily complex; however, if over the course of a multi-step reaction a transient intermediate is formed, the steady state approximation can be used to simplify the resulting rate equations. The steady state approximation assumes that the transient intermediate C reacts quickly and is thus always low in concentration. Using this approximation, the concentration of this fleeting intermediate is assumed to be constant during the course of the reaction (Eq. 3.16). Rearrangement of Eq. 3.16 and substitution of Eq. 3.17 into Eq. 3.15 gives Eq. 3.18, which predicts first order behavior with respect to A.

$$\frac{d[P]}{dt} = k_2[C] \quad (\text{Eq. 3.15})$$

$$\frac{d[I]}{dt} = k_1[A] - k_2[C] = 0 \quad (\text{Eq. 3.16})$$

$$[C] = \frac{k_1[A]}{k_2} \quad (\text{Eq. 3.17})$$

$$\frac{d[P]}{dt} = k_1[A] \quad (\text{Eq. 3.18})$$

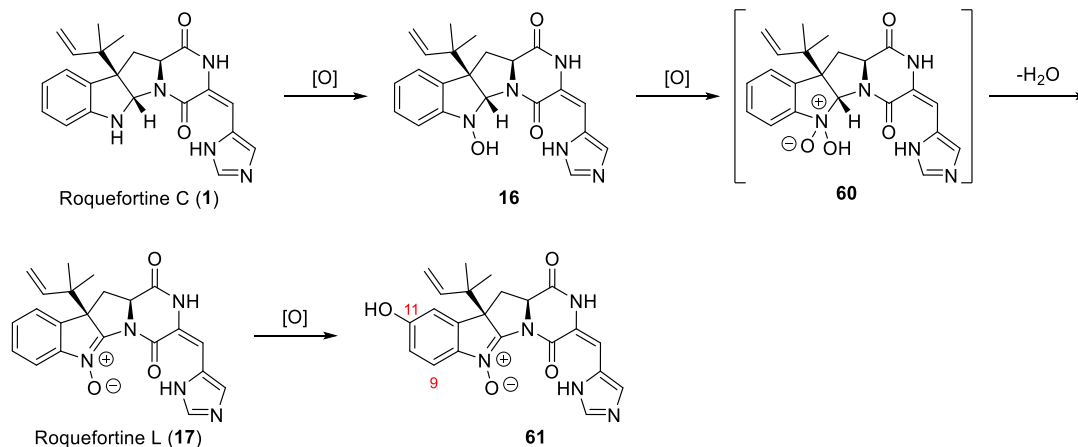
Using reaction progress kinetics techniques to monitor the concentration of each reactant as a function of time allows one to solve for each reactant's partial reaction order and the rate constant. These values can provide insight into the mechanism of a reaction or the reactivity of a particular species. Reaction progress kinetics can be analyzed using a number of experimental techniques, including UV-Vis spectroscopy, IR spectroscopy, high performance liquid

chromatography (HPLC), liquid chromatography-mass spectrometry (LC-MS), and NMR spectroscopy.

### III. Results and Discussion

#### A. Roquefortine C N-Oxidation Products

A recently published method using a hydrogen peroxide-trichloroacetonitrile system for the oxidation of secondary amines to nitrones<sup>11</sup> prompted us to investigate the kinetics of roquefortine C oxidation (Scheme 3.3). This oxidant was particularly interesting given that it yielded higher percentages of the hydroxylamine intermediate (**16**) than other more reactive oxidants such as *m*-chloroperbenzoic acid (mCPBA).



**Scheme 3.3:** Roquefortine C N-oxidation products

In addition, roquefortine L was shown to be further oxidized to a compound of novel structure (**61**). LC-MS analysis indicated the addition of 16 Da following the oxidation of roquefortine L, pointing to overall addition of one atom of oxygen.

Additionally,  $^1\text{H}$  NMR of the unknown oxidation product in methanol- $d_4$  revealed a doublet at 6.60 ppm ( $J = 1.3$  Hz), a doublet of doublets at 6.63 ppm ( $J = 1.4, 9.7$  Hz), and a doublet at 7.60 ppm ( $J = 9.7$  Hz). This splitting pattern is indicative of oxidative substitution at C11, *para* to the nitronone functionality.  $^1\text{H}$ - $^{13}\text{C}$  HMBC analysis also showed a strong correlation between the C9 hydrogen at 7.60 ppm and the 186.7 ppm peak in the  $^{13}\text{C}$  NMR spectrum. As  $^3J_{\text{CH}}$  is generally larger than  $^2J_{\text{CH}}$  and  $^4J_{\text{CH}}$  for aromatic systems, this correlation also points to oxidative substitution at C11.<sup>12</sup>

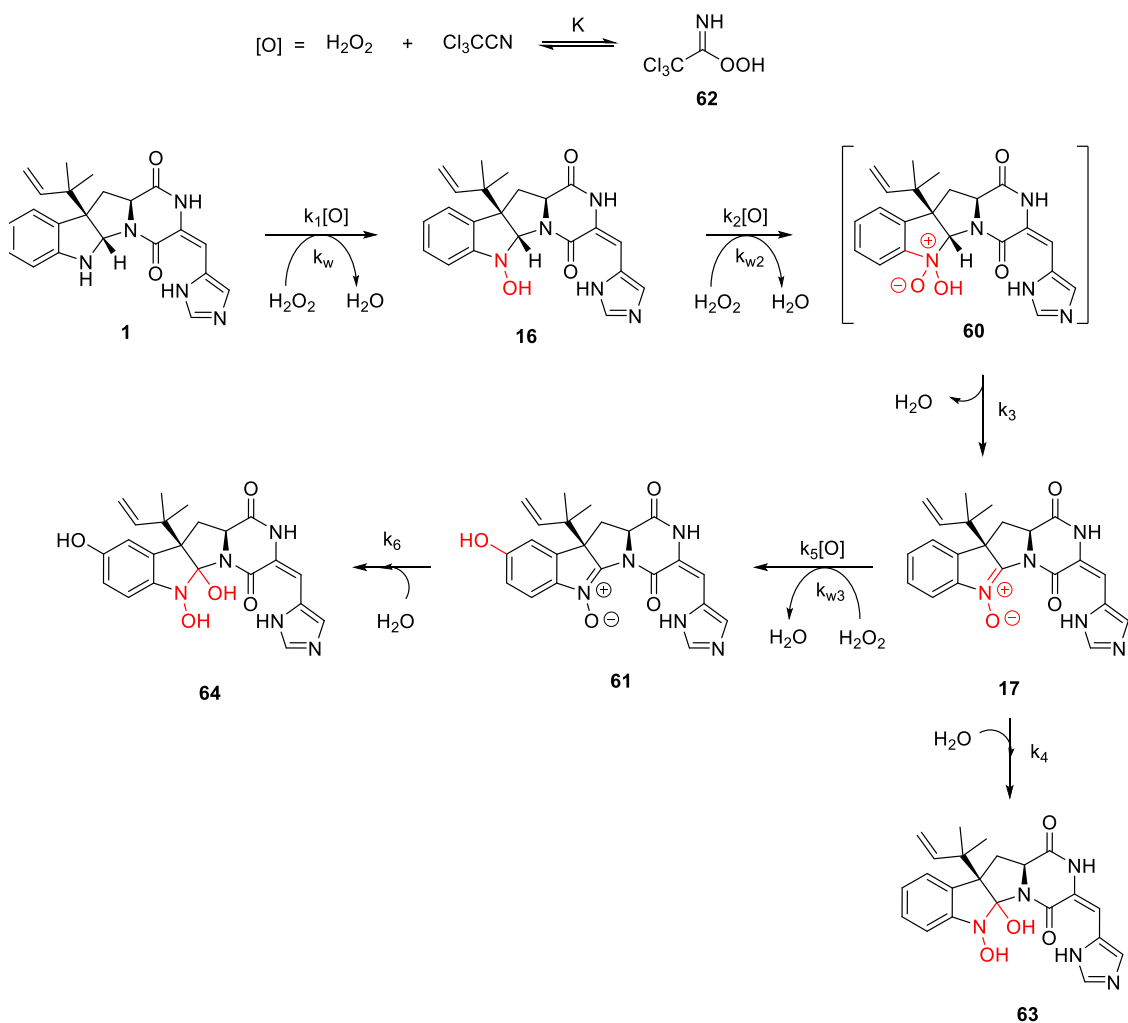
The formation of phenol **61** was an unexpected result that warranted further discussion. The hydroxylation of an *N*-aryl nitronone has been observed in only one other instance in the literature.<sup>13</sup> Electrophilic aromatic hydroxylation with mCPBA has been observed, however only in activated arenes.<sup>14</sup> Formation of **61** is particularly interesting in this instance as hydroxylation occurs *para* to the nitronone and not at the *meta* position as one might expect for electrophilic aromatic substitution of a deactivated arene. This result leads us to believe that the hydroxylation is occurring via a non-electrophilic mechanism. Given the substitution pattern, one might imagine this reaction proceeding via a nucleophilic mechanism. Vicarious nucleophilic substitution of nitroarenes to form *o*- and *p*-nitrophenols has been reported with *tert*-butyl and cumene hydroperoxides;<sup>15</sup> however, these reactions were carried out in strongly basic conditions to form the necessary nucleophilic alkyl hydroperoxide anions.

One could also imagine this reaction to proceed through a free radical process. Homolysis of the peroxy bond of peracids and peroxyimidic acids has been suggested based upon density functional theory (DFT) calculations;<sup>16</sup> however, attempts to inhibit free radicals using butylated hydroxytoluene (BHT) did not affect formation of **61**. This experiment leads us to believe that either this reaction is not occurring by a free radical mechanism or **17** is more effective at trapping free radicals than BHT, which is possible given that nitrones are known spin traps. Given these conflicting results, it is difficult at this time to ascertain the mechanism of formation of compound **61**.

## B. Derivation of N-Oxidation Rate Laws

Due to the unique kinetics of this oxidant, it was of interest to examine the kinetics of this reaction sequence as compared to other electrophilic oxidants (Scheme 3.4). The kinetics of this reaction sequence can be described by Equations 3.19-3.24. The generation of the reactive peroxyimidic acid species **62** is expressed by the equilibrium constant  $K$  (Eq. 3.19). Using a large excess of hydrogen peroxide and trichloroacetonitrile, and thus peroxyimidic acid, the rate of consumption of roquefortine C (**1**) can be expressed as pseudo first order, assuming the rate of oxidation by hydrogen peroxide alone is negligible (Equation 3.20). Similarly, the rate of consumption of the hydroxylamine **16** can be expressed as a pseudo first order reaction (Equation 3.21). Assuming the dehydration of **60** is extremely rapid, we can simplify the rate expression for **60** using the steady state approximation (Equation 3.22). The equations expressing the concentration of the

nitrone roquefortine L (**17**) versus time and the concentration of the phenol (**61**) versus time were derived using the integrating factor method (Equations 3.23 and 3.24).



**Scheme 3.4:** Roquefortine C oxidation pathway

$$[\mathbf{62}] = K[H_2O_2][Cl_3CCN] \quad (\text{Eq. 3.19})$$

$$[\mathbf{1}] = [\mathbf{1}]_0 e^{-Zt} \quad (\text{Eq. 3.20})$$

$$\text{where } Z = (k_1 K[Cl_3CCN]_0 + k_w)[H_2O_2]_0$$

$$[\mathbf{16}] = \frac{Z[\mathbf{1}]_0}{Y-Z} (e^{-Zt} - e^{-Yt}) \quad (\text{Eq. 3.21})$$

$$\text{where } Y = (k_2K[Cl_3CCN]_0 + k_{w2})[H_2O_2]_0$$

$$[\mathbf{60}] = \frac{Y[\mathbf{16}]}{k_3} \quad (\text{Eq. 3.22})$$

$$[\mathbf{17}] = \frac{YZ[\mathbf{1}]_0 e^{-(k'_4+U)t}}{Y-Z} \left( \frac{e^{(k'_4+U-Z)t} - 1}{k'_4+U-Z} + \frac{e^{(k'_4+U-Y)t} - 1}{k'_4+U-Y} \right) \quad (\text{Eq. 3.23})$$

$$\text{where } k'_4 = k_4[H_2O], \quad U = k_5K[Cl_3CCN]_0[H_2O_2]_0$$

$$[\mathbf{61}] = \frac{UYZ[\mathbf{1}]_0 e^{-(k'_6)t}}{Y-Z} \left( \frac{1}{k'_4+U-Z} \left( \frac{e^{(k'_6-Z)t} - 1}{k'_6-Z} - \frac{e^{(k'_6-k'_4-U)t} - 1}{k'_6-k'_4-U} \right) - \frac{1}{k'_4+U-Y} \left( \frac{e^{(k'_6-Y)t} - 1}{k'_6-Y} - \frac{e^{(k'_6-k'_4-U)t} - 1}{k'_6-k'_4-U} \right) \right) \quad (\text{Eq. 3.24})$$

$$\text{where } k'_6 = k_6[H_2O]$$

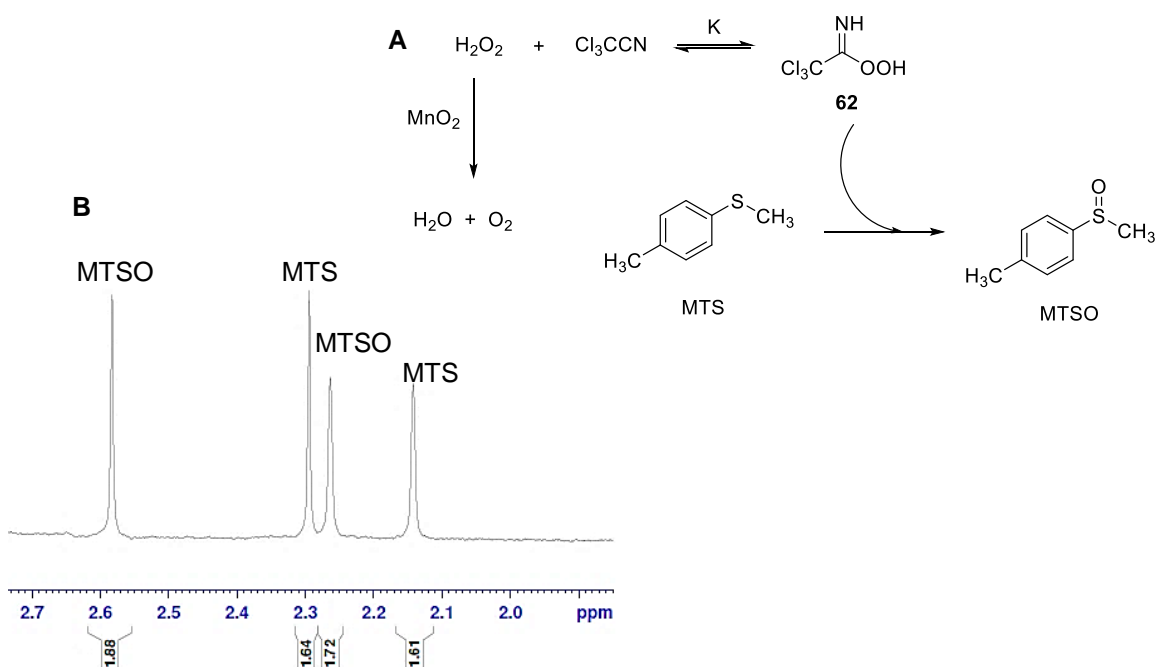
### C. Attempts to Monitor Reaction Kinetics

The equilibrium constant  $K$  for the formation of **62** was determined through reaction with methyl *p*-tolyl sulfide (MTS) and analysis of the sulfide/sulfoxide ratio by  $^1\text{H}$  NMR (Scheme 3.5). Simultaneous addition of manganese dioxide to rapidly decompose the hydrogen peroxide prevented any shift in equilibrium following the addition of methyl *p*-tolyl sulfide.<sup>17</sup> The equilibrium constant  $K$  was determined to be  $K = 23.0 \pm 3.99 \text{ M}$  ( $n=3$ ).

A number of methods were attempted to observe the reaction progress kinetics of this reaction. The various oxidized species did not possess unique enough UV absorbances to carry out this analysis by UV-Vis spectroscopy. Gas chromatography-mass spectrometry (GC-MS) analysis resulted in significant



fragmentation of the oxidized species, precluding accurate analysis. As acidic conditions are known to drastically increase the rate of hydrolysis of nitron, HPLC and LC-MS analysis was carried out in neutral conditions. This resulted in severe line broadening and overlap of the peaks of interest. Each of the species in this reaction sequence could be resolved by  $^1\text{H}$  NMR (Figure 3.1); however, in situ monitoring of this reaction by  $^1\text{H}$  NMR proved fruitless due to the significant changes in shimming over the course of the reaction as well as interference by hydrogen peroxide.



**Scheme 3.5:** Determination of K for the formation of peroxyimidic acid **62**

(A) Oxidation of methyl *p*-tolyl sulfide (MTS) by peroxyimidic acid **62**; (B)  $^1\text{H}$  NMR spectrum of MTS/MTSO mixture

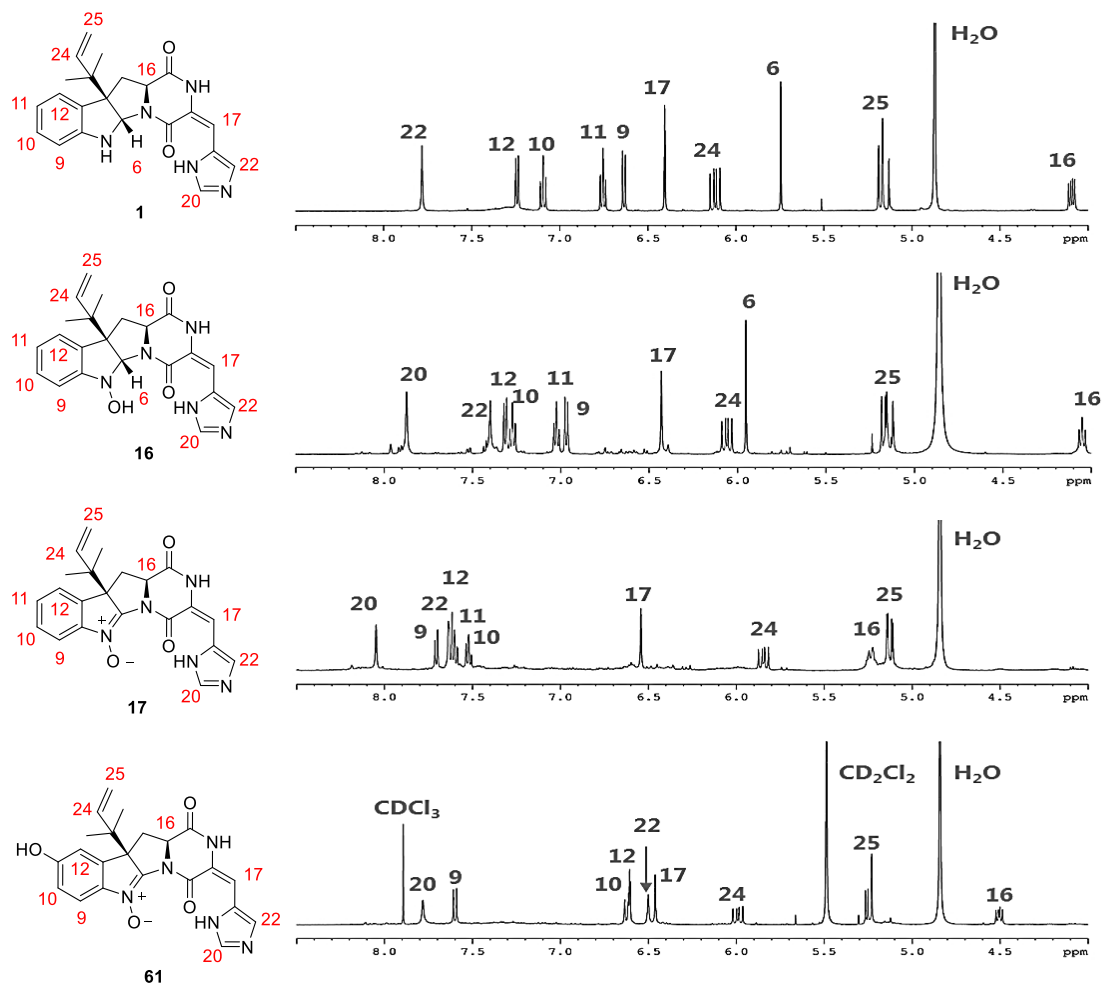


**Figure 3.1:**  $^1\text{H}$  NMR spectra of roquefortine C (**1**) and N-oxidation products  
 $^1\text{H}$  NMR spectra taken in methanol- $d_4$

#### D. N-Oxidation Product Analysis

With previous attempts to monitor the reaction progress kinetics of this reaction sequence proving unsuccessful, we turned our attention towards the analysis of the product mixture of roquefortine C N-oxidation using two equivalents of oxidant. The trichloroacetonitrile-hydrogen peroxide oxidation system was analyzed along with mCPBA, DMDO,  $\text{Na}_2\text{WO}_4/\text{H}_2\text{O}_2$ , potassium

peroxymonosulfate (OXONE ®), and Davis oxaziridine. All of the oxidants investigated gave mixtures of starting material and various oxidized compounds (Table 3.1). Compound **61** was the most abundant product in the majority of the reactions, indicating that the nitrene roquefortine L is most reactive towards oxidation as compared to **1** or the hydroxylamine (**16**). DMDO (Entry 2) and OXONE ® (Entry 4) exhibited the best conversion from **1**, indicating that these oxidants were sufficiently reactive with roquefortine C. The other oxidants featured higher levels of unreacted starting material, indicating that the oxidized products were much more reactive towards further oxidation by the oxidant than the starting amine. Reactions carried out at 0 °C (Entries 7-10) exhibited greater conversion of starting material, indicating that the rapid conversion to **17** and **61** was inhibited by colder temperatures. Davis oxaziridine (Entry 6) and sodium tungstate-hydrogen peroxide (Entry 3) proved to be ineffective at promoting the N-oxidation of **1**.

In an attempt to elucidate the fundamental reasons behind the difference in reactivity of the oxidants, molecular energy calculations were carried out to estimate the partial charge of the electrophilic oxygen atom in each oxidant (Table 3.2). The results of these calculations generally correlate with experimental observations as mCPBA and DMDO, the two oxidants with the least negative partial charges on their electrophilic oxygens, displayed the fastest reaction times. The electrophilicity of the oxidants is not the only factor when determining reaction efficiency, however. Davis oxaziridine, which has comparable electrophilicity to

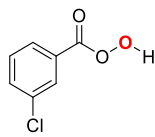
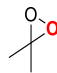
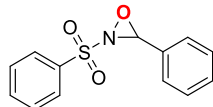
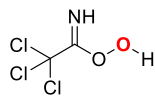
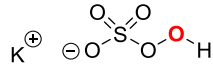
DMDO, displayed poor reactivity with roquefortine C, likely due to the increased steric bulk of this oxidant.

**Table 3.1:** Roquefortine C N-oxidation distribution of products

Entry	Oxidizing agent	Time (h)	Temp (°C)	Products (%)			
				<b>1</b>	<b>5</b>	<b>2</b>	<b>6</b>
1	mCPBA	0.25	25	35	10	34	20
2	DMDO	0.25	25	12	18	29	40
3	Na <sub>2</sub> WO <sub>4</sub> /H <sub>2</sub> O <sub>2</sub>	4	25	88	2	3	7
4	OXONE®	4	25	17	18	29	34
5	<b>62</b> (Cl <sub>3</sub> CCN/H <sub>2</sub> O <sub>2</sub> )	4	25	24	19	15	40
6	Davis oxaziridine	4 (96)	25	85 (75)	5 (6)	7 (3)	3 (15)
7	mCPBA	0.25	0	30	7	37	25
8	DMDO	0.25	0	18	33	13	35
9	OXONE®	4	0	9	15	33	42
10	<b>62</b> (Cl <sub>3</sub> CCN/H <sub>2</sub> O <sub>2</sub> )	4	0	15	16	13	55

While N-oxidations involving organic oxidants are generally thought to involve a concerted mechanism, the mechanism of oxidation by mononuclear tungsten peroxo complexes is still debated. As there is also debate surrounding the active structure of mononuclear tungsten peroxo complexes,<sup>18-20</sup> this oxidant was not included in the partial charge calculations.

**Table 3.2:** Electrophilicity of electrophilic oxidizing reagents

Entry	Oxidant	Oxygen partial charge (e) <sup>a</sup>
1	 mCPBA	-0.352038
2	 DMDO	-0.372807
3	 Davis oxaziridine	-0.386358
4	 <b>62</b>	-0.414521
5	 OXONE®	-0.47801

<sup>a</sup> Calculations carried out at HF/6-311+G(2d,p) level of theory

#### IV. Conclusions

The oxidation of roquefortine C to roquefortine L was demonstrated using a number of different electrophilic oxidizing reagents. While nitrene formation on a complex substrate such as roquefortine C proves feasible, it is evident that oxidizing agents cannot compete with enzymatic approaches with respect to selectivity and efficiency. In general, mCPBA and OXONE® gave the greatest yields of **17** at both room temperature and at 0 °C. Production of **17** using DMDO

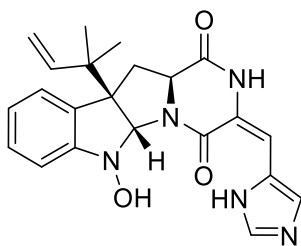
was comparable to mCPBA at room temperature but was retarded when the reaction was performed at 0 °C. N-Oxidation of roquefortine C was found to be highly influenced by sterics, as the bulky Davis oxaziridine was shown to be ineffective at the transformation. Additionally, each of the oxidants was shown to produce the phenol nitron **61**, an unexpected reaction with minimal literature precedent. As nitron incorporation in naturally occurring products could produce new biological activity, it is of interest to elucidate the reactivity of various oxidants on complex molecules. With the increase of molecular complexity of today's pharmaceutical compounds, late stage modification of complex molecules is now more important than ever and thoughtful implementation of these reagents can only be accomplished through study of their reactivity with complex systems.

## **V. Experimental Section**

### **General Information**

Starting materials, reagents and solvents were purchased from commercial suppliers and used without further purification unless otherwise noted. DMDO was prepared as a solution in acetone as described by Murray and Singh.<sup>21</sup> DMDO content of the solution was determined by reaction with thioanisole and subsequent <sup>1</sup>H NMR analysis. All reactions were conducted in oven-dried glassware. Products were purified by flash column chromatography (FCC) on 230-400 mesh silica gel. <sup>1</sup>H and <sup>13</sup>C NMR spectra were recorded on a spectrometer operating at 500 MHz for <sup>1</sup>H and 125 MHz for <sup>13</sup>C unless otherwise stated. Chemical shifts are reported in ppm relative to tetramethylsilane (TMS) as the

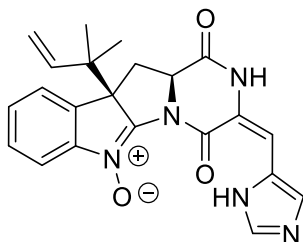
internal standard for  $^1\text{H}$  and chloroform as the internal standard for  $^{13}\text{C}$ . NMR data is reported as follows: chemical shift, multiplicity (s = singlet, d = doublet, dd = doublet of doublets, t = triplet, q = quartet, br = broad, m = multiplet), coupling constants (Hz), and integration. High-resolution mass spectra (HRMS) were recorded on an ESI-TOF spectrometer (Agilent). Waters software calibrates and reports by use of neutral atomic mass. The mass of the electron is not included. Liquid-chromatography-mass spectrometry (LC-MS) experiments were carried out using a Waters 2767 sample manager comprised of a Waters 2525 binary gradient HPLC with diode array detector and a Waters Micromass ZQ mass spectrometer with S-4 electro-spray ionization. The LC-MS chromatography was carried out on an Atlantis-C18 column (4.6  $\times$  50 mm; 5  $\mu\text{m}$ ) with a linear gradient of 10-90% acetonitrile in water (15 minutes, 2 mL/min).



### Roquefortine C hydroxylamine (16)

Roquefortine C (100 mg, 0.26 mmol) was dissolved in dry dichloromethane (5 mL) in a round-bottomed flask. mCPBA (77%, 172.6 mg, 0.78 mmol) was added, and the reaction was allowed to stir for 20 minutes.  $\text{NaBH}_4$  (160 mg, 4.24 mmol) was then added, and the reaction was allowed to stir until bubbling initiated by addition of  $\text{NaBH}_4$  had subsided. The reaction was quenched with methanol (1 mL), and

the reaction mixture was concentrated by rotary evaporation. The residue was purified first by column chromatography (0-7% CH<sub>3</sub>OH/CH<sub>2</sub>Cl<sub>2</sub>, deactivated with Et<sub>3</sub>N) then by prep plate (5% CH<sub>3</sub>OH/CH<sub>2</sub>Cl<sub>2</sub>) to afford the hydroxylamine (12 mg, 11%) as a single stereoisomer. <sup>1</sup>H NMR (500 MHz, CD<sub>3</sub>OD) δ 7.74 (s, 1H), 7.30 (s, 1H), 7.25 (d, *J* = 8 Hz, 1H), 7.21 (t, *J* = 8 Hz, 1H), 6.96 (t, *J* = 7.5 Hz, 1H), 6.90 (d, *J* = 7.5 Hz, 1H), 6.36 (s, 1H), 5.99 (dd, *J* = 6.5, 11 Hz, 1H), 5.89 (s, 1H), 5.09 (m, 2H), 3.98 (t, *J* = 8.5 Hz, 1H), 2.41 (m, 2H), 1.08 (s, 1H), 0.95 (s, 1H). <sup>13</sup>C NMR (125 MHz, CD<sub>3</sub>OD) δ 168.0, 159.8, 154.2, 145.0, 137.7, 131.8, 130.3, 126.0, 125.0, 124.4, 119.7, 115.9, 115.3, 111.1, 110.2, 87.9, 62.3, 59.7, 42.5, 40.1, 24.3, 23.5. HRMS (ESI-TOF) *m/z* [M + H]<sup>+</sup> calcd for C<sub>22</sub>H<sub>24</sub>N<sub>5</sub>O<sub>3</sub> 406.1879, found 406.1890.

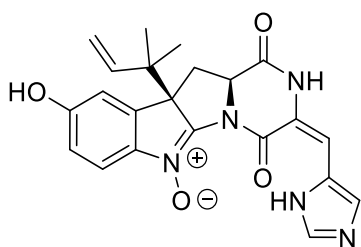


### Roquefortine L (17)

Roquefortine C (200 mg, 0.51 mmol) was dissolved in dry dichloromethane (10 mL) in a round-bottomed flask and chilled in an ice bath under argon. The reaction mixture was stirred over 3Å molecular sieves. In a separate vial, mCPBA (77%, 571 mg, 2.55 mmol) was dissolved in dichloromethane (10 mL) and washed twice with phosphate buffer, pH 7.5. The mCPBA solution was dried over Na<sub>2</sub>SO<sub>4</sub> and was added dropwise over 10 minutes to the roquefortine C solution. The



reaction mixture was stirred for 30 minutes, after which the reaction was quenched with two drops of dimethyl sulfide. The reaction mixture was concentrated by rotary evaporation and was purified by column chromatography (0-40% *i*-PrOH/CH<sub>2</sub>Cl<sub>2</sub>) on silica gel deactivated with Et<sub>3</sub>N to give roquefortine L (20 mg, 10%). <sup>1</sup>H NMR (600 MHz, DMSO-*d*<sub>6</sub>/CHCl<sub>3</sub>) δ 10.69 (s, 1H), 7.75 (s, 1H), 7.60 (s, 1H), 7.58 (d, *J* = 8.0 Hz, 1H), 7.48 (m, 2H), 7.40 (t, *J* = 7.4 Hz; 1H), 6.53 (s, 1H), 5.76 (dd, *J* = 11.0, 17.3 Hz, 1H), 5.08 (dd, *J* = 3.7, 11.4 Hz, 1H), 5.03 (d, *J* = 11.4 Hz, 1H), 4.99 (s, 1H), 2.86 (dd, *J* = 3.8, 14.1 Hz, 1H), 2.21 (dd, *J* = 11.5, 13.6 Hz, 1H), 1.03 (s, 3H), 0.83 (s, 3H). <sup>13</sup>C NMR (150 MHz, CDCl<sub>3</sub>) δ 164.7, 156.4, 148.6, 146.8, 141.7, 138.0, 128.7, 128.3, 124.1, 121.6, 115.5, 114.5, 63.4, 27.9, 42.8, 22.3, 22.2. IR (KBr): 2961.82, 1682.40, 1384.58, 1258.38, 1091.79, 1014.45, 794.80 cm<sup>-1</sup>; HRMS (ESI-TOF) *m/z* [M + H]<sup>+</sup> calcd for C<sub>22</sub>H<sub>22</sub>N<sub>5</sub>O<sub>3</sub> 404.1723, found 404.1727 (lit. (Vreeken et al., 2013))<sup>22</sup> HRMS (FTICR-MS) *m/z* [M + H]<sup>+</sup> calcd for C<sub>22</sub>H<sub>22</sub>N<sub>5</sub>O<sub>3</sub> 404.1723, found 404.1706).



### 11-Hydroxyroquefortine L (61)

Roquefortine C (200 mg, 0.51 mmol) was dissolved in dry dichloromethane (10 mL) in a round-bottomed flask and chilled in an ice bath under argon. The reaction mixture was stirred over 3Å molecular sieves. In a separate vial, mCPBA (77%,

571 mg, 2.55 mmol) was dissolved in dichloromethane (10 mL) and washed twice with phosphate buffer, pH 7.5. The mCPBA solution was dried over Na<sub>2</sub>SO<sub>4</sub> and was added dropwise over 10 minutes to the roquefortine C solution. The reaction mixture was stirred for 30 minutes, after which the reaction was quenched with two drops of dimethyl sulfide. The reaction mixture was concentrated by rotary evaporation and purified by column chromatography (0-40% *i*-PrOH/CH<sub>2</sub>Cl<sub>2</sub>) on silica gel deactivated with Et<sub>3</sub>N to give 11-hydroxyroquefortine L (30 mg, 15%). <sup>1</sup>H NMR (500 MHz, CD<sub>3</sub>OD) δ 7.69 (s, 1H), 7.52 (d, *J* = 9.5 Hz, 1 H), 6.58 (d, *J* = 9.5 Hz, 1H), 6.53, (s, 1H), 6.46 (s, 1H), 6.36 (s, 1H), 5.87 (dd, *J* = 10.5, 17.5 Hz, 1H), 5.33 (d, *J* = 5.5 Hz, 1H), 5.18 (m, 1H), 4.33 (dd, *J* = 6.5, 11.5 Hz, 1 H), 2.58 (dd, *J* = 6.0, 13.0 Hz), 2.50 (t, *J* = 11.5 Hz, 1H), 1.16 (s, 3H), 1.11 (s, 1H). <sup>13</sup>C NMR (125 MHz, DMSO-*d*<sub>6</sub>) δ 185.7, 163.6, 156.8, 151.1, 142.4, 141.2, 132.7, 122.6, 122.3, 121.8, 115.5, 88.5, 57.8, 55.8, 48.6, 40.7, 22.9, 22.1. HRMS (ESI-TOF) *m/z* [M + H]<sup>+</sup> calcd for C<sub>22</sub>H<sub>22</sub>N<sub>5</sub>O<sub>4</sub> 420.1672, found 420.1668.

### **Oxidation with DMDO**

Roquefortine C (15 mg, 0.038 mmol) was dissolved in acetone (0.4 mL) in a vial. DMDO (1.3 mL, 0.059 M in acetone, 0.077 mmol) was added dropwise and stirred until DMDO was consumed (15 minutes, monitored by potassium iodide starch paper). A 200 μL aliquot was removed from the reaction mixture and diluted to 1 mL with dry CH<sub>2</sub>Cl<sub>2</sub> for LC-MS analysis.

### **Oxidation with mCPBA**

Roquefortine C (15 mg, 0.038 mmol) was dissolved in chloroform (0.4 mL) in a vial. mCPBA (77%, 10 mg, 0.077 mmol) was dissolved in chloroform (0.8 mL) and was added dropwise to roquefortine C. The reaction was stirred until mCPBA was consumed (15 minutes, monitored by potassium iodide starch paper). A 100  $\mu$ L aliquot was removed from the reaction mixture and diluted to 1 mL with dry  $\text{CH}_2\text{Cl}_2$  for LC-MS analysis.

### **Oxidation with sodium tungstate/hydrogen peroxide**

Roquefortine C (40 mg, 0.10 mmol) was suspended in methanol (2.0 mL) in a vial.  $\text{Na}_2\text{WO}_4 \cdot 2\text{H}_2\text{O}$  (3 mg, 0.010 mmol) and  $\text{H}_2\text{O}_2$  (30% in  $\text{H}_2\text{O}$ , 23  $\mu$ L, 0.20 mmol) were added sequentially and stirred for 4 hours. A 75  $\mu$ L aliquot was removed from the reaction mixture and diluted to 1 mL with dry  $\text{CH}_2\text{Cl}_2$  for LC-MS analysis.

### **Oxidation with trichloroacetonitrile/hydrogen peroxide**

$\text{H}_2\text{O}_2$  (30% in  $\text{H}_2\text{O}$ , 8.7  $\mu$ L, 0.077 mmol) and  $\text{Cl}_3\text{CCN}$  (7.7  $\mu$ L, 0.077 mmol) were dissolved in methanol (0.38 mL) in a vial. Roquefortine C was added and stirred for 4 hours. A 50  $\mu$ L aliquot was removed from the reaction mixture and diluted to 1 mL with dry  $\text{CH}_2\text{Cl}_2$  for LC-MS analysis.

### **Oxidation with Davis oxaziridine**

Roquefortine C (30 mg, 0.077 mmol) was dissolved in dichloromethane (0.77 mL) in a vial. Davis oxaziridine (40 mg, 0.15 mmol) was dissolved in dichloromethane

(1.5 mL) in a separate vial and was added dropwise to roquefortine C. The reaction mixture stirred for 4 hours. A 50  $\mu$ L aliquot was removed from the reaction mixture and diluted to 1 mL with dry  $\text{CH}_2\text{Cl}_2$  for LC-MS analysis.

#### **Oxidation with OXONE $\text{\textcircled{R}}$**

Roquefortine C (15 mg, 0.038 mmol) was dissolved in 1:4 THF: $\text{CH}_3\text{CN}$  (0.5 mL) in a vial. EDTA-2Na (0.01 M in  $\text{H}_2\text{O}$ , 0.38 mL, 0.0038 mmol),  $\text{NaHCO}_3$  (16 mg, 0.19 mmol), and OXONE  $\text{\textcircled{R}}$  (47 mg, 0.077 mmol) were added sequentially to the roquefortine C solution and stirred for 4 hours. A 50  $\mu$ L aliquot was removed from the reaction mixture and diluted to 1 mL with dry  $\text{CH}_2\text{Cl}_2$  for LC-MS analysis.

#### **LC-MS calibration**

Roquefortine C (50 mg, 0.13 mmol) was dissolved in dry dichloromethane (3 mL) in a round-bottomed flask and chilled in an ice bath. In a separate vial, mCPBA (77%, 85 mg, 0.64 mmol) was dissolved in dichloromethane (6 mL) and washed twice with phosphate buffer, pH 7.5. The mCPBA solution was dried over  $\text{Na}_2\text{SO}_4$  and was added dropwise over 10 minutes to the roquefortine C solution. The reaction mixture was stirred for 30 minutes, after which the reaction was quenched with two drops of dimethyl sulfide. The reaction mixture was concentrated by rotary evaporation and the residue was washed three times with diethyl ether. A sample of the residue was analyzed by  $^1\text{H}$  NMR to quantify the amount of each reaction intermediate present in the sample. LC-MS response factors (Supplementary

Table 3.1) were determined using calibration standards of five different concentrations.

**Supplementary Table 3.1:** LC-MS response ratios for roquefortine C and oxidation products

Compound	Response factor
Roquefortine C ( <b>1</b> )	103945 ± 30 M <sup>-1</sup>
Roquefortine C hydroxylamine ( <b>16</b> )	169810 ± 24 M <sup>-1</sup>
Roquefortine L ( <b>17</b> )	41410 ± 27 M <sup>-1</sup>
11-Hydroxyroquefortine L ( <b>61</b> )	37988 ± 13 M <sup>-1</sup>

Errors represent the standard error of the estimate ( $\sigma_{\text{est}}$ ).

## VI. References

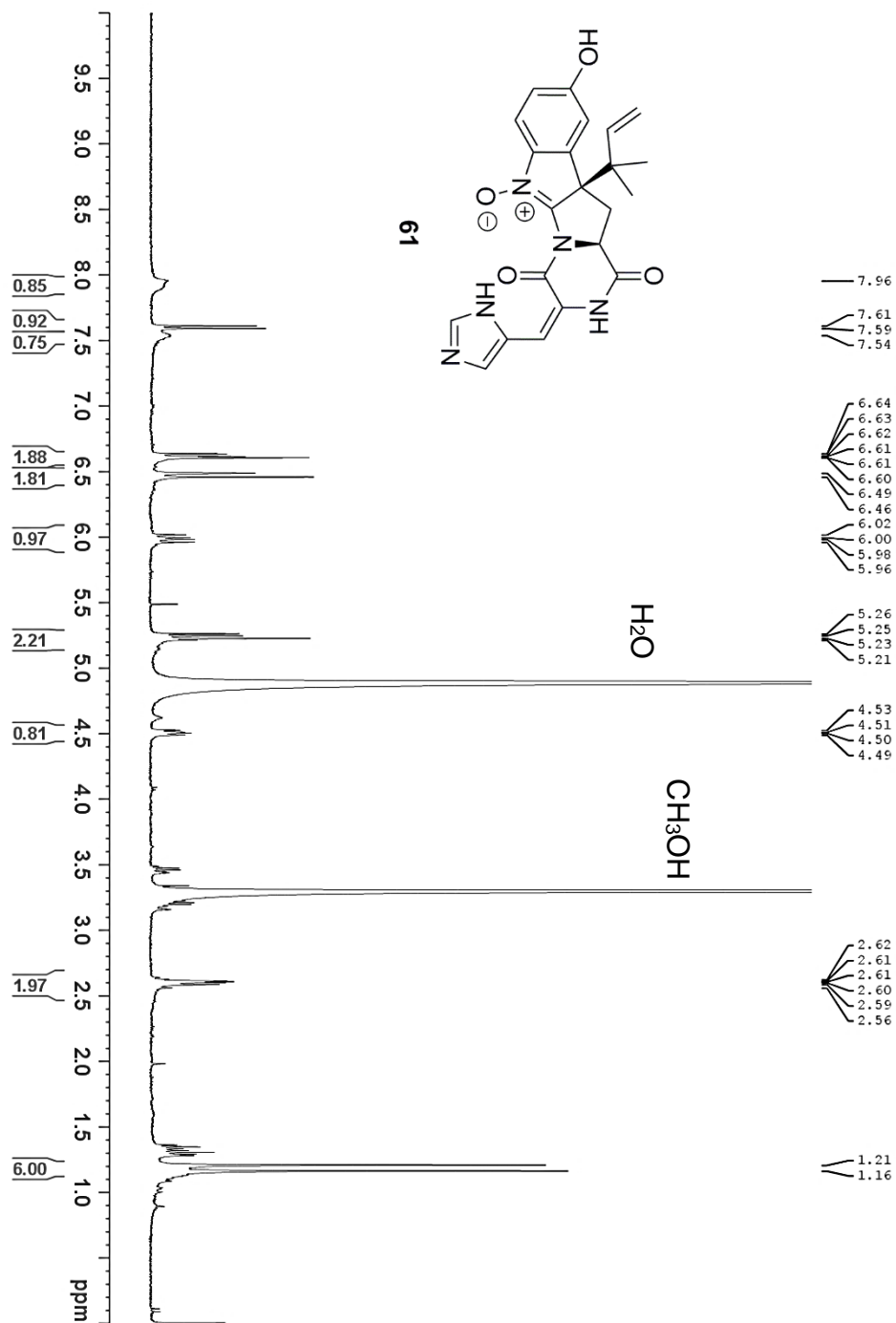
- (1) Newmister, S. A.; Gober, C. M.; Romminger, S.; Yu, F.; Tripathi, A.; Parra, L. L. L.; Williams, R. M.; Berlinck, R. G. S.; Joullié, M. M.; Sherman, D. H. *J. Am. Chem. Soc.* **2016**, *138*(35), 11176-11184.
- (2) Barbati, S.; Clément, J.-L.; Fréjaville, C.; Bouteiller, J.-C.; Tordo, P.; Michel, J.-C.; Yadan, J.-C. *Synthesis* **1999**, *12*, 2036-2040.
- (3) Hanessian, S.; Bayrakdarian, M. *Tetrahedron Lett.* **2002**, *43*, 967-971.
- (4) Villamena, F. A.; Dickman, M. H.; Crist, D. R. *Inorg. Chem.* **1998**, *37*, 1446-1453.
- (5) Floyd, R. A. *Aging Cell* **2006**, *5*, 51-57.

- (6) Wulff, J. E.; Siegrist, R.; Myers, A. G. *J. Am. Chem. Soc.* **2007**, *129*(46), 14444-14451.
- (7) Griffing, B. F.; West, P. R., A method of enhancing the contrast of images and materials thereof. EP0110165A3, 1987.
- (8) Marcantoni, E.; Petrini, M.; Polimanti, O. *Tetrahedron Lett.* **1995**, *36*(20), 3561-3562.
- (9) Ballistreri, F. P.; Chiacchio, U.; Rescifina, A.; Tomaselli, G. A.; Toscano, R. M. *Tetrahedron* **1992**, *48*(40), 8677-8684.
- (10) Davis, G. C., Storage stable aryl nitrene compositions. EP0187303, 1986.
- (11) Nikbakht, F.; Heydari, A. *Tetrahedron Lett.* **2014**, *55*(15), 2513-2516.
- (12) Field, L. D.; Li, H. L.; Magill, A. M. *Organic Structures from 2D NMR Spectra*; John Wiley & Sons Ltd: Chichester, West Sussex, 2015.
- (13) Yamada, T.; Ideguchi-Matsushita, T.; Hirose, T.; Shirahata, T.; Hokari, R.; Ishiyama, A.; Iwatsuki, M.; Sugawara, A.; Kobayashi, Y.; Otaguro, K.; Ōmura, S.; Sunazuka, T. *Chem. Eur. J.* **2015**, *21*(33), 11855-11864.
- (14) Bjørsvik, H.-R.; Occhipinti, G.; Gambarotti, C.; Cerasino, L.; Jensen, V. R. *J. Org. Chem.* **2005**, *70*, 7290-7296.
- (15) Makosza, M.; Sienkiewicz, K. *J. Org. Chem.* **1998**, *63*, 4199-4208.

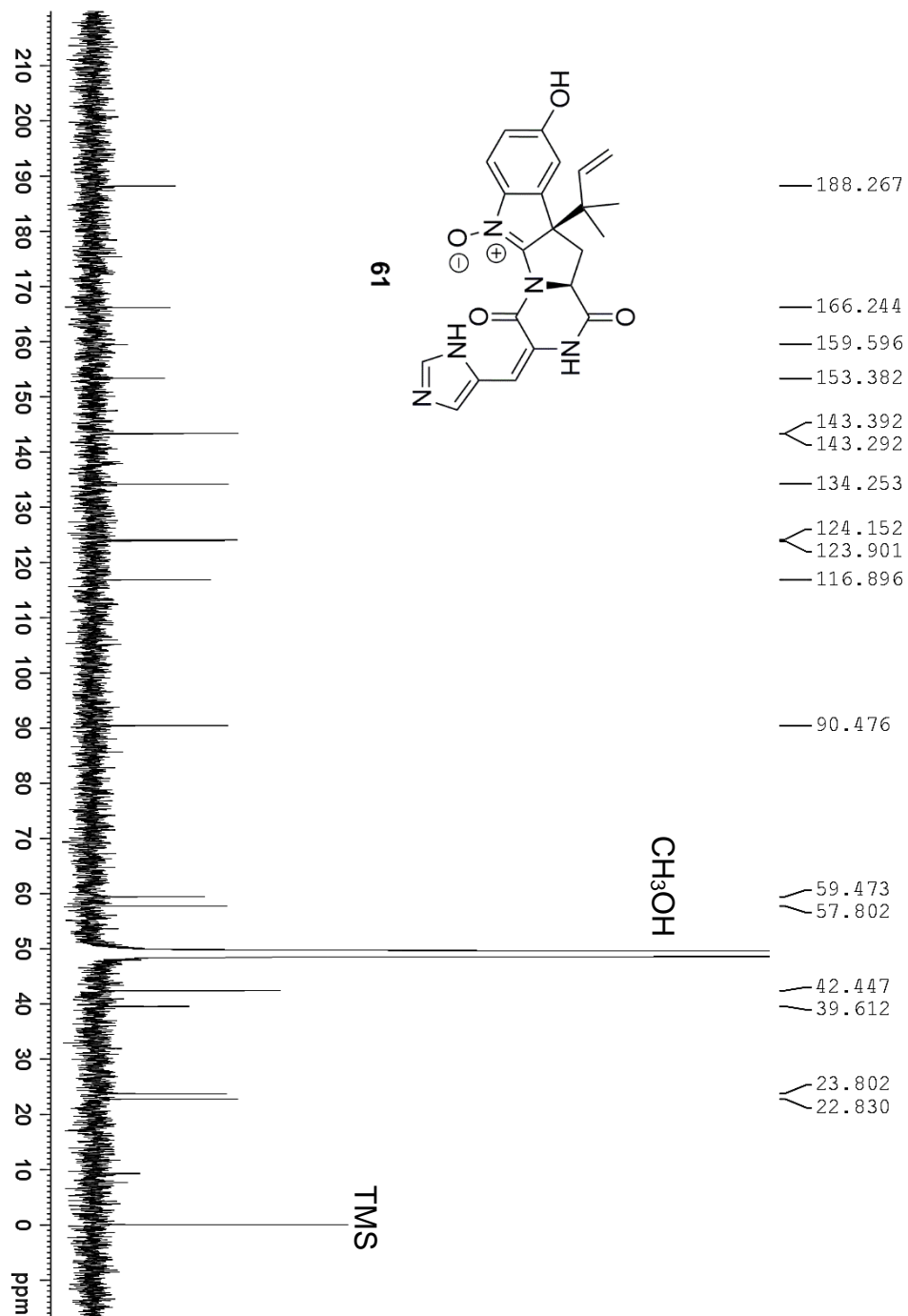
- (16) Shi, H.-C.; Li, Y. *J. Mol. Catal. A: Chem.* **2007**, 271(1-2), 32-41.
- (17) Pinkernell, U.; Effkemann, S.; Nitzsche, F.; Karst, U. *J. Chromatogr. A* **1996**, 730, 203-208.
- (18) Jin, P.; Wei, D.; Wen, Y.; Luo, M.; Wang, X.; Tang, M. *J. Mol. Struct.* **2011**, 992(1-3), 19-26.
- (19) Jacobson, S. E.; Muccigrosso, D. A.; Mares, F. *J. Org. Chem.* **1979**, 44(6), 921-924.
- (20) Valentin, C. D.; Gisdakis, P.; Yudanov, I. V.; Rösch, N. *J. Org. Chem.* **2000**, 65, 2996-3004.
- (21) Murray, R. W.; Singh, M. *Org. Synth.* **1997**, 74, 91.
- (22) Ries, M. I.; Ali, H.; Lankhorst, P. P.; Hankemeier, T.; Bovenberg, R. A.; Driessen, A. J.; Vreeken, R. J. *J. Biol. Chem.* **2013**, 288(52), 37289-37295.

## **Appendix 3A: Spectra Relevant to Chapter 3**

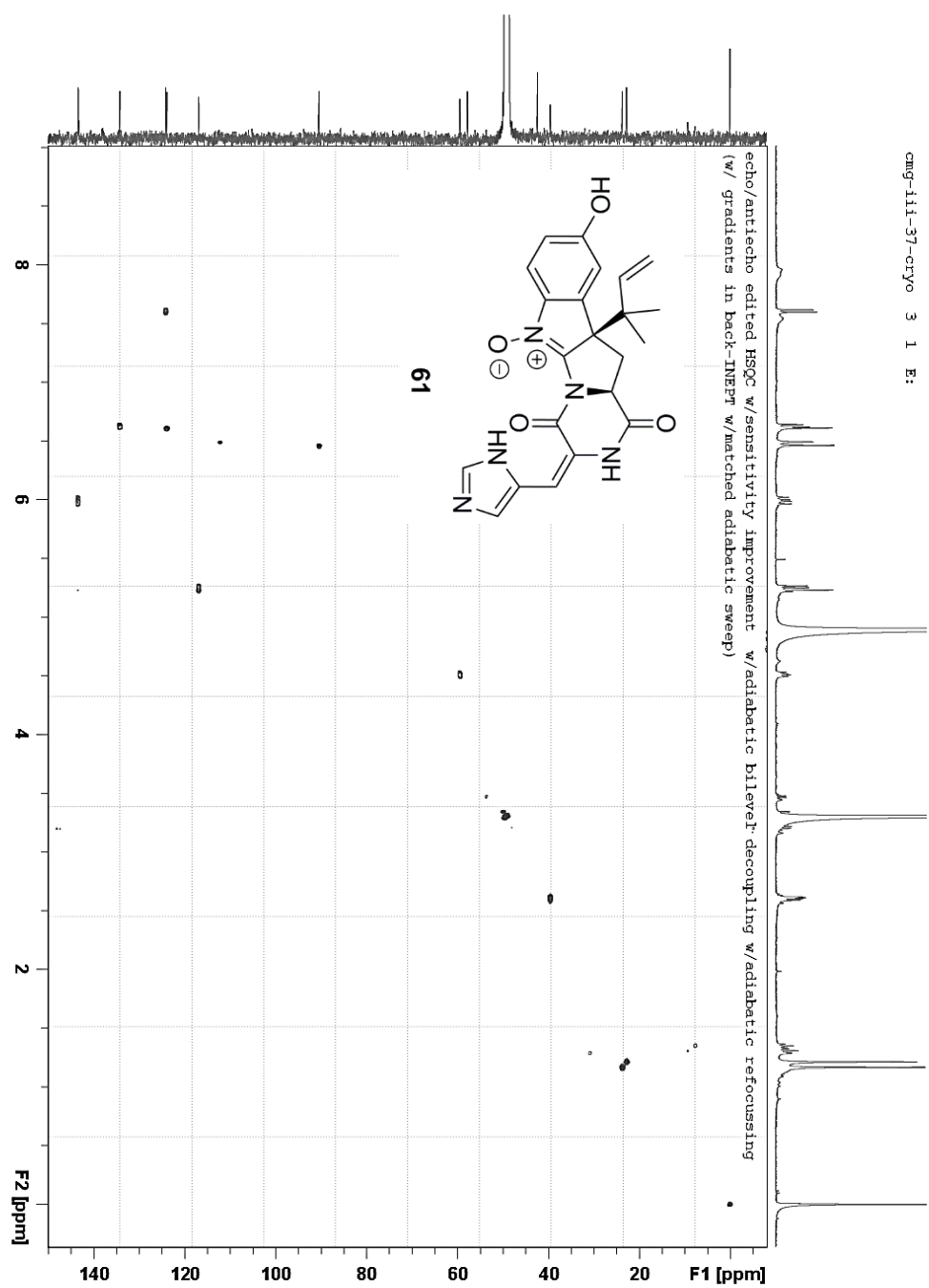




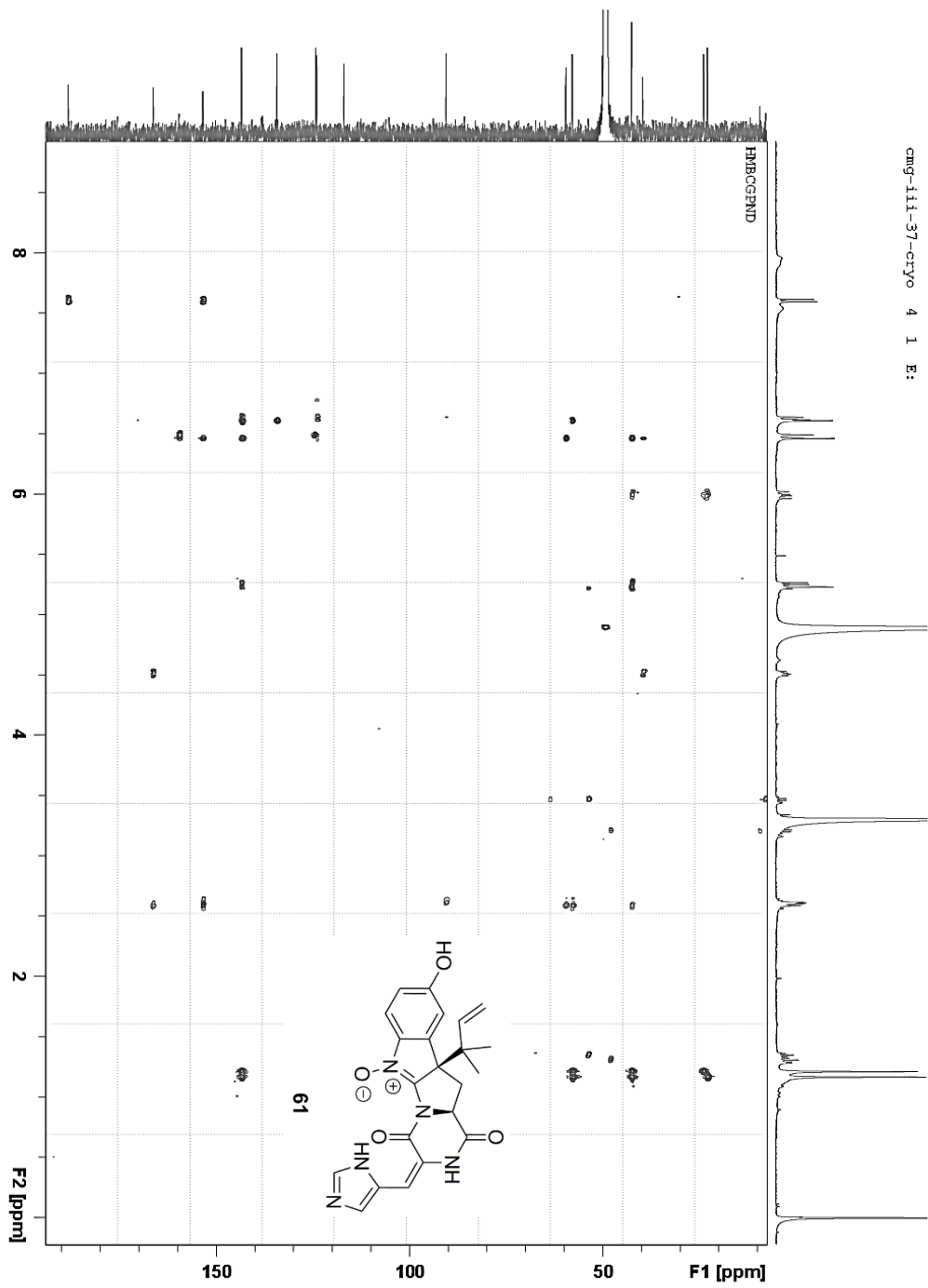
**Supplementary Figure 3.1: <sup>1</sup>H NMR (500 MHz, CD<sub>3</sub>OD) Spectrum of 61**



Supplementary Figure 3.2: <sup>13</sup>C NMR (125 MHz, CD<sub>3</sub>OD) Spectrum of 61



Supplementary Figure 3.3:  $^1\text{H}$ - $^{13}\text{C}$  HSQC (500 MHz,  $\text{CD}_3\text{OD}$ ) Spectrum of **61**



Supplementary Figure 3.4:  $^1\text{H}$ - $^{13}\text{C}$  HMBC (500 MHz,  $\text{CD}_3\text{OD}$ ) Spectrum of **61**

**CHAPTER FOUR**  
**SYNTHETIC INVESTIGATIONS TOWARDS TRIAZASPIROCYCLES**

Material in this chapter reproduced in part with permission from:

Gober, C.; Carroll, P. J.; Joullié, M. M. *Mini Rev. Org. Chem.* **2016**, *13*, 126-142.

Copyright 2016 Bentham Science

## I. Introduction

Triazaspirocycles are unique chemical motifs found in several biologically active natural products. These compounds feature three nitrogen atoms attached to one quaternary carbon forming a spirocyclic scaffold. The rigid chemical backbone of these structures contributes towards their application in both the materials and pharmaceuticals industries. Despite their industrial promise, few syntheses of these compounds exist in the literature. The biosynthesis of roquefortine C, however, provides inspiration for the synthesis of these compounds, namely through a nitrene-promoted transannular rearrangement. This type of internal rearrangement has never been carried out synthetically and would provide an efficient stereoselective synthesis of triazaspirocycles. Herein are reported synthetic efforts towards triazaspirocycles.

## II. Background

### A. Triazaspirocycle Natural Products

A number of natural products contain the triazaspiro motif, most commonly in the form of a tethered triazaspirocycle (Figure 4.1).<sup>1</sup>

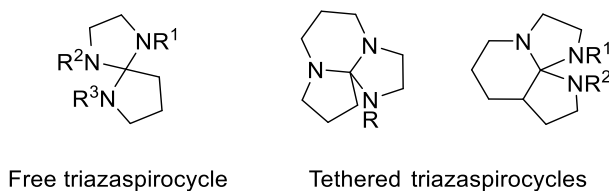


**Figure 4.1:** Triazaspirocycle scaffolds

The majority of naturally derived triazaspirocyclics are of *Penicillium* origin (Figure 4.2), and of those, most have been shown to originate from biosynthetic transformations of roquefortine C (**1**).<sup>2-7</sup>

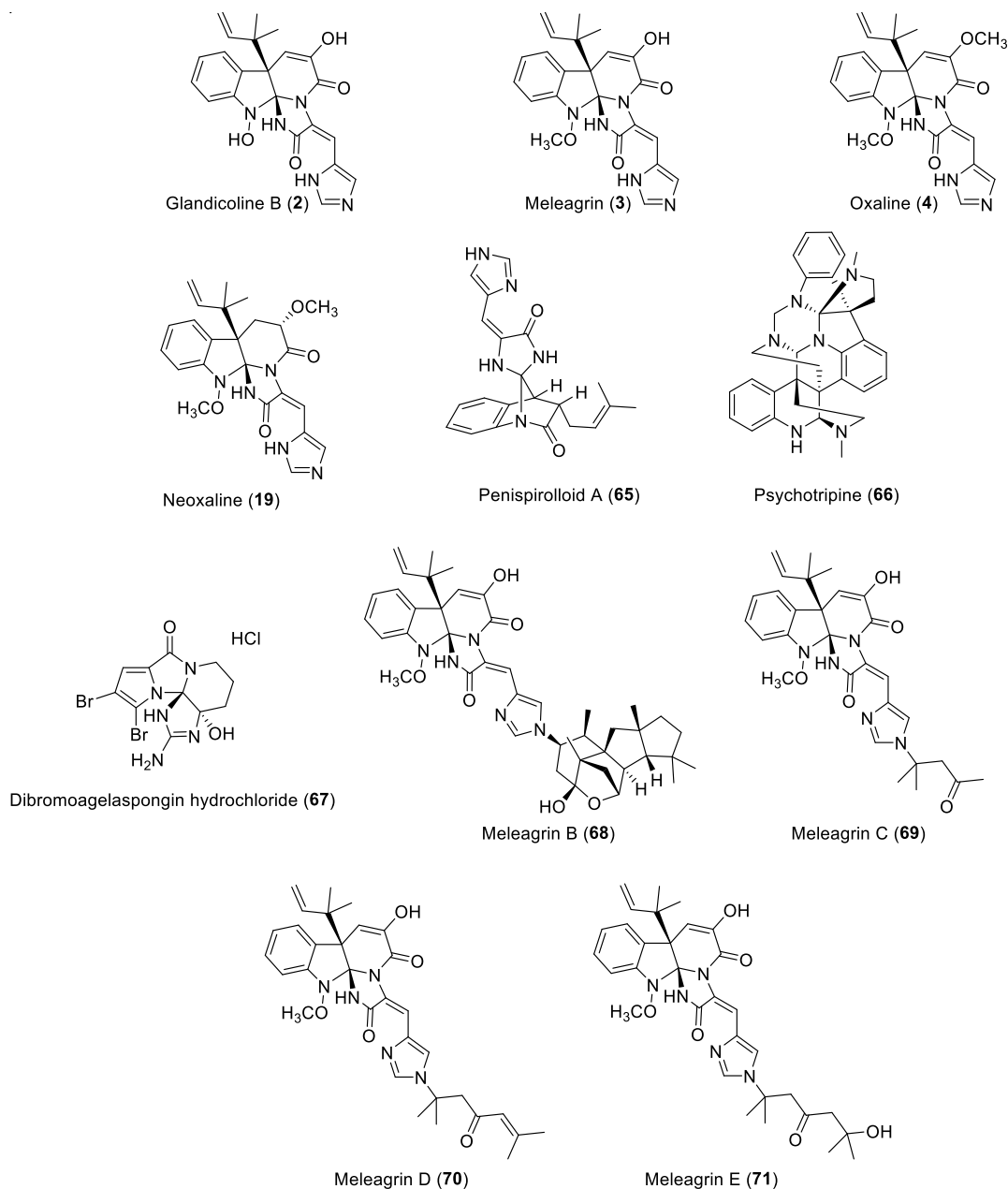
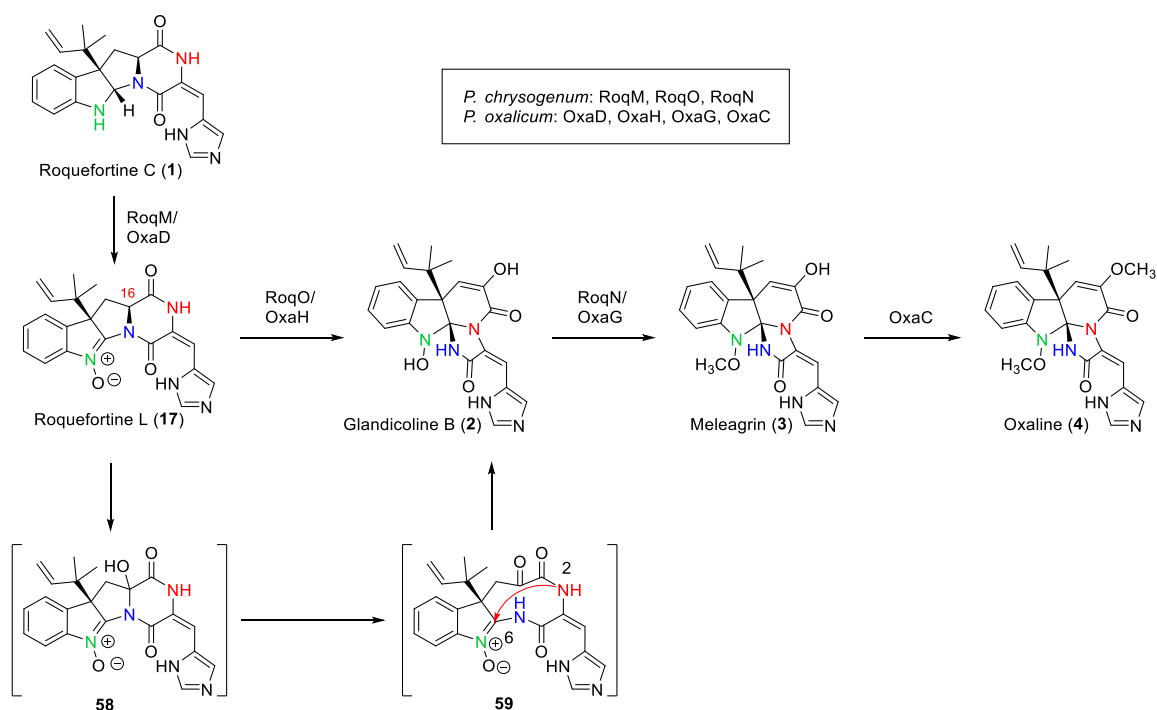


**Figure 4.2:** Triazaspirocyclic natural products

As mentioned in Chapters 1 and 2, the biosynthesis of roquefortine C derived triazaspirocycles in *P. chrysogenum* and *P. oxalicum* is initiated by indoline N-oxidation to give roquefortine L (**17**). A cytochrome P450 monooxygenase (RoqO/OxaH) is then proposed to promote  $\alpha$ -hydroxylation. The newly-generated hemiaminal is proposed to open to the 9-membered  $\alpha$ -diketone, which, upon transannular attack of the nitron  $\alpha$ -carbon by N2, gives the triazaspirocyclic core of glandicoline B (**2**) (Scheme 4.1).<sup>3</sup>



**Scheme 4.1:** Biogenesis of roquefortine C derived triazaspirocycles in *P. chrysogenum* and *P. oxalicum*

## B. Triazaspirocycles: Properties and Applications

Natural products containing the triazaspirocyclic motif display a wide range of biological activity. Oxaline (**4**), whose structure has been established by X-ray



crystallography,<sup>8</sup> and neoxaline have been observed to exhibit antiproliferative activity and to arrest the cell cycle at the M phase in Jurkat cells via inhibition of tubulin polymerization (see Appendix 4A for description of cell lines).<sup>9</sup>

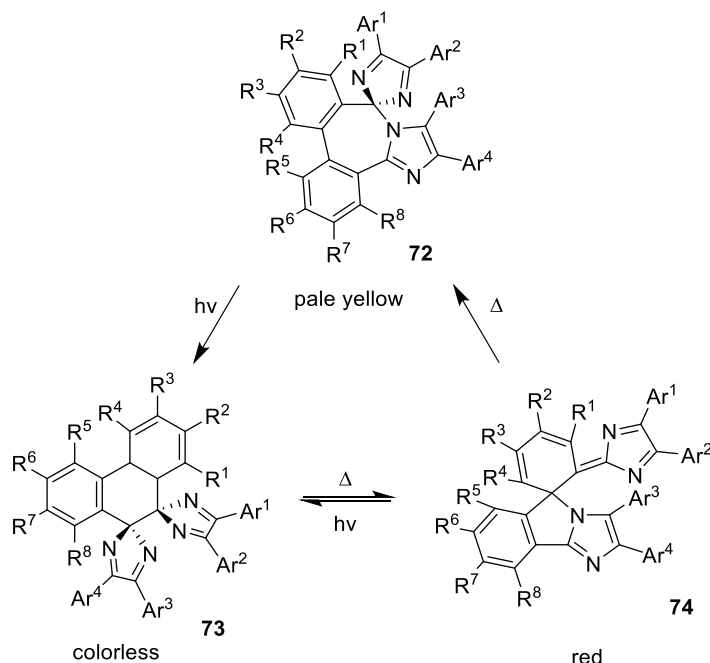
Meleagrins (**3**) and several of its semisynthetic derivatives have shown activity against several strains of multiple-drug resistant bacteria, whose rapid emergence has ignited a threat to global health in recent years. Meleagrins were observed to inhibit the bacterial enoyl-acyl carrier protein reductase FabI, a novel antibacterial target and key enzyme in the synthesis of bacterial type 2 fatty acid, which is essential for bacterial cell growth.<sup>10</sup> Meleagrins were also shown to possess moderate antitumor activity when applied to cell lines A-549 and HL-60 and caused cell cycle arrest in the G<sub>2</sub>/M phase, presumably by inhibiting tubulin polymerization (see Appendix 4A for description of cell lines).<sup>11</sup> Recent reports indicate that meleagrins are also a promising lead for the treatment of breast cancer.<sup>12</sup> Additionally, meleagrins have been reported to be a fibrinolysis inhibitor.<sup>13</sup>

Both meleagrins and glandicolins B (**2**) have shown anti-fouling activity against the barnacle larva *Balanus amphitrite*, inhibiting their attachment to wetted surfaces.<sup>14,15,16</sup> Glandicolins B (**2**) were also found to be active at 100 µg/mL against *S. aureus*, *Micrococcus luteus*, and *E. coli*.<sup>17</sup>

Several imidazole-substituted biosynthetic derivatives of meleagrins have been isolated from deep sea *Penicillium* fungi (Figure 4.2) and were shown to exhibit a range of cytotoxic effects against HL-60, MOLT-4, A-549, and BEL-7402

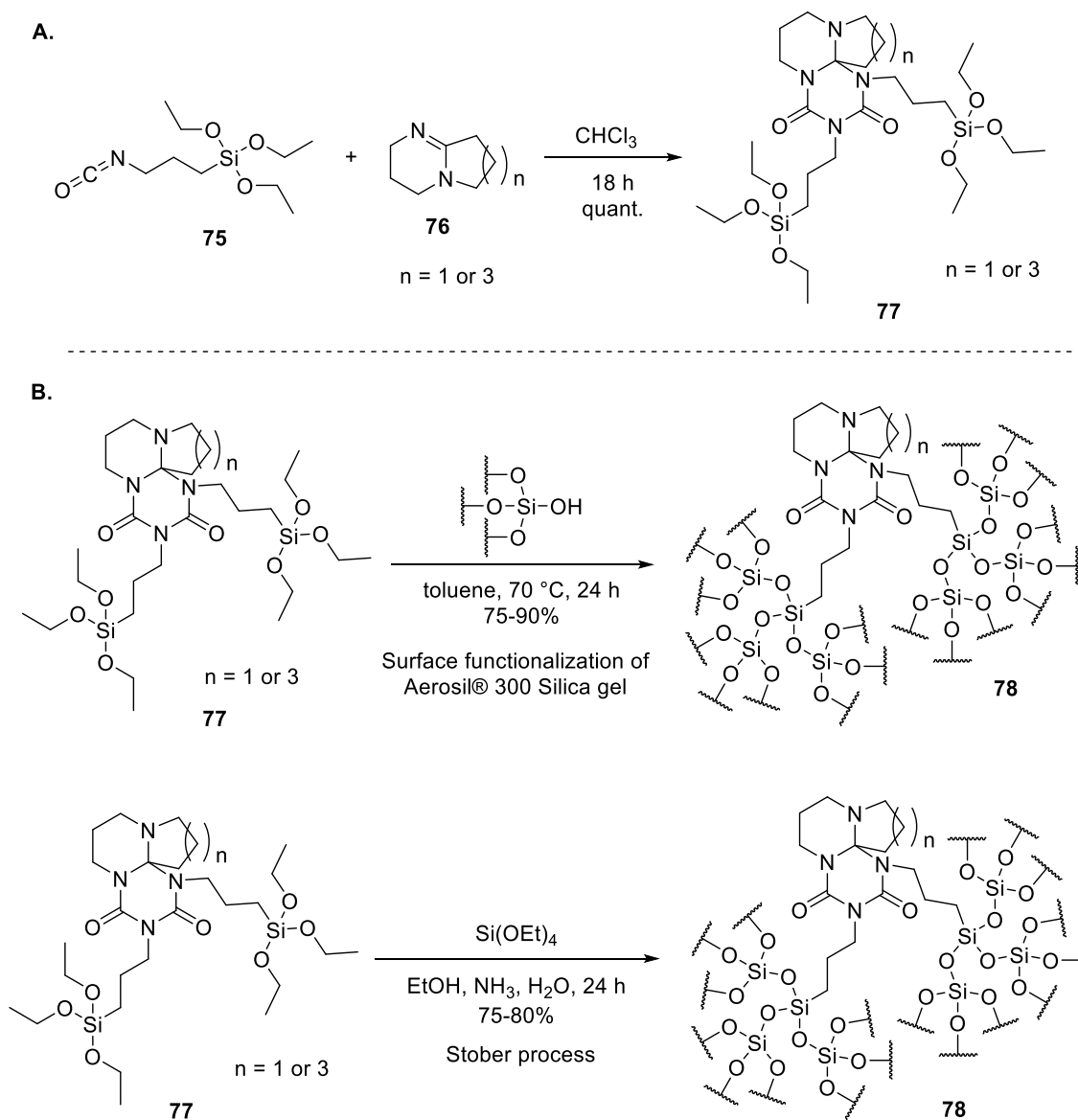
cell lines (see Appendix 4A for description of cell lines).<sup>11</sup> Meleagrins B (**68**) displayed moderate cytotoxicity, with half maximal inhibitory concentration ( $IC_{50}$ ) values in the 1.8 to 6.7  $\mu$ M range for each cell line. Meleagrins C (**69**) displayed less potent activity, particularly against the HL-60 cell line, where  $IC_{50}$  values were greater than 50  $\mu$ M. Meleagrins D (**70**) and E (**71**) showed significantly weaker activity than meleagrins A-C against the A-549 cell line and displayed virtually no activity against the HL-60 cell line ( $IC_{50} > 100 \mu$ M).

In addition to their biological activity, triazaspirocycles have found use in several other applications. In 2013, Horino, Tokita, and Oshima patented a biimidazole-based photochromic material that demonstrates negative photochromism (Scheme 4.2).<sup>18</sup> Photochromic materials undergo reversible color change as a result of isomerization. They can be broadly categorized as inducing negative photochromism, a change from colored to uncolored accompanying isomerization, or positive photochromism, a change from uncolored to colored accompanying isomerization. Compounds with photochromic properties have applications in color changing lens and molecular switches, among others. Horino, Tokita, and Oshima found that, in compounds where  $R^4$  and  $R^5$  were sterically bulky groups, irradiation with visible light caused isomerization from the pale yellow [4.6] triazaspirocycle **72** to the colorless dispirocyclic system **73**. Further isomerization to a red colored [4.5] spirocyclic system (**74**) was observed when **73** was shielded from light, after which further isomerization restored the original pale yellow color.



**Scheme 4.2:** Photochromic triazaspirocycles

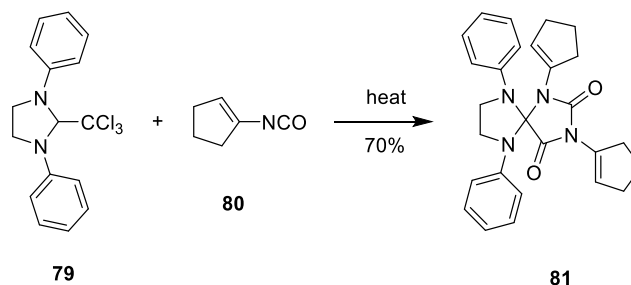
Triazaspirocycles have also demonstrated applications in surface functionalization (Scheme 4.3).<sup>19</sup> Following the synthesis of triazaspirocycles via the addition of isocyanates bearing silyl ethers to 1,5-diazabicyclo[4.3.0]non-5-ene (DBN) and 1,8-diazabicyclo[5.4.0]undec-7-ene (DBU, Scheme 4.3A), functionalization of silicon dioxide surfaces was carried out via one of two methods; the first involving the reaction of the silyl ether functionalized triazaspirocycles with fumed silica and the second involving functionalization via the Stöber process (Scheme 4.3B).<sup>20</sup>



### C. Synthesis of Triazaspirocycles

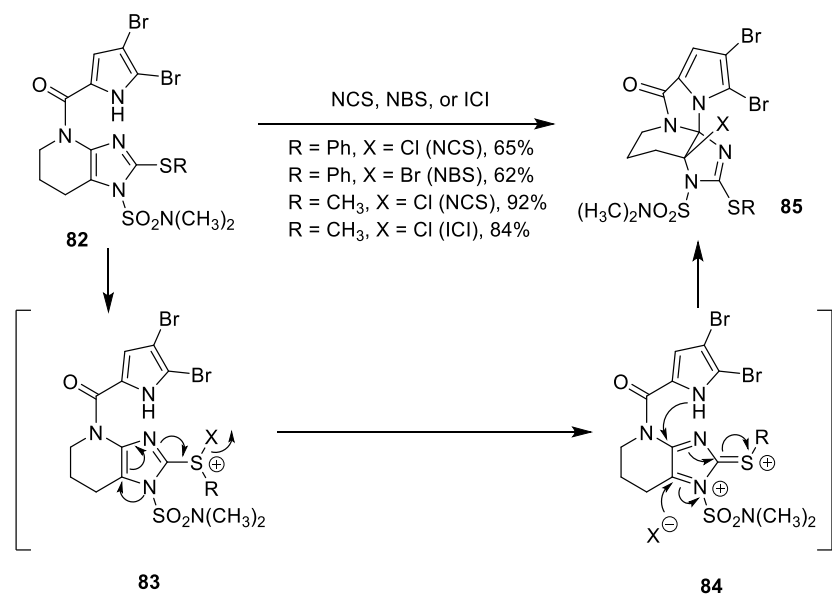
The most common synthetic method for the construction of triazaspirocycles is 1,3 dipolar cycloaddition (Scheme 4.4). In this particular reaction, a 1,3 dipole undergoes a [3+2] cycloaddition with a dipolarophile to form

a five-membered ring. 1,3 Dipoles share four electrons across a  $\pi$  system of three atoms and typically react with dipolarophiles such as olefins and isocyanates.<sup>21</sup>

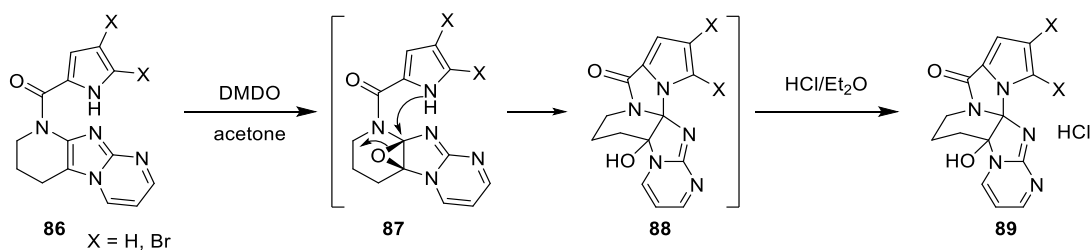


**Scheme 4.4:** Synthesis of triazaspirocycles via 1,3-dipolar cycloaddition

Unlike bimolecular cycloadditions, intramolecular cyclizations often proceed stereo- and regioselectively and are thus advantageous in achieving asymmetric syntheses of triazaspirocyclic systems. In the total synthesis of dibromoagelaspongin by Feldman et al., oxidative cyclization to form the tethered triazaspirocycle was shown to occur in the presence of NBS, *N*-chlorosuccinimide (NCS), or ICl (Scheme 4.5).<sup>22-24</sup> Following mechanistic investigation of this reaction, Feldman et al. demonstrated this transformation takes place via a Pummerer reaction, in which electrophilic halogenation of the -SR group leads to elimination to form sulfonium intermediate **84**, which subsequently undergoes nucleophilic attack by the adjacent dibromopyrrole ring. Feldman et al. had initially synthesized the triazaspirocyclic core of dibromoagelaspongin via intramolecular ring opening of an epoxide, which led to the triazaspirocyclic hemiaminal **89** following acidic workup (Scheme 4.6).<sup>25</sup>

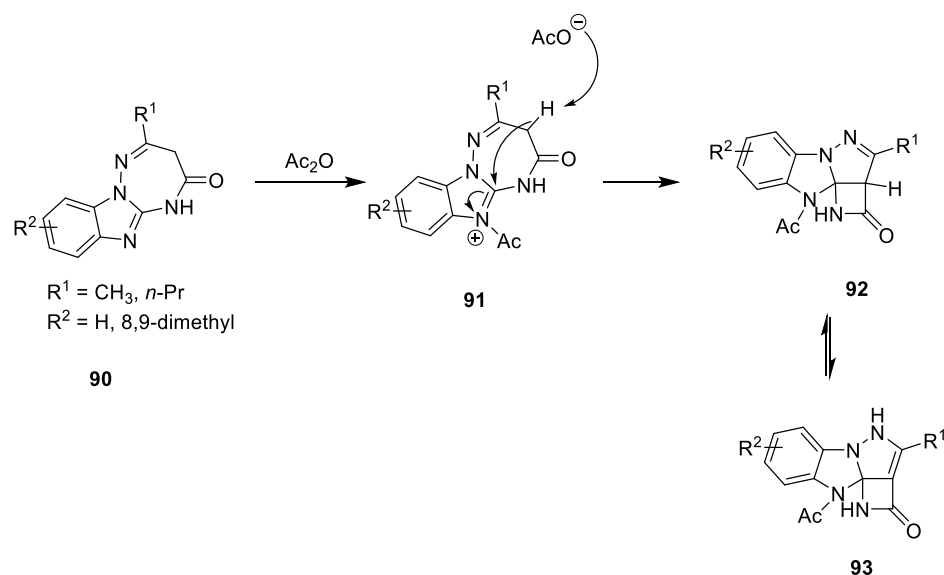


**Scheme 4.5:** Pummerer reaction to access dibromoagelaspongine triazaspirocyclic core



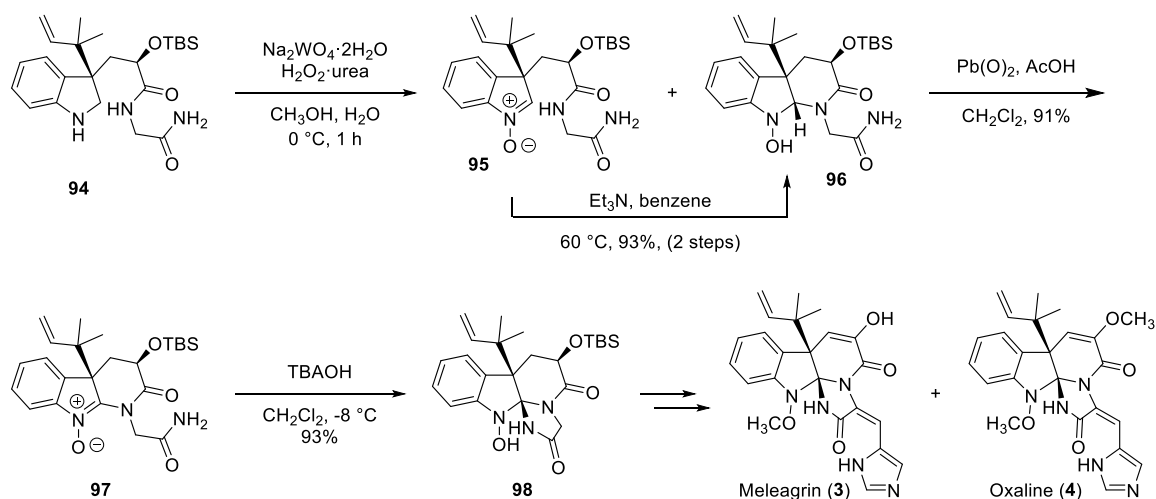
**Scheme 4.6:** Synthesis of dibromoagelaspongine core via intramolecular epoxide ring opening

A transannular ring contraction promoted by acetic anhydride has been shown by Avendaño et al. to produce novel triazaspirocyclic  $\beta$ -lactams (Scheme 4.7).<sup>26</sup>



**Scheme 4.7:** Synthesis of fused  $\beta$ -lactams via acetic anhydride promoted transannular rearrangements

The first asymmetric total synthesis of neoxaline (**19**) was accomplished in 2013,<sup>27</sup> and the first asymmetric total syntheses of meleagrins (**3**) and oxaline (**4**) and a second-generation asymmetric total synthesis of neoxaline were completed in 2015.<sup>28</sup> The construction of the triazaspiro core in each of these syntheses was carried out in a stepwise fashion of oxidation and cyclization. Oxidation of **94** with  $\text{H}_2\text{O}_2$ -urea in the presence of  $\text{NaWO}_4 \cdot 2\text{H}_2\text{O}$  provides a mixture of nitron **95** and diaminal **96**. Treatment of the crude mixture with triethylamine in benzene converts nitron **95** to diaminal **96**, and subsequent oxidation affords *N*-oxoamidine **97**. Finally, cyclization using tetrabutylammonium hydroxide (TBAOH) affords indoline spiroaminal **98** (Scheme 4.8).<sup>27-29</sup>



**Scheme 4.8:** Triazaspirocycle formation in the total syntheses of oxaline and meleagrins

### III. Results and Discussion

#### A. Geometry Optimization Studies of Roquefortine C Transannular Rearrangement

While the synthesis of triazaspirocycles has been described in the literature, there are relatively few instances of stereoselective formation of triazaspirocycles. As roquefortine C-derived triazaspirocycles have already demonstrated a wide range of biological activity,<sup>9,10,14</sup> we proposed to expand the scope of transannular ring contractions by exploring the synthesis of triazaspirocycles via transannular ring contraction of indoline nitrones. We believe it is possible to achieve the desired transformation in a single step following the generation of the indoline nitrone.

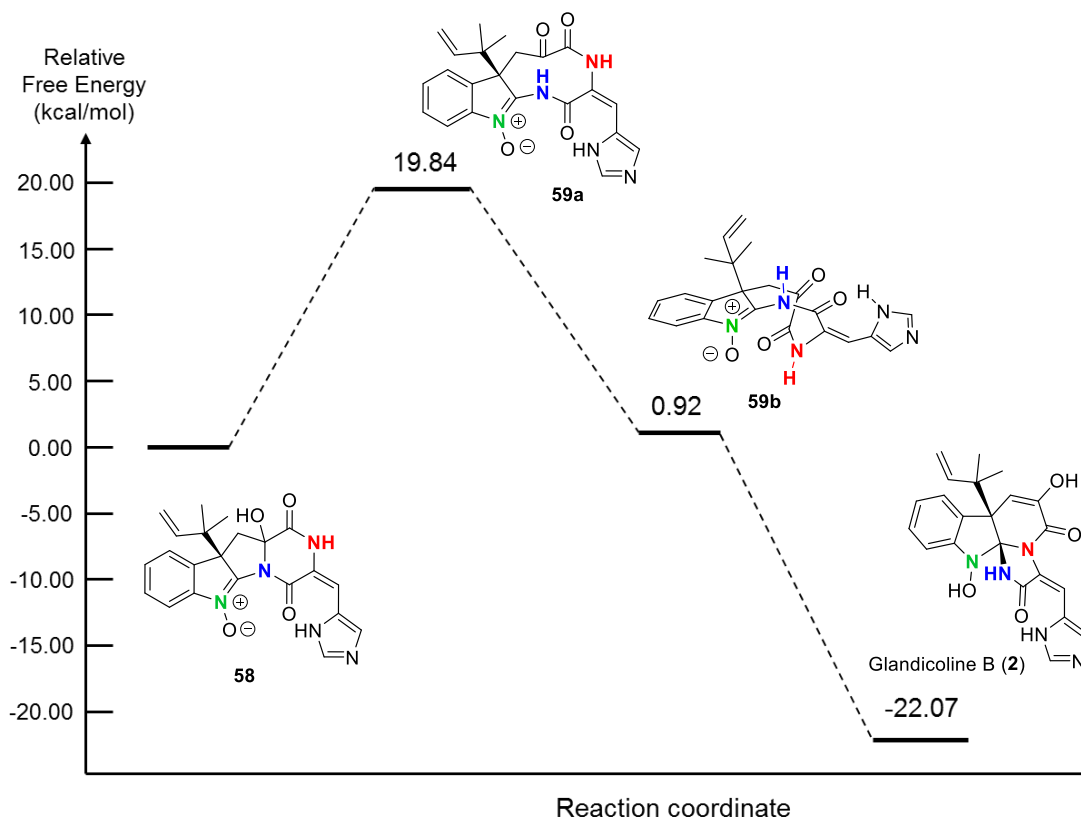
As our inspiration for this methodology draws heavily on the roquefortine C biosynthetic pathway, it seemed most logical to investigate this methodology using roquefortine C as our initial substrate. The proposed biosynthetic mechanism of



triazaspirocycle formation of glandicoline B (**2**) from roquefortine C (Scheme 4.1) is thought to involve four distinct steps: 1) N-oxidation of roquefortine C (**1**) to nitronone roquefortine L (**17**); 2)  $\alpha$ -hydroxylation of roquefortine L at C16; 3) ring expansion of the newly formed hemiaminal; and 4) transannular attack of the nitronone  $\alpha$ -carbon by N2. The ultimate success of this methodology lies in the energetic viability of ring expansion and subsequent contraction to form the triazaspirocycle. One might imagine that the energetic barrier of progressing from a fused 5,6-bicycle to a 9-membered ring could be too high to be achieved without assistance from an enzyme to lower the activation energy. Additionally, it is unclear whether the geometry of compound **59** lends itself to stereospecific ring contraction. Therefore, it was of interest to carry out computational studies of this rearrangement to determine its viability.

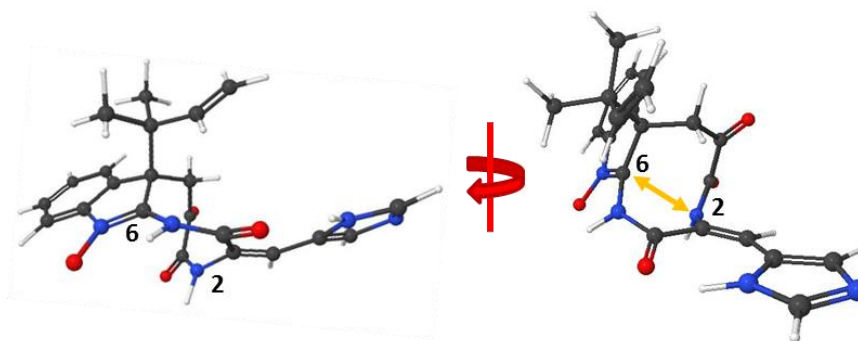
Geometry optimization of compounds **58**, **59**, and **2** was carried out at the HF/6-311+G(2d,p) level of theory using WebMO (Figure 4.3). These computational studies suggest compound **59** exists in two conformations, one adopting a planar conformation (**59a**) and one adopting a folded configuration (**59b**). As compound **58** is also rather planar in structure, compound **59a** is presumed to be the first conformation adopted following cleavage of the hemiaminal C-N bond. Computational analysis suggests subsequent conformational isomerism of **59a** to **59b** would result in a stabilization of nearly 20 kcal/mol. The curvature of compound **59b** also places N2 within 2.7 Å of C6 with a trajectory consistent with the observed stereochemistry of glandicoline B (Figure 4.4). The transannular

reaction forming glandicoline B is also predicted to be thermodynamically favorable, resulting in a stabilization of 22.07 kcal/mol.



Geometry optimization was carried out at HF/6-311+G(2d,p) level of theory.

**Figure 4.3:** Reaction coordinate diagram of roquefortine C transannular rearrangement to glandicoline B



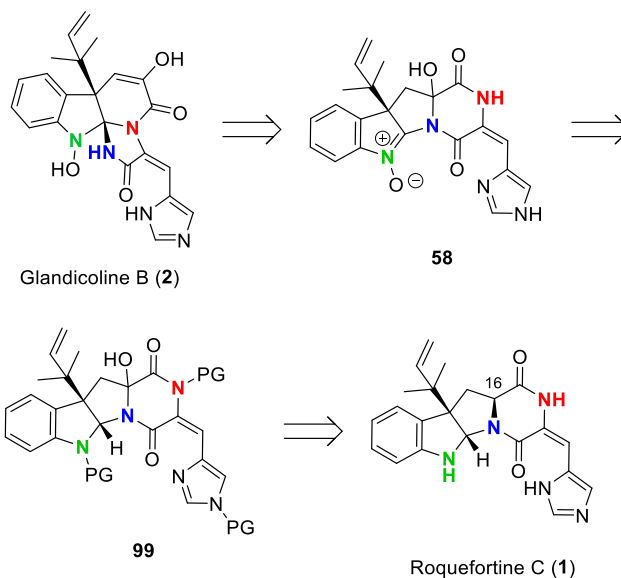
Geometry optimization was carried out at HF/6-311+G(2d,p) level of theory.

**Figure 4.4:** Geometry optimized structure of compound **59b**

Taken together, these computational studies indicate that transannular rearrangement from roquefortine C to glandicoline B is synthetically achievable and that the key intermediate **59** adopts a more thermodynamically favorable conformation to afford the stereochemistry observed in glandicoline B.

### **B. Efforts toward Transannular Rearrangement Methodology using Roquefortine C**

Given the promising results of the geometry optimization studies, a synthetic route was established to explore the transannular rearrangement of roquefortine C to glandicoline B (Scheme 4.9). Retrosynthetically, following protection of the imidazole, diketopiperazine, and indoline nitrogens, a hydroxyl group would be installed at the C16 position. Oxidations of this nature are well documented for diketopiperazines, most notably in the syntheses of epidithiodiketopiperazine alkaloids by Movassaghi and Sodeoka (Figure 4.5).<sup>30-36</sup> These syntheses implemented free-radical oxidants to install  $\alpha$ -hydroxy groups as precursors to the disulfide bridge. Electrophilic addition of oxygen to enolates is also well-documented for amides. Electrophilic oxygen species used in these transformations include DMDO, Davis oxaziridine, oxodiperoxymolybdenum-(pyridine)(hexamethylphosphoric triamide) (MoOPH), and more.<sup>33,37</sup>



**Scheme 4.9:** Retrosynthetic analysis of glandicoline B formation

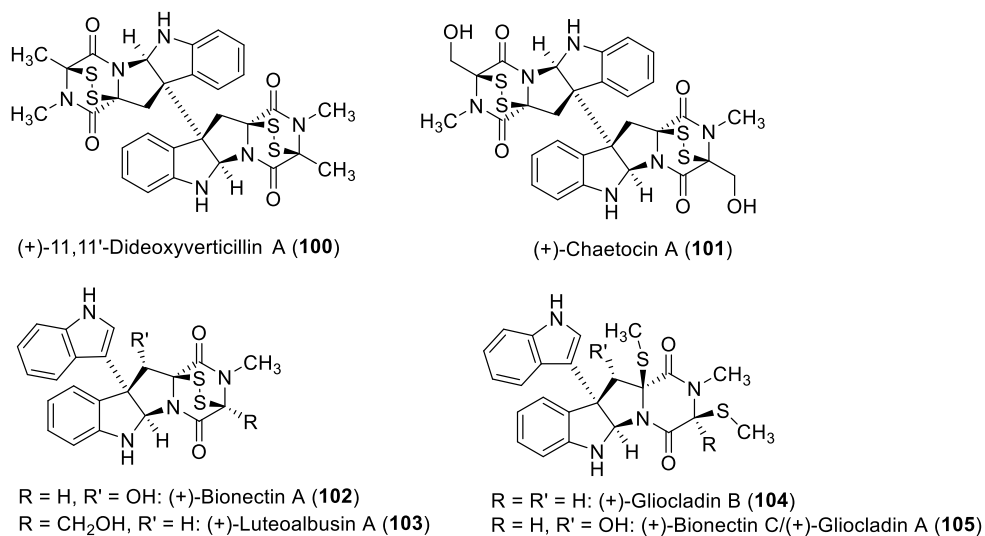
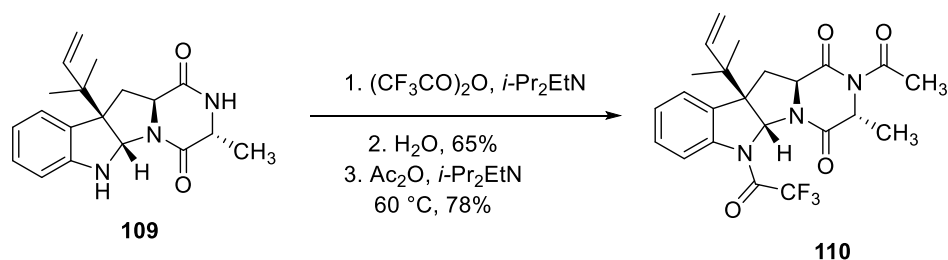


**Figure 4.5:** Representative epidithiodiketopiperazine alkaloids synthesized by Movassaghi and Sodeoka

Subsequent removal of the protecting groups and indoline N-oxidation would set the stage for transannular rearrangement to glandicoline B. Addition of a weak base is proposed to oxidize the hemiaminal to the 9-membered  $\alpha$ -diketo species.



nucleophilic diketopiperazine due to steric hindrance at the indoline nitrogen.<sup>39</sup>  $\alpha$ -Hydroxylation did not proceed with this species, and attempts to trap the corresponding enolate as a silyl enol ether were unsuccessful as the Boc groups were cleaved in the presence of silyl chlorides and triflates. Protection using benzoyl, carbamate (fluorenylmethyloxycarbonyl (Fmoc) or Cbz), or sulfonamide (mesyl (Ms) or tosyl (Ts)) groups yielded only mono protection of the imidazole. These results were in contrast to literature precedent in which similar compounds were shown to undergo protection of the indoline nitrogen (Scheme 4.11).<sup>40</sup>



**Scheme 4.11:** Representative protection of a pyrroloindoline diketopiperazine

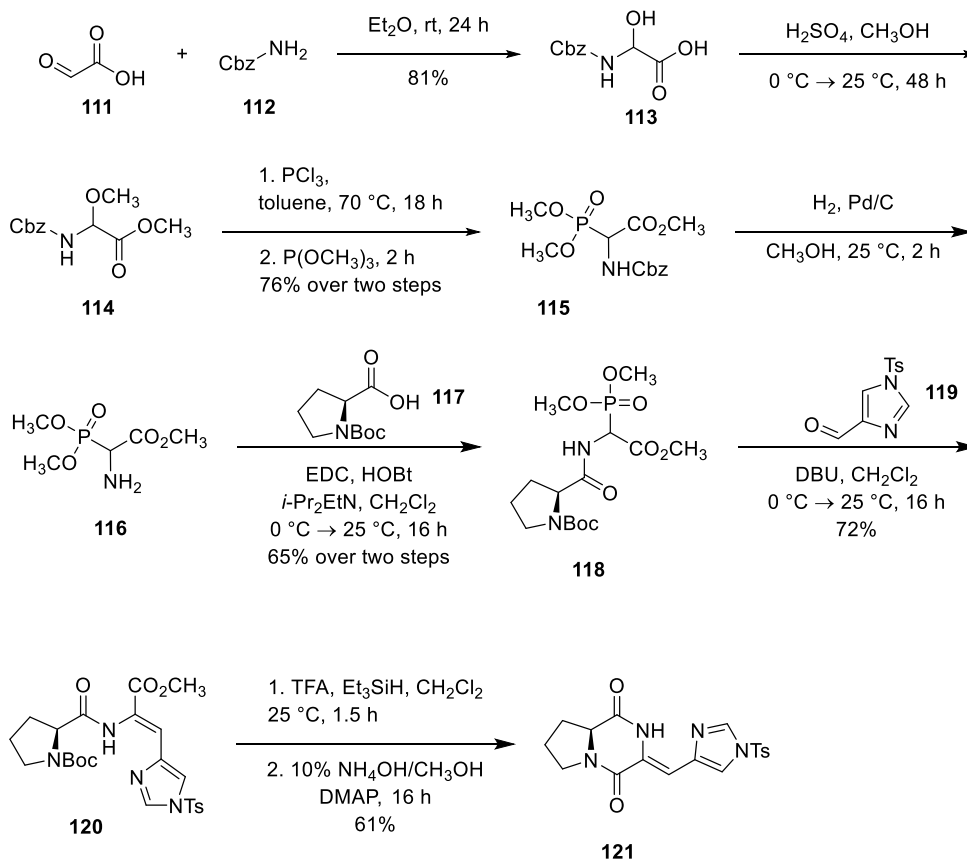
### C. First Generation Model System

With efforts to synthesize glandicoline B from roquefortine C proving ultimately unsuccessful, we turned our attention towards the design of a model system to investigate conditions for  $\alpha$ -hydroxylation. This first generation model system (**121**) incorporated the diketopiperazine and imidazole functionalities of roquefortine C while eliminating the indoline portion that had proven difficult to protect in roquefortine C.

The route to compound **121** implements methodology originally developed by Schmidt et al. for the synthesis of dehydroamino acid esters (Scheme 4.12).<sup>41</sup> Glyoxylic acid monohydrate was coupled to benzyl carbamate to give the  $\alpha$ -hydroxyglycine **113**, which was converted to the methyl ether under acidic conditions. Reaction with phosphorus trichloride gave the  $\alpha$ -chloride, and a subsequent Michaelis–Arbuzov reaction with trimethyl phosphite gave dimethoxyphosphorylacetate **115** in 76% yield over two steps. Hydrogenolysis followed by coupling to *N*-Boc D-proline provided compound **118**. Horner-Wadsworth-Emmons reaction of compound **118** with aldehyde **118** followed by ring closing led to the exclusive isolation of the undesired *Z* isomer. We hypothesize that unfavorable lone pair interactions between the methyl ester and imidazole discourage formation of the *trans* oxaphosphetane ***trans*-122** (Scheme 4.13). Additionally, oxaphosphetane ***cis*-122**, formed following *anti* addition of the aldehyde to the phosphonate ester, likely adopts an internal hydrogen bond, further aiding in the preferential formation of the *Z* isomer.

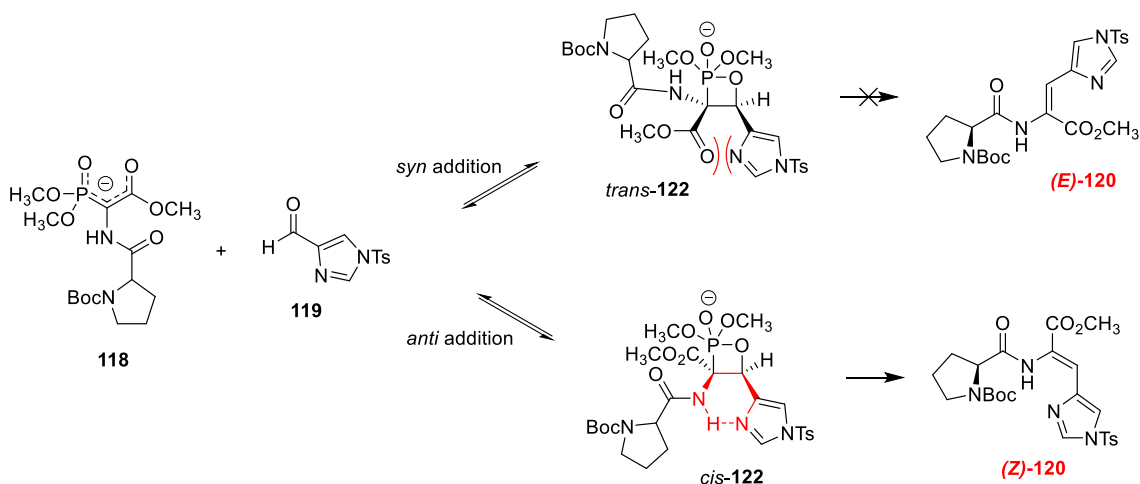
Carrying out the Horner-Wadsworth-Emmons reaction following cyclization to the diketopiperazine also gave the undesired *Z* isomer as the internal interactions of the two oxaphosphetanes remained unchanged following cyclization. Attempts to alkylate the amide nitrogen in hopes of disrupting the internal hydrogen bonding network proved unsuccessful.

While this synthetic route ultimately did not lead to the desired *E* isomer,  $\alpha$ -hydroxylation conditions were nevertheless investigated using compound **121**. Unfortunately, these efforts were not successful, as the presence of the *Z* dehydrohistidine moiety blocked functionalization of the amide nitrogen.  $\alpha$ -Hydroxylation did not proceed in the presence of the unprotected amide.



**Scheme 4.12:** Synthetic route towards first generation model system **121**



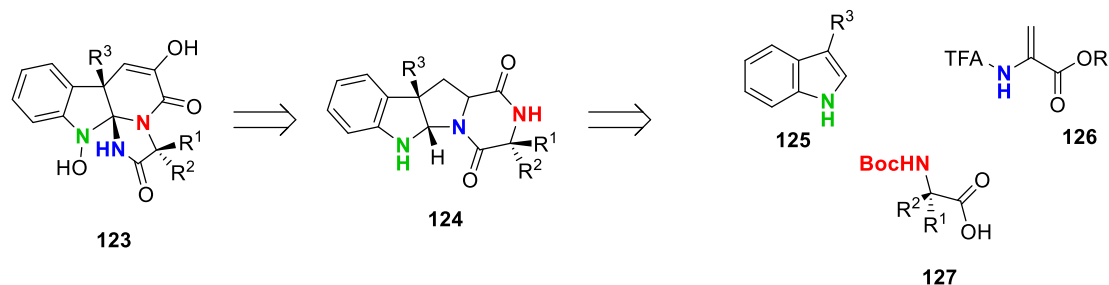


**Scheme 4.13:** Oxaphosphetane internal hydrogen bonding leads to exclusive formation of the *Z* isomer

#### D. Second Generation Model System: Design and Computational Studies

In light of the shortcomings of our first generation model system to develop an  $\alpha$ -hydroxylation methodology, a second generation model system was designed, incorporating the pyrroloindoline diketopiperazine skeleton of roquefortine C (Scheme 4.14). Transannular formation of triazaspirocycle **123** would proceed following  $\alpha$ -hydroxylation, as planned in our initial synthetic route to glandicoline B. As mentioned previously, this hydroxylation could be carried out through use of a free-radical oxidant or through electrophilic addition of oxygen to an enolate. The construction of this model system would be carried out using simple amino acid building blocks, which could be derivatized to achieve the same folded conformation required for the stereospecific transannular rearrangement. The pyrroloindoline core would be synthesized via [3+2] cycloaddition of a 3-substituted indole (**125**) with a 2-(2,2,2-trifluoroacetamido)acrylate (**126**). Coupling

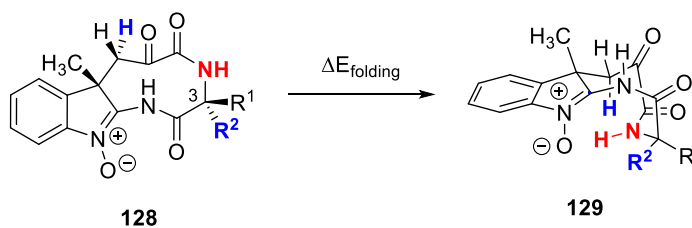
of the pyrroloindoline skeleton to Boc-protected amino acid **127** would provide diketopiperazine **124**.



**Scheme 4.14:** Retrosynthesis of second generation model system **124** and triazaspirocycle **123**

Several factors played a role in the design of the second generation model system. As the ultimate success of this model system hinges on its ability to mimic the folded conformation of compound **59b**, geometry optimization studies were carried out for a number of derivatives of diketoamine **128**. All derivatives investigated were found to adopt both a planar conformation (**128**) as well as a folded conformation (**129**) (Table 4.1). The desired folded conformation was found to be thermodynamically favored when either  $R^1$  or  $R^2$  was a phenyl group; however, due to the fact that many of the reactions proposed to synthesize triazaspirocycle **123** are base-promoted, mono-substitution at C3 would likely result in epimerization and unwanted side reactions. We therefore elected to synthesize the  $R^1 = R^2 = \text{CH}_3$  model system **124a**. While this species is predicted to favor the planar conformation, the activation energy required to achieve the desired folded conformation is attainable through heating of the reaction mixture.

**Table 4.1:** Calculated folding energy ( $\Delta E_{\text{folding}}$ ) of **128**



Entry	R <sup>1</sup>	R <sup>2</sup>	$\Delta E_{\text{folding}}$ (kcal/mol)
a	CH <sub>3</sub>	CH <sub>3</sub>	12.02
b	H	Ph	-5.82
c	Ph	H	-1.19
d	H	<i>t</i> -Bu	7.60
e	<i>t</i> -Bu	H	16.74
f	H	CH <sub>3</sub>	9.25
g	H	H	10.83

Geometry optimization was carried out at HF/6-311+G(2d,p) level of theory.

Geometry optimization calculations were carried out for all intermediates involved in the transannular rearrangement from **130** to **123a** (Figure 4.6). These calculations revealed that the planar **128a** exhibits thermodynamic stability of nearly 12 kcal/mol as compared to compound **130**. Conversion of **128a** to **129a** appears experimentally achievable, with subsequent triazaspirocycle formation imparting a 26.74 kcal/mol stabilization. The results of these calculations indicate that the synthetic route proposed to access triazaspirocycle **123a** is reasonable and that this model system is a satisfactory mimic for roquefortine C.

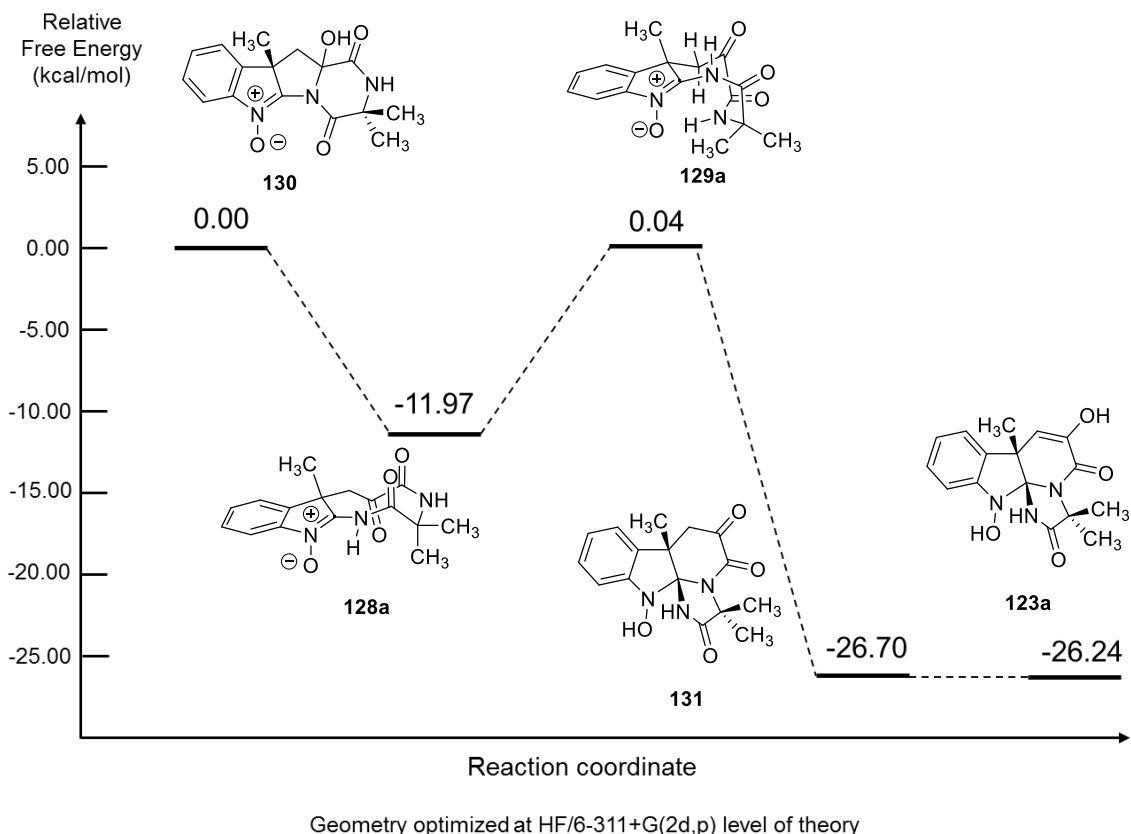
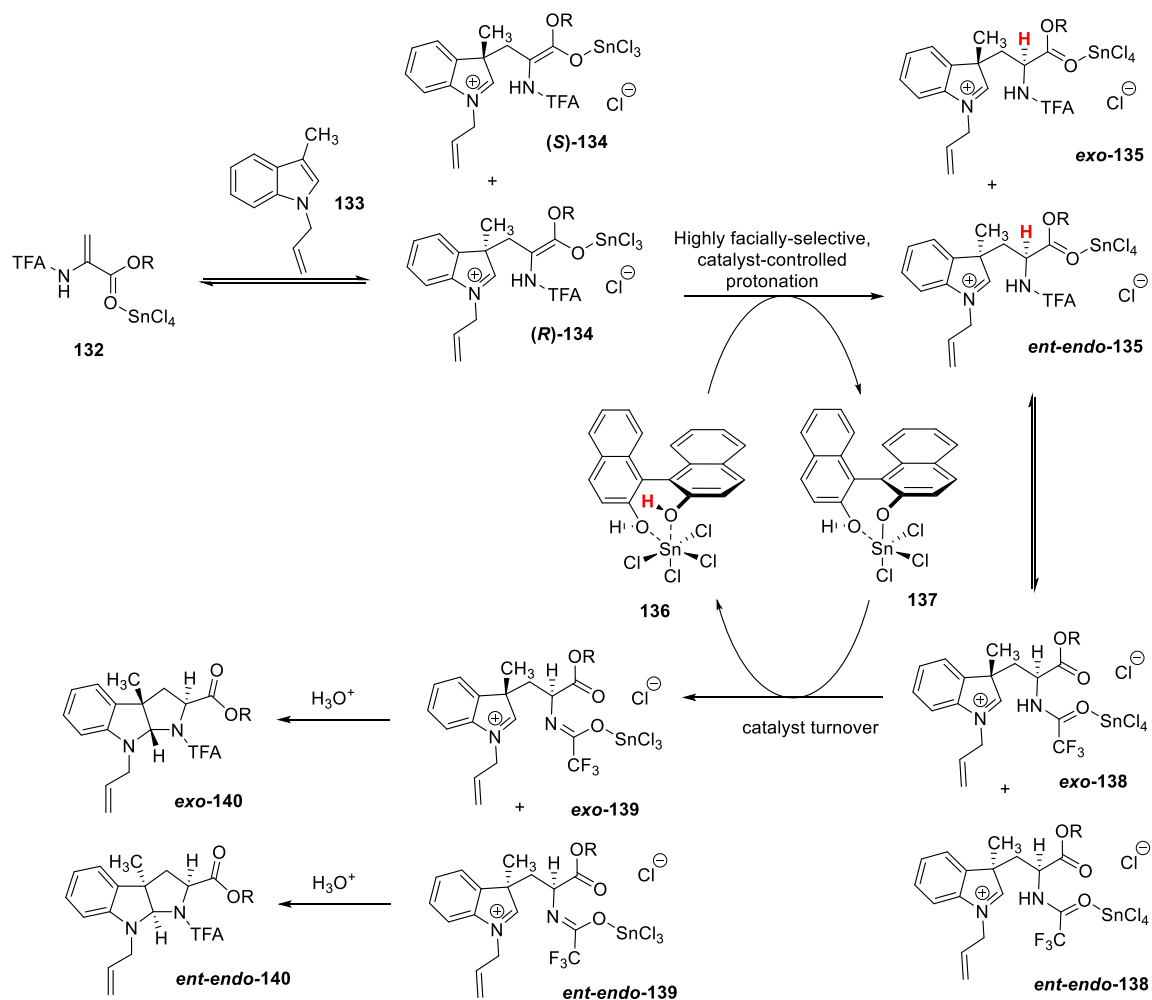


**Figure 4.6:** Reaction coordinate diagram of transannular rearrangement to **123a**

### E. Second Generation Model System: Synthetic Efforts

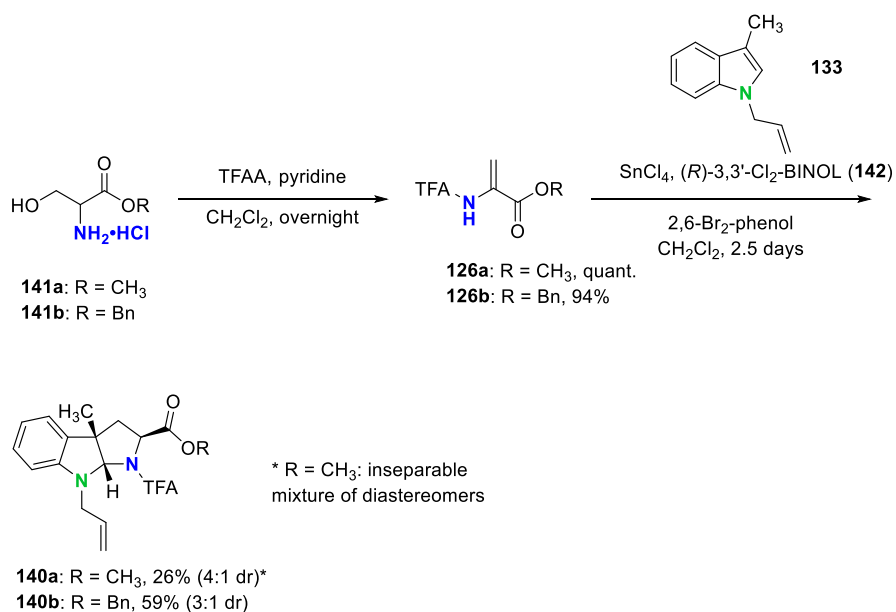
The first step towards the construction of model system **123a** was synthesis of the pyrroloindoline moiety. This step was accomplished using methodology developed by Reisman et al.<sup>42-44</sup> This methodology consists of a tin(IV) chloride promoted formal [3+2] cycloaddition between a 3-substituted indole and a 2-amidoacrylate (Scheme 4.15). Highly facially-selective protonation is achieved through use of an (*R*)-BINOL (1,1'-bi-2-naphthol) ligand. The matching and mismatching effects of the chiral catalyst complex with the chiral enolates allow for preferential formation of the *exo* diastereomer **exo-140**.



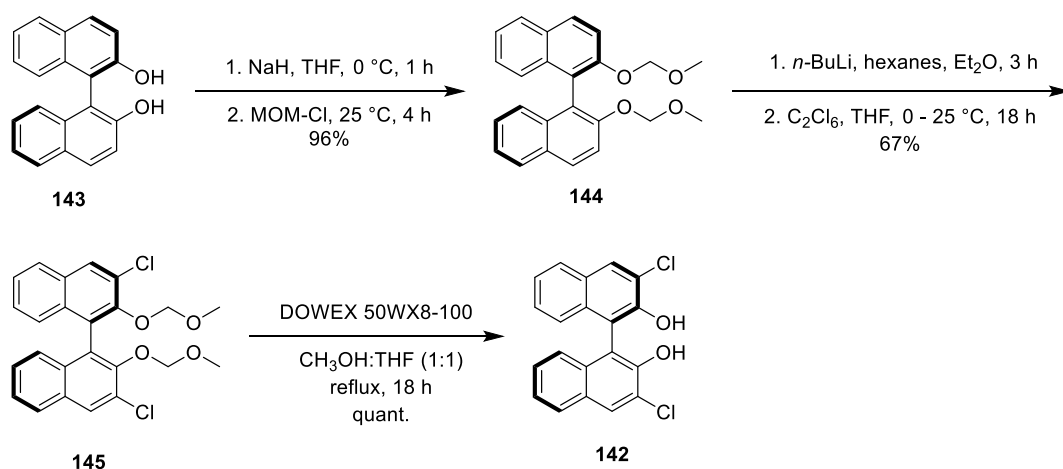
**Scheme 4.15:** Proposed mechanism of pyrroloindoline synthesis by formal [3+2] cycloaddition

2-Amidoacrylate **126a** had been shown by Reisman and coworkers to provide exo pyrroloindolines in greater diastereoselectivity as compared to the corresponding benzyl acrylate **126b**, giving compound **140a** in 84% yield with 5:1 diastereomeric ratio (dr) (Scheme 4.16).<sup>42,43</sup> In our hands, this reaction gave a similar diastereomeric ratio using 2-amidoacrylate **126a**; however, the exo and ent-endo diastereomers proved to be inseparable by flash chromatography.

Implementing benzyl trifluoroacetamidoacrylate **126b** for the cycloaddition reaction allowed for the synthesis and separation of the *exo* and *ent-endo* diastereomers in comparable yield and dr to that reported by Reisman.<sup>44</sup> (*R*)-3,3'-Cl<sub>2</sub>-BINOL **142** had been identified by Reisman et al. from a screen of BINOL ligands to give optimal yields and diastereomeric ratios for this reaction. The synthesis of this ligand, however, required four steps (Scheme 4.17) and the high ligand loading concentration coupled with the difficulty of recycling the ligand following the reaction led us to implement commercially-available (*R*)-BINOL **143** for the majority of **140b** syntheses, which provided the desired *exo* product in 54% yield.



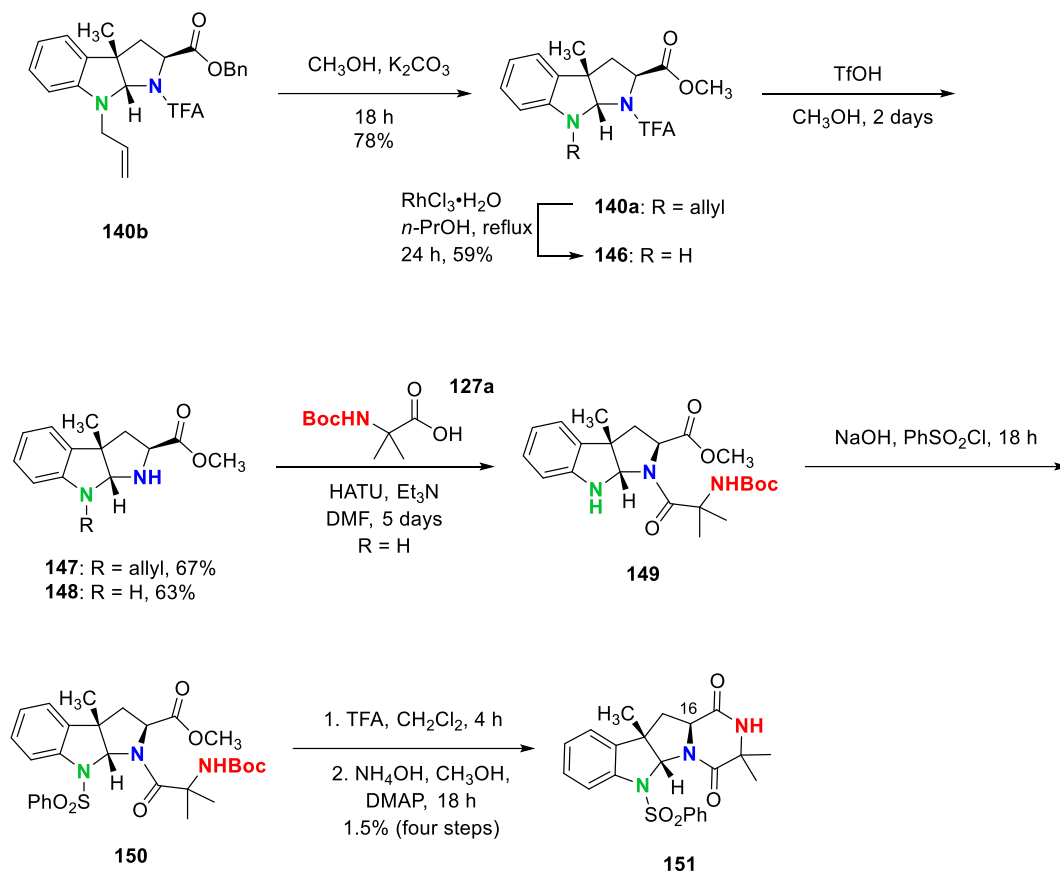
**Scheme 4.16:** Synthesis of pyrroloindolines **140a** and **140b**



**Scheme 4.17:** Synthesis of (*R*)-3,3'-Cl<sub>2</sub>-BINOL **142**

Transesterification of **140b** to methyl ester **140a** proceeded smoothly (Scheme 4.18). Following trifluoroacetyl (TFA) deprotection by triflic acid, peptide coupling of **147** to **127a** was attempted; however, unfavorable steric interactions from the neighboring allyl group significantly hindered coupling. The indoline *N*-allyl group was removed via a RhCl<sub>3</sub>-catalyzed deallylation reaction in *n*-propanol prior to the removal of the TFA moiety.<sup>45</sup> Attempts to remove the allyl group following TFA deprotection resulted in low yields and numerous side reactions. Coupling of the less hindered **148** still proceeded with great difficulty, given the steric bulk of both the proline amine and the  $\alpha$ -disubstituted carboxylic acid coupling partners. Increased concentration, prolonged reaction time, and excess base, coupling reagent, and **127a** were needed to drive the reaction to modest yields. Smaller amine bases such as Et<sub>3</sub>N gave more rapid reaction times than *i*-Pr<sub>2</sub>EtN or 2,4,6-collidine. Formation of the indoline sulfonamide proceeded only under aqueous basic conditions; as such, protection of the indoline nitrogen was

carried out prior to formation of the diketopiperazine to prevent hydrolysis. TFA deprotection of the Boc group and subsequent cyclization gave diketopiperazine **151**.

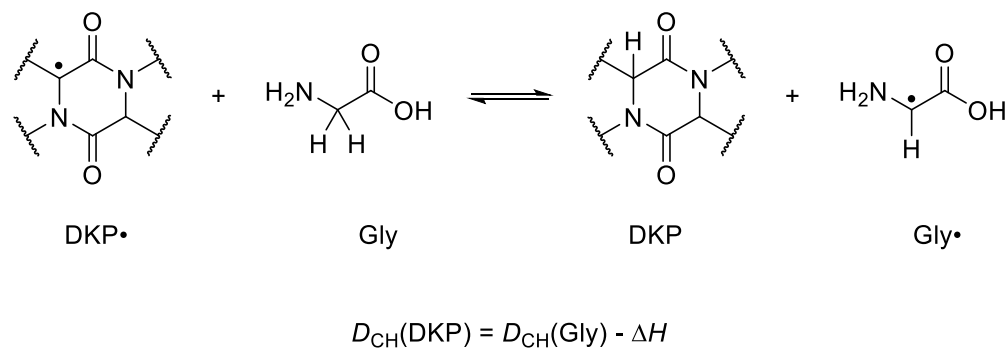


**Scheme 4.18:** Synthesis of phenylsulfonyl protected model system **151**

With compound **151** in hand, we have initiated efforts towards the synthesis of triazaspirocycle **123a**. As mentioned previously, the key reaction of this transformation involves the  $\alpha$ -hydroxylation of the C16 position. Efforts to install this functionality via electrophilic hydroxylation of the corresponding enolate proved fruitless, so we turned our attention towards radical hydroxylation. As

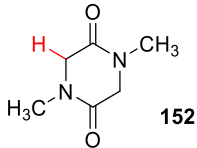
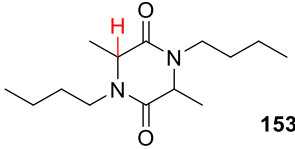
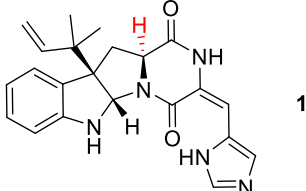
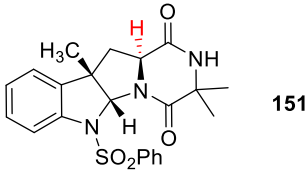


mentioned previously, permanganate-based oxidants such as *n*-Bu<sub>4</sub>NMnO<sub>4</sub> and bis(pyridine) silver (I) permanganate (Py<sub>2</sub>AgMnO<sub>4</sub>) have been implemented for this transformation, notably in the synthesis of epidithiodiketopiperazines by Movassaghi and Sodeoka.<sup>30-36</sup> Diketopiperazines are known to stabilize radicals at the α position, and this method of hydroxylation would take advantage of the captodative character of the C16 position (Table 4.2). The captodative character for several diketopiperazines, including roquefortine C and **151**, was calculated using an isodesmic reaction. Direct calculation of bond dissociation energies (BDE) of radical hydrogen abstraction can result in significant computational errors; as such, diketopiperazine BDEs were calculated as the heats of isodesmic reactions ( $\Delta H$ ) using the known enthalpy of bond dissociation ( $D_{\text{CH}}$ ) for glycine (Scheme 4.19).<sup>46</sup>



**Scheme 4.19:** Calculation of diketopiperazine <sup>α</sup>C-H BDE as heat of reaction  $\Delta H$

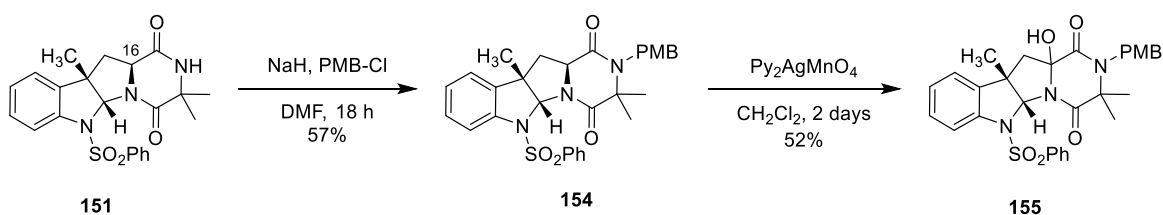
**Table 4.2:** Captodative character of select diketopiperazines

Species	$\alpha$ C-H BDE (kJ/mol)
 152	387 <sup>47</sup>
 153	374 <sup>48</sup>
 1	341
 151	319

Calculations for roquefortine C and **151** performed at B3LYP/6-311+G(2d,p) level of theory, using neutral glycine in an isodesmic reaction<sup>46</sup>

Appropriate protection of the indoline and diketopiperazine nitrogens proved to be a critical factor in this transformation. Protection of these positions was necessary as radical abstraction of the N-H hydrogen atom at either of these positions results in a resonance stabilized radical that effectively halts chain propagation. Secondly, the choice of protecting group for the indoline nitrogen in particular was shown to influence the reactivity of the oxidant. Implementing electron rich protecting groups such as *para*-methoxybenzyl (PMB) did not

significantly reduce the nucleophilicity of the indoline nitrogen and gave rise to indoline *N*-oxide formation. Protection of both the indoline and the diketopiperazine nitrogens with *tert*-butoxycarbonyl (Boc) groups failed to give any reaction under these conditions.  $\alpha$ -Hydroxylation was finally achieved using phenylsulfonyl protected **154** and  $\text{Py}_2\text{AgMnO}_4$  (Scheme 4.20). This reaction proceeded quite slowly and required excess oxidant and long reaction times to obtain modest yields. Additionally, it was observed that upon standing in solution, compound **155** underwent isomerization, as evidenced by  $^1\text{H}$  NMR. This isomerization is likely a result of the opening and subsequent reformation of the hemiaminal bond.

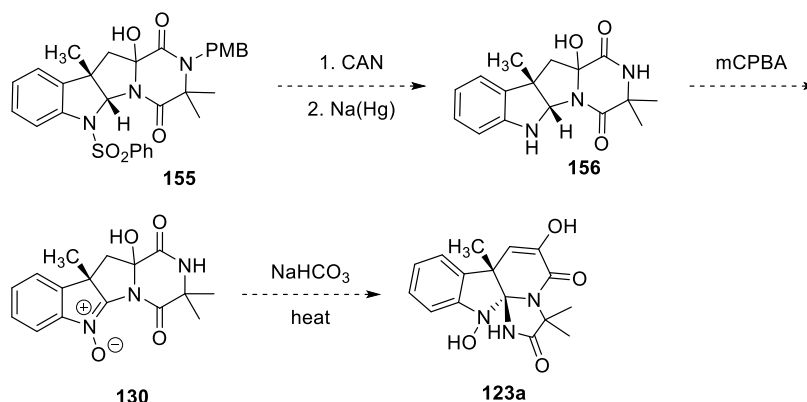


**Scheme 4.20:**  $\alpha$ -Hydroxylation of model system **155**

#### IV. Conclusions and Future Directions

While the biomimetic semisynthesis of glandicoline B from roquefortine C was ultimately unsuccessful, two model systems were synthesized to investigate the transannular synthesis of triazaspirocycles. The  $\alpha$ -hydroxylation of compound **153** was achieved using radical oxidant  $\text{Py}_2\text{AgMnO}_4$ . Future work to complete this synthetic route includes deprotection of the PMB and  $\text{SO}_2\text{Ph}$  protecting groups, *N*-oxidation of the indoline nitrogen to the nitrene, and rearrangement to give the desired triazaspirocycle (Scheme 4.21). The observed isomerization of compound

**155** upon standing in solution demonstrates the potential for transannular rearrangement, as breaking of the hemiaminal bond appears to occur spontaneously at room temperature.



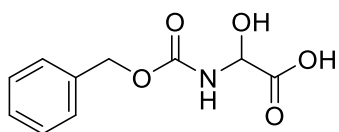
**Scheme 4.21:** Future work towards the synthesis of triazaspirocycle **123a**

## V. Experimental Details

### General information

Starting materials, reagents and solvents were purchased from commercial suppliers and used without further purification unless otherwise noted. Anhydrous Et<sub>2</sub>O, THF, and CH<sub>2</sub>Cl<sub>2</sub> were obtained from a solvent dispensing system stored under positive pressure of argon. All reactions were conducted in oven-dried glassware. The progress of reactions was monitored by silica gel thin layer chromatography (TLC) plates (250 μm with fluorescent indicator), visualized under UV, and stained using a phosphomolybdic acid (PMA) stain. Products were purified by flash column chromatography (FCC) on 230-400 mesh silica gel. <sup>1</sup>H and <sup>13</sup>C NMR spectra were recorded on a spectrometer operating at 500 MHz for <sup>1</sup>H and 125 MHz for <sup>13</sup>C unless otherwise stated. Chemical shifts are reported in

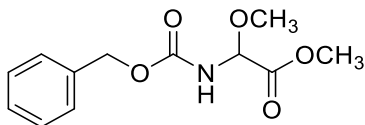
ppm relative to tetramethylsilane (TMS) as the internal standard for  $^1\text{H}$  and chloroform as the internal standard for  $^{13}\text{C}$ .  $^1\text{H}$ - $^{13}\text{C}$  Heteronuclear single quantum correlation experiment (HSQC) NMR spectra were recorded on a spectrometer operating at 500 MHz. NMR data is reported as follows: chemical shift, multiplicity (s = singlet, d = doublet, dd = doublet of doublets, t = triplet, td = triplet of doublets, q = quartet, br = broad, m = multiplet), coupling constants (Hz), and integration. Accurate mass measurement data (HRMS) were acquired on ESI-TOF or electron ionization (EI) spectrometers (Waters). Waters software calibrates and reports by use of neutral atomic mass. The mass of the electron is not included.



### **2-(((Benzyloxy)carbonyl)amino)-2-hydroxyacetic acid (113)**

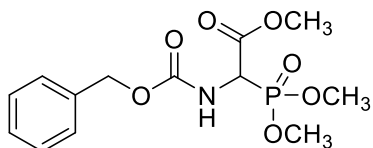
Glyoxylic acid monohydrate (1.33 g, 14.40 mmol) and benzyl carbamate (2.00 g, 13.00 mmol) were dissolved in dry  $\text{Et}_2\text{O}$  (13 mL), and the solution was stirred at room temperature for 18 hours, forming a white precipitate. An additional 30 mL of ether was added to the reaction mixture, and the precipitate was isolated via filtration to give 2-(((benzyloxy)carbonyl)amino)-2-hydroxyacetic acid as a fluffy white solid (2.36 g, 81% yield).  $^1\text{H}$  NMR (500 MHz,  $\text{DMSO-d}_6$ )  $\delta$  12.79 (br s, 1H), 8.12 (d,  $J = 8.7$  Hz, 1H), 7.34 (m, 5H), 6.24 (br s, 1H), 5.21 (d,  $J = 8.8$  Hz, 1H), 5.05 (s, 2H). HRMS (EI)  $m/z$   $[\text{M} + \text{H}]^+$  calcd for  $\text{C}_{10}\text{H}_{12}\text{NO}_5$  226.0715, found

226.0715 (lit. (Azuma et al., 2011)<sup>49</sup> HRMS  $m/z$   $[M + H]^+$  calcd for  $C_{10}H_{12}NO_5$  226.0715, found 226.0716).



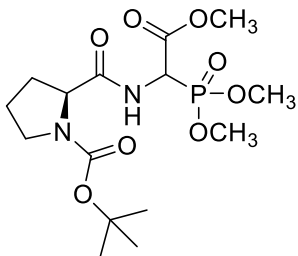
#### **Methyl 2-(((benzyloxy)carbonyl)amino)-2-methoxyacetate (114)**

2-(((Benzyloxy)carbonyl)amino)-2-hydroxyacetic acid (2.36 g, 10.40 mmol) was dissolved in  $CH_3OH$  (24 mL) and chilled in an ice bath for 10 minutes. Concentrated  $H_2SO_4$  (0.42 mL) was then added dropwise via syringe. As ice melted, reaction mixture was allowed to gradually warm to room temperature as it was stirred for 48 hours. The reaction was then quenched by pouring over a mixture of ~50 g ice and ~60 mL saturated aqueous  $NaHCO_3$ , causing a white precipitate to crash out of solution. The reaction mixture was then extracted three times with EtOAc, dried over  $MgSO_4$  and concentrated to give a clear oil that crystallized after ~1 hour at room temperature to give methyl 2-(((benzyloxy)carbonyl)amino)-2-methoxyacetate as a white crystalline solid (2.35 g, 89%).  $^1H$  NMR (500 MHz,  $CDCl_3$ )  $\delta$  7.31 (m, 5H), 5.81 (br s, 1H), 5.32 (d,  $J = 9.5$  Hz, 1H), 5.12 (s, 2H), 3.77 (s, 3H), 3.40 (s, 3H). HRMS (ESI-TOF)  $m/z$   $[M + Na]^+$  calcd for  $C_{12}H_{15}NO_5$  276.0848, found 276.0835. (lit. (Azuma et al., 2011)<sup>49</sup> HRMS  $m/z$   $[M + Na]^+$  calcd for  $C_{12}H_{15}NNaO_5$  276.0848, found 276.0846).



**Methyl 2-(((benzyloxy)carbonyl)amino)-2-(dimethoxyphosphoryl)acetate (115)**

Methyl 2-(((benzyloxy)carbonyl)amino)-2-methoxyacetate (2.35 g, 9.30 mmol) was dissolved in dry toluene (10 mL) and was heated to 70 °C under argon.  $\text{PCl}_3$  (0.81 mL, 9.30 mmol) was added dropwise via syringe and the reaction mixture was allowed to stir for 18 hours at 70 °C.  $\text{P}(\text{OCH}_3)_3$  (1.10 mL, 9.30 mmol) was then added via syringe and stirring was continued for an additional 2 hours. The reaction mixture was then concentrated to give a pale yellow oil, which was dissolved in EtOAc and washed three times with saturated aqueous  $\text{NaHCO}_3$ . The EtOAc layer was dried over  $\text{Na}_2\text{SO}_4$  and concentrated to ~10 mL. Hexanes were added while stirring until a precipitate formed, which was subsequently isolated via filtration to give methyl 2-(((benzyloxy)carbonyl)amino)-2-(dimethoxyphosphoryl)acetate as a white crystalline solid (2.36 g, 76%).  $^1\text{H NMR}$  ( $\text{CDCl}_3$ )  $\delta$  7.33 (m, 5H), 5.56 (d,  $J = 9.0$  Hz, 1H), 5.13 (s, 2H), 4.92 (dd,  $J = 9$  Hz, 22 Hz, 1H), 3.80 (m, 9H). HRMS (ESI-TOF)  $m/z$   $[\text{M} + \text{H}]^+$  calcd for  $\text{C}_{13}\text{H}_{19}\text{NO}_7\text{P}$  332.0899, found 332.0912. (lit. (Azuma et al., 2011)<sup>49</sup> HRMS  $m/z$   $[\text{M} + \text{H}]^+$  calcd for  $\text{C}_{13}\text{H}_{19}\text{NO}_7\text{P}$  332.0899, found 332.0905).

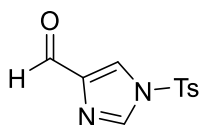


***tert*-Butyl (2S)-2-((1-(dimethoxyphosphoryl)-2-methoxy-2-oxoethyl)carbamoyl)pyrrolidine-1-carboxylate (118)**

Methyl 2-(((benzyloxy)carbonyl)amino)-2-(dimethoxyphosphoryl)acetate (1.50 g, 4.50 mmol) was dissolved in CH<sub>3</sub>OH (15 mL) under argon. Palladium on carbon (10 wt. % loading, matrix activated carbon support, 0.056 g) was added and the reaction mixture was evacuated and fitted with a balloon of hydrogen gas. The reaction mixture was allowed to stir for 2 hours at room temperature, after which it was filtered through a Celite plug and rinsed with EtOAc. The EtOAc solution was concentrated to give methyl 2-amino-2-(dimethoxyphosphoryl)acetate as a clear oil, which was immediately dissolved in dry CH<sub>2</sub>Cl<sub>2</sub> (45 mL) and cooled in an ice bath under argon. *N*-Boc-D-proline (1.11 g, 5.20 mmol) was then added, followed by sequential addition of *N*-(3-dimethylaminopropyl)-*N'*-ethylcarbodiimide hydrochloride (EDC, 1.07 g, 5.60 mmol), 1-hydroxybenzotriazole hydrate (HOBT, 0.64 g, 4.70 mmol), and *N,N*-diisopropylethylamine (1.18 mL, 6.8 mmol). The reaction mixture was allowed to slowly warm to room temperature as it was stirred for 20 hours. The reaction mixture was then sequentially washed with 10% aqueous HCl, 5% aqueous NaHCO<sub>3</sub>, and saturated aqueous NaCl. The organic solution was dried over Na<sub>2</sub>SO<sub>4</sub> and was concentrated by rotary evaporation to give a pale yellow oil. The oil was purified via column chromatography (1:4

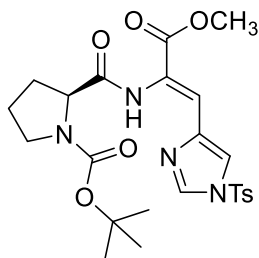


acetone:CH<sub>2</sub>Cl<sub>2</sub>) to give *tert*-butyl (2*S*)-2-((1-(dimethoxyphosphoryl)-2-methoxy-2-oxoethyl)carbamoyl)-pyrrolidine-1-carboxylate as a clear oil (1.16 g, 65% over two steps). <sup>1</sup>H NMR (CDCl<sub>3</sub>) δ 5.17 (dd, *J* = 9.1, 22.1 Hz, 1H), 4.31 (br s, 1H), 3.78 (m, 9H), 3.43 (br s, 2H), 2.13 (br s, 2H), 1.85 (br s, 1H), 1.44 (s, 9H). <sup>13</sup>C NMR (125 MHz, CDCl<sub>3</sub>) δ 172.1, 167.1, 155.9, 80.8, 61.0, 60.1, 54.3, 54.2, 53.4, 47.2, 29.8, 28.4, 24.6, 23.7. HRMS (EI) *m/z* [M – Boc – OCH<sub>3</sub>]<sup>+</sup> calcd for C<sub>9</sub>H<sub>15</sub>N<sub>2</sub>O<sub>5</sub>P 262.0719, found 262.0724 (parent ion not observed).



### 1-Tosyl-1*H*-imidazole-4-carbaldehyde (119)

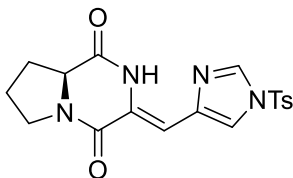
1*H*-Imidazole-4-carbaldehyde (1.32 g, 13.70 mmol) was dissolved in dry CH<sub>2</sub>Cl<sub>2</sub> (38 mL) in a round-bottomed flask under argon. Et<sub>3</sub>N (2.3 mL, 16.40 mmol) and TsCl (2.65 g, 13.80 mmol) were added sequentially, and the reaction was allowed to stir overnight at room temperature. After stirring for 18 hours, the reaction mixture was quenched with saturated aqueous NH<sub>4</sub>Cl. The aqueous layer was washed twice with CH<sub>2</sub>Cl<sub>2</sub>, and the combined organic layers were dried over Na<sub>2</sub>SO<sub>4</sub> and concentrated in vacuo to give 1-tosyl-1*H*-imidazole-4-carbaldehyde (3.42 g, 99%) as an off white solid. <sup>1</sup>H NMR (500 MHz, CDCl<sub>3</sub>) δ 9.85 (s, 1H), 8.02 (d, *J* = 1.5 Hz, 1H), 7.89 (d, *J* = 1.0 Hz, 1H), 7.85 (d, *J* = 8.5 Hz, 2H), 7.38 (d, *J* = 8.5 Hz, 2H), 2.44 (s, 3H). HRMS (ESI-TOF) *m/z* [M + Na]<sup>+</sup> calcd for C<sub>11</sub>H<sub>10</sub>N<sub>2</sub>NaO<sub>3</sub>S 273.0310, found 273.0302 (lit (Arndt et al., 2016)<sup>50</sup> HRMS (ESI) *m/z* [M + H]<sup>+</sup> calcd for C<sub>11</sub>H<sub>11</sub>N<sub>2</sub>O<sub>3</sub>S 251.0485, found 251.0487).



***tert*-Butyl (*S,Z*)-2-((3-methoxy-3-oxo-1-(1-tosyl-1*H*-imidazol-4-yl)prop-1-en-2-yl)carbamoyl)pyrrolidine-1-carboxylate (**120**)**

*tert*-Butyl (2*S*)-2-((1-(dimethoxyphosphoryl)-2-methoxy-2-oxoethyl)carbamoyl)-pyrrolidine-1-carboxylate (0.67 g, 1.70 mmol) was dissolved in dry CH<sub>2</sub>Cl<sub>2</sub> (68 mL) under argon and chilled in an ice bath. DBU (0.51 mL, 3.40 mmol) was added slowly via syringe, and the reaction mixture was allowed to stir for 10 minutes. 1-Tosyl-1*H*-imidazole-4-carbaldehyde (0.68 g, 2.70 mmol) was then added, and the reaction mixture was allowed to stir overnight at room temperature. After stirring 18 hours, the reaction was quenched with saturated aqueous NH<sub>4</sub>Cl and washed with 1 N KHSO<sub>4</sub> (aq.), saturated aqueous NaHCO<sub>3</sub>, and saturated aqueous NaCl. The organic solution was dried over Na<sub>2</sub>SO<sub>4</sub> and concentrated by rotary evaporation. The crude product was purified by column chromatography (1:4 acetone:CH<sub>2</sub>Cl<sub>2</sub>) to give *tert*-butyl (*S,Z*)-2-((3-methoxy-3-oxo-1-(1-tosyl-1*H*-imidazol-4-yl)prop-1-en-2-yl)carbamoyl)-pyrrolidine-1-carboxylate (0.66 g, 72%) as a white solid. <sup>1</sup>H NMR (500 MHz, CDCl<sub>3</sub>) δ 10.72 (br s, 1H), 8.02 (s, 1H), 7.83 (d, *J* = 7.9 Hz, 2H), 7.37 (d, *J* = 8.1 Hz, 2H), 7.28 (s, 1H), 6.29 (s, 1H), 4.24 (d, *J* = 5.1 Hz, 1H), 3.81 (s, 3H), 3.81 (m, 1H), 3.65 (m, 1H), 2.45 (s, 3H), 2.21 (m, 1H), 2.13 (m, 1H), 1.95 (m, 1H), 1.90 (m, 1H), 1.24 (s, 9H). <sup>13</sup>C NMR (125 MHz, CDCl<sub>3</sub>) δ 171.8, 165.5, 154.4, 146.9, 139.8, 136.6, 134.6, 130.7, 130.1, 127.7, 116.7,

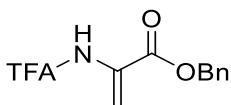
109.1, 80.4, 61.7, 52.6, 46.9, 31.1, 28.2, 23.9, 21.9. HRMS (ESI-TOF)  $m/z$  [M + H]<sup>+</sup> calcd for C<sub>24</sub>H<sub>31</sub>N<sub>4</sub>O<sub>7</sub>S 519.1913, found 519.1926.



**(S,Z)-3-((1-Tosyl-1H-imidazol-4-yl)methylene)hexahydropyrrolo[1,2-a]pyrazine-1,4-dione (121)**

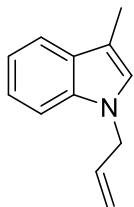
*tert*-Butyl (S,Z)-2-((3-methoxy-3-oxo-1-(1-tosyl-1H-imidazol-4-yl)prop-1-en-2-yl)-carbamoyl)pyrrolidine-1-carboxylate (0.10 g, 0.19 mmol) was dissolved in CH<sub>2</sub>Cl<sub>2</sub> (0.4 mL) and trifluoroacetic acid (TFA, 0.18 mL, 2.47 mmol) and Et<sub>3</sub>SiH (0.08 mL, 0.48 mmol) were added via syringe. The reaction mixture was allowed to stir at room temperature, and following full conversion of starting material after 1.5 hours (determined by TLC), the reaction mixture was concentrated by rotary evaporation. The crude residue was then dissolved in 10% NH<sub>4</sub>OH in CH<sub>3</sub>OH (2.7 mL). 4-Dimethylaminopyridine (DMAP, 0.005 g, 0.038 mmol) was then added, and the reaction mixture was allowed to stir overnight at room temperature. After stirring for 17 hours, the reaction mixture was concentrated by rotary evaporation and purified by column chromatography (1:9 acetone:CH<sub>2</sub>Cl<sub>2</sub>) to give (S,Z)-3-((1-tosyl-1H-imidazol-4-yl)methylene)hexahydropyrrolo[1,2-a]pyrazine-1,4-dione as a white solid (0.56 g, 61%). <sup>1</sup>H NMR (500 MHz, CDCl<sub>3</sub>) δ 10.96 (s, 1H), 7.98 (s, 1H), 7.81 (d, *J* = 8.4 Hz, 2H), 7.37 (d, *J* = 8.0 Hz, 2H), 7.2965 (d, *J* = 1.2 Hz, 1H), 6.52 (s, 1H), 4.17 (dd, *J* = 6.2, 10.6 Hz, 1H), 3.80 (m, 1H), 3.56 (m, 1H), 2.45 (m, 1H), 2.42

(s, 3H), 1.96 (m, 3H).  $^{13}\text{C}$  NMR (125 MHz,  $\text{CDCl}_3$ )  $\delta$  165.5, 157.6, 147.1, 140.2, 136.5, 134.5, 130.8, 129.5, 127.7, 116.9, 102.3, 59.5, 45.8, 29.5, 22.0, 21.8. HRMS (ESI-TOF)  $m/z$   $[\text{M} + \text{H}]^+$  calcd for  $\text{C}_{18}\text{H}_{19}\text{N}_4\text{O}_4\text{S}$  387.1127, found 387.1125.



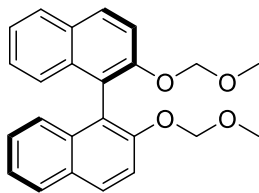
### **Benzyl 2-(2,2,2-trifluoroacetamido)acrylate (126b)**

L-Serine benzyl ester hydrochloride (1.32 g, 5.70 mmol) was dissolved in  $\text{CH}_2\text{Cl}_2$  (9.5 mL) and chilled in an ice bath. Trifluoroacetic anhydride (TFAA, 4 mL, 28.60 mmol) and pyridine (2.8 mL, 34.30 mmol) were added sequentially via syringe, and the reaction mixture was stirred and allowed to warm to room temperature. After stirring overnight, the reaction mixture was chilled in an ice bath, diluted with  $\text{CH}_2\text{Cl}_2$ , and quenched with water. The organic layer was then washed with water and saturated aqueous NaCl, dried over  $\text{Na}_2\text{SO}_4$ , and concentrated by rotary evaporation. The crude residue was purified by column chromatography (2:3 EtOAc:hexanes) to give benzyl 2-(2,2,2-trifluoroacetamido)acrylate (1.03 g, 66%) as a clear oil.  $^1\text{H}$  NMR (500 MHz,  $\text{CDCl}_3$ )  $\delta$  8.53 (br s, 1H), 7.41 (m, 5H), 6.74 (s, 1H), 6.20 (d,  $J$  = 0.8 Hz, 1H), 5.33 (s, 2H). HRMS (EI)  $m/z$   $[\text{M}]^+$  calcd for  $\text{C}_{12}\text{H}_{10}\text{F}_3\text{NO}_3$  273.0613, found 273.0618.



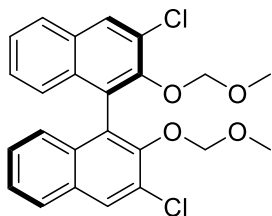
### 1-Allyl-3-methyl-1*H*-indole (133)

A slurry of NaH (60% in mineral oil, 4.60 g, 114.30 mmol) in DMF (67 mL) was prepared in a round-bottomed flask under argon. 3-Methylindole (5.00 g, 38.10 mmol) was dissolved in DMF (32 mL) in a separate round-bottomed flask and was then added slowly via syringe to NaH slurry. The reaction mixture was allowed to stir 1 hour at room temperature, after which allyl bromide (4.3 mL, 49.60 mmol) was added. After stirring overnight under argon, the reaction was poured over saturated aqueous NH<sub>4</sub>Cl and extracted with Et<sub>2</sub>O. The organic layer was washed with saturated aqueous NaCl, dried over MgSO<sub>4</sub>, and concentrated by rotary evaporation. The residue was purified by column chromatography (1:99 EtOAc:hexanes) to give 1-allyl-3-methyl-1*H*-indole (5.77 g, 88%) as a pale yellow oil. <sup>1</sup>H NMR (500 MHz, CDCl<sub>3</sub>) δ 7.61 (d, *J* = 7.9 Hz, 1H), 7.32 (d, *J* = 8.2 Hz, 1H), 7.22 (td, *J* = 1.0, 7.0 Hz, 1H), 7.14 (td, *J* = 1.0, 7.4 Hz, 1H), 6.89 (s, 1H), 6.01 (m, 1H), 5.21 (dd, *J* = 1.5, 10.3 Hz, 1H), 5.12 (dd, *J* = 1.5, 17.0 Hz, 1H), 4.70 (td, *J* = 1.6, 5.4 Hz, 2H), 2.37 (d, *J* = 1.0 Hz, 1H). HRMS (EI) *m/z* [M]<sup>+</sup> calcd for C<sub>12</sub>H<sub>13</sub>N 171.1048, found 171.1043.



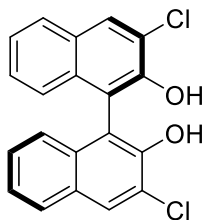
**(*R*)-2,2'-Bis(methoxymethoxy)-1,1'-binaphthalene (144)**

NaH (60% in mineral oil, 0.308 g, 7.7 mmol) was suspended in dry THF (17 mL) in a round-bottomed flask under argon and was chilled in an ice bath. (*R*)-BINOL (1.00 g, 3.50 mmol) was dissolved in dry THF (6 mL) in a separate round-bottomed flask and was added slowly to NaH mixture via syringe. The reaction mixture was allowed to stir 1 hour at 0 °C and then allowed to warm to room temperature for 15 minutes. MOM-Cl (0.6 mL, 7.70 mmol) was then added slowly via syringe, and the reaction mixture was stirred at room temperature for 4 hours. The reaction was quenched with saturated aqueous NH<sub>4</sub>Cl and was concentrated by rotary evaporation. The residue was suspended in CH<sub>2</sub>Cl<sub>2</sub> and H<sub>2</sub>O and the aqueous layer was extracted three times with CH<sub>2</sub>Cl<sub>2</sub>. The combined organic extracts were then washed with saturated aqueous NaCl, dried over Na<sub>2</sub>SO<sub>4</sub>, and concentrated by rotary evaporation to give (*R*)-2,2'-bis(methoxymethoxy)-1,1'-binaphthalene (1.27 g, 96%) as a white crystalline solid. <sup>1</sup>H NMR (500 MHz, CDCl<sub>3</sub>) δ 7.92 (d, *J* = 9.0 Hz, 2H), 7.84 (d, *J* = 8.2 Hz, 2H), 7.55 (d, *J* = 9.0 Hz, 2H), 7.32 (td, *J* = 1.2, 6.7 Hz, 2H), 7.19 (td, *J* = 1.3, 6.7 Hz, 2H), 7.12 (d, *J* = 8.6 Hz, 2H), 5.05 (d, *J* = 6.8 Hz, 2H), 4.95 (d, *J* = 6.8 Hz, 2H), 3.11 (s, 6H). HRMS (ESI-TOF) *m/z* [M]<sup>+</sup> calcd for C<sub>24</sub>H<sub>22</sub>O<sub>4</sub> 374.1510, found 374.1518 (lit (Hediger, Reymond, et al., 2015)<sup>51</sup> HRMS *m/z* [M + Na]<sup>+</sup> calcd for C<sub>24</sub>H<sub>22</sub>NaO<sub>4</sub> 397.1410, found 374.1518).



**(*R*)-3,3'-Dichloro-2,2'-bis(methoxymethoxy)-1,1'-binaphthalene (145)**

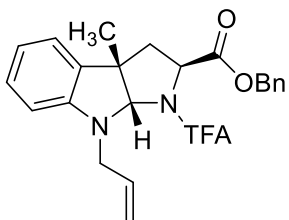
(*R*)-2,2'-Bis(methoxymethoxy)-1,1'-binaphthalene (1.27 g, 3.38 mmol) was added to an oven-dried round-bottomed flask under argon and dissolved in dry degassed Et<sub>2</sub>O (56 mL). *n*-BuLi (0.93M in hexanes, 12.7 mL, 11.84 mmol) was added dropwise via syringe and the reaction mixture was allowed to stir 3 hours at room temperature. The reaction mixture was then cooled in an ice bath, and dry degassed THF (37 mL) and C<sub>2</sub>Cl<sub>6</sub> (2.40 g, 10.40 mmol) were then added. The reaction mixture was gradually warmed to room temperature and stirred overnight. The reaction mixture was then quenched with saturated aqueous NH<sub>4</sub>Cl and the layers were separated. The aqueous layer was extracted three times with CH<sub>2</sub>Cl<sub>2</sub>, and the combined organic layers were dried over Na<sub>2</sub>SO<sub>4</sub> and concentrated by rotary evaporation. The residue was purified by column chromatography (1:10 Et<sub>2</sub>O:hexanes) to give (*R*)-3,3'-dichloro-2,2'-bis(methoxymethoxy)-1,1'-binaphthalene (1.00 g, 67%) as a white solid. <sup>1</sup>H NMR (500 MHz, CDCl<sub>3</sub>) δ 8.07 (s, 2H), 7.79 (d, *J* = 8.3 Hz, 2H), 7.43 (td, *J* = 1.1, 6.8 Hz, 2H), 7.27 (td, *J* = 1.2, 6.8 Hz, 2H), 7.19 (d, *J* = 8.5 Hz, 2H), 4.84 (dd, *J* = 5.9, 15.7 Hz, 4H), 2.58 (s, 6H). HRMS (ESI-TOF) *m/z* [M]<sup>+</sup> calcd for C<sub>24</sub>H<sub>20</sub><sup>35</sup>Cl<sub>2</sub>O<sub>4</sub> 442.0739, found 442.0735 (lit (Chong et al., 2011)<sup>52</sup> HRMS *m/z* [M]<sup>+</sup> calcd for C<sub>24</sub>H<sub>20</sub><sup>35</sup>Cl<sub>2</sub>O<sub>4</sub> 442.0740, found 442.0756).



**(R)-3,3'-Dichloro-BINOL (142)**

(*R*)-3,3'-Dichloro-2,2'-bis(methoxymethoxy)-1,1'-binaphthalene (1.00 g, 2.26 mmol) was dissolved in 1:1 CH<sub>3</sub>OH:THF (40 mL). DOWEX 50WX8-100 (1.50 g) was added, and the reaction mixture was refluxed overnight. After refluxing for 18 hours, the DOWEX 50WX8-100 was filtered off, and the organic solution was concentrated. The residue was purified by column chromatography (1:10 EtOAc:hexanes) to give (*R*)-3,3'-dichloro-BINOL (0.80 g, quant.) as a pale yellow solid. <sup>1</sup>H NMR (500 MHz, CDCl<sub>3</sub>) δ 8.08 (s, 2H), 7.83 (d, *J* = 8.2 Hz, 2H), 7.40 (td, *J* = 1.0, 6.8 Hz, 2H), 7.32 (td, *J* = 1.2, 6.9 Hz, 2H), 7.13 (d, *J* = 8.5 Hz, 2H), 5.59 (s, 2H). HRMS (EI) *m/z* [M]<sup>+</sup> calcd for C<sub>20</sub>H<sub>12</sub><sup>35</sup>Cl<sub>2</sub>O<sub>2</sub> 354.0214, found 354.0228 (lit (Chong et al., 2011)<sup>52</sup> HRMS *m/z* [M]<sup>+</sup> calcd for C<sub>20</sub>H<sub>12</sub><sup>35</sup>Cl<sub>2</sub>O<sub>2</sub> 354.0214, found 354.0211).

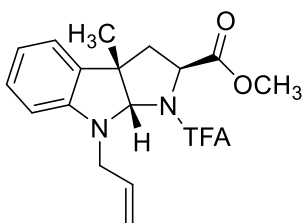




**Benzyl (2S,3aS,8aS)-8-allyl-3a-methyl-1-(2,2,2-trifluoroacetyl)-1,2,3,3a,8,8a-hexahydropyrrolo[2,3-*b*]indole-2-carboxylate (140b)**

To an oven-dried round-bottomed flask under argon, the following reagents were added sequentially: 1-allyl-3-methyl-1*H*-indole (3.66 g, 21.40 mmol), CH<sub>2</sub>Cl<sub>2</sub> (152 mL), benzyl 2-(2,2,2-trifluoroacetamido)acrylate (6.98 g, 25.60 mmol), (*R*)-BINOL (1.20 g, 4.30 mmol), and 2,6-dibromophenol (2.10 g, 8.50 mmol). SnCl<sub>4</sub> (1 M in CH<sub>2</sub>Cl<sub>2</sub>, 34 mL, 34.16 mmol) was then added slowly via syringe. The reaction mixture was allowed to stir at room temperature for 2 days, after which it was diluted with CH<sub>3</sub>CN and quenched with 1 M HCl. The reaction mixture was further diluted with H<sub>2</sub>O and CH<sub>2</sub>Cl<sub>2</sub>, and the layers were separated. The aqueous layer was extracted three times with Et<sub>2</sub>O. The combined organic layers were washed three times with 3 M NaOH, dried over MgSO<sub>4</sub>, and concentrated. The residue was purified by column chromatography (1-8% EtOAc in hexanes) to give benzyl (2S,3aS,8aS)-8-allyl-3a-methyl-1-(2,2,2-trifluoroacetyl)-1,2,3,3a,8,8a-hexahydro-pyrrolo[2,3-*b*]indole-2-carboxylate (5.15 g, 54%) as a pale yellow oil. <sup>1</sup>H NMR (500 MHz, CDCl<sub>3</sub>, compound exists as a 6.1:1 mixture of rotamers, the major rotamer is denoted by \*, minor rotamer denoted by §) δ 7.40 (br s, 5H\*, 5H§), 7.1 (t, *J* = 7.6 Hz, 1H\*, 1H§), 7.01 (d, *J* = 7.1 Hz, 1H\*, 1H§), 6.84 (br s, 1H§), 6.77 (t, *J* = 7.2 Hz, 1H\*), 6.64 (br s, 1H§), 6.55 (d, *J* = 7.8 Hz, 1H\*), 5.83 (m, 1H\*, 1H§),

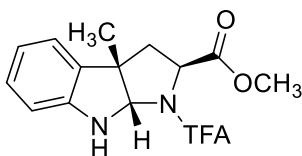
5.74 (s, 1H<sup>\*</sup>), 5.53 (br s, 1H§), 5.30-5.15 (m, 4H<sup>\*</sup>, 4H§), 4.75 (d, *J* = 9.0 Hz, 1H<sup>\*</sup>), 4.42 (br s, 1H§), 4.27 (d, *J* = 15.2 Hz, 1H<sup>\*</sup>), 4.05 (dd, *J* = 5.8, 16.5 Hz, 1H<sup>\*</sup>, 1H§), 3.84 (br s, 1H§), 2.60 (dd, *J* = 10.1, 13.2 Hz, 1H<sup>\*</sup>, 1H§), 2.36 (d, *J* = 13.4 Hz, 1H<sup>\*</sup>), 2.11 (br s, 1H§), 1.28 (s, 3H<sup>\*</sup>, 3H§). HRMS (ESI-TOF) *m/z* [M + H]<sup>+</sup> calcd for C<sub>24</sub>H<sub>24</sub>F<sub>3</sub>N<sub>2</sub>O<sub>3</sub> 445.1739, found 445.1713 (lit (Reisman et al., 2010)<sup>42</sup> HRMS (ESI) *m/z* [M + H]<sup>+</sup> calcd for C<sub>24</sub>H<sub>24</sub>F<sub>3</sub>N<sub>2</sub>O<sub>3</sub> 445.1734, found 445.1750).



**Methyl (2S,3aS,8aS)-8-allyl-3a-methyl-1-(2,2,2-trifluoroacetyl)-1,2,3,3a,8,8a-hexahydropyrrolo[2,3-*b*]indole-2-carboxylate (140a)**

Benzyl (2S,3aS,8aS)-8-allyl-3a-methyl-1-(2,2,2-trifluoroacetyl)-1,2,3,3a,8,8a-hexahydropyrrolo[2,3-*b*]indole-2-carboxylate (393 mg, 0.88 mmol) was dissolved in dry CH<sub>3</sub>OH (9 mL) in a round-bottomed flask. K<sub>2</sub>CO<sub>3</sub> (24 mg, 0.18 mmol) was added, and the reaction mixture was stirred overnight. The reaction was quenched with 1 M HCl and extracted three times with EtOAc. The organic layers were washed with saturated aqueous NaHCO<sub>3</sub>, dried over Na<sub>2</sub>SO<sub>4</sub>, and concentrated. The residue was purified by column chromatography (0-15% EtOAc in hexanes) to give methyl (2S,3aS,8aS)-8-allyl-3a-methyl-1-(2,2,2-trifluoroacetyl)-1,2,3,3a,8,8a-hexahydropyrrolo[2,3-*b*]indole-2-carboxylate (252 mg, 78%) as a white crystalline solid. <sup>1</sup>H NMR (500 MHz, CDCl<sub>3</sub>) δ 7.15 (t, *J* = 7.7 Hz, 1H), 7.06 (d, *J* = 7.2 Hz, 1H), 6.81 (t, *J* = 7.0 Hz, 1H), 6.58 (d, *J* = 7.6 Hz, 1H), 5.82 (m, 2H), 5.28

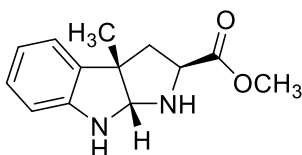
(d,  $J = 17.2$  Hz, 1H), 5.15 (d,  $J = 10.1$  Hz, 1H), 4.73 (d,  $J = 8.5$  Hz, 1H), 4.26 (d,  $J = 15.7$  Hz, 1H), 4.05 (dd,  $J = 5.5, 16.4$  Hz, 1H), 3.81 (s, 3H), 2.60 (dd,  $J = 10.4, 12.9$  Hz, 1H), 2.41 (d,  $J = 13.3$  Hz, 1H), 1.40 (s, 3H). HRMS (ESI-TOF)  $m/z$   $[M]^+$  calcd for  $C_{18}H_{19}F_3N_2O_3$  368.1348, found 368.1344 (lit (Reisman et al., 2013)<sup>43</sup> HRMS (APCI)  $m/z$   $[M + H]^+$  calcd for  $C_{18}H_{20}F_3N_2O_3$  369.1421, found 369.1416).



**Methyl (2S,3aS,8aS)-3a-methyl-1-(2,2,2-trifluoroacetyl)-1,2,3,3a,8,8a-hexahydropyrrolo[2,3-*b*]indole-2-carboxylate (146)**

Methyl (2S,3aS,8aS)-8-allyl-3a-methyl-1-(2,2,2-trifluoroacetyl)-1,2,3,3a,8,8a-hexahydropyrrolo[2,3-*b*]indole-2-carboxylate (60 mg, 0.16 mmol) was suspended in *n*-PrOH (5 mL), sparged with argon for 10 minutes, and heated to dissolution.  $RhCl_3 \cdot 3H_2O$  (4 mg, 0.008 mmol) was added, and the reaction mixture was refluxed overnight under argon. The reaction was cooled to room temperature, diluted with a large amount of  $H_2O$ , and extracted three times with  $CH_2Cl_2$ . The organic layers were dried over  $Na_2SO_4$  and concentrated by rotary evaporation. The residue was purified by column chromatography (0-10% EtOAc in hexanes) to give methyl (2S,3aS,8aS)-3a-methyl-1-(2,2,2-trifluoroacetyl)-1,2,3,3a,8,8a-hexahydropyrrolo[2,3-*b*]indole-2-carboxylate (27 mg, 51%) as a pale yellow oil.  $^1H$  NMR (500 MHz,  $CDCl_3$ , compound exists as a 1:1 mixture of rotamers)  $\delta$  7.10 (m, 2H), 6.84 (t,  $J = 7.4$  Hz, 0.5H), 6.78 (t,  $J = 7.4$  Hz, 0.5H), 6.65 (d,  $J = 7.8$  Hz, 0.5H), 6.61 (d,  $J = 7.8$  Hz, 0.5H), 5.64 (s, 0.5H), 5.59 (s, 0.5H), 5.33 (br s, 0.5H), 4.77 (s, 0.5H), 4.63

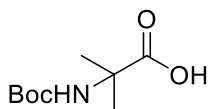
(ddd,  $J = 1.3, 4.1, 9.1$  Hz, 0.5H), 4.46 (t,  $J = 7.4$  Hz, 0.5H), 3.83 (s, 1.5H), 3.76 (s, 1.5H), 2.76 (dd,  $J = 9.2, 13.5$  Hz, 0.5H), 2.61 (dd,  $J = 8.5, 13.2$  Hz, 0.5H), 2.38 (dd,  $J = 4.3, 13.4$  Hz, 0.5H), 2.22 (dd,  $J = 7.0, 13.2$  Hz, 0.5H), 1.50 (s, 1.5H), 1.41 (s, 1.5H).  $^{13}\text{C}$  NMR (125 MHz,  $\text{CDCl}_3$ , compound exists as a 1:1 mixture of rotamers)  $\delta$  172.3, 171.1, 147.1, 146.6, 133.4, 133.4, 129.1, 129.0, 122.5, 122.4, 120.5, 119.6, 110.2, 109.6, 86.7, 84.7, 61.4, 59.8, 54.8, 53.2, 52.9, 50.5, 43.9, 40.6, 31.8, 24.5, 24.2. HRMS (ESI-TOF)  $m/z$   $[\text{M} + \text{H}]^+$  calcd for  $\text{C}_{15}\text{H}_{16}\text{F}_3\text{N}_2\text{O}_3$  329.1113, found 329.1095.



**Methyl (2S,3aS,8aR)-3a-methyl-1,2,3,3a,8,8a-hexahydropyrrolo[2,3-b]indole-2-carboxylate (148)**

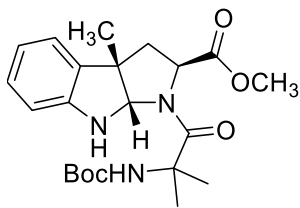
Methyl (2S,3aS,8aS)-3a-methyl-1-(2,2,2-trifluoroacetyl)-1,2,3,3a,8,8a-hexahydropyrrolo[2,3-b]indole-2-carboxylate (1.81 g, 5.51 mmol) was dissolved in methanol (55 mL) in a round-bottomed flask. Triflic acid (4.8 mL, 55.10 mmol) was added slowly, and the reaction mixture was stirred at room temperature for 2 days. The reaction was then slowly quenched with saturated aqueous  $\text{NaHCO}_3$  and extracted three times with  $\text{CH}_2\text{Cl}_2$ . The organic layers were dried over  $\text{Na}_2\text{SO}_4$  and concentrated. The residue was purified by column chromatography (100% EtOAc) to give methyl (2S,3aS,8aR)-3a-methyl-1,2,3,3a,8,8a-hexahydropyrrolo[2,3-b]indole-2-carboxylate (0.96 g, 75%) as a pale yellow oil.  $^1\text{H}$  NMR (500 MHz,  $\text{CDCl}_3$ )  $\delta$  7.03 (m, 2H), 6.74 (td,  $J = 0.9, 7.4$  Hz, 1H), 6.56 (d,  $J = 7.6$  Hz, 1H), 4.91

(s, 1H), 3.74 (dd,  $J = 6.0, 10.4$  Hz, 1H), 3.71 (s, 3H), 2.43 (dd,  $J = 6.0, 12.2$  Hz, 1H), 1.96 (dd,  $J = 10.4, 12.1$  Hz, 1H), 1.48 (s, 3H).  $^{13}\text{C}$  NMR (125 MHz,  $\text{CDCl}_3$ )  $\delta$  174.5, 149.6, 134.6, 128.3, 123.2, 119.2, 109.2, 84.9, 59.9, 54.6, 52.3, 46.5, 26.0. HRMS (ESI-TOF)  $m/z$   $[\text{M} + \text{H}]^+$  calcd for  $\text{C}_{13}\text{H}_{17}\text{N}_2\text{O}_2$  233.1290, found 233.1274.



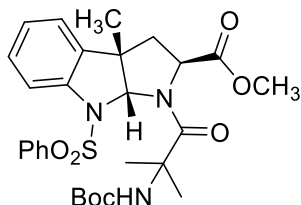
### **2-((*tert*-Butoxycarbonyl)amino)-2-methylpropanoic acid (127a)**

In a round-bottomed flask, 2-methylalanine (1.00 g, 9.70 mmol) was stirred with  $\text{Boc}_2\text{O}$  (4.2 g, 19.40 mmol), 1 M NaOH (40 mL), and 1,4-dioxane (40 mL) overnight at room temperature. The reaction mixture was then concentrated to remove the dioxane, acidified to pH 3 with 1 M HCl, and extracted three times with EtOAc. The organic layers were dried over  $\text{MgSO}_4$  and concentrated to give 2-((*tert*-butoxycarbonyl)amino)-2-methylpropanoic acid (1.35 g, 68%) as a white crystalline solid.  $^1\text{H}$  NMR (500 MHz,  $\text{CDCl}_3$ )  $\delta$  5.10 (br s, 1H), 1.53 (s, 6H), 1.42 (s, 9H). HRMS (ESI-TOF)  $m/z$   $[\text{M} - \text{H}]^-$  calcd for  $\text{C}_9\text{H}_{16}\text{NO}_4$  202.1079, found 202.1097 (lit (Balamurugan and Muraleedharan, 2012)<sup>53</sup> HRMS (ESI)  $m/z$   $[\text{M} + \text{H}]^+$  calcd for  $\text{C}_9\text{H}_{18}\text{NO}_4$  204.1236, found 204.1239).



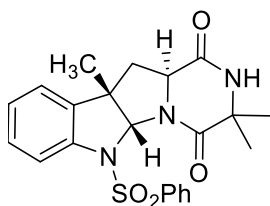
**Methyl (2S,3aS,8aS)-1-(2-((*tert*-butoxycarbonyl)amino)-2-methylpropanoyl)-3a-methyl-1,2,3,3a,8,8a-hexahydropyrrolo[2,3-*b*]indole-2-carboxylate (149)**

In a round-bottomed flask, 2-((*tert*-butoxycarbonyl)amino)-2-methylpropanoic acid (800 mg, 3.94 mmol) was dissolved in DMF (33 mL). 1-[Bis(dimethylamino)methylene]-1*H*-1,2,3-triazolo[4,5-*b*]pyridinium 3-oxid hexafluorophosphate (HATU, 1.49 g, 3.94 mmol) and Et<sub>3</sub>N (1.4 mL, 9.84 mmol) were added, and the reaction mixture was allowed to stir for 10 minutes. Methyl (2*S*,3a*S*,8a*R*)-3a-methyl-1,2,3,3a,8,8a-hexahydropyrrolo[2,3-*b*]indole-2-carboxylate (380 mg, 1.64 mmol) was then added, and the reaction mixture was allowed to stir overnight at room temperature. The reaction mixture was then diluted with water and extracted three times with EtOAc. The combined organic layers were washed with saturated aqueous NaHCO<sub>3</sub> and saturated aqueous NaCl, and were dried over Na<sub>2</sub>SO<sub>4</sub> and concentrated. The combined product and 1-hydroxy-7-azabenzotriazole (HOAt) activated carboxylic acid were purified from the starting material via column chromatography (100% EtOAc). The crude product (629 mg), an inseparable mixture of several compounds, was carried on without further purification.



**Methyl (2S,3aS,8aR)-1-(2-((*tert*-butoxycarbonyl)amino)-2-methylpropanoyl)-3a-methyl-8-(phenylsulfonyl)-1,2,3,3a,8,8a-hexahydropyrrolo[2,3-*b*]indole-2-carboxylate (150)**

A crude mixture containing methyl (2S,3aS,8aS)-1-(2-((*tert*-butoxycarbonyl)amino)-2-methylpropanoyl)-3a-methyl-1,2,3,3a,8,8a-hexahydropyrrolo[2,3-*b*]indole-2-carboxylate (730 mg) was suspended in 1 M aqueous NaOH (4.4 mL) in a round-bottomed flask. To this suspension was added benzenesulfonyl chloride (245  $\mu$ L, 1.93 mmol), and the reaction mixture was stirred for 18 hours. The mixture was then acidified with 1 M aqueous HCl and extracted three times with Et<sub>2</sub>O. The ether extracts were washed with saturated aqueous NaCl, dried over Na<sub>2</sub>SO<sub>4</sub>, and concentrated in vacuo. The crude residue was purified by column chromatography (25-50% EtOAc in hexanes) to give 617.9 mg of methyl (2S,3aS,8aR)-1-(2-((*tert*-butoxycarbonyl)amino)-2-methylpropanoyl)-3a-methyl-8-(phenylsulfonyl)-1,2,3,3a,8,8a-hexahydropyrrolo[2,3-*b*]indole-2-carboxylate as an inseparable mixture with several unidentified compounds. The crude product was carried on without further purification.

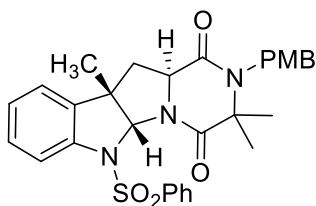


**(5aR,10bS,11aS)-3,3,10b-Trimethyl-6-(phenylsulfonyl)-2,3,6,10b,11,11a-hexahydro-4H-pyrazino[1',2':1,5]pyrrolo[2,3-b]indole-1,4(5aH)-dione (151)**

The crude methyl (2S,3aS,8aR)-1-(2-((*tert*-butoxycarbonyl)amino)-2-methylpropanoyl)-3a-methyl-8-(phenylsulfonyl)-1,2,3,3a,8,8a-hexahydropyrrolo[2,3-*b*]indole-2-carboxylate (96.3 mg) was dissolved in CH<sub>2</sub>Cl<sub>2</sub> (2.5 mL) in a round-bottomed flask and chilled to 0 °C in an ice bath. TFA (640 μL, 8.63 mmol) was added, and the reaction mixture was allowed to slowly warm to room temperature and stir for 3 hours. The reaction mixture was concentrated to remove the CH<sub>2</sub>Cl<sub>2</sub>, and the residue was then dissolved in 10% NH<sub>4</sub>OH in CH<sub>3</sub>OH (2.5 mL). DMAP (4 mg, 0.034 mmol) was added, and the reaction mixture was allowed to stir overnight at room temperature. The reaction mixture was then concentrated and purified by column chromatography (100% EtOAc) to give (5aR,10bS,11aS)-3,3,10b-trimethyl-6-(phenylsulfonyl)-2,3,6,10b,11,11a-hexahydro-4H-pyrazino[1',2':1,5]pyrrolo[2,3-*b*]indole-1,4(5aH)-dione (25 mg, 1.5 % over four steps) as a yellow solid. <sup>1</sup>H NMR (500 MHz, CDCl<sub>3</sub>) δ 7.89 (d, *J* = 7 Hz, 2H), 7.66 (d, *J* = 8.1 Hz, 1H), 7.55 (d, *J* = 7.4 Hz, 1H), 7.44 (t, *J* = 8.0 Hz, 2H), 7.30 (td, *J* = 1.4, 7.0 Hz, 1H), 7.13 (m, 2H), 6.84 (br s, 1H), 6.07 (s, 1H), 4.00 (dd, *J* = 6.0, 11.2 Hz, 1H), 2.63 (dd, *J* = 6.0, 12.7 Hz, 1H), 2.07 (dd, *J* = 11.4, 12.6 Hz, 1H), 1.51 (s, 3H), 1.41 (s, 3H), 1.03 (s, 3H). <sup>13</sup>C NMR (125 MHz, CDCl<sub>3</sub>) δ 168.1, 167.8, 141.6, 138.7, 136.1,



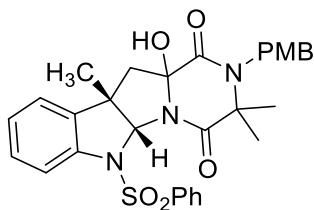
133.5, 129.2, 127.6, 125.6, 123.3, 117.0, 83.2, 58.6, 57.5, 50.7, 44.2, 29.0, 25.7, 24.9. HRMS (ESI-TOF)  $m/z$   $[M + Na]^+$  calcd for  $C_{22}H_{23}N_3NaO_4S$  448.1307, found 448.1325.



**(5aR,10bS,11aS)-2-(4-Methoxybenzyl)-3,3,10b-trimethyl-6-(phenylsulfonyl)-2,3,6,10b,11,11a-hexahydro-4H-pyrazino[1',2':1,5]pyrrolo[2,3-b]indole-1,4(5aH)-dione (154)**

(5aR,10bS,11aS)-3,3,10b-Trimethyl-6-(phenylsulfonyl)-2,3,6,10b,11,11a-hexahydro-4H-pyrazino[1',2':1,5]pyrrolo[2,3-b]indole-1,4(5aH)-dione (18 mg, 0.042 mmol) was dissolved in DMF (1 mL) in a round-bottomed flask under argon and chilled in an ice bath to 0 °C. NaH (60% in mineral oil, 2 mg, 0.046 mmol) was added, and the reaction mixture was allowed to stir for 30 minutes. PMB-Cl (5.7  $\mu$ L, 0.042 mmol) was then added, and the reaction mixture was allowed to slowly warm to room temperature overnight. After stirring for 18 hours, the reaction was quenched with saturated aqueous  $NH_4Cl$ , diluted with water, and extracted three times with EtOAc. The combined EtOAc extracts were washed three times with water and once with saturated aqueous NaCl. The EtOAc extracts were then dried over  $MgSO_4$  and concentrated in vacuo. The crude product was purified by column chromatography (1:1 EtOAc:hexanes) to give (5aR,10bS,11aS)-2-(4-methoxybenzyl)-3,3,10b-trimethyl-6-(phenylsulfonyl)-2,3,6,10b,11,11a-hexa-

hydro-4*H*-pyrazino[1',2':1,5]pyrrolo[2,3-*b*]indole-1,4(5*aH*)-dione (13 mg, 57%) as a pale yellow oil. <sup>1</sup>H NMR (500 MHz, CDCl<sub>3</sub>) δ 7.87 (d, *J* = 7.4 Hz, 2H), 7.66 (d, *J* = 8.1 Hz, 1H), 7.54 (t, *J* = 7.5 Hz, 1H), 7.44 (t, *J* = 8.0 Hz, 2H), 7.32 (td, *J* = 1.9, 7.0 Hz, 1H), 7.15 (m, 4H), 6.82 (d, *J* = 8.7 Hz, 2H), 6.09 (s, 1H), 4.62 (dd, *J* = 15.7, 24.8 Hz, 2H), 4.05 (dd, *J* = 5.9, 11.0 Hz, 1H), 3.78 (s, 3H), 2.76 (dd, *J* = 5.9, 12.8 Hz, 1H), 2.14 (dd, *J* = 11.2, 12.7 Hz, 1H), 1.56 (s, 3H), 1.22 (s, 3H), 1.01 (s, 3H). <sup>13</sup>C NMR (125 MHz, CDCl<sub>3</sub>) δ 167.7, 167.4, 159.0, 141.6, 138.9, 136.4, 133.4, 130.4, 129.2, 129.2, 128.9, 127.6, 125.7, 123.3, 117.2, 114.2, 83.5, 62.8, 58.3, 55.4, 50.7, 45.0, 44.8, 26.8, 24.8, 23.6. HRMS (ESI-TOF) *m/z* [M + H]<sup>+</sup> calcd for C<sub>30</sub>H<sub>32</sub>N<sub>3</sub>O<sub>5</sub>S 546.2063, found 546.2072.



**(5*aR*,10*bS*)-11*a*-Hydroxy-2-(4-methoxybenzyl)-3,3,10*b*-trimethyl-6-(phenylsulfonyl)-2,3,6,10*b*,11,11*a*-hexahydro-4*H*-pyrazino[1',2':1,5]pyrrolo[2,3-*b*]indole-1,4(5*aH*)-dione (155)**

5*aR*,10*bS*,11*aS*)-2-(4-Methoxybenzyl)-3,3,10*b*-trimethyl-6-(phenylsulfonyl)-2,3,6,10*b*,11,11*a*-hexahydro-4*H*-pyrazino[1',2':1,5]pyrrolo[2,3-*b*]indole-1,4(5*aH*)-dione (13 mg, 0.024 mmol) was dissolved in dry CH<sub>2</sub>Cl<sub>2</sub> (1 mL) in a round-bottomed flask. Py<sub>2</sub>AgMnO<sub>4</sub> (184 mg, 0.48 mmol) was added, and the dark purple reaction mixture was stirred at room temperature for 48 h. The reaction was quenched with 10% aqueous Na<sub>2</sub>S<sub>2</sub>O<sub>3</sub> and diluted with CH<sub>2</sub>Cl<sub>2</sub> and water. The

biphasic system was extracted three times with CH<sub>2</sub>Cl<sub>2</sub>, and the combined organic extracts were washed once with 30% aqueous CuSO<sub>4</sub>, dried over Na<sub>2</sub>SO<sub>4</sub>, and concentrated in vacuo. The crude product was purified by column chromatography (1:1 EtOAc:hexanes) to give (5a*R*,10b*S*)-11a-hydroxy-2-(4-methoxybenzyl)-3,3,10b-trimethyl-6-(phenylsulfonyl)-2,3,6,10b,11,11a-hexa-hydro-4*H*-pyrazino[1',2':1,5]pyrrolo[2,3-*b*]indole-1,4(5a*H*)-dione (7 mg, 52 %) as a pale yellow oil. <sup>1</sup>H NMR (500 MHz, CDCl<sub>3</sub>) δ 7.81 (dd, *J* = 1.0, 8.6 Hz, 2H), 7.56 (d, *J* = 8.1 Hz, 1H), 7.52 (t, *J* = 7.5 Hz, 1H), 7.40 (t, *J* = 8.1 Hz, 2H), 7.30 (td, *J* = 1.1, 8.7 Hz, 1H), 7.15 (td, *J* = 0.8, 7.6 Hz, 1H), 7.07 (d, *J* = 7.6 Hz, 1H), 6.97 (d, *J* = 8.6 Hz, 2H), 6.75 (d, *J* = 8.7 Hz, 2H), 6.04 (s, 1H), 4.69 (d, *J* = 15.6 Hz, 1H), 4.38 (d, *J* = 15.6 Hz, 1H), 3.76 (s, 3H), 2.90 (d, *J* = 14.3 Hz, 1H), 2.42 (d, *J* = 14.3 Hz, 1H), 1.54 (s, 3H), 1.47 (s 3 H), 1.06 (s 3 H). <sup>13</sup>C NMR (125 MHz, CDCl<sub>3</sub>) δ 172.2, 167.5, 158.6, 140.0, 138.5, 133.3, 133.1, 128.9, 128.6, 128.3, 128.2, 127.7, 125.9, 123.0, 118.1, 114.0, 86.8, 85.1, 64.8, 55.2, 50.0, 49.4, 45.1, 26.6, 26.3, 25.2. HRMS (ESI-TOF) *m/z* [M + Na]<sup>+</sup> calcd for C<sub>30</sub>H<sub>31</sub>N<sub>3</sub>NaO<sub>6</sub>S 584.1831, found 584.1852.

## VI. References

- (1) Gober, C.; Carroll, P. J.; Joullié, M. M. *Mini Rev. Org. Chem.* **2016**, *13*, 126-142.
- (2) García-Estrada, C.; Ullán, R. V.; Albillos, S. M.; Fernández-Bodega, M. A.; Durek, P.; von Döhren, H.; Martín, J. F. *Chem. Biol.* **2011**, *18*(11), 1499-1512.

- (3) Ries, M. I.; Ali, H.; Lankhorst, P. P.; Hankemeier, T.; Bovenberg, R. A.; Driessen, A. J.; Vreeken, R. J. *J. Biol. Chem.* **2013**, *288*(52), 37289-37295.
- (4) Ali, H.; Ries, M. I.; Nijland, J. G.; Lankhorst, P. P.; Hankemeier, T.; Bovenberg, R. A.; Vreeken, R. J.; Driessen, A. J. *PLoS ONE* **2013**, *8*(6), e65328.
- (5) Fedoreyev, S. A.; Ilyin, S. G.; Utkina, N. K.; Maximov, O. B.; Reshetnyak, M. V. *Tetrahedron* **1989**, *45*(11), 3487-3492.
- (6) Reshetilova, T. A.; Vinokurova, N. G.; Khmelenina, V. N.; Kozlovskii, A. G. *Microbiology* **1995**, *64*(1), 27-29.
- (7) Overy, D. P.; Nielsen, K. F.; Smedsgaard, J. *J. Chem. Ecol.* **2005**, *31*(10), 2373-2390.
- (8) Nagel, D. W.; Pachler, K. G. R.; Steyn, P. S.; Wessels, P. L.; Gafner, G.; Kruger, G. J. *J. Chem. Soc. Chem. Commun.* **1974**(24), 1021.
- (9) Koizumi, Y.; Arai, M.; Tomoda, H.; Ōmura, S. *Biochim. Biophys. Acta.* **2004**, *1693*(1), 47-55.
- (10) Zheng, C. J.; Sohn, M.-J.; Lee, S.; Kim, W.-G. *PLoS ONE* **2013**, *8*(11), e78922.
- (11) Du, L.; Li, D.; Zhu, T.; Cai, S.; Wang, F.; Xiao, X.; Gu, Q. *Tetrahedron* **2009**, *65*(5), 1033-1039.

- (12) Mady, M. S.; Mohyeldin, M. M.; Ebrahim, H. Y.; Elsayed, H. E.; Houssen, W. E.; Haggag, E. G.; Soliman, R. F.; El Sayed, K. A. *Bioorg. Med. Chem.* **2015**, *24*(2), 113-122.
- (13) Felser, B.; Preiss, D. U., Novel fibrinolysis inhibitors and medical application thereof. DE 102011013326, 2011.
- (14) Han, Z.; Sun, J.; Zhang, Y.; He, F.; Xu, Y.; Matsumura, K.; He, L. S.; Qiu, J. W.; Qi, S. H.; Qian, P. Y. *J. Proteome Res.* **2013**, *12*(5), 2090-2100.
- (15) Qi, S.; He, F., Indole alkaloid in the preparation of marine antifouling coating. CN 102757677, 2012.
- (16) He, F.; Han, Z.; Peng, J.; Qian, P. Y.; Qi, S. H. *Nat. Prod. Commun.* **2013**, *8*(3), 329-332.
- (17) Koolen, H. H. F.; Soares, E. R.; da Silva, F. M. A.; de Almeida, R. A.; de Souza, A. D. L.; de Medeiros, L. S.; Filho, E. R.; de Souza, A. Q. L. *Quim. Nova* **2012**, *35*(4), 771-774.
- (18) Horino, T.; Tokita, A.; Oshima, T., Photochromic material. 0102775, 2013.
- (19) Schmidt, F. G.; Spange, S.; Polenz, I., Basen/isocyanat-initiierte polymerisation an oxidischen oberflächen. 117379, 2013.
- (20) Stöber, W.; Fink, A. *J. Colloid Interface Sci.* **1968**, *26*, 62-69.

- (21) Rigby, J. H.; Wang, Z. *Org. Lett.* **2002**, 4(24), 4289-4291.
- (22) Feldman, K. S.; Fodor, M. D. *J. Am. Chem. Soc.* **2008**, 130, 14964-14965.
- (23) Feldman, K. S.; Fodor, M. D. *J. Org. Chem.* **2009**, 74, 3449-3461.
- (24) Feldman, K. S.; Fodor, M. D.; Skoumbourdis, A. P. *Synthesis-Stuttgart* **2009**, 18, 3162-3173.
- (25) Feldman, K. S.; Fodor, M. D. *J. Am. Chem. Soc.* **2006**, 130, 14964-14965.
- (26) Romano, C.; de la Cuesta, E.; Avendaño, C. *J. Org. Chem.* **1991**, 56(1), 74-78.
- (27) Ideguchi, T.; Yamada, T.; Shirahata, T.; Hirose, T.; Sugawara, A.; Kobayashi, Y.; Omura, S.; Sunazuka, T. *J. Am. Chem. Soc.* **2013**, 135(34), 12568-12571.
- (28) Yamada, T.; Ideguchi-Matsushita, T.; Hirose, T.; Shirahata, T.; Hokari, R.; Ishiyama, A.; Iwatsuki, M.; Sugawara, A.; Kobayashi, Y.; Otaguro, K.; Ōmura, S.; Sunazuka, T. *Chem. Eur. J.* **2015**, 21(33), 11855-11864.
- (29) Sunazuka, T.; Shirahata, T.; Tsuchiya, S.; Hirose, T.; Mori, R.; Harigaya, Y.; Kuwajima, I.; Ōmura, S. *Org. Lett.* **2005**, 7(5), 941-943.
- (30) Kim, J.; Ashenhurst, J. A.; Movassaghi, M. *Science* **2009**, 324, 238-241.
- (31) Kim, J.; Movassaghi, M. *J. Am. Chem. Soc.* **2010**, 132, 14376-14378.

- (32) Boyer, N.; Movassaghi, M. *Chem. Sci.* **2012**, *3*, 1798-1803.
- (33) Coste, A.; Kim, J.; Adams, T. C.; Movassaghi, M. *Chem. Sci.* **2013**, *4*(8), 3191-3197.
- (34) Adams, T. C.; Payette, J. N.; Cheah, J. H.; Movassaghi, M. *Org. Lett.* **2015**, *17*, 4268-4271.
- (35) Iwasa, E.; Hamashima, Y.; Fujishiro, S.; Higuchi, E.; Ito, A.; Yoshida, M.; Sodeoka, M. *J. Am. Chem. Soc.* **2010**, *132*, 4078-4079.
- (36) Iwasa, E.; Hamashima, Y.; Fujishiro, S.; Hashizume, D.; Sodeoka, M. *Tetrahedron* **2011**, *67*, 6587-6599.
- (37) Allan, K. M.; Kobayashi, K.; Rawal, V. H. *J. Am. Chem. Soc.* **2012**, *134*(3), 1392-1395.
- (38) Beshore, D. C.; Smith, A. B., III. *J. Am. Chem. Soc.* **2008**, *130*, 13778-13789.
- (39) Depew, K. M.; Marsden, S. P.; Zatorska, D.; Zatorski, A.; Bornmann, W. G.; Danishefsky, S. J. *J. Am. Chem. Soc.* **1999**, *121*, 11953-11963.
- (40) Danishefsky, S. J.; Depew, K. M.; Marsden, S. P.; Bornmann, W. G.; Chou, T.-C.; Schkeryantz, J.; Zatorski, A., Analogues of N-Acetylardeemin, Method of Preparation and Uses Thereof. WO 018215, 1997.

- (41) Schmidt, U.; Lieberknecht, A.; Schanbacher, U.; Beuttler, T.; Wild, J. *Angew. Chem. Int. Ed.* **1982**, 21(10), 776-777.
- (42) Repka, L. M.; Ni, J.; Reisman, S. E. *J. Am. Chem. Soc.* **2010**, 132, 14418-14420.
- (43) Ni, J.; Wang, H.; Reisman, S. E. *Tetrahedron* **2013**, 69(27-28), 5622-5633.
- (44) Wang, H.; Reisman, S. E. *Angew. Chem. Int. Ed.* **2014**, 53(24), 6206-6210.
- (45) Zacuto, M. J.; Xu, F. *J. Org. Chem.* **2007**, 72, 6298-6300.
- (46) Rauk, A.; Yu, D.; Taylor, J.; Shustov, G. V.; Block, D. A.; Armstrong, D. A. *Biochemistry* **1999**, 38, 9089-9096.
- (47) Brocks, J. J.; Welle, F. M.; Beckhaus, H.-D.; Ruchardt, C. *Tetrahedron Lett.* **1997**, 38(44), 7721-7724.
- (48) Brocks, J. J.; Beckhaus, H.-D.; Beckwith, A. L. J.; Ruchardt, C. *J. Org. Chem.* **1998**, 63, 1935-1943.
- (49) Azuma, H.; Okano, K.; Fukuyama, T.; Tokuyama, H. *Org. Synth.* **2011**, 88, 152-161.
- (50) Wojtas, K. P.; Lu, J.-Y.; Krahn, D.; Arndt, H.-D. *Chem. Asian J.* **2016**, 11(20), 2859-2862.



(51) Simonin, C.; Awale, M.; Brand, M.; van Deursen, R.; Schwartz, J.; Fine, M.; Kovacs, G.; Häfliger, P.; Gyimesi, G.; Sithampari, A.; Charles, R.-P.; Hediger, M. A.; Reymond, J.-L. *Angew. Chem. Int. Ed.* **2015**, *54*, 14748-14752.

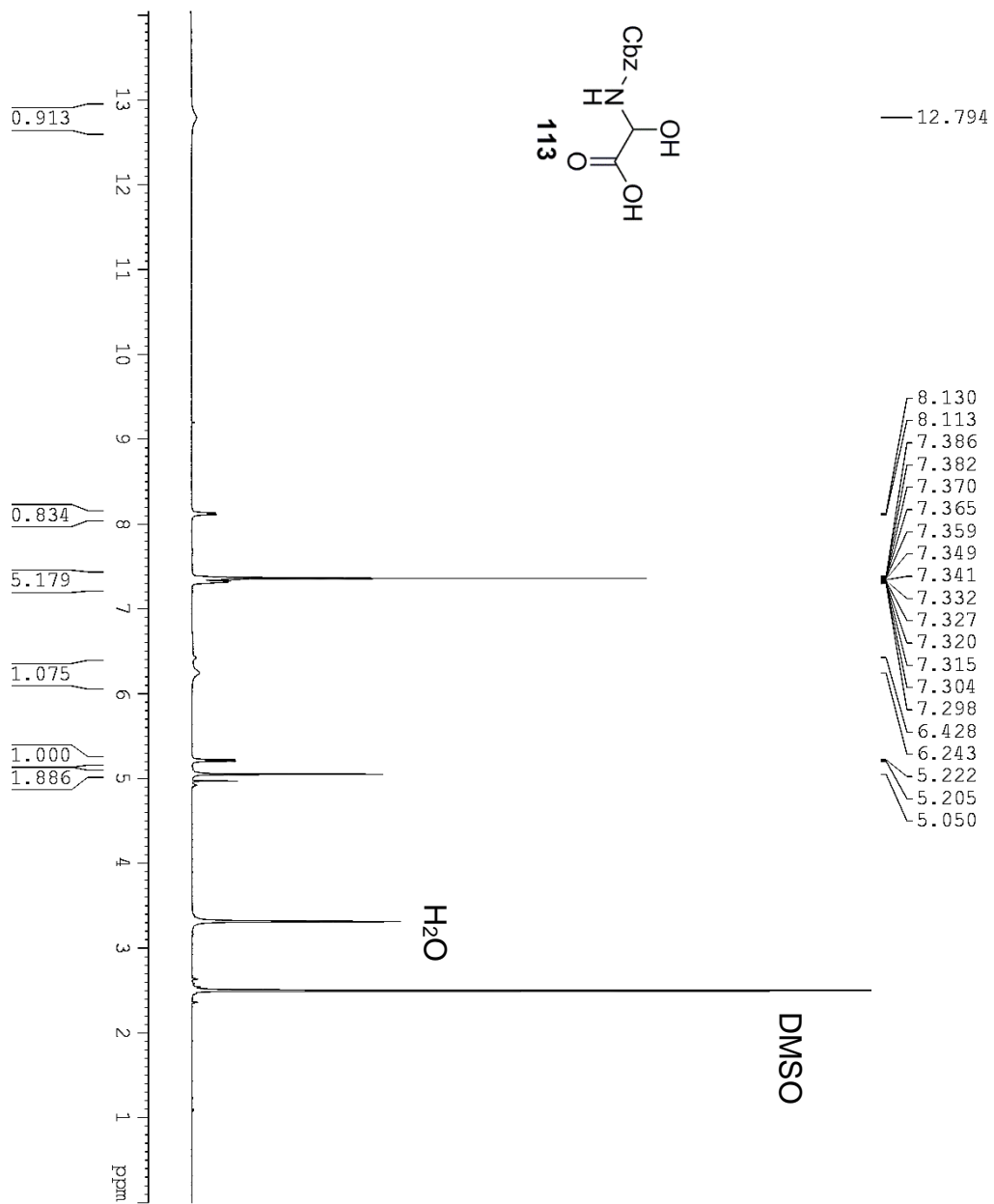
(52) Turner, H. M.; Patel, J.; Niljianskul, N.; Chong, J. M. *Org. Lett.* **2011**, *13*(21), 5796-5799.

(53) Balamurugan, D.; Muraleedharan, K. M. *Chem. Eur. J.* **2012**, *18*, 9516-9520.

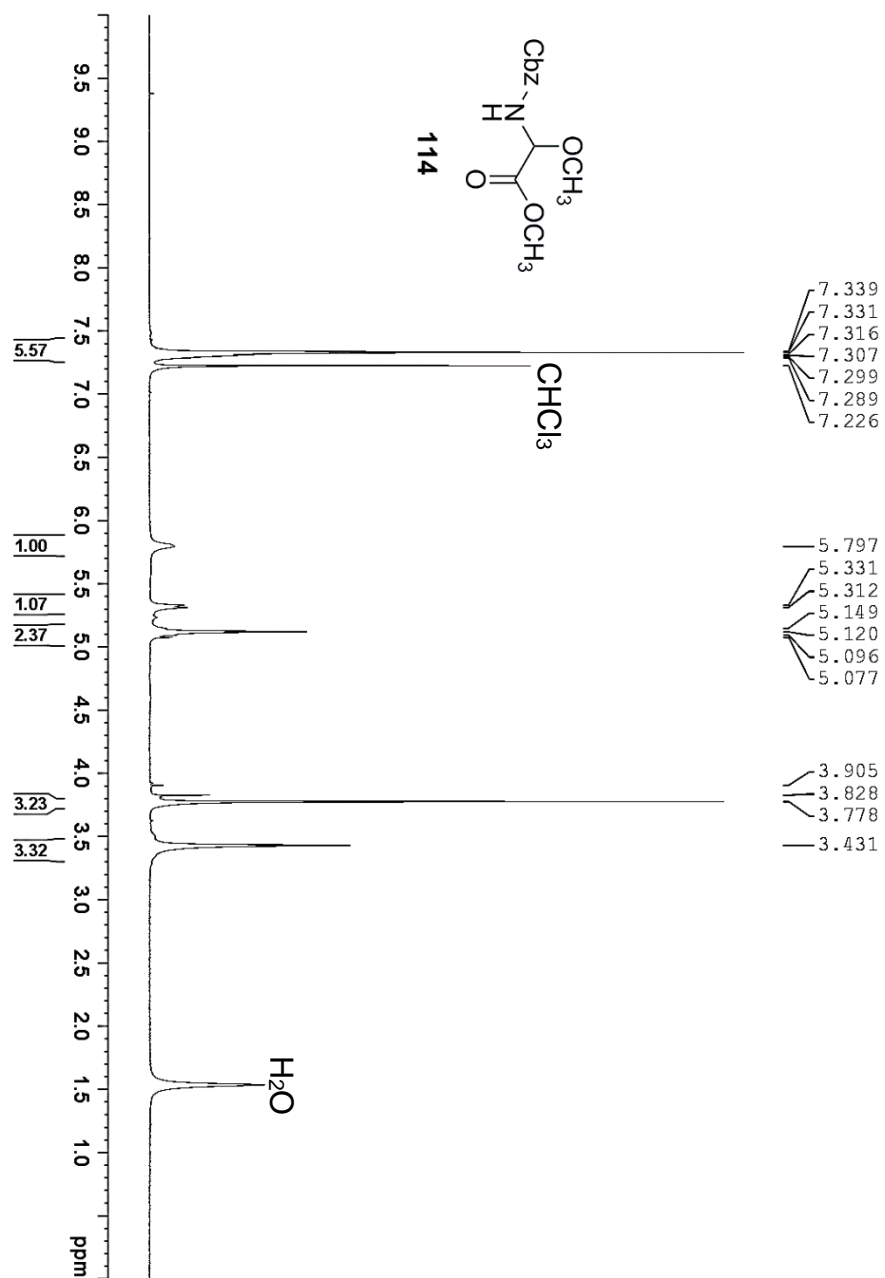
#### Appendix 4A: Description of Human Cell Lines

<b>Cell line</b>	<b>Tissue/cell type</b>	<b>Disease</b>
A-549	Lung	Carcinoma
BEL-7402	Liver	Hepatocellular carcinoma
HL-60	Promyeloblast	Acute promyelocytic leukemia
Jurkat	T lymphocyte	Acute T cell leukemia
MOLT-4	T lymphoblast	Acute lymphoblastic leukemia

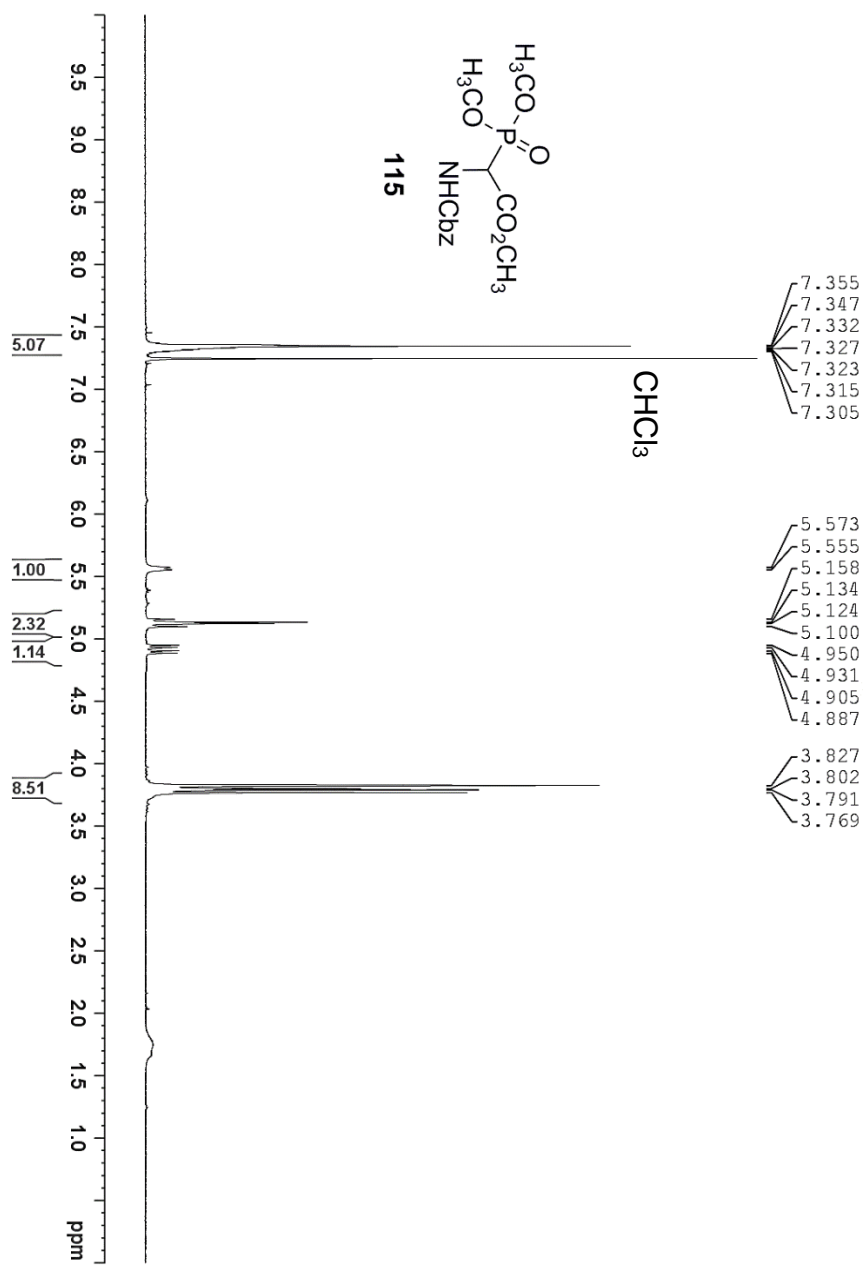
## **Appendix 4B: Spectra Relevant to Chapter 4**



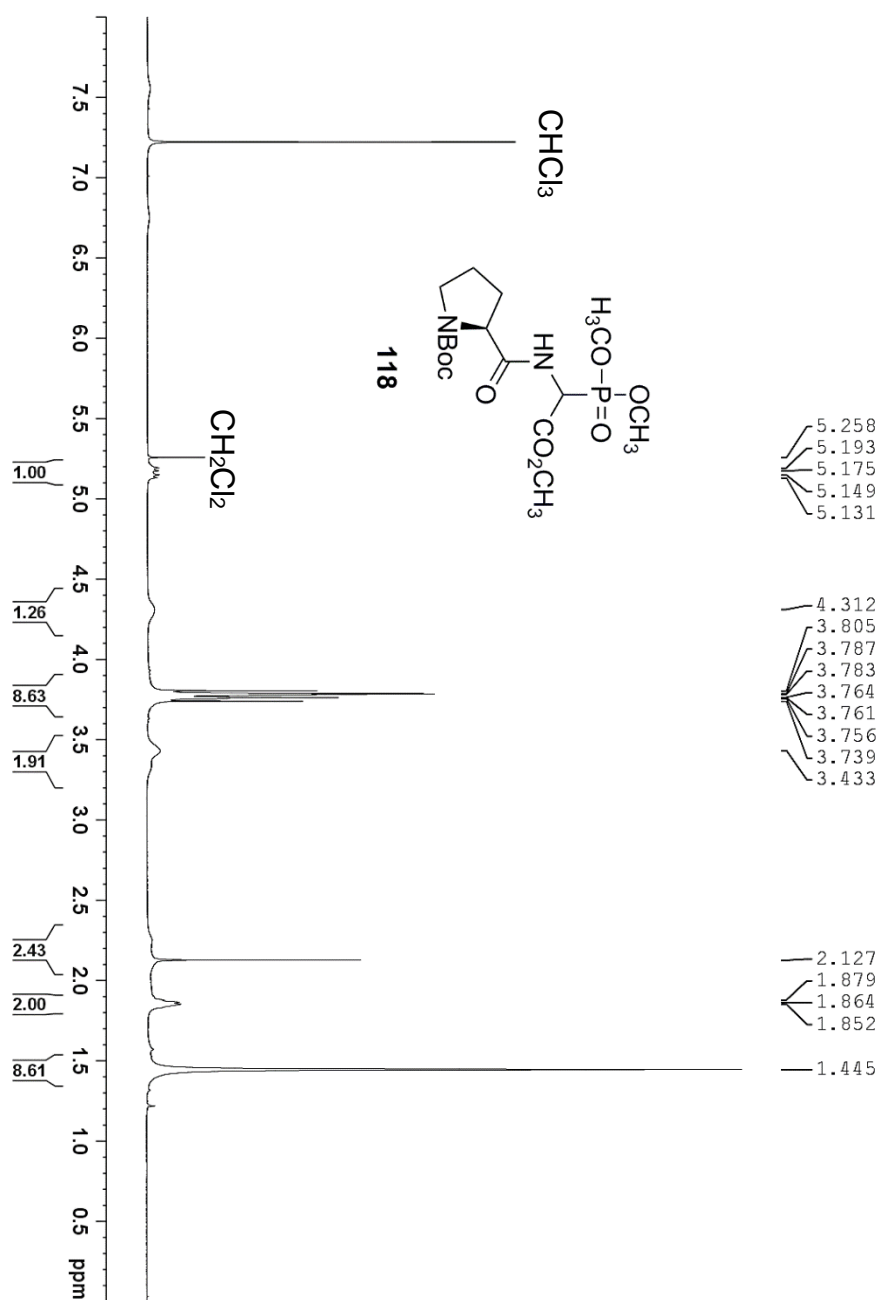
Supplementary Figure 4.1: <sup>1</sup>H NMR (500 MHz, DMSO-*d*<sub>6</sub>) Spectrum of 113



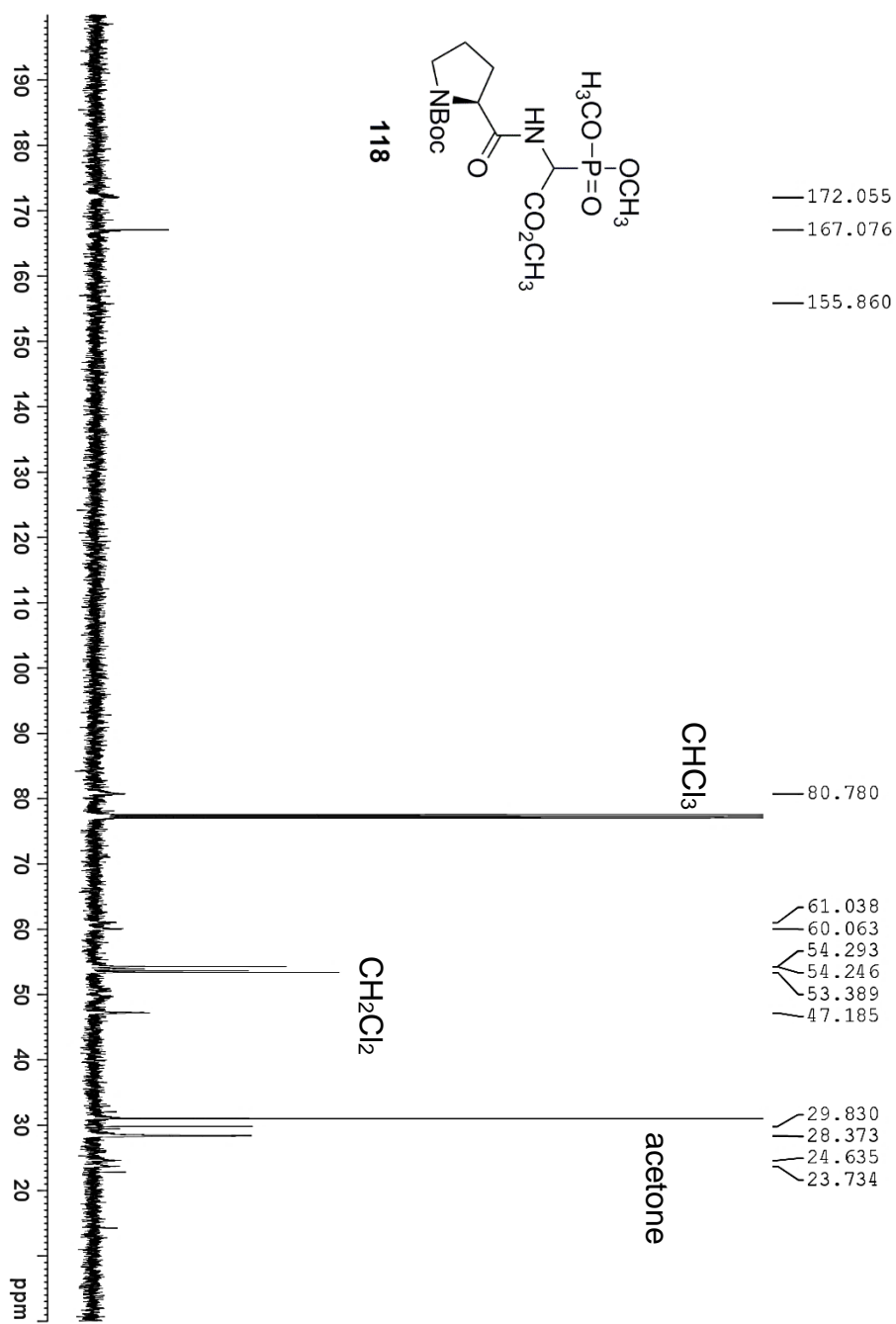
Supplementary Figure 4.2: <sup>1</sup>H NMR (500 MHz, CDCl<sub>3</sub>) Spectrum of 114



**Supplementary Figure 4.3:**  $^1\text{H}$  NMR (500 MHz,  $\text{CDCl}_3$ ) Spectrum of **115**

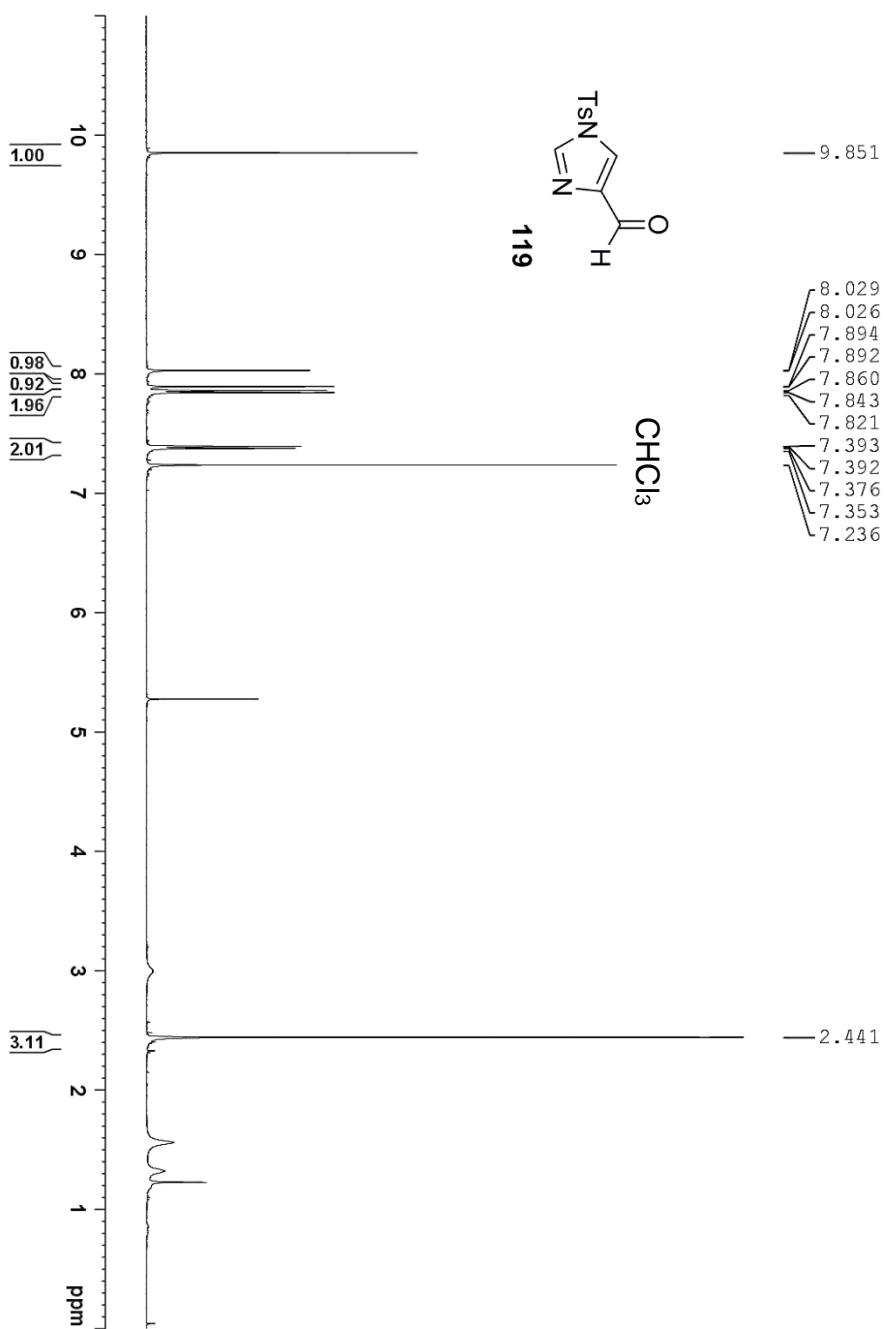


**Supplementary Figure 4.4:**  $^1\text{H NMR}$  (500 MHz,  $\text{CDCl}_3$ ) Spectrum of **118**

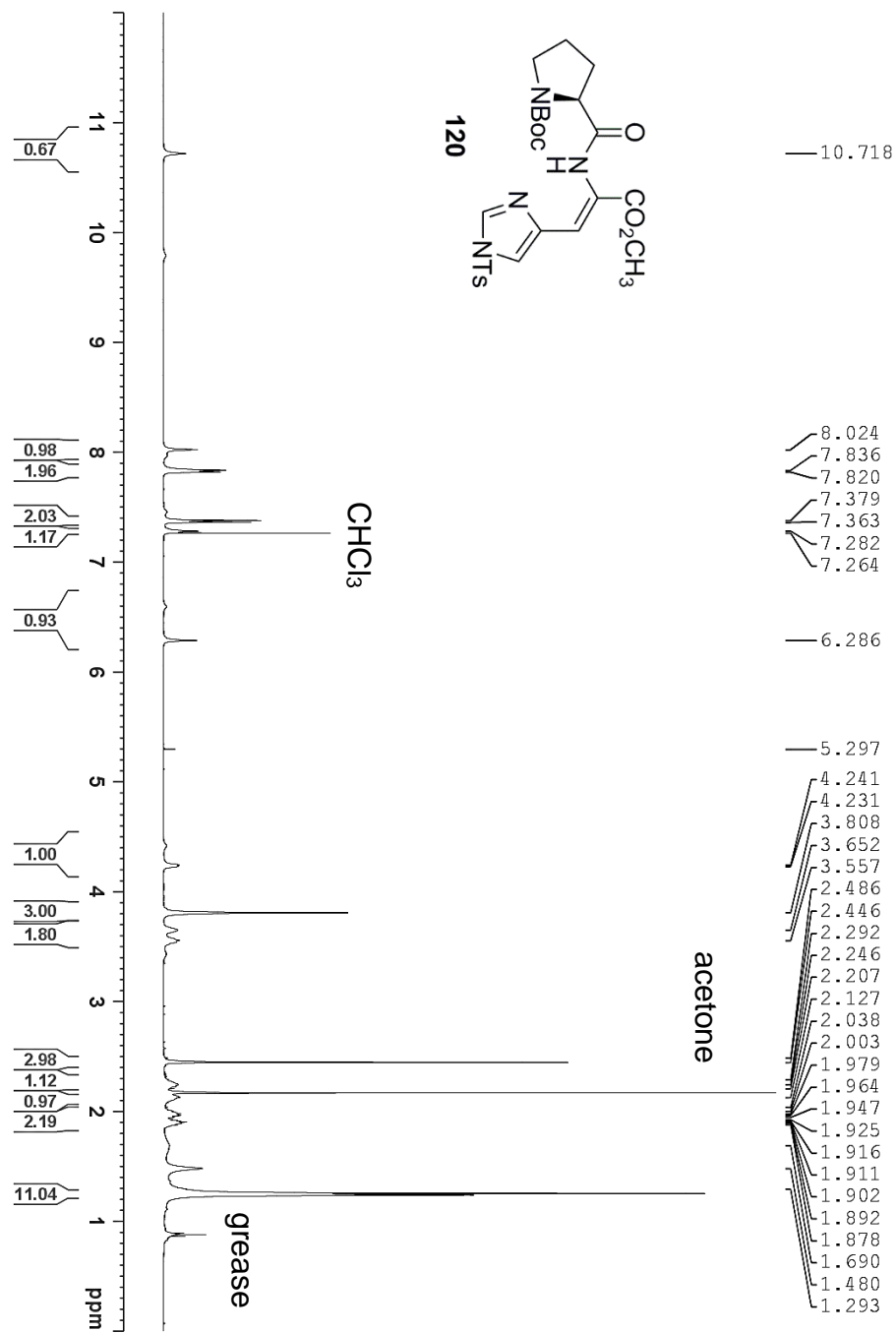


Supplementary Figure 4.5: <sup>13</sup>C NMR (125 MHz, CDCl<sub>3</sub>) Spectrum of **118**

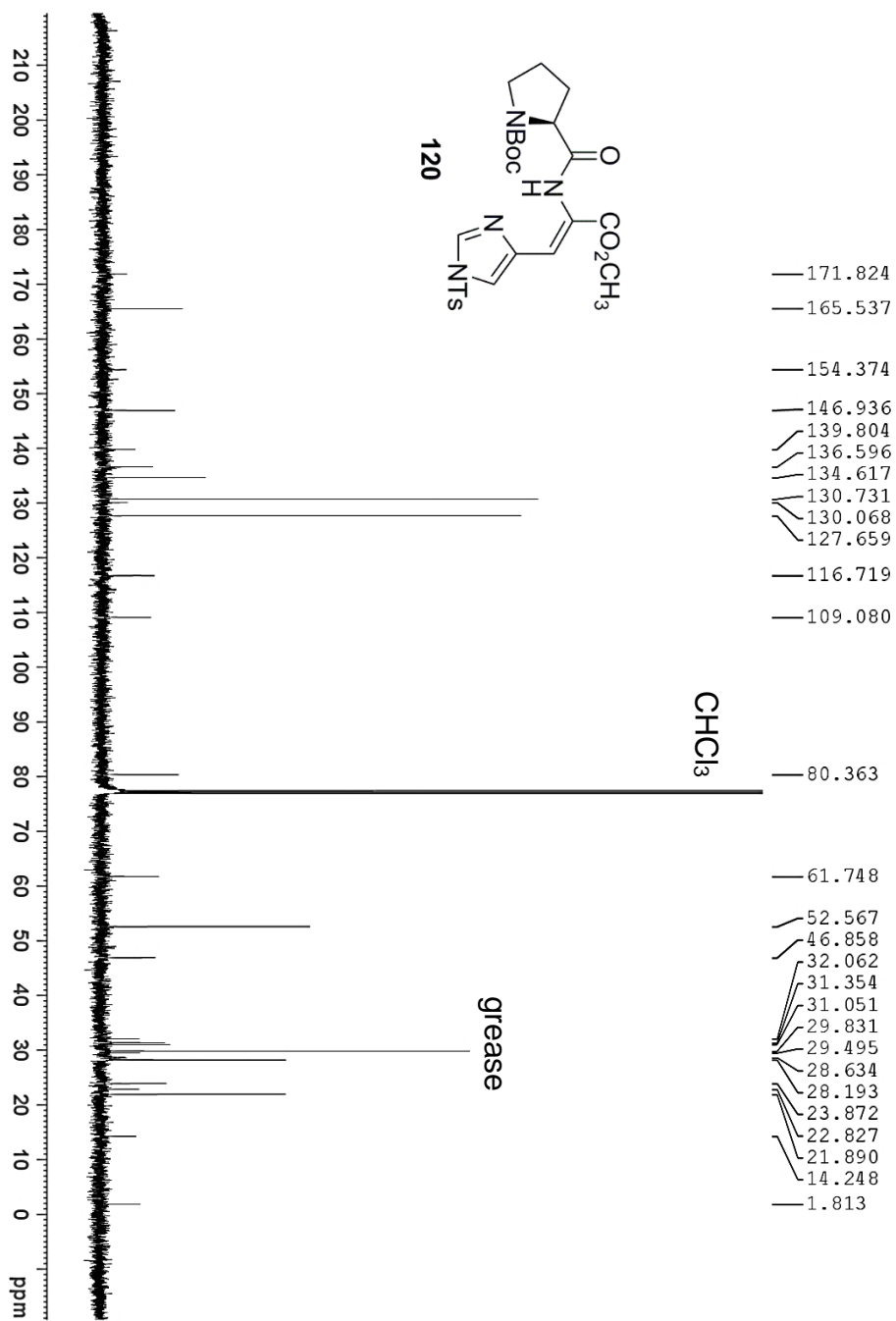




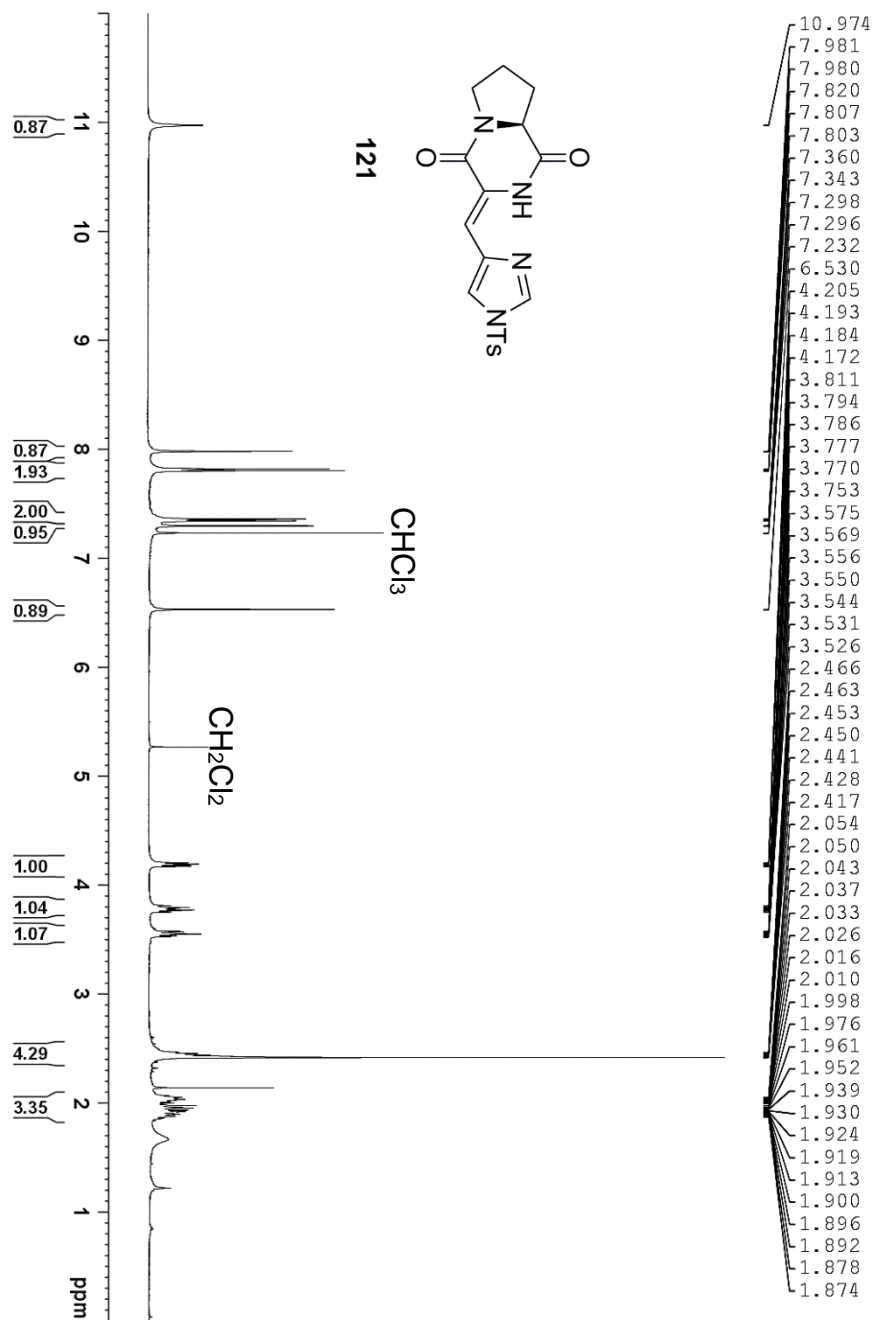
Supplementary Figure 4.6:  $^1\text{H}$  NMR (500 MHz,  $\text{CDCl}_3$ ) Spectrum of **119**



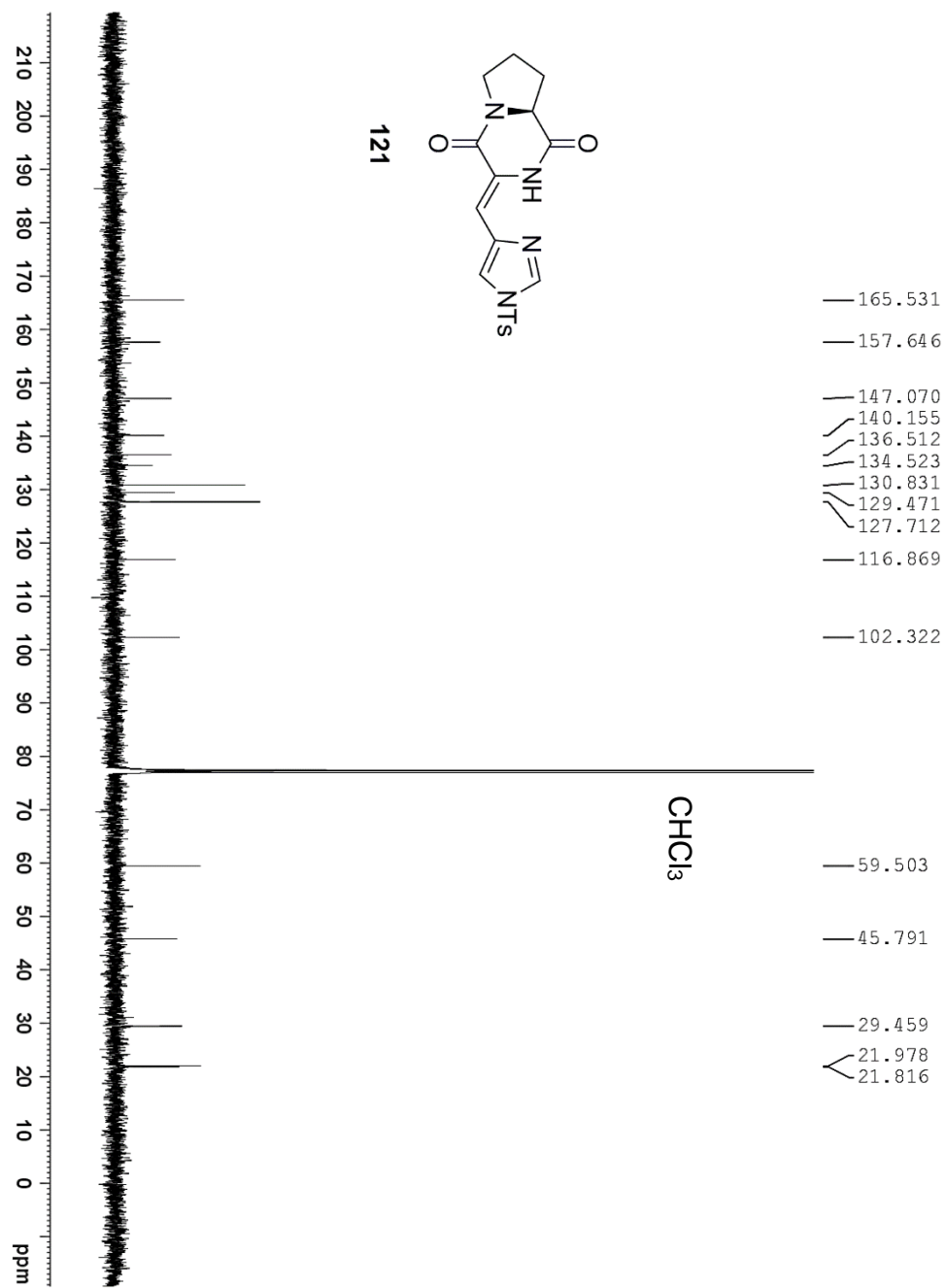
**Supplementary Figure 4.7:** <sup>1</sup>H NMR (500 MHz, CDCl<sub>3</sub>) Spectrum of **120**



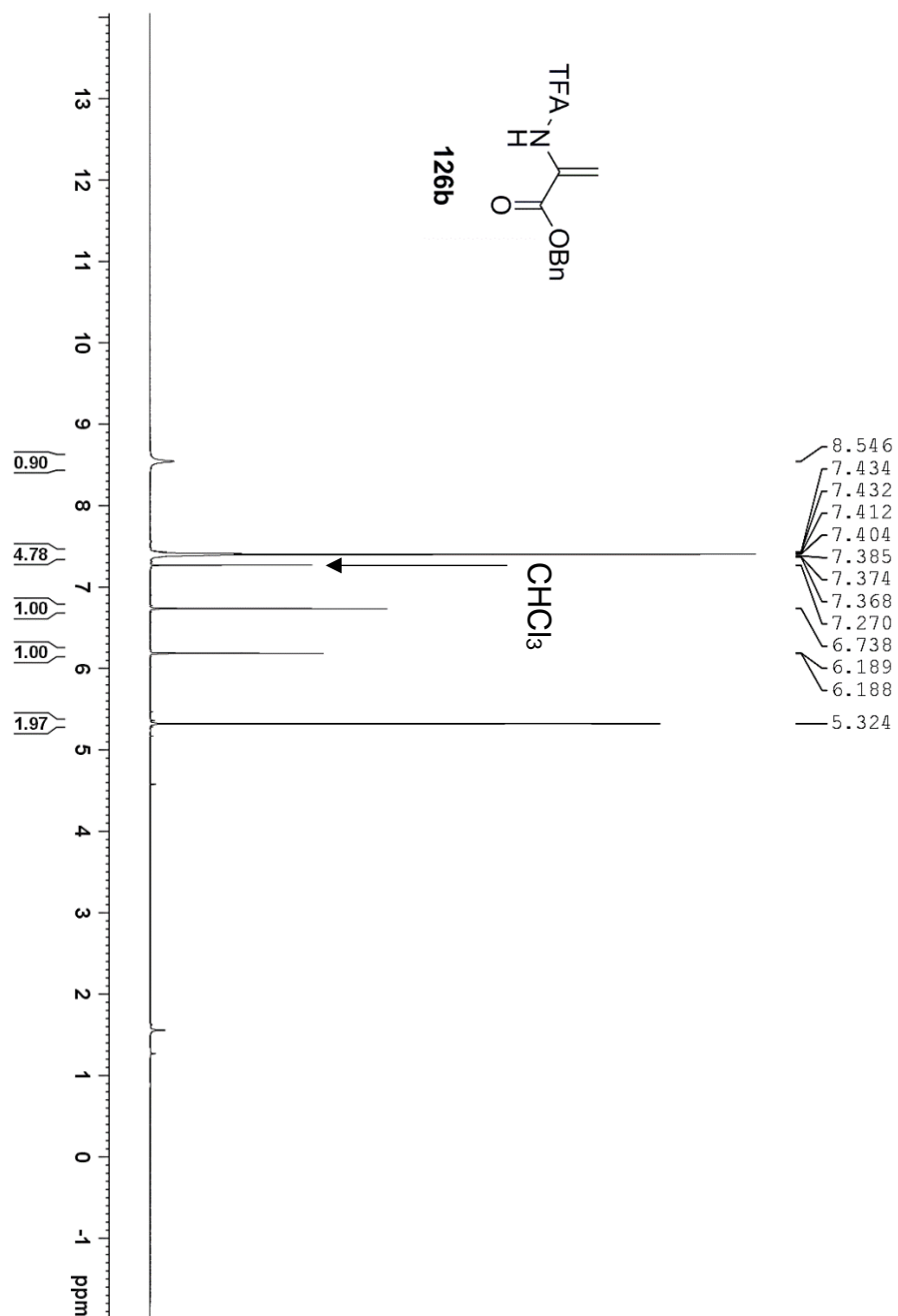
Supplementary Figure 4.8: <sup>13</sup>C NMR (125 MHz, CDCl<sub>3</sub>) Spectrum of **120**



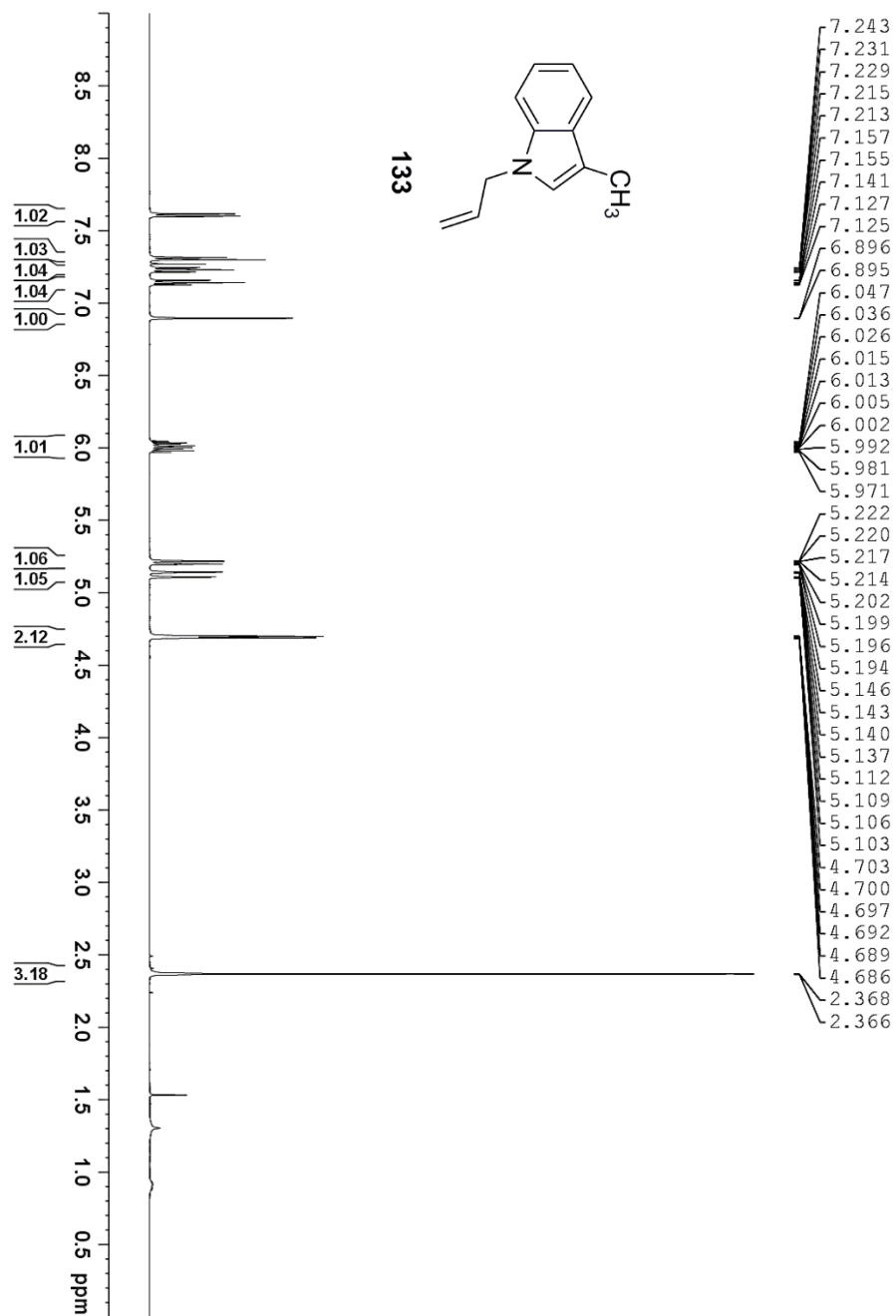
Supplementary Figure 4.9: <sup>1</sup>H NMR (500 MHz, CDCl<sub>3</sub>) Spectrum of 121



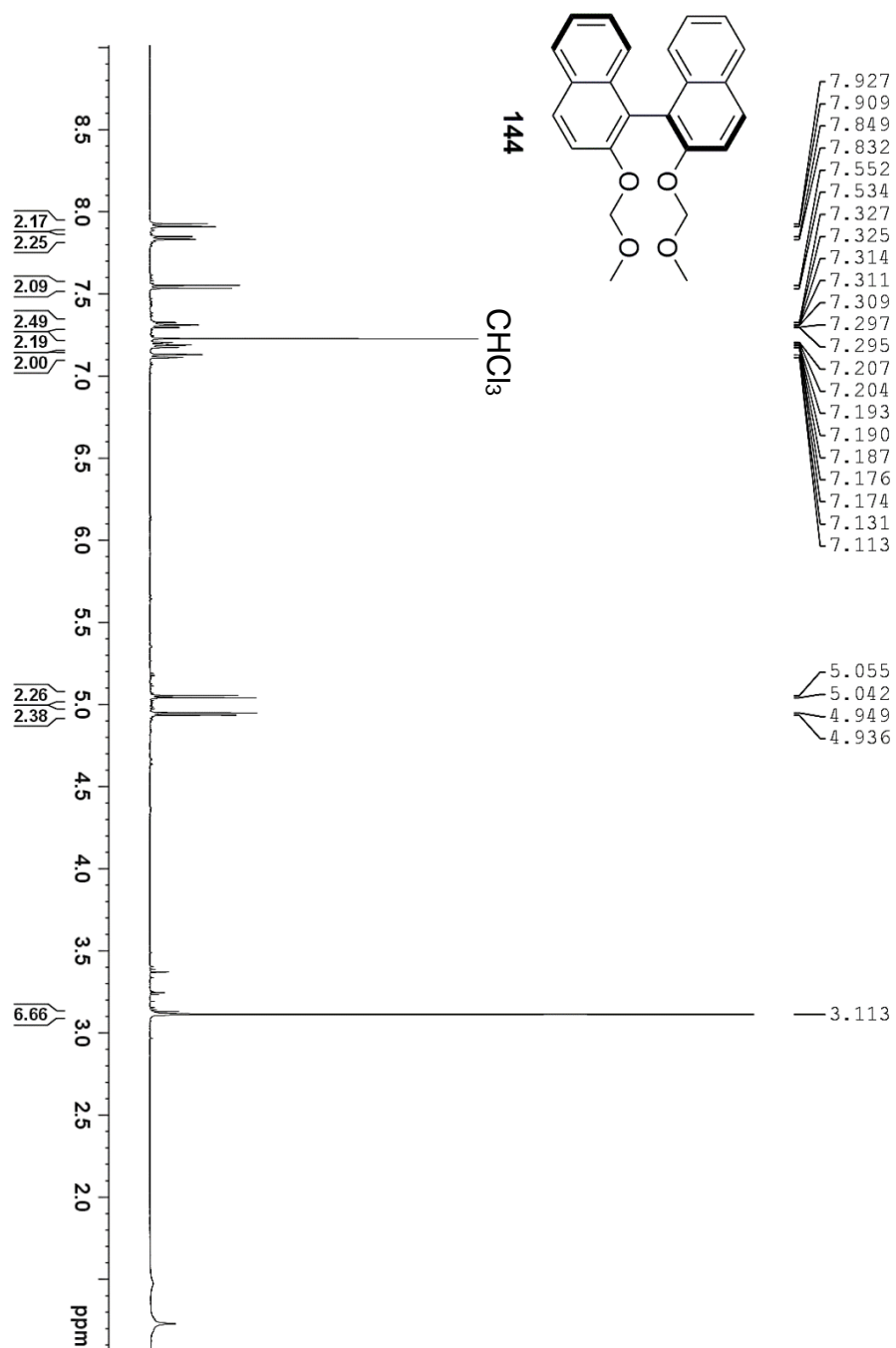
**Supplementary Figure 4.10:**  $^{13}\text{C}$  NMR (125 MHz,  $\text{CDCl}_3$ ) Spectrum of **121**



Supplementary Figure 4.11:  $^1\text{H}$  NMR (500 MHz,  $\text{CDCl}_3$ ) Spectrum of 126b

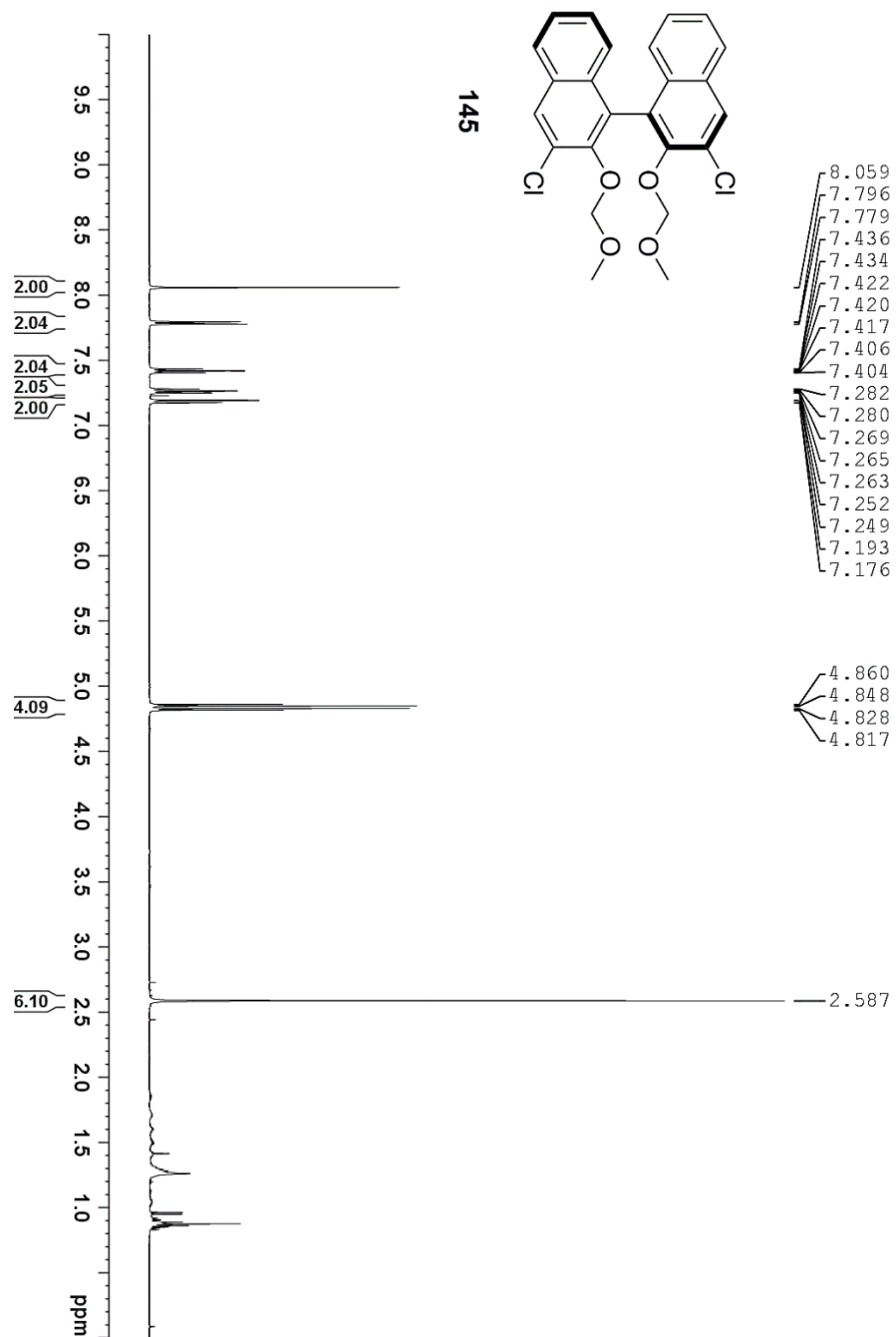


**Supplementary Figure 4.12: <sup>1</sup>H NMR (500 MHz, CDCl<sub>3</sub>) Spectrum of 133**

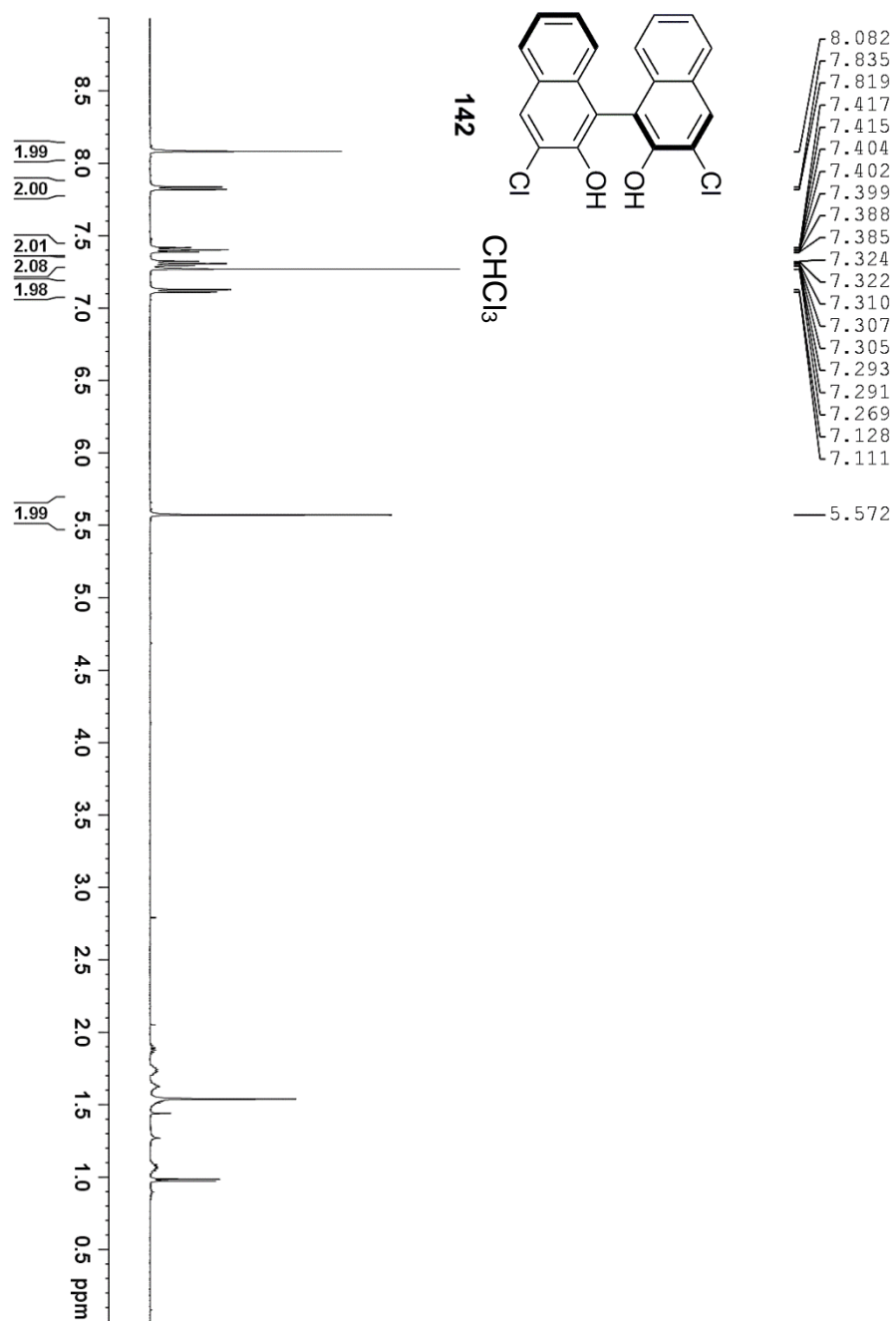


Supplementary Figure 4.13:  $^1\text{H}$  NMR (500 MHz,  $\text{CDCl}_3$ ) Spectrum of **144**

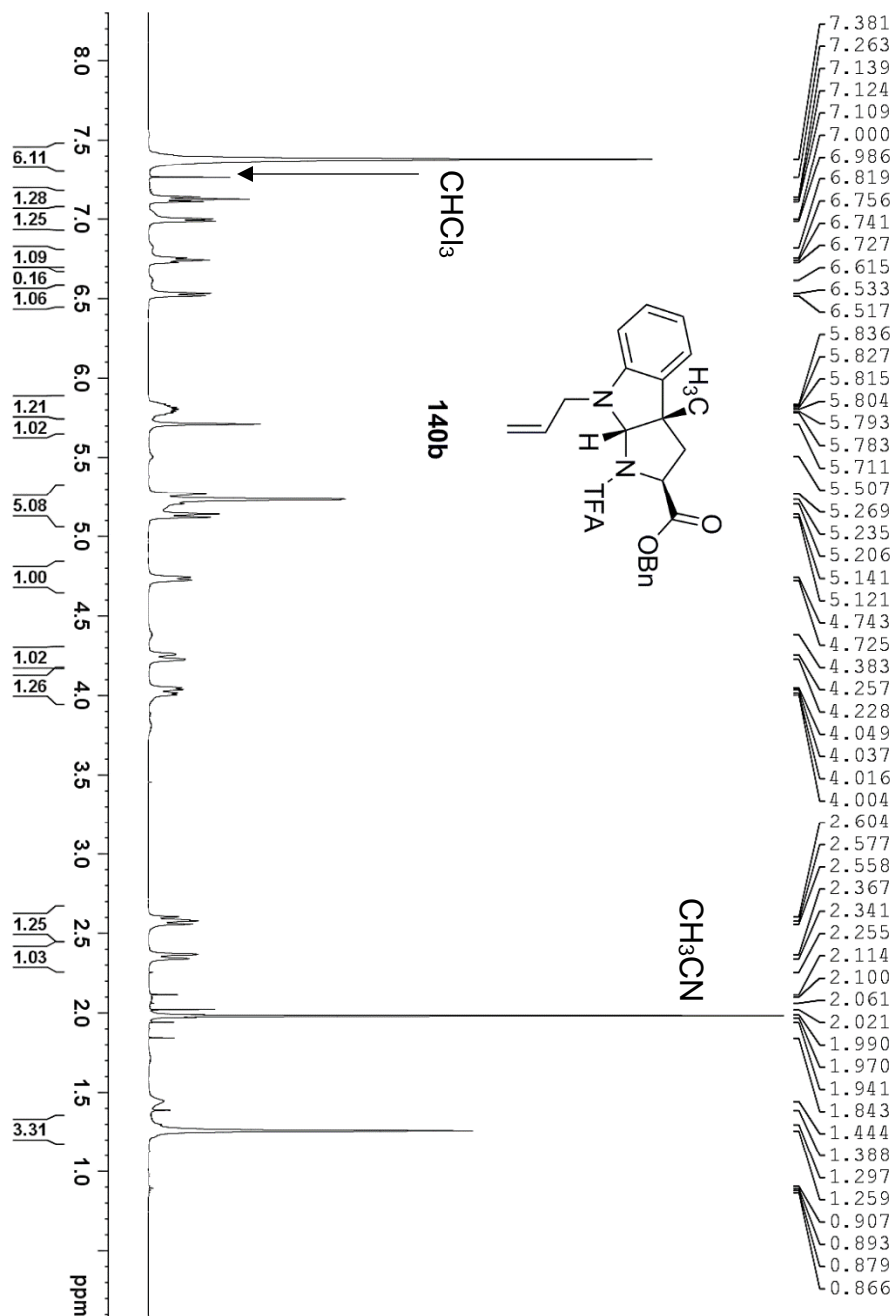




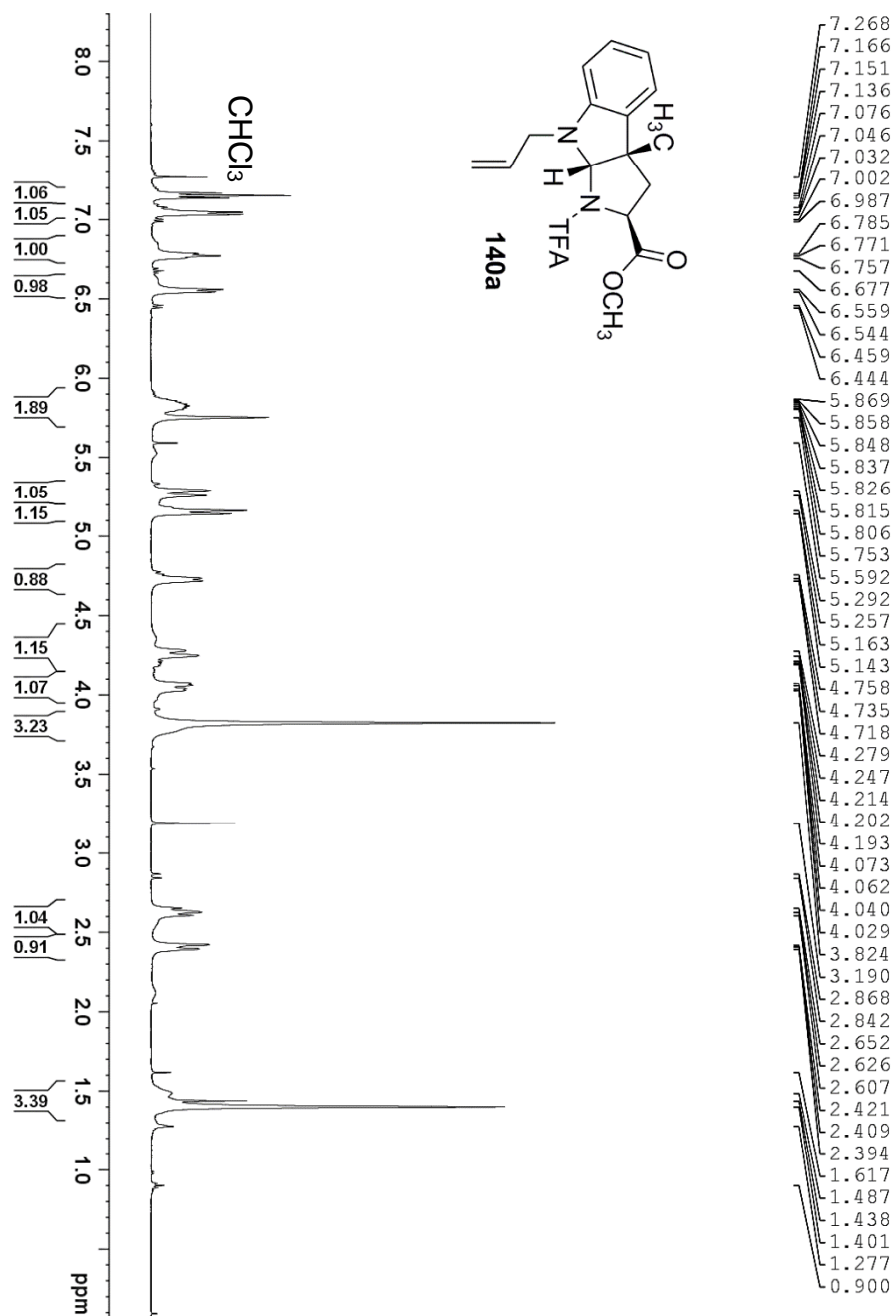
Supplementary Figure 4.14:  $^1\text{H}$  NMR (500 MHz,  $\text{CDCl}_3$ ) Spectrum of 145



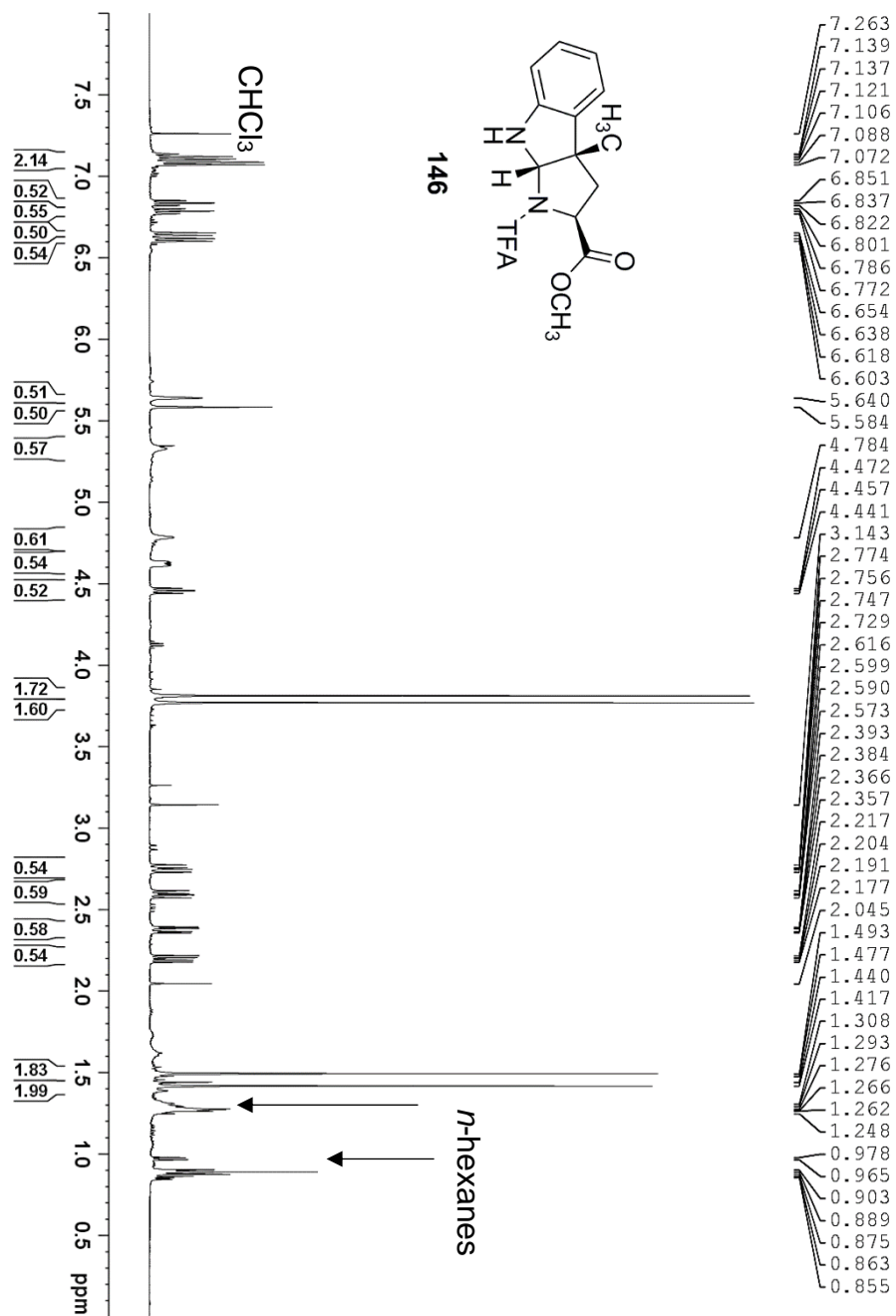
Supplementary Figure 4.15:  $^1\text{H}$  NMR (500 MHz,  $\text{CDCl}_3$ ) Spectrum of 142



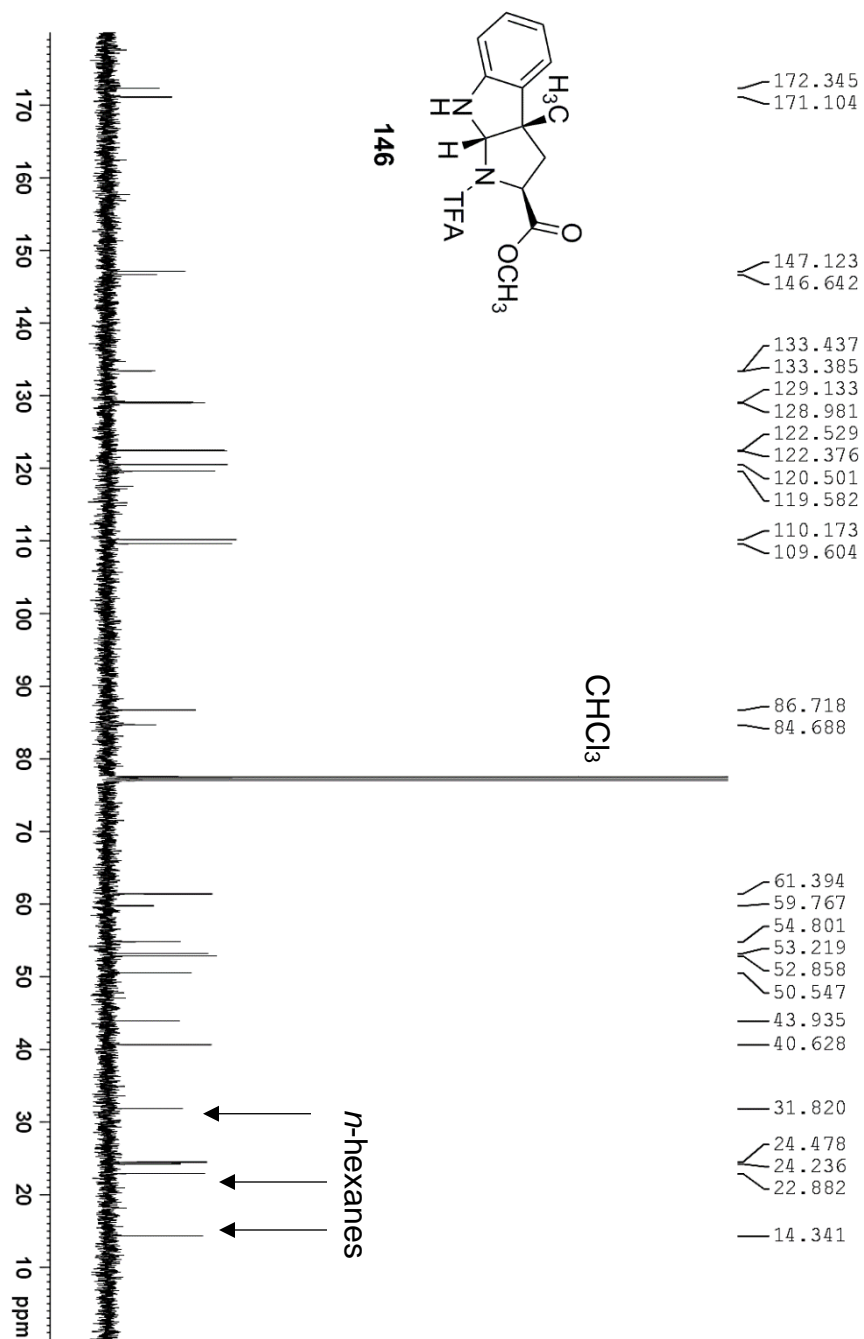
Supplementary Figure 4.16:  $^1\text{H}$  NMR (500 MHz,  $\text{CDCl}_3$ ) Spectrum of **140b**



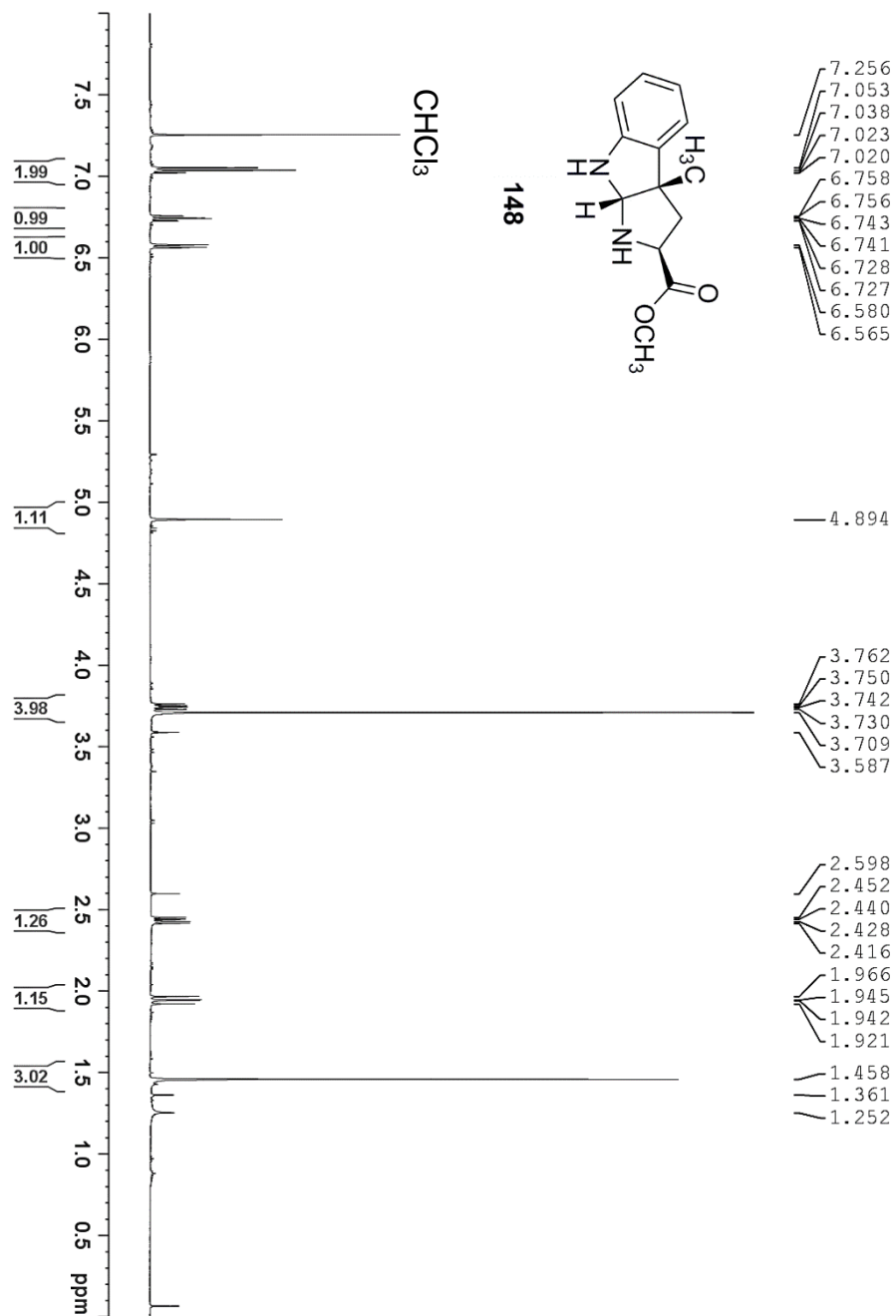
Supplementary Figure 4.17: <sup>1</sup>H NMR (500 MHz, CDCl<sub>3</sub>) Spectrum of 140a



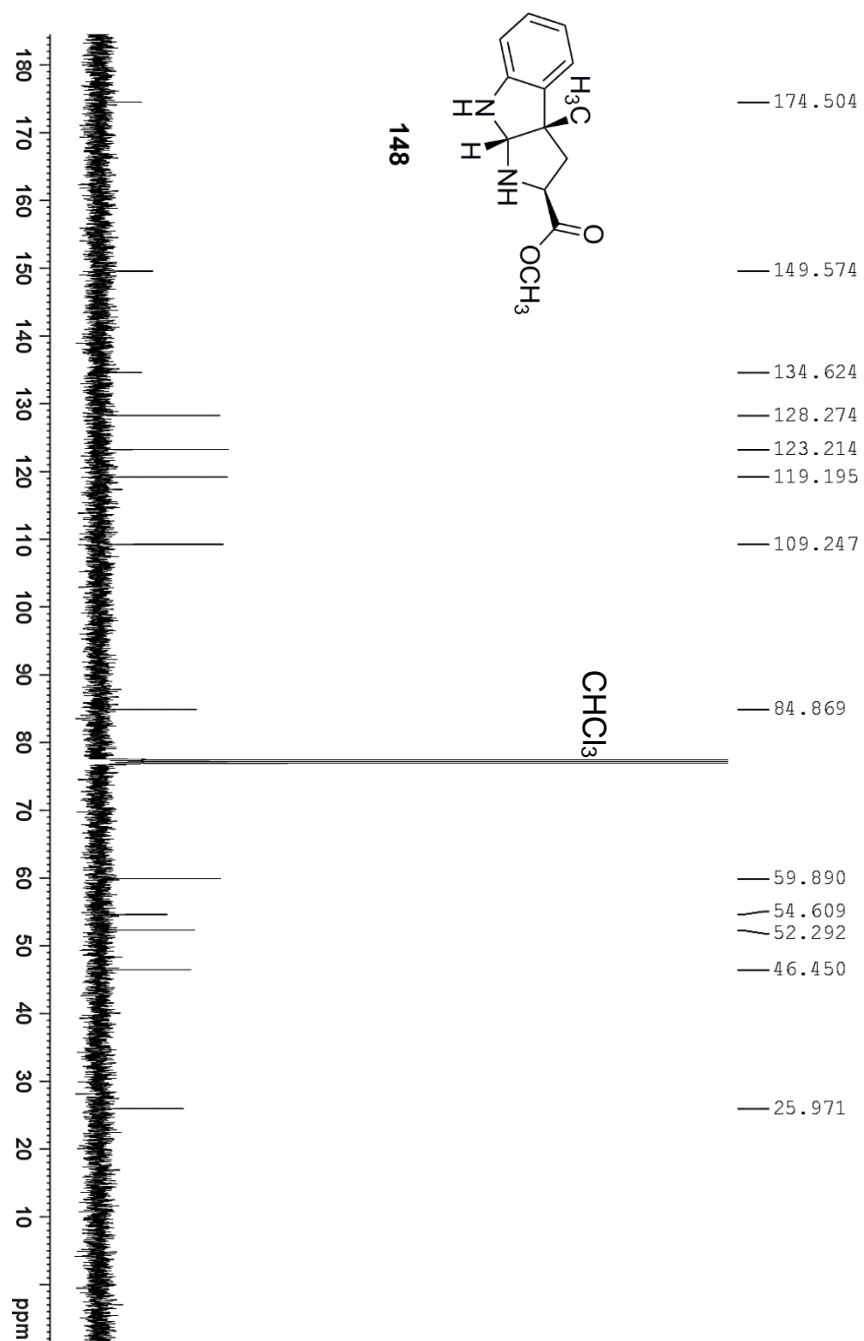
Supplementary Figure 4.18: <sup>1</sup>H NMR (500 MHz, CDCl<sub>3</sub>) Spectrum of **146**



Supplementary Figure 4.19: <sup>13</sup>C NMR (125 MHz, CDCl<sub>3</sub>) Spectrum of **146**

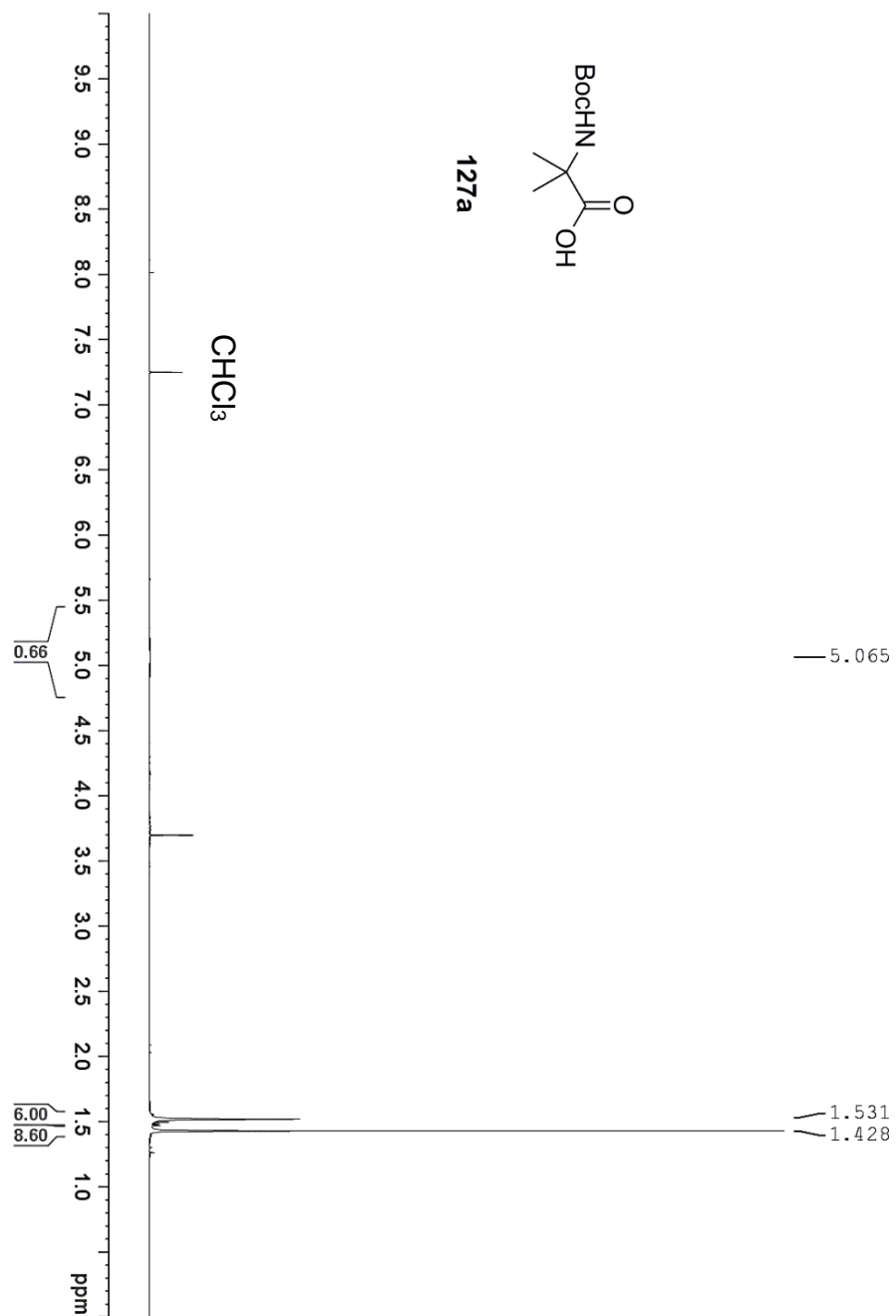


**Supplementary Figure 4.20:**  $^1\text{H}$  NMR (500 MHz,  $\text{CDCl}_3$ ) Spectrum of **148**

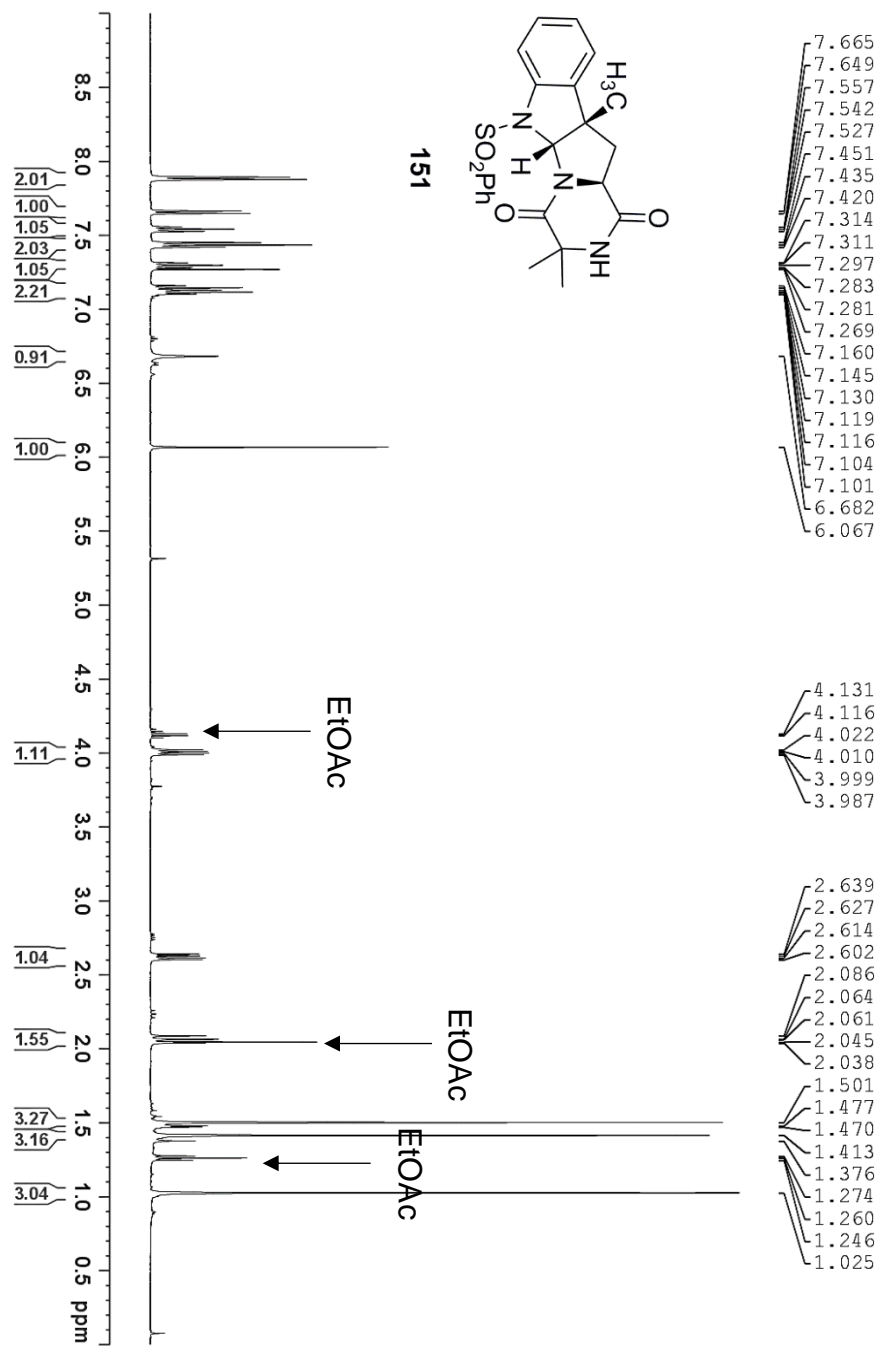


Supplementary Figure 4.21:  $^{13}\text{C}$  NMR (125 MHz,  $\text{CDCl}_3$ ) Spectrum of 148

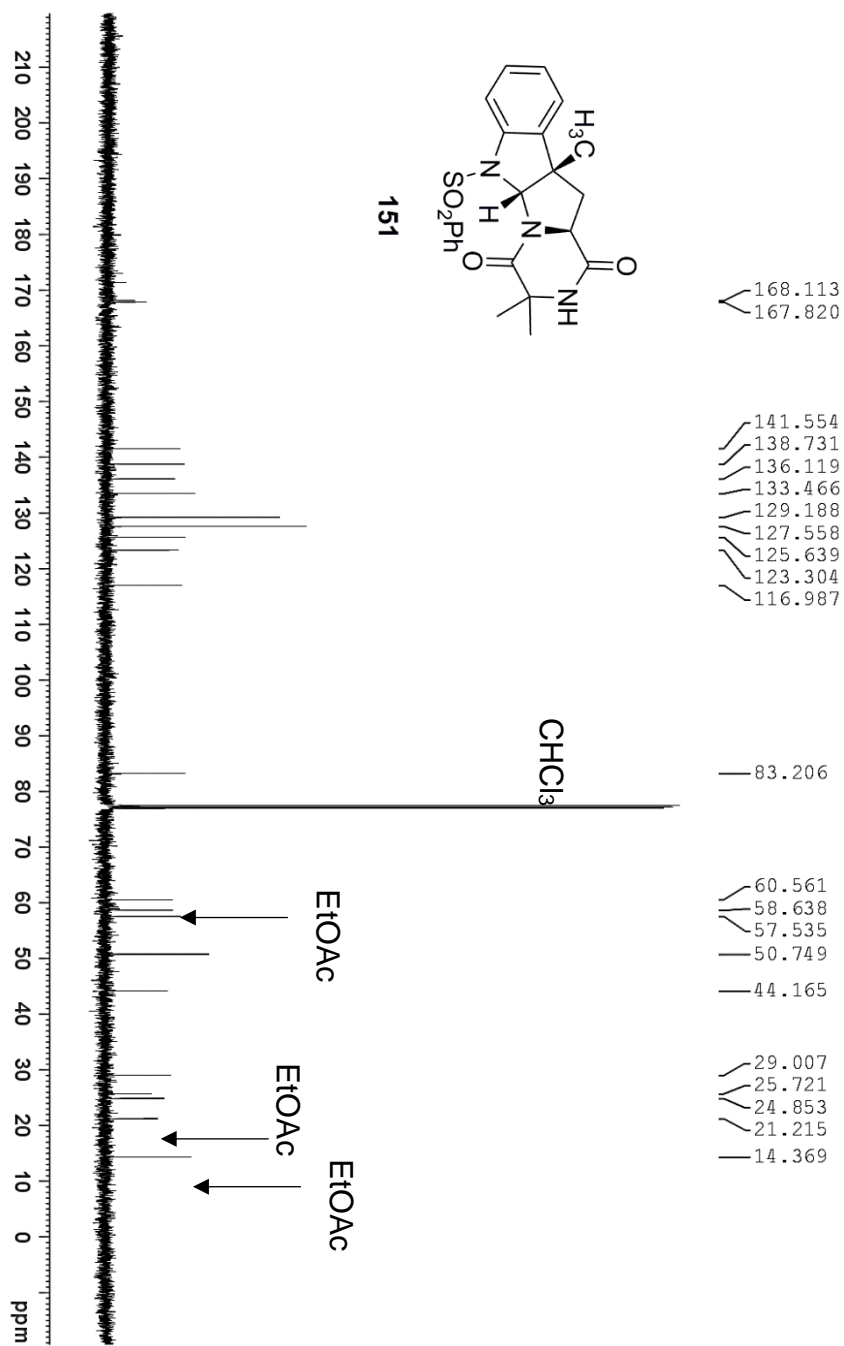




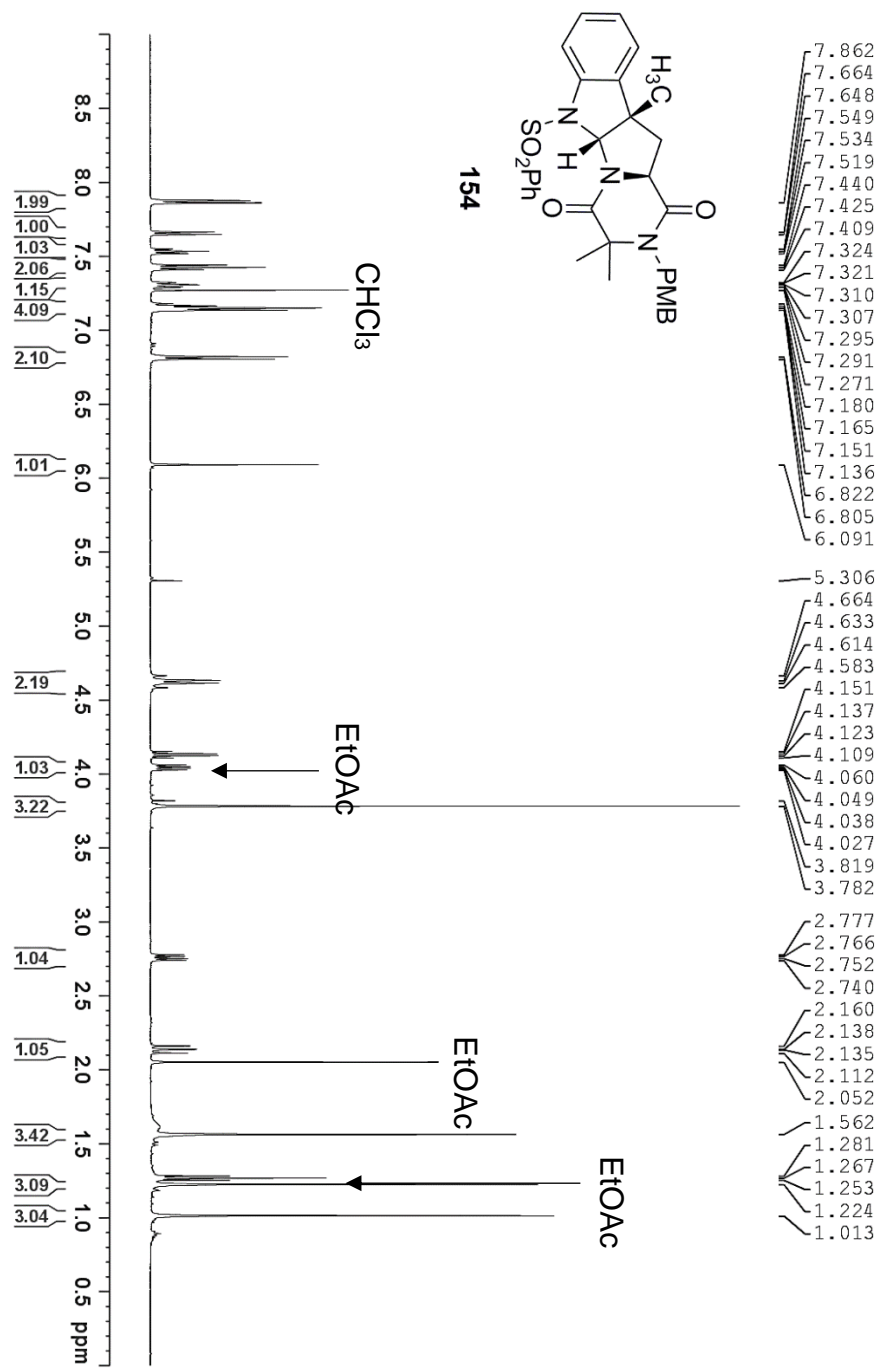
Supplementary Figure 4.22:  $^1\text{H NMR}$  (500 MHz,  $\text{CDCl}_3$ ) Spectrum of **127a**



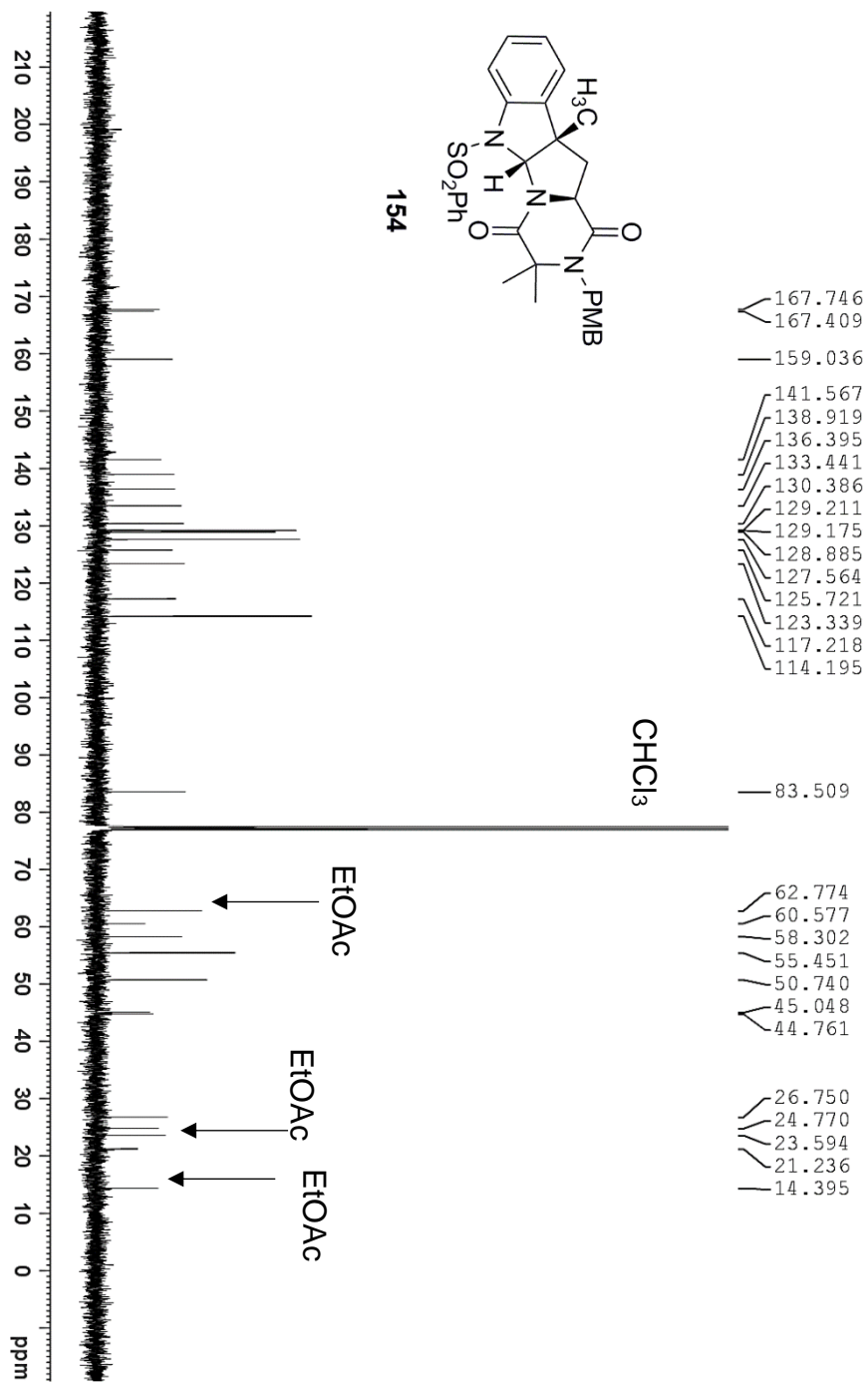
**Supplementary Figure 4.23:  $^1\text{H}$  NMR (500 MHz,  $\text{CDCl}_3$ ) Spectrum of **151****



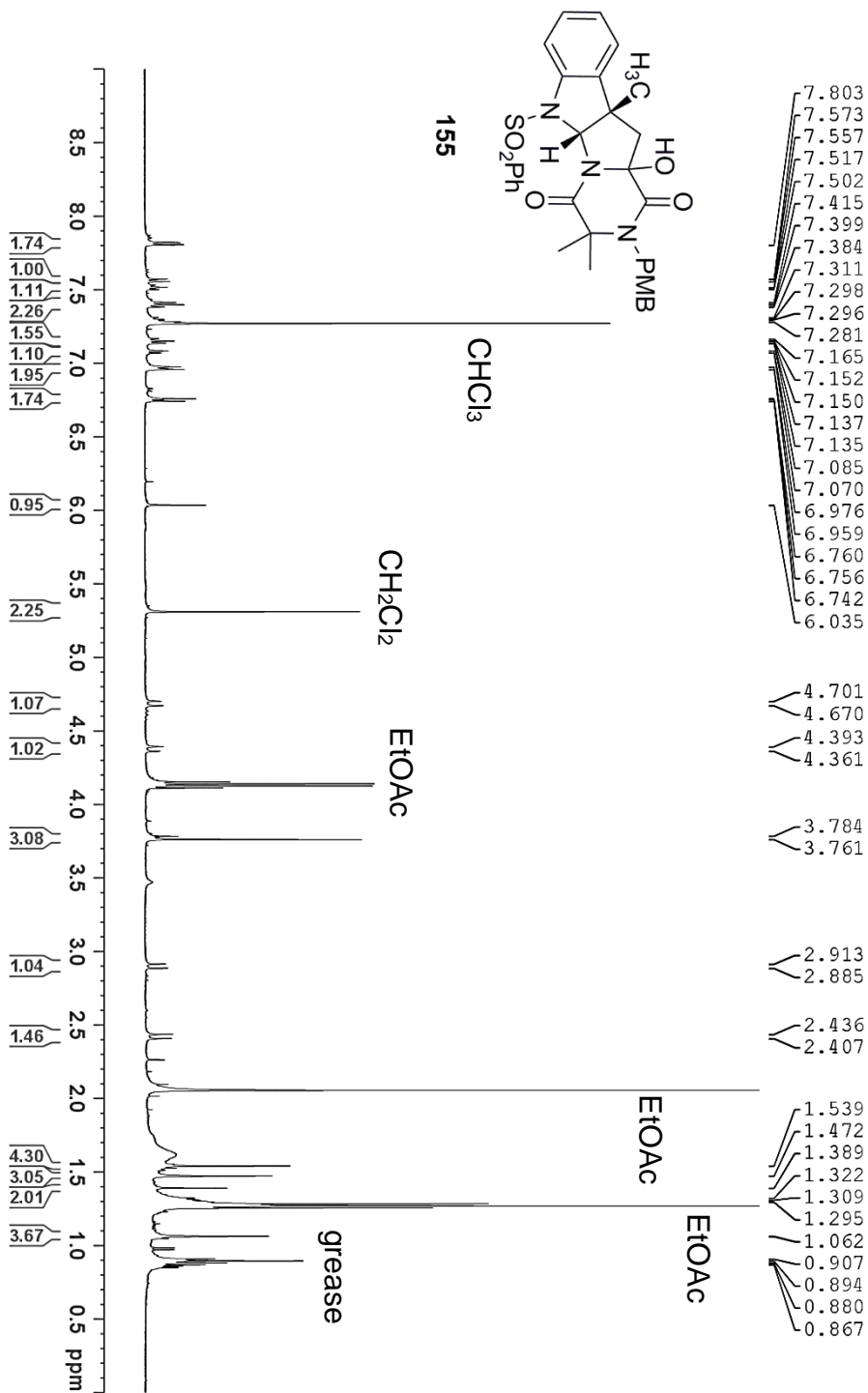
Supplementary Figure 4.24: <sup>13</sup>C NMR (125 MHz, CDCl<sub>3</sub>) Spectrum of **151**



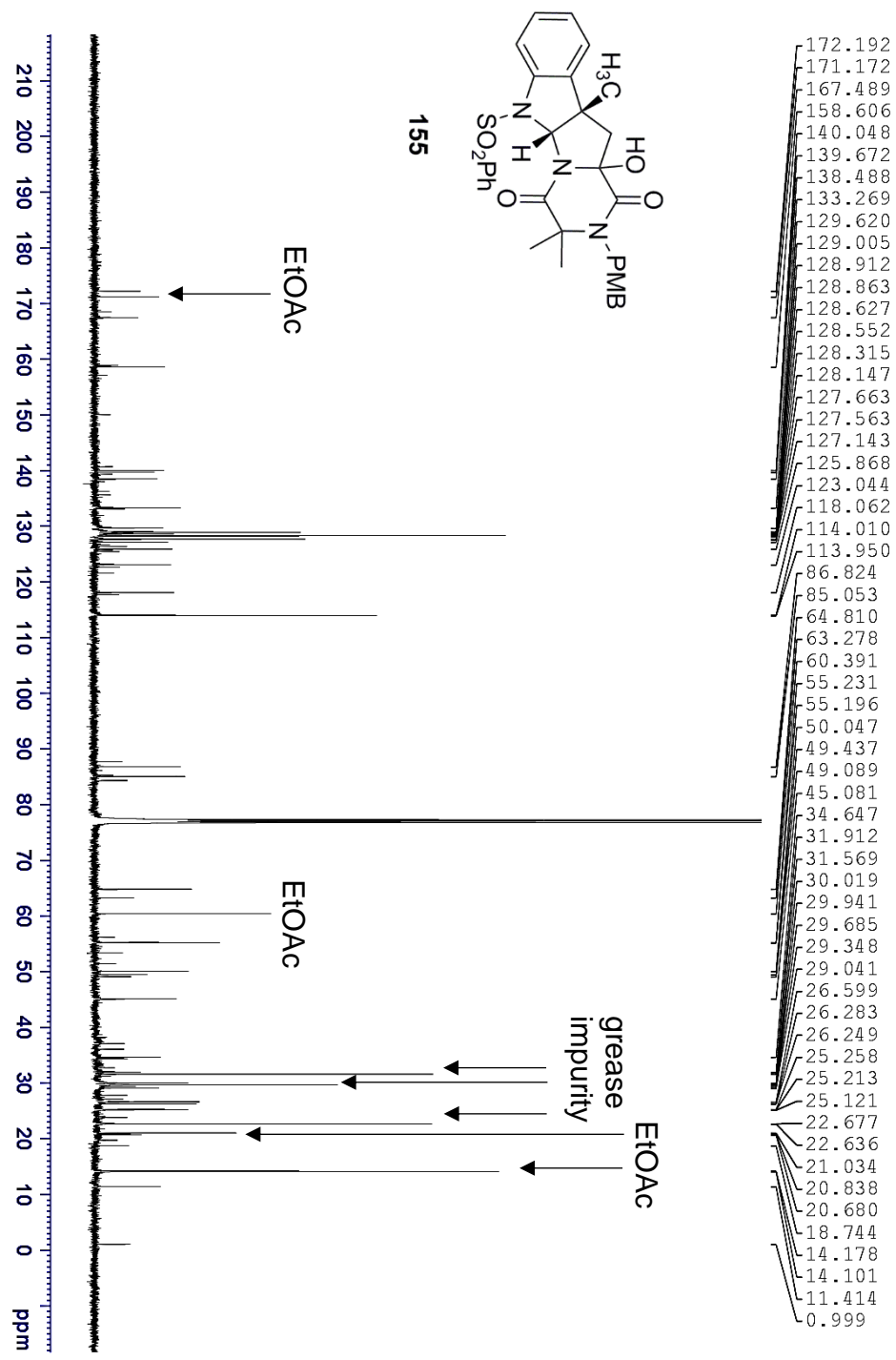
Supplementary Figure 4.25: <sup>1</sup>H NMR (500 MHz, CDCl<sub>3</sub>) Spectrum of **154**



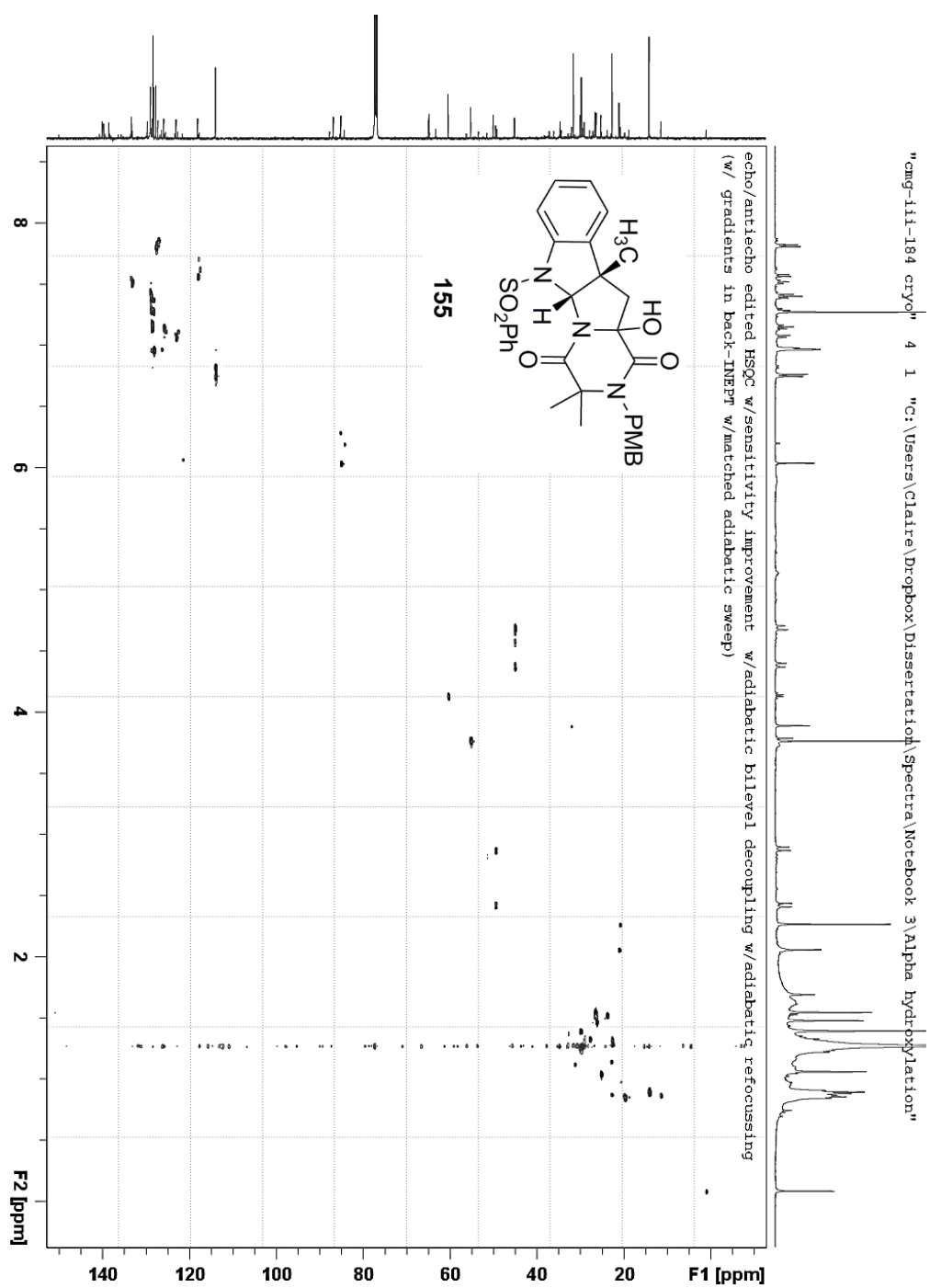
Supplementary Figure 4.26:  $^{13}C$  NMR (125 MHz,  $CDCl_3$ ) Spectrum of **154**



Supplementary Figure 4.27: <sup>1</sup>H NMR (500 MHz, CDCl<sub>3</sub>) Spectrum of **155**



Supplementary Figure 4.28: <sup>13</sup>C NMR (125 MHz, CDCl<sub>3</sub>) Spectrum of **155**



Supplementary Figure 4.29:  $^1\text{H}$ - $^{13}\text{C}$  HSQC NMR (500 MHz,  $\text{CDCl}_3$ ) Spectrum of 155



## Appendix 4C: X-Ray Crystal Structures Relevant to Chapter 4

### X-ray Structure Determination of Compound **121**

Compound **121**, C<sub>18</sub>H<sub>18</sub>N<sub>4</sub>SO<sub>4</sub>, crystallizes in the triclinic space  $P\bar{1}$  with  $a=8.0132(4)\text{\AA}$ ,  $b=8.0532(4)\text{\AA}$ ,  $c=13.8714(6)\text{\AA}$ ,  $\alpha=101.108(2)^\circ$ ,  $\beta=97.013(2)^\circ$ ,  $\gamma=95.669(2)^\circ$ ,  $V=864.90(7)\text{\AA}^3$ ,  $Z=2$ , and  $d_{\text{calc}}=1.484\text{ g/cm}^3$ . X-ray intensity data were collected on a Bruker APEXII CCD area detector employing graphite-monochromated Mo-K $\alpha$  radiation ( $\lambda=0.71073\text{ \AA}$ ) at a temperature of 100(1)K. Preliminary indexing was performed from a series of thirty-six 0.5° rotation frames with exposures of 10 seconds. A total of 2301 frames were collected with a crystal to detector distance of 37.6 mm, rotation widths of 0.5° and exposures of 3 seconds:

scan type	2 $\theta$	$\omega$	$\varphi$	$\chi$	frames
$\varphi$	19.50	59.55	348.71	-26.26	739
$\varphi$	-20.50	342.55	321.55	-73.06	739
$\omega$	-10.50	352.00	80.80	-60.33	84
$\varphi$	-23.00	315.83	12.48	28.88	739

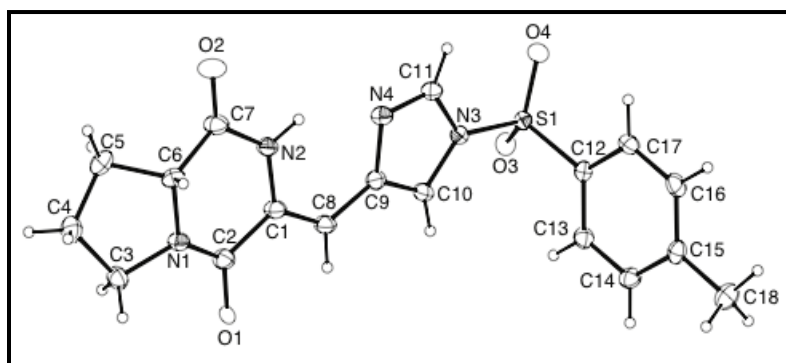
Rotation frames were integrated using SAINT<sup>i</sup>, producing a listing of unaveraged  $F^2$  and  $\sigma(F^2)$  values which were then passed to the SHELXTL<sup>ii</sup>

program package for further processing and structure solution. A total of 17301 reflections were measured over the ranges  $2.58 \leq \theta \leq 25.38^\circ$ ,  $-9 \leq h \leq 9$ ,  $-9 \leq k \leq 9$ ,  $-16 \leq l \leq 16$  yielding 3146 unique reflections ( $R_{int} = 0.0177$ ). The intensity data were corrected for Lorentz and polarization effects and for absorption using SADABS<sup>iii</sup> (minimum and maximum transmission 0.6977, 0.7452).

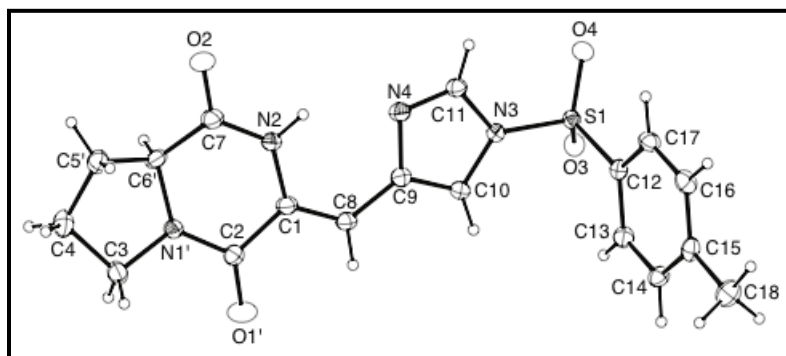
The structure was solved by direct methods (SHELXS-97<sup>iv</sup>). During development of the structure, some “extra” electron density was apparent in the C5-C6-N1 area. A disorder model was devised that included alternate locations for these three atoms resulting from the superposition of the two molecules depicted in Figures 1. and 2. The two disorder models had relative occupancies of 0.55/0.45. Refinement was by full-matrix least squares based on  $F^2$  using SHELXL-97.<sup>v</sup> All reflections were used during refinement. The weighting scheme used was  $w=1/[\sigma^2(F_o^2) + (0.0338P)^2 + 0.31336435P]$  where  $P = (F_o^2 + 2F_c^2)/3$ . Non-hydrogen atoms were refined anisotropically and hydrogen atoms were refined using a riding model. Refinement converged to  $R1=0.0318$  and  $wR2=0.0825$  for 3040 observed reflections for which  $F > 4\sigma(F)$  and  $R1=0.0326$  and  $wR2=0.0831$  and  $GOF = 1.106$  for all 3146 unique, non-zero reflections and 282 variables.<sup>vi</sup> The maximum  $\Delta/\sigma$  in the final cycle of least squares was 0.002 and the two most prominent peaks in the final difference Fourier were +0.412 and -0.372  $e/\text{\AA}^3$ .

Supplementary Table 4.1 lists cell information, data collection parameters, and refinement data. Final positional and equivalent isotropic thermal parameters

are given in Supplementary Tables 4.2 and 4.3. Anisotropic thermal parameters are in Supplementary Table 4.4. Supplementary Tables 4.5 and 4.6 list bond distances and bond angles. Supplementary Figures 4.26 and 4.27 are ORTEP<sup>vii</sup> representations of the molecule with 50% probability thermal ellipsoids displayed.



Supplementary Figure 4.26: ORTEP drawing of disorder model no. 1 of the asymmetric with 50% probability thermal ellipsoids.



Supplementary Figure 4.27: ORTEP drawing of disorder model no. 2 of the asymmetric with 50% probability thermal ellipsoids.

**Supplementary Table 4.1: Summary of Structure Determination of  
Compound 121**

Empirical formula	C <sub>18</sub> H <sub>18</sub> N <sub>4</sub> SO <sub>4</sub>
Formula weight	386.42
Temperature	100(1) K
Wavelength	0.71073 Å
Crystal system	triclinic
Space group	P $\bar{1}$
Cell constants:	
a	8.0132(4) Å
b	8.0532(4) Å
c	13.8714(6) Å
a	101.108(2)°
b	97.013(2)°
g	95.669(2)°
Volume	864.90(7) Å <sup>3</sup>
Z	2
Density (calculated)	1.484 Mg/m <sup>3</sup>
Absorption coefficient	0.222 mm <sup>-1</sup>
F(000)	404
Crystal size	0.25 x 0.22 x 0.15 mm <sup>3</sup>

Theta range for data collection	2.58 to 25.38°
Index ranges	-9 ≤ h ≤ 9, -9 ≤ k ≤ 9, -16 ≤ l ≤ 16
Reflections collected	17301
Independent reflections	3146 [R(int) = 0.0177]
Completeness to theta = 25.38°	98.7 %
Absorption correction	Semi-empirical from equivalents
Max. and min. transmission	0.7452 and 0.6977
Refinement method	Full-matrix least-squares on F <sup>2</sup>
Data / restraints / parameters	3146 / 0 / 282
Goodness-of-fit on F <sup>2</sup>	1.106
Final R indices [I > 2σ(I)]	R1 = 0.0318, wR2 = 0.0825
R indices (all data)	R1 = 0.0326, wR2 = 0.0831
Largest diff. peak and hole	0.412 and -0.372 e.Å <sup>-3</sup>

**Supplementary Table 4.2: Refined Positional Parameters for Compound 121**

Atom	x	y	z	U <sub>eq</sub> , Å <sup>2</sup>
C1	0.6649(2)	0.48482(19)	0.43450(12)	0.0189(3)
C2	0.7730(2)	0.5283(2)	0.53377(12)	0.0205(3)
C3	0.9251(2)	0.4121(2)	0.66531(12)	0.0220(3)
C4	0.9480(2)	0.2272(2)	0.67058(13)	0.0258(4)
C5	0.8748(6)	0.1266(5)	0.5670(3)	0.0243(9)
C6	0.7225(4)	0.2180(3)	0.5415(2)	0.0178(6)
N1	0.7894(6)	0.3973(8)	0.5807(4)	0.0175(10)
O1	0.8218(14)	0.6747(17)	0.5758(10)	0.018(3)
C5'	0.8092(7)	0.1154(6)	0.5900(4)	0.0223(10)
C6'	0.8152(5)	0.2155(4)	0.5083(3)	0.0199(7)
N1'	0.8406(8)	0.3940(10)	0.5628(5)	0.0176(12)
O1'	0.829(2)	0.677(2)	0.5756(14)	0.035(5)
C7	0.6540(2)	0.1775(2)	0.43121(12)	0.0230(4)
C8	0.6278(2)	0.6083(2)	0.38616(12)	0.0197(3)
C9	0.53425(19)	0.58446(19)	0.28718(11)	0.0171(3)
C10	0.5099(2)	0.7061(2)	0.23277(11)	0.0186(3)
C11	0.38706(19)	0.45197(19)	0.14816(11)	0.0173(3)
C12	0.20155(19)	0.83555(19)	0.08551(11)	0.0158(3)
C13	0.25426(19)	0.99682(19)	0.14546(12)	0.0184(3)
C14	0.1331(2)	1.09395(19)	0.18064(12)	0.0196(3)
C15	-0.0397(2)	1.0347(2)	0.15444(12)	0.0190(3)
C16	-0.0885(2)	0.8746(2)	0.09319(12)	0.0213(3)
C17	0.0308(2)	0.7730(2)	0.05926(12)	0.0198(3)
C18	-0.1698(2)	1.1419(2)	0.19391(14)	0.0280(4)
N2	0.61064(17)	0.31197(16)	0.39343(10)	0.0188(3)
N3	0.41533(16)	0.62128(16)	0.14317(9)	0.0160(3)

N4	0.45616(17)	0.42501(16)	0.23242(10)	0.0182(3)
O2	0.60708(17)	0.03014(14)	0.38878(9)	0.0289(3)
O3	0.49787(13)	0.81381(14)	0.03153(8)	0.0189(2)
O4	0.27594(14)	0.56404(14)	-0.03040(8)	0.0193(2)
S1	0.35327(4)	0.70729(5)	0.04492(3)	0.01467(11)
$U_{eq} = \frac{1}{3} [U_{11}(aa^*)^2 + U_{22}(bb^*)^2 + U_{33}(cc^*)^2 + 2U_{12}aa^*bb^*\cos\gamma + 2U_{13}aa^*cc^*\cos\beta + 2U_{23}bb^*cc^*\cos\alpha]$				

**Supplementary Table 4.3: Positional Parameters for Hydrogens in Compound 121**

Atom	x	y	z	U <sub>iso</sub> , Å <sup>2</sup>
H3a	0.8918	0.4717	0.7263	0.029
H3b	1.0291	0.4728	0.6539	0.029
H3a'	0.8548	0.4598	0.7131	0.029
H3b'	1.0334	0.4834	0.6767	0.029
H4A	1.0668	0.2147	0.6862	0.034
H4B	0.8867	0.1898	0.7203	0.034
H5a	0.8402	0.0080	0.5675	0.032
H5b	0.9555	0.1329	0.5208	0.032
H6	0.6322	0.1858	0.5786	0.024
H5a'	0.8379	0.0009	0.5694	0.030
H5b'	0.6991	0.1095	0.6124	0.030
H6'	0.9136	0.1918	0.4747	0.027
H8	0.6656	0.7200	0.4192	0.026
H10	0.5487	0.8220	0.2517	0.025
H11	0.3260	0.3673	0.0974	0.023
H13	0.3689	1.0382	0.1615	0.024
H14	0.1669	1.2002	0.2223	0.026
H16	-0.2032	0.8350	0.0747	0.028
H17	-0.0028	0.6650	0.0196	0.026
H18a	-0.2812	1.0883	0.1637	0.042
H18b	-0.1510	1.2529	0.1786	0.042
H18c	-0.1602	1.1527	0.2646	0.042
H2	0.5426	0.2894	0.3383	0.025



**Supplementary Table 4.4: Refined Thermal Parameters (U's) for  
Compound 121**

Atom	U <sub>11</sub>	U <sub>22</sub>	U <sub>33</sub>	U <sub>23</sub>	U <sub>13</sub>	U <sub>12</sub>
C1	0.0232(8)	0.0145(7)	0.0175(8)	0.0012(6)	0.0023(6)	0.0005(6)
C2	0.0266(8)	0.0160(8)	0.0182(8)	0.0041(7)	0.0010(6)	0.0015(6)
C3	0.0235(8)	0.0236(8)	0.0184(8)	0.0061(6)	-0.0007(6)	0.0022(7)
C4	0.0262(9)	0.0258(9)	0.0276(9)	0.0120(7)	0.0014(7)	0.0048(7)
C5	0.028(2)	0.0187(17)	0.030(2)	0.0091(15)	0.0085(17)	0.0075(18)
C6	0.0219(15)	0.0128(14)	0.0196(15)	0.0041(11)	0.0067(13)	0.0006(11)
N1	0.021(3)	0.0147(15)	0.015(2)	0.0022(14)	0.0029(16)	-0.0003(19)
O1	0.021(3)	0.014(6)	0.016(5)	0.001(4)	-0.008(3)	0.004(3)
C5'	0.025(3)	0.021(2)	0.023(2)	0.0073(17)	0.0040(19)	0.005(2)
C6'	0.026(2)	0.0122(17)	0.0218(19)	0.0019(14)	0.0046(17)	0.0046(14)
N1'	0.023(3)	0.0143(18)	0.015(3)	0.0030(18)	0.001(2)	0.001(2)
O1'	0.057(8)	0.015(8)	0.029(8)	0.002(6)	0.001(6)	-0.007(5)
C7	0.0332(9)	0.0154(8)	0.0194(8)	0.0033(6)	0.0022(7)	0.0004(7)
C8	0.0249(8)	0.0140(7)	0.0179(8)	0.0009(6)	0.0000(6)	0.0001(6)
C9	0.0171(7)	0.0161(7)	0.0176(8)	0.0021(6)	0.0029(6)	0.0020(6)
C10	0.0210(8)	0.0151(7)	0.0172(8)	0.0007(6)	-0.0020(6)	0.0005(6)
C11	0.0191(7)	0.0143(7)	0.0175(8)	0.0020(6)	0.0027(6)	0.0001(6)
C12	0.0153(7)	0.0163(7)	0.0166(7)	0.0047(6)	0.0018(6)	0.0036(6)
C13	0.0158(7)	0.0167(7)	0.0218(8)	0.0048(6)	0.0007(6)	-0.0008(6)
C14	0.0230(8)	0.0142(7)	0.0215(8)	0.0043(6)	0.0031(6)	0.0008(6)
C15	0.0198(8)	0.0211(8)	0.0194(8)	0.0090(6)	0.0048(6)	0.0061(6)
C16	0.0133(7)	0.0269(8)	0.0224(8)	0.0040(7)	-0.0001(6)	0.0006(6)
C17	0.0176(8)	0.0195(8)	0.0194(8)	0.0004(6)	-0.0010(6)	-0.0007(6)
C18	0.0252(9)	0.0282(9)	0.0332(10)	0.0060(7)	0.0098(7)	0.0093(7)
N2	0.0244(7)	0.0143(6)	0.0157(6)	0.0013(5)	-0.0001(5)	0.0012(5)

N3	0.0172(6)	0.0146(6)	0.0154(6)	0.0025(5)	0.0001(5)	0.0023(5)
N4	0.0206(7)	0.0154(6)	0.0177(7)	0.0018(5)	0.0030(5)	0.0008(5)
O2	0.0468(8)	0.0141(6)	0.0230(6)	0.0018(5)	0.0008(5)	-0.0002(5)
O3	0.0159(5)	0.0206(6)	0.0210(6)	0.0063(4)	0.0033(4)	0.0017(4)
O4	0.0199(6)	0.0194(6)	0.0166(5)	0.0004(4)	0.0006(4)	0.0018(4)
S1	0.01374(19)	0.01536(19)	0.01446(19)	0.00272(14)	0.00096(14)	0.00174(14)
The form of the anisotropic displacement parameter is: $\exp[-2\pi^2(a^2U_{11}h^2+b^2U_{22}k^2+c^2U_{33}l^2+2b^*c^*U_{23}kl+2a^*c^*U_{13}hl+2a^*b^*U_{12}hk)]$						

**Supplementary Table 4.5: Bond Distances in Compound 121, Å**

C1-C8	1.339(2)	C1-N2	1.4020(19)	C1-C2	1.494(2)
C2-O1	1.213(14)	C2-O1'	1.236(19)	C2-N1	1.351(7)
C2-N1'	1.362(8)	C3-N1'	1.472(8)	C3-N1	1.477(7)
C3-C4	1.533(2)	C4-C5	1.521(5)	C4-C5'	1.552(5)
C5-C6	1.525(5)	C6-N1	1.463(7)	C6-C7	1.522(3)
C5'-C6'	1.515(6)	C6'-N1'	1.471(8)	C6'-C7	1.537(4)
C7-O2	1.219(2)	C7-N2	1.347(2)	C8-C9	1.450(2)
C9-C10	1.361(2)	C9-N4	1.4024(19)	C10-N3	1.3878(19)
C11-N4	1.298(2)	C11-N3	1.3763(19)	C12-C17	1.389(2)
C12-C13	1.395(2)	C12-S1	1.7473(15)	C13-C14	1.383(2)
C14-C15	1.399(2)	C15-C16	1.391(2)	C15-C18	1.506(2)
C16-C17	1.386(2)	N3-S1	1.6885(13)	O3-S1	1.4250(11)
O4-S1	1.4293(11)				

**Supplementary Table 4.6: Bond Angles in Compound 121, °**

C8-C1-N2	122.11(14)	C8-C1-C2	120.15(14)	N2-C1-C2	117.69(14)
O1-C2-O1'	2.6(14)	O1-C2-N1	121.5(6)	O1'-C2-N1	121.3(9)
O1-C2-N1'	122.1(6)	O1'-C2-N1'	120.8(8)	N1-C2-N1'	21.4(2)
O1-C2-C1	122.0(5)	O1'-C2-C1	122.7(8)	N1-C2-C1	115.6(3)
N1'-C2-C1	114.5(3)	N1'-C3-N1	19.7(2)	N1'-C3-C4	102.2(3)
N1-C3-C4	104.4(3)	C5-C4-C3	103.86(19)	C5-C4-C5'	24.58(15)
C3-C4-C5'	105.5(2)	C4-C5-C6	102.0(3)	N1-C6-C7	113.9(3)
N1-C6-C5	102.3(3)	C7-C6-C5	113.2(3)	C2-N1-C6	126.8(5)
C2-N1-C3	120.4(4)	C6-N1-C3	110.1(4)	C6'-C5'-C4	100.1(3)
N1'-C6'-C5'	103.2(4)	N1'-C6'-C7	111.7(4)	C5'-C6'-C7	113.7(3)
C2-N1'-C6'	127.1(6)	C2-N1'-C3	120.0(5)	C6'-N1'-C3	112.0(5)
O2-C7-N2	122.92(15)	O2-C7-C6	119.75(17)	N2-C7-C6	115.23(16)
O2-C7-C6'	118.49(18)	N2-C7-C6'	114.83(18)	C6-C7-C6'	35.02(17)
C1-C8-C9	126.21(14)	C10-C9-N4	109.77(13)	C10-C9-C8	127.16(14)
N4-C9-C8	123.07(14)	C9-C10-N3	105.76(13)	N4-C11-N3	111.65(13)
C17-C12-C13	121.36(14)	C17-C12-S1	119.21(12)	C13-C12-S1	119.41(11)
C14-C13-C12	118.81(14)	C13-C14-C15	120.94(14)	C16-C15-C14	118.93(14)
C16-C15-C18	120.87(15)	C14-C15-C18	120.19(15)	C17-C16-C15	121.12(14)
C16-C17-C12	118.80(14)	C7-N2-C1	126.82(14)	C11-N3-C10	106.86(13)
C11-N3-S1	126.38(11)	C10-N3-S1	126.72(11)	C11-N4-C9	105.97(13)
O3-S1-O4	121.49(7)	O3-S1-N3	106.06(6)	O4-S1-N3	104.12(6)
O3-S1-C12	108.88(7)	O4-S1-C12	110.67(7)	N3-S1-C12	104.02(7)

---

<sup>i</sup>Bruker (2009) SAINT. Bruker AXS Inc., Madison, Wisconsin, USA.

<sup>ii</sup>Bruker (2009) SHELXTL. Bruker AXS Inc., Madison, Wisconsin, USA.

<sup>iii</sup>Sheldrick, G.M. (2007) SADABS. University of Gottingen, Germany.

<sup>iv</sup>Sheldrick, G.M. (2008) Acta Cryst. A64,112-122.

<sup>v</sup>Sheldrick, G.M. (2008) Acta Cryst. A64,112-122.

$$^viR1 = \frac{\sum ||F_o| - |F_c||}{\sum |F_o|}$$

$$wR2 = [\frac{\sum w(F_o^2 - F_c^2)^2}{\sum w(F_o^2)^2}]^{1/2}$$

$$GOF = [\frac{\sum w(F_o^2 - F_c^2)^2}{(n - p)}]^{1/2}$$

where n = the number of reflections and p = the number of parameters refined.

<sup>vii</sup>“ORTEP-II: A Fortran Thermal Ellipsoid Plot Program for Crystal Structure Illustrations”. C.K. Johnson (1976) ORNL-5138.

## List of Acronyms and Abbreviations

°C: degrees Celsius

Å: angstroms

AA: amino acid

antiSMASH: antibiotics & Secondary Metabolite Analysis Shell

B3LYP: Becke, three-parameter, Lee-Yang-Parr

BDE: bond dissociation energy

BHT: *tert*-butylhydroxytoluene

BINOL: 1,1'-bi-2-naphthol

Boc: *tert*-butyloxycarbonyl

Boc<sub>2</sub>O: di-*tert*-butyl dicarbonate

br s: broad singlet

CAN: cerium ammonium nitrate

Cbz: carboxybenzyl

cDNA: complementary DNA

CDY: Czapek-Dox yeast extract

COSY: homonuclear correlation spectroscopy

d: doublet

Da: Dalton

DBN: 1,5-diazabicyclo[4.3.0]non-5-ene

DBU: 1,8-diazabicyclo[5.4.0]undec-7-ene

dd: doublet of doublets

dd H<sub>2</sub>O: double distilled water

DFT: density functional theory

DHTD: dehydrohistidyltryptophanyldiketopiperazine

DMAP: 4-dimethylaminopyridine

DMAPP: dimethylallyl pyrophosphate

DMDO: dimethyldioxirane

DMF: dimethylformamide

DMSO: dimethylsulfoxide

dr: diastereomeric ratio

dT: deoxy-thymidine

e: elementary charge

EDC: 1-ethyl-3-(3-dimethylaminopropyl)carbodiimide

EDTA: ethylenediaminetetraacetic acid

EI: electron ionization

Equiv: equivalent

ESI-TOF: electrospray ionization time-of-flight

Et: ethyl

Et<sub>3</sub>N: triethylamine

FAD: flavin adenine dinucleotide

FCC: flash column chromatography

Fmoc: fluorenylmethyloxycarbonyl

F-TEDA-PF<sub>6</sub>: 1-(chloromethyl)-4-fluoro-1,4-diazoniabicyclo[2.2.2]octane dihexafluorophosphate

g: grams

g: standard acceleration due to gravity at the Earth's surface

G<sub>2</sub> phase: Gap 2 phase

GC-MS: gas chromatography-mass spectrometry



gCOSY: gradient correlation spectroscopy

gHMBCAD: gradient heteronuclear multiple bond correlation adiabatic

gHSQCAD: gradient heteronuclear single quantum coherence adiabatic

h: hours

HATU: 1-[Bis(dimethylamino)methylene]-1*H*-1,2,3-triazolo[4,5-*b*]pyridinium 3-oxid hexafluorophosphate

HEPES: 4-(2-hydroxyethyl)-1-piperazineethanesulfonic acid

HF: Hartree-Fock

His: histidine

HMBC: heteronuclear multiple bond correlation

HMQC: heteronuclear multiple quantum coherence

HOAt: 1-hydroxy-7-azabenzotriazole

HOBt: hydroxybenzotriazole

HOMO: highest occupied molecular orbital

hp: hypothetical protein

HPLC: high-performance liquid chromatography

HPLC-MS: high-performance liquid chromatography-mass spectrometry

HRMS: high resolution mass spectrometry

HSQC: heteronuclear single quantum coherence

HTD: histidyltryptophanyldiketopiperazine

Hz: hertz

IC<sub>50</sub>: half maximal inhibitory concentration

IPTG: Isopropyl  $\beta$ -D-1-thiogalactopyranoside

IR: infrared

k: rate constant

K: equilibrium constant

k<sub>cat</sub>: turnover number

kDa: kilodaltons

kJ: kilojoules

K<sub>M</sub>: Michaelis constant

k-mer: all possible subsequences obtained from DNA sequencing

L: liter

LB: lysogeny broth

LC-MS: liquid chromatography-mass spectrometry

LiHMDS: lithium bis(trimethylsilyl)amide

LUMO: lowest unoccupied molecular orbital

M: molar

m: multiplet

M phase: mitotic phase

m/z: mass-to-charge ratio

mCPBA: *meta*-chloroperbenzoic acid

mg: milligrams

MGS: mannitol, glucose, succinic acid

MHz: megahertz

mL: milliliters

mM: millimolar

mmol: millimoles

mol: moles

MoOPH: oxodiperoxymolybdenum(pyridine)-(hexamethylphosphoric triamide)

Ms: mesyl

MTS: methyl *p*-tolyl sulfide

MTSO: methyl *p*-tolyl sulfoxide

N: normal

N50: the shortest sequence length at 50% of the genome

NADH: nicotinamide adenine dinucleotide

NADPH: nicotinamide adenine dinucleotide phosphate

NBS: *N*-bromosuccinimide

NCS: *N*-chlorosuccinimide

NFSI: *N*-fluorobenzenesulfonimide

Ni-NTA: nickel- nitrilotriacetic acid

NIS: *N*-iodosuccinimide

nM: nanomolar

NMR: nuclear magnetic resonance

NOESY: nuclear Overhauser effect spectroscopy

NPSP: *N*-(phenylseleno)phthalimide

NRPS: nonribosomal peptide synthase

ORF: open reading frame

PCR: polymerase chain reaction

PMA: phosphomolybdic acid

PMB: *para*-methoxybenzyl

PPTS: pyridinium *p*-toluenesulfonate

Py<sub>2</sub>AgMnO<sub>4</sub>: bis(pyridine) silver (I) permanganate

q: quartet

R<sub>f</sub>: retention factor

RT-PCR: reverse transcription- polymerase chain reaction

s: singlet

SET: single electron transfer

t: triplet

TBAOH: tetrabutylammonium hydroxide

TCEP: tris(2-carboxyethyl)phosphine

td: triplet of doublets

TEV: tobacco etch virus

TFA: trifluoroacetic acid; trifluoroacetyl

TFAA: trifluoroacetic anhydride

TfOH: triflic acid

THF: tetrahydrofuran

TLC: thin-layer chromatography

TMS: tetramethylsilane

TMSI: trimethylsilyl iodide

Ts: tosyl

TTN: total turnover number

UV: ultraviolet

UV-Vis: ultraviolet-visible

$\mu\text{g}$ : microgram

$\mu\text{L}$ : microliter

$\mu\text{M}$ : micromolar

## Bibliography

Adams, T. C.; Payette, J. N.; Cheah, J. H.; Movassaghi, M. *Org. Lett.* **2015**, *17*, 4268-4271.

Ali, H.; Ries, M. I.; Nijland, J. G.; Lankhorst, P. P.; Hankemeier, T.; Bovenberg, R. A.; Vreeken, R. J.; Driessen, A. J. *PLoS ONE* **2013**, *8*(6), e65328.

Allan, K. M.; Kobayashi, K.; Rawal, V. H. *J. Am. Chem. Soc.* **2012**, *134*(3), 1392-1395.

Aninat, C.; Andre, F.; Delaforge, M. *Food Addit. Contam.* **2005**, *22*(4), 361-368.

Arnold, D. L.; Scott, P. M.; McGuire, P. F.; Harwig, J.; Nera, E. A. *Food Cosmet. Toxicol.* **1978**, *16*, 369-371.

Artman, G. D.; Grubbs, A. W.; Williams, R. M. *J. Am. Chem. Soc.* **2007**, *129*(19), 6336-6342.

Azuma, H.; Okano, K.; Fukuyama, T.; Tokuyama, H. *Org. Synth.* **2011**, *88*, 152-161.

Balamurugan, D.; Muraleedharan, K. M. *Chem. Eur. J.* **2012**, *18*, 9516-9520.

Ballistreri, F. P.; Chiacchio, U.; Rescifina, A.; Tomaselli, G. A.; Toscano, R. M. *Tetrahedron* **1992**, *48*, 8677-8684.

Banke, S.; Frisvad, J. C.; Rosendahl, S. *Mycol. Res.* **1997**, *101*(5), 617-624.

- Baran, P. S.; Guerrero, C. A.; Hafensteiner, B. D.; Ambhaikar, N. B. *Angew. Chem. Int. Ed.* **2005**, *44*(25), 3892-3895.
- Barbati, S.; Clément, J.-L.; Fréjaville, C.; Bouteiller, J.-C.; Tordo, P.; Michel, J.-C.; Yadan, J.-C. *Synthesis* **1999**, *12*, 2036-2040.
- Beshore, D. C.; Smith, A. B., III. *J. Am. Chem. Soc.* **2008**, *130*, 13778-13789.
- Bjørsvik, H.-R.; Occhipinti, G.; Gambarotti, C.; Cerasino, L.; Jensen, V. R. *J. Org. Chem.* **2005**, *70*, 7290-7296.
- Blake, K. W.; Sammes, P. G. *J. Chem. Soc. C.* **1970**, *7*, 980-984.
- Bondon, A.; Macdonald, T. L.; Harris, T. M.; Guengerich, F. P. *J. Biol. Chem.* **1989**, *264*(4), 1988-1997.
- Boyer, N.; Movassaghi, M. *Chem. Sci.* **2012**, *3*, 1798-1803.
- Boysen, M.; Skouboe, P.; Frisvad, J.; Rossen, L. *Microbiology* **1996**, *142*, 541-549.
- Brocks, J. J.; Beckhaus, H.-D.; Beckwith, A. L. J.; Ruchardt, C. *J. Org. Chem.* **1998**, *63*, 1935-1943.
- Brocks, J. J.; Welle, F. M.; Beckhaus, H.-D.; Ruchardt, C. *Tetrahedron Lett.* **1997**, *38*(44), 7721-7724.
- Bunger, J.; Westphal, G.; Monnich, A.; Hinnendahl, B.; Hallier, E.; Muller, M. *Toxicology* **2004**, *202*(3), 199-211.



- Cashman, J. R.; Xiong, Y. N.; Xu, L.; Janowsky, A. *J. Pharmacol. Exp. Ther.* **1999**, *288*(3), 1251-1260.
- Cashman, J. R.; Yang, Z.-c.; Hogberg, T. *Chemical Research in Toxicology* **1990**, *3*, 428-432.
- Chen, H.; Fan, Y.; Du, N.; Li, P., Roquefortine C preparing method. CN 104894182, 2015.
- Clement, B.; Lustig, K. L.; Ziegler, D. M. *Drug Metab. Dispos.* **1993**, *21*(1), 24-29.
- Coste, A.; Kim, J.; Adams, T. C.; Movassaghi, M. *Chem. Sci.* **2013**, *4*(8), 3191-3197.
- da Silva, J. V.; Fill, T. P.; Lotufo, L. V.; do Ó. Pessoa, C.; Rodrigues-Filho, E. *Helv. Chim. Act.* **2014**, *97*, 1345-1353.
- Danishefsky, S. J.; Depew, K. M.; Marsden, S. P.; Bornmann, W. G.; Chou, T.-C.; Schkeryantz, J.; Zatorski, A., Analogues of N-Acetylardeemin, Method of Preparation and Uses Thereof. WO 018215, 1997.
- Davis, G. C., Storage stable aryl nitron compositions. EP 0187303, 1986.
- Depew, K. M.; Marsden, S. P.; Zatorska, D.; Zatorski, A.; Bornmann, W. G.; Danishefsky, S. J. *J. Am. Chem. Soc.* **1999**, *121*, 11953-11963.

Driehuis, F.; Spanjer, M. C.; Scholten, J. M.; te Giffel, M. C. *J. Dairy Sci.* **2008**, *91*(11), 4261-4271.

Du, L.; Li, D.; Zhu, T.; Cai, S.; Wang, F.; Xiao, X.; Gu, Q. *Tetrahedron* **2009**, *65*(5), 1033-1039.

El-Banna, A. A.; Pitt, J. I.; Leistner, L. *Syst. Appl. Microbiol.* **1987**, *10*, 42-46.

Fedoreyev, S. A.; Ilyin, S. G.; Utkina, N. K.; Maximov, O. B.; Reshetnyak, M. V. *Tetrahedron* **1989**, *45*(11), 3487-3492.

Feldman, K. S.; Fodor, M. D. *J. Am. Chem. Soc.* **2006**, *130*, 14964-14965.

Feldman, K. S.; Fodor, M. D. *J. Am. Chem. Soc.* **2008**, *130*, 14964-14965.

Feldman, K. S.; Fodor, M. D. *J. Org. Chem.* **2009**, *74*, 3449-3461.

Feldman, K. S.; Fodor, M. D.; Skoumbourdis, A. P. *Synthesis-Stuttgart* **2009**, *18*, 3162-3173.

Felser, B.; Preiss, D. U., Novel fibrinolysis inhibitors and medical application thereof. DE 102011013326, 2011.

Fenical, W.; Jensen, P. R.; Cheng, X. C., Avrainvillamide, a cytotoxic marine natural product, and derivatives thereof. US 6,066,635, May 23, 2000.

Ferreira Koolen, H. H.; Ribeiro Soares, E.; Moura Araujo da Silva, F.; Alves de Almeida, R.; Leao de Souza, A. D.; Soman de Medeiros, L.; Rodrigues Filho, E.; Lima de Souza, A. Q. *Quim. Nova* **2012**, *35*(4), 771–774.

Field, L. D.; Li, H. L.; Magill, A. M. *Organic Structures from 2D NMR Spectra*; John Wiley & Sons Ltd: Chichester, West Sussex, 2015.

Floyd, R. A. *Aging Cell* **2006**, *5*, 51-57.

Frisvad, J. C.; Filtenborg, O. *Appl. Environ. Microb.* **1983**, *46*(6), 1301-1310.

Frisvad, J. C.; Filtenborg, O. In *Modern concepts in Penicillium and Aspergillus classification*; Samson, R. A., Pitt, J. I., Eds.; Plenum Press: New York, 1990, p 159-170.

Frisvad, J. C.; Filtenborg, O. In *Modern concepts in Penicillium and Aspergillus classification*; Samson, R. A., Pitt, J. I., Eds.; Plenum Press: New York, 1990, p 373-384.

Frisvad, J. C.; Filtenborg, O. *Mycologia* **1989**, *81*(6), 837-861.

Frisvad, J. C.; Smedsgaard, J.; Larsen, T. O.; Samson, R. A. *Stud. Mycol.* **2004**, *49*, 201-241.

García-Estrada, C.; Ullán, R. V.; Albillos, S. M.; Fernández-Bodega, M. A.; Durek, P.; von Döhren, H.; Martín, J. F. *Chem. Biol.* **2011**, *18*(11), 1499-1512.

- Gober, C.; Carroll, P. J.; Joullié, M. M. *Mini Rev. Org. Chem.* **2016**, *13*, 126-142.
- Gober, C.; Joullié, M. M. *Athens Journal of Science* **2015**, *3*(4), 257-264.
- Gober, C.; Joullié, M. M. *Isr. J. Chem.* **2016**, *57*, 303-308.
- Griffing, B. F.; West, P. R., A method of enhancing the contrast of images and materials thereof. EP 0110165A3, 1987.
- Hafensteiner, B. D.; Escribano, M.; Petricci, E.; Baran, P. S. *Bioorg. Med. Chem. Lett.* **2009**, *19*(14), 3808-3810.
- Han, Z.; Sun, J.; Zhang, Y.; He, F.; Xu, Y.; Matsumura, K.; He, L. S.; Qiu, J. W.; Qi, S. H.; Qian, P. Y. *J. Proteome Res.* **2013**, *12*(5), 2090-2100.
- Han, Z.; Sun, J.; Zhang, Y.; He, F.; Xu, Y.; Matsumura, K.; He, L. S.; Qiu, J. W.; Qi, S. H.; Qian, P. Y. *J. Proteome Res.* **2013**, *12*(5), 2090-2100.
- Hanessian, S.; Bayrakdarian, M. *Tetrahedron Lett.* **2002**, *43*, 967-971.
- He, F.; Han, Z.; Peng, J.; Qian, P. Y.; Qi, S. H. *Nat. Prod. Commun.* **2013**, *8*(3), 329-332.
- Herzon, S. B.; Myers, A. G. *J. Am. Chem. Soc.* **2005**, *127*(15), 5342-5344.
- Horino, T.; Tokita, A.; Oshima, T., Photochromic material. US 0102775, 2013.

- Hymery, N.; Vasseur, V.; Coton, M.; Mounier, J.; Jany, J. L.; Barbier, G.; Coton, E.  
*Compr Rev Food Sci F* **2014**, *13*(4), 437-456.
- Ideguchi, T.; Yamada, T.; Shirahata, T.; Hirose, T.; Sugawara, A.; Kobayashi, Y.;  
Omura, S.; Sunazuka, T. *J. Am. Chem. Soc.* **2013**, *135*(34), 12568-12571.
- Iwasa, E.; Hamashima, Y.; Fujishiro, S.; Hashizume, D.; Sodeoka, M. *Tetrahedron*  
**2011**, *67*, 6587-6599.
- Iwasa, E.; Hamashima, Y.; Fujishiro, S.; Higuchi, E.; Ito, A.; Yoshida, M.; Sodeoka,  
M. *J. Am. Chem. Soc.* **2010**, *132*, 4078-4079.
- Jacobson, S. E.; Muccigrosso, D. A.; Mares, F. *J. Org. Chem.* **1979**, *44*(6), 921-  
924.
- Jin, P.; Wei, D.; Wen, Y.; Luo, M.; Wang, X.; Tang, M. *J. Mol. Struct.* **2011**, *992*(1-  
3), 19-26.
- Kadlubar, F. F.; McKee, E. M.; Ziegler, D. M. *Arch. Biochem. Biophys.* **1973**, *156*,  
46-57.
- Kim, J.; Ashenurst, J. A.; Movassaghi, M. *Science* **2009**, *324*, 238-241.
- Kim, J.; Movassaghi, M. *J. Am. Chem. Soc.* **2010**, *132*, 14376-14378.
- Koizumi, Y.; Arai, M.; Tomoda, H.; Ōmura, S. *Biochim. Biophys. Acta.* **2004**,  
*1693*(1), 47-55.

- Koolen, H. H. F.; Soares, E. R.; da Silva, F. M. A.; de Almeida, R. A.; de Souza, A. D. L. *Quim. Nova* **2012**, 35(4), 771-774.
- Kopp, B.; Rehm, H. J. *Eur. J. Appl. Microbiol. Biotechnol.* **1979**, 6, 397-401.
- Kopp-Holtwiesche, B. B. *J. Environ. Pathol. Toxicol. Oncol.* **1990**, 10(1-2), 41-44.
- Kozlovsky, A. G.; Vinokurova, N. G.; Reshetilova, T. A.; Sakharovsky, V. G.; Baskunov, B. P.; Seleznyov, S. G. *Prikl. Biokhim. Mikrobiol.* **1994**, 30, 410-414.
- Kozlovsky, A. G.; Solovieva, T. F.; Reshetilova, T. A.; Skryabin, G. K. *Experientia* **1981**, 37, 472-473.
- Kyriakidis, N.; Waight, E. S.; Day, J. B.; Mantle, P. G. *Appl. Environ. Microb.* **1981**, 42(1), 61-62.
- Larsen, T. O.; Gareis, M.; Frisvad, J. C. *J. Agric. Food Chem.* **2002**, 50, 6148-6152.
- Li, S.; Finefield, J. M.; Sunderhaus, J. D.; McAfoos, T. J.; Williams, R. M.; Sherman, D. H. *J. Am. Chem. Soc.* **2012**, 134(2), 788-791.
- Mady, M. S.; Mohyeldin, M. M.; Ebrahim, H. Y.; Elsayed, H. E.; Houssen, W. E.; Haggag, E. G.; Soliman, R. F.; El Sayed, K. A. *Bioorg. Med. Chem.* **2015**, 24(2), 113-122.

- Makosza, M.; Sienkiewicz, K. *J. Org. Chem.* **1998**, 63, 4199-4208.
- Mansfield, M. A.; Jones, A. D.; Kuldau, G. A. *Phytopathology* **2008**, 98(3), 330-336.
- Mantle, P. G.; Perera, K. P. W. C.; Maishman, N. J.; Mundy, G. R. *Appl. Environ. Microb.* **1983**, 45(5), 1486-1490.
- Marcantoni, E.; Petrini, M.; Polimanti, O. *Tetrahedron Lett.* **1995**, 36(20), 3561-3562.
- McAfoos, T. J.; Li, S.; Tsukamoto, S.; Sherman, D. H.; Williams, R. M. *Heterocycles* **2010**, 82(1), 461-472.
- Mikkola, R.; Andersson, M. A.; Hautaniemi, M.; Salkinoja-Salonen, M. S. *Toxicon* **2015**, 99, 58-67.
- Monbaliu, S.; Van Poucke, C.; Detavernier, C.; Dumoulin, F.; Van De Velde, M.; Schoeters, E.; Van Dyck, S.; Averkieva, O.; Van Peteghem, C.; De Saeger, S. *J. Agric. Food Chem.* **2010**, 58(1), 66-71.
- Murray, R. W.; Singh, M. *Org. Synth.* **1997**, 74, 91.
- Nagel, D. W.; Pachler, K. G. R.; Steyn, P. S.; Wessels, P. L.; Gafner, G.; Kruger, G. J. *J. Chem. Soc. Chem. Commun.* **1974**(24), 1021.

- Newmister, S. A.; Gober, C. M.; Romminger, S.; Yu, F.; Tripathi, A.; Parra, L. L. L.; Williams, R. M.; Berlinck, R. G. S.; Joullié, M. M.; Sherman, D. H. *J. Am. Chem. Soc.* **2016**, *138*(35), 11176-11184.
- Ni, J.; Wang, H.; Reisman, S. E. *Tetrahedron* **2013**, *69*(27-28), 5622-5633.
- Nikbakht, F.; Heydari, A. *Tetrahedron Letters* **2014**, *55*(15), 2513-2516.
- Nising, C. F. *Chem. Soc. Rev.* **2010**, *39*(2), 591-599.
- Ohmomo, S.; Ohashi, T.; Abe, M. *Agr. Biol. Chem. Tokyo* **1980**, *44*(8), 1929-1930.
- Ohmomo, S.; Sato, T.; Utagawa, T.; Abe, M. *Agr. Biol. Chem. Tokyo* **1975**, *39*(6), 1333-1334.
- Ohmomo, S.; Utagawa, T.; Abe, M. *Agr. Biol. Chem. Tokyo* **1977**, *41*(10), 2097-2098.
- Ouchaou, K.; Maire, F.; Salo, O.; Ali, H.; Hankemeier, T.; van der Marel, G. A.; Filippov, D. V.; Bovenberg, R. A.; Vreeken, R. J.; Driessen, A. J.; Overkleeft, H. S. *ChemBioChem* **2015**, *16*(6), 915-923.
- Overy, D. P.; Frisvad, J. C. *Syst. Appl. Microbiol.* **2003**, *26*(4), 631-639.
- Overy, D. P.; Nielsen, K. F.; Smedsgaard, J. *J. Chem. Ecol.* **2005**, *31*(10), 2373-2390.
- Padwa, A.; Koehler, K. F. *Heterocycles* **1986**, *24*(2), 611-615.



- Peng, J. X.; Gao, H. Q.; Li, J.; Ai, J.; Geng, M. Y.; Zhang, G. J.; Zhu, T. J.; Gu, Q. Q.; Li, D. H. *J. Org. Chem.* **2014**, *79*(17), 7895-7904.
- Pinkernell, U.; Effkemann, S.; Nitzsche, F.; Karst, U. *J. Chromatogr. A* **1996**, *730*, 203-208.
- Qi, S.; He, F., Indole alkaloid in the preparation of marine antifouling coating. CN 102757677, 2012.
- Qian-Cutrone, J.; Huang, S.; Shu, Y. Z.; Vyas, D.; Fairchild, C.; Menendez, A.; Krampitz, K.; Dalterio, R.; Klohr, S. E.; Gao, Q. *J. Am. Chem. Soc.* **2002**, *124*(49), 14556-14557.
- Rand, T. G.; Giles, S.; Flemming, J.; Miller, J. D.; Puniani, E. *Toxicol. Sci.* **2005**, *87*(1), 213-222.
- Rasmussen, R. R.; Rasmussen, P. H.; Larsen, T. O.; Bladt, T. T.; Binderup, M. L. *Food Chem. Toxicol.* **2011**, *49*(1), 31-44.
- Rauk, A.; Yu, D.; Taylor, J.; Shustov, G. V.; Block, D. A.; Armstrong, D. A. *Biochemistry* **1999**, *38*, 9089-9096.
- Repka, L. M.; Ni, J.; Reisman, S. E. *J. Am. Chem. Soc.* **2010**, *132*, 14418-14420.
- Reshetilova, T. A.; Kozlovsky, A. G. *J. Basic Microbiol.* **1990**, *30*(2), 109-114.

- Reshetilova, T. A.; Vinokurova, N. G.; Khmelenina, V. N.; Kozlovskii, A. G.  
*Microbiology* **1995**, *64*(1), 27-29.
- Reshetilova, T. A.; Vinokurova, N. G.; Khmelenina, V. N.; Kozlovskii, A. G.  
*Microbiology* **1995**, *64*(1), 27-29.
- Ries, M. I.; Ali, H.; Lankhorst, P. P.; Hankemeier, T.; Bovenberg, R. A.; Driessen,  
A. J.; Vreeken, R. J. *J. Biol. Chem.* **2013**, *288*(52), 37289-37295.
- Rigby, J. H.; Wang, Z. *Org. Lett.* **2002**, *4*(24), 4289-4291.
- Rodriguez, R. J.; Proteau, P. J.; Marquez, B. L.; Hetherington, C. L.; Buckholz, C.  
J.; O'Connell, K. L. *Drug Metab. Dispos.* **1999**, *27*(8), 880-886.
- Romano, C.; de la Cuesta, E.; Avendaño, C. *J. Org. Chem.* **1991**, *56*, 74-78.
- Roy, A.; Schneller, S. W. *Org. Lett.* **2005**, *7*, 3889-3891.
- Schiavi, B. M.; Richard, D. J.; Joullié, M. M. *J. Org. Chem.* **2002**, *67*, 620-624.
- Schmidt, F. G.; Spange, S.; Polenz, I., Basen/isocyanat-initiierte polymerisation an  
oxidischen oberflächen. WO 117379, 2013.
- Schmidt, U.; Lieberknecht, A.; Schanbacher, U.; Beuttler, T.; Wild, J. *Angew.  
Chem. Int. Ed.* **1982**, *21*(10), 776-777.
- Scott, P. M.; Kennedy, B. P.; Harwig, J.; Blanchfield, B. J. *Appl. Environ. Microb.*  
**1977**, *33*(2), 249-253.

- Scott, P. M.; Merrien, M. A.; Polonsky, J. *Experientia* **1976**, 32(2), 140-142.
- Scott, P. M.; Polonsky, J.; Merrien, M. A. *J. Agric. Food Chem.* **1979**, 27(1), 201-202.
- Shan, W. G.; Ying, Y. M.; Yu, H. N.; Liu, W. H.; Zhan, Z. J. *Helv. Chim. Act.* **2010**, 93(4), 772-776.
- Shangguan, N.; Hehre, W. J.; Ohlinger, W. S.; Beavers, M. P.; Joullié, M. M. *J. Am. Chem. Soc.* **2008**, 130(19), 6281-6287.
- Shi, H.-C.; Li, Y. *J. Mol. Catal. A: Chem.* **2007**, 271(1-2), 32-41.
- Shindo, H.; Umezawa, B. *Chem. Pharm. Bull. (Tokyo)* **1962**, 10, 492-503.
- Simonin, C.; Awale, M.; Brand, M.; van Deursen, R.; Schwartz, J.; Fine, M.; Kovacs, G.; Häfliger, P.; Gyimesi, G.; Sithampari, A.; Charles, R.-P.; Hediger, M. A.; Reymond, J.-L. *Angew. Chem. Int. Ed.* **2015**, 54, 14748-14752.
- Spanjer, M. C.; Rensen, P. M.; Scholten, J. M. *Food Addit. Contam. Part A Chem. Anal. Control Expo. Risk Assess.* **2008**, 25(4), 472-489.
- Steyn, P. S.; Vleggaar, R. *J. Chem. Soc. Chem. Commun.* **1983**, 10, 560.
- Stöber, W.; Fink, A. *J. Colloid Interface Sci.* **1968**, 26, 62-69.

- Sugie, Y.; Hirai, H.; Inagaki, T.; Ishiguro, M.; Kim, Y. J.; Kojima, Y.; Sakakibara, T.; Sakemi, S.; Sugiura, A.; Suzuki, Y.; Brennan, L.; Duignan, J.; Huang, L. H.; Sutcliffe, J.; Kojima, N. *J. Antibiot. (Tokyo)* **2001**, *54*(11), 911-916.
- Sun, H.; Ehlhardt, W. J.; Kulanthaivel, P.; Lanza, D. L.; Reilly, C. A.; Yost, G. S. *J. Pharmacol. Exp. Ther.* **2007**, *322*(2), 843-851.
- Sunazuka, T.; Shirahata, T.; Tsuchiya, S.; Hirose, T.; Mori, R.; Harigaya, Y.; Kuwajima, I.; Ōmura, S. *Org. Lett.* **2005**, *7*(5), 941-943.
- Sustmann, R.; Trill, H. *Angew. Chem. Int. Ed.* **1972**, *11*(9), 838-&.
- Tang, P.; Furuya, T.; Ritter, T. *J. Am. Chem. Soc.* **2010**, *132*, 12150-12154.
- Taubel, M.; Sulyok, M.; Vishwanath, V.; Bloom, E.; Turunen, M.; Jarvi, K.; Kauhanen, E.; Krska, R.; Hyvarinen, A.; Larsson, L.; Nevalainen, A. *Indoor Air* **2011**, *21*(5), 368-375.
- Trimble, L. A.; Sumarah, M. W.; Blackwell, B. A.; Wrona, M. D.; Miller, J. D. *Tetrahedron Lett.* **2012**, *53*(8), 956-958.
- Turner, H. M.; Patel, J.; Niljianskul, N.; Chong, J. M. *Org. Lett.* **2011**, *13*(21), 5796-5799.
- Valentin, C. D.; Gisdakis, P.; Yudanov, I. V.; Rösch, N. *J. Org. Chem.* **2000**, *65*, 2996-3004.

van den Berg, M. A.; Albang, R.; Albermann, K.; Badger, J. H.; Daran, J. M.;  
Driessen, A. J.; García-Estrada, C.; Fedorova, N. D.; Harris, D. M.; Heijne,  
W. H.; Joardar, V.; Kiel, J. A.; Kovalchuk, A.; Martín, J. F.; Nierman, W. C.;  
Nijland, J. G.; Pronk, J. T.; Roubos, J. A.; van der Klei, I. J.; van Peij, N. N.;  
Veenhuis, M.; von Döhren, H.; Wagner, C.; Wortman, J.; Bovenberg, R. A.  
*Nat. Biotechnol.* **2008**, *26*, 1161-1168.

Villamena, F. A.; Dickman, M. H.; Crist, D. R. *Inorg. Chem.* **1998**, *37*, 1446-1453.

Vishwanath, V.; Sulyok, M.; Labuda, R.; Bicker, W.; Krska, R. *Anal. Bioanal. Chem.*  
**2009**, *395*(5), 1355-1372.

Vishwanath, V.; Sulyok, M.; Weingart, G.; Kluger, B.; Taubel, M.; Mayer, S.;  
Schuhmacher, R.; Krska, R. *Talanta* **2011**, *85*(4), 2027-2038.

von Nussbaum, F. *Angew. Chem. Int. Ed.* **2003**, *42*(27), 3068-3071.

Wagener, R. E.; Davis, N. D.; Diener, U. L. *Appl. Environ. Microb.* **1980**, *39*, 882-  
887.

Wang, H.; Reisman, S. E. *Angew. Chem. Int. Ed.* **2014**, *53*(24), 6206-6210.

Wang, X. R.; You, J. L.; King, J. B.; Powell, D. R.; Cichewicz, R. H. *J. Nat. Prod.*  
**2012**, *75*(4), 707-715.

Williamson, K. S.; Michaelis, D. J.; Yoon, T. P. *Chem. Rev.* **2014**, *114*(16), 8016-  
8036.

Wojtas, K. P.; Lu, J.-Y.; Krahn, D.; Arndt, H.-D. *Chem. Asian J.* **2016**, *11*(20), 2859-2862.

Wulff, J. E.; Herzon, S. B.; Siegrist, R.; Myers, A. G. *J. Am. Chem. Soc.* **2007**, *129*(16), 4898-4899.

Wulff, J. E.; Siegrist, R.; Myers, A. G. *J. Am. Chem. Soc.* **2007**, *129*(46), 14444-14451.

Yamada, T.; Ideguchi-Matsushita, T.; Hirose, T.; Shirahata, T.; Hokari, R.; Ishiyama, A.; Iwatsuki, M.; Sugawara, A.; Kobayashi, Y.; Otoguro, K.; Ōmura, S.; Sunazuka, T. *Chem. Eur. J.* **2015**, *21*(33), 11855-11864.

Yamaguchi, T.; Nozawa, K.; Nakajima, S.; Kawai, K.; Udagawa, S. *Maikotokishin* **1991**, *34*, 485-487.

Zacuto, M. J.; Xu, F. *J. Org. Chem.* **2007**, *72*, 6298-6300.

Zheng, C. J.; Sohn, M.-J.; Lee, S.; Kim, W.-G. *PLoS ONE* **2013**, *8*(11), e78922.